Testing the role of extracellular vesicles in early left-right patterning

SARA FILIPA SILVA PESTANA

Tese para obtenção do grau de Doutor em Mecanismos de Doença e Medicina Regenerativa

Doutoramento em associação entre:
Universidade NOVA de Lisboa (Faculdade de Ciências Médicas | NOVA Medical School)
Universidade do Algarve (UAlg)

Setembro, 2022

Testing the role of extracellular vesicles in early left-right patterning

Sara Filipa Silva Pestana

Orientadores:
Susana Lopes, Investigador Principal da Faculdade de Ciências Médicas | NOVA Medical School, Universidade Nova de Lisboa
Duarte Barral, Professor Associado da Faculdade de Ciências Médicas | NOVA Medical School, Universidade Nova de Lisboa

Tese para obtenção do grau de Doutor em Doutor em Mecanismos de Doença e Medicina Regenerativa

Doutoramento em associação entre:
Universidade NOVA de Lisboa (Faculdade de Ciências Médicas | NOVA Medical School)
Universidade do Algarve (UAlg)

Setembro, 2022

The research described here was performed at NOVA Medical School | Faculdade de Ciências Médicas, NMS|FCM, Universidade Nova de Lisboa; Lisboa, Portugal, between 2018 and 2022. Its execution was supported by a PhD fellowship from the Portuguese Foundation for Science and Technology (SFRH/BD/130272/2017).

The procedures performed in the context of my thesis were approved by the NMS | FCM-UNL Ethics Research Committee (nº 207/2021/CEFCM).

LIST OF CONTENTS

Acknowledgements

Fazer um doutoramento é sem dúvida uma longa jornada com muitos altos e baixos, não só em busca de uma descoberta científica, mas também de crescimento pessoal. Felizmente tive bons exemplos em meu redor que me apoiaram e nunca me deixaram desistir.

Em primeiro lugar, gostaria de agradecer à Susana Lopes que me aceitou no seu laboratório durante o meu mestrado. Tinha acabado de sair do primeiro ano de mestrado fascinada com biologia do desenvolvimento. A capacidade de apenas uma célula dar origem a um organismo completamente diferenciado e funcional fez-me prosseguir uma carreira científica e foi a Susana Lopes quem me proporcionou um projeto nessa área. Deste então, tive a oportunidade de trabalhar ao lado de pessoas brilhantes, conhecer os especialistas do campo, apresentar o meu trabalho em conferências internacionais e muito mais. Nada disto teria sido possível, se não tivesses acreditado em mim e nas minhas capacidades. E por isso, estou-te eternamente grata, Susana. Fizeste de mim, como a célula que se tornou num organismo independente, uma cientista.

Gostaria também de agradecer ao Duarte Barral, que amavelmente aceitou ser meu co-orientador. A tua disponibilidade, críticas construtivas e reflexões foram indispensáveis para a realização deste trabalho. És um exemplo de que tudo se faz com boa organização e foco, sem nunca perder a boa disposição.

Ao longo desde tempo tive também o privilégio de partilhar o meu dia-a-dia no laboratório da Susana Lopes com pessoas incríveis, que me proporcionaram um ambiente seguro para aprender e crescer, com uma camaradagem irrepreensível. Festejámos as experiências bem-sucedidas e os artigos aceites uns dos outros como se fossem nossos e ninguém virou costas nos momentos de maior aperto. Não podia ter pedido uma "família" de laboratório melhor.

Mónica, tu és uma força da natureza. A tua disciplina e perseverança são uma fonte de inspiração. Nunca tinha conhecido uma pessoa com tanta integridade pessoal e profissional e empatia emocional, como tu. Um dos muitos conselhos que me deste foi o de pensar se algo que nos chateia hoje terá algum efeito na nossa vida ao fim de cinco anos. E assim pretendo levar a vida, de forma pragmática com uma atitude positiva, como tu sempre mostraste, e focando-me nas coisas boas e bonitas que temos. Por tudo isto e muito mais, muito obrigada!

Petra, és igualmente incrível. Contigo aprendi que tudo é eterno até deixar de o ser. Partilhámos gargalhadas e confidências, planeámos ideias milionárias e discutimos pró e contras de experiências. Com o teu pensamento crítico e afiado estiveste sempre pronta para arranjar uma solução fácil e eficaz para qualquer que fosse o meu problema. Não teria chegado até aqui sem ti, obrigada! E não tenhas receio de te atirares de cabeça, pois eu sei o quanto tu és capaz de voar alto!

Raquel, não tenho palavras suficientes para te agradecer. Acolheste-me de braços abertos no laboratório e ao longo do tempo esta amizade transbordou do ambiente profissional e tornaste-te numa irmã mais velha. Obrigada por todos os conselhos, os raspanetes e o apoio incondicional! Obrigada pela ajuda, pelos brindes no quiosque da avenida ao fim do dia e por acreditares em mim, mesmo quando eu própria não acreditava! Obrigada, também por me mostrares que há um mundo melhor para lá do horizonte. Por outro lado, tive a oportunidade

de te ver crescer. Sempre trabalhadora e dona de seu nariz, amiga e carinhosa, tu foste e continuas a ser uma inspiração. Tenho muito orgulho em ti, Raquelinda!

Pedrocas, foste o melhor companheiro de experiências que alguém pode ter. Sempre pronto para o próximo desafio, fossem noitadas de experiências dificílimas, slides no surfskate ou a pedalar mobikes, mostraste-me que com calma e persistência, conseguimos alcançar os nossos objetivos. Obrigada por todas as gargalhadas que partilhámos dentro e fora do laboratório e por todas aquelas que ainda estão para vir! Obrigada, também pela paciência e disponibilidade para me ensinares a manipular KVs e quantificar flow, sem ti não tinha feito metade! Espero que saibas que podes contar sempre comigo.

Raquel e Pedro, muito do que sei hoje como cientista aprendi convosco, não fossem vocês os fillet mignon mais talentosos que conheço. Agradeço-vos de coração cheio!

Catarina, fizesse chuva ou sol, não houve um momento aborrecido ao teu lado. Entre histórias caricatas e peripécias, tu animaste os meus dias no laboratório. Sem ti, não ter tido a mesma piada. Obrigada, também pela camaradagem, que tantas vezes me safou de ir trabalhar ao fim-de-semana. És uma miúda cheia de valor, não te esqueças disso.

Quero também agradecer à Margarida por toda a disponibilidade em ajudar, as bolachas e chocolates, e por me relembrares, quando pensava que estava a ficar louca, que há pessoas que acreditam que os aminoácidos se podem enviar por Bluetooth. À Raquel Domingues que neste último ano teve a paciência de me ouvir. E ao Fábio, que cuidou dos meus peixinhos e que me aconselhou as melhores séries televisivas, com uma prestação superior ao IMDb.

Uma palavra de apreço aos meu colegas de doutoramento, que tornaram esta 5ª e última edição do ProRegeM inesquecível. A pandemia impediu-nos de ir ao Algarve uma última vez, mas em breve teremos de marcar um reencontro.

No CEDOC encontrei ainda outras pessoas maravilhosas que sempre estiveram prontas para me ajudar e apoiar, que tornaram os meus dias mais felizes e que hoje posso também chamar de amigos.

Bitoque, Ana e Illy, vocês são impecáveis! Sem vocês para me encorajarem, teria desistido a meio. Obrigada por todos os momentos, as conversas, as idas ao churrasco coreano, aos aperoles (!), as idas do ginásio e aos caracóis. Vocês mantiveram a minha saúde mental em dia!

Borbinha, foste fundamental nesta última fase. Com o doutoramento a terminar e a querermos passar para novas aventuras, entre respostas negativas e entrevistas falhadas, tu nunca me deixaste desistir! Hoje posso dizer que conseguimos e, por isso, estou-te imensamente grata.

Fui também uma afortunada por ter grandes amigos fora do CEDOC, que me conhecem melhor que eu própria, e que estiveram ao meu lado desde sempre.

Inês, you're my person. És a Yang da minha Grey e o Pumba do meu Timon. E por mais palavras houvesse, eu não teria como explicar o quanto tu és importante para mim. Trabalhadora, persistente, inteligente e engraçada, és o pacote completo. E o que eu mais desejo é que sejas feliz!

Marta Moniz, Adriana e Carina, as minhas CB queens. Vocês ensinaram-me que não precisamos de estar todos os dias juntas para manter uma amizade. Os nossos reencontros são sempre de alegria e partilha, como se o tempo nunca tivesse passado.

Tânia, Sara e Neuza, a vocês devo-vos muito. Obrigada por todo o apoio e preocupação, os conselhos e os sorrisos no rosto. Obrigada, também ao Rui e ao Fábio, que foram excelentes adições ao grupo. Não teria sobrevivido sem os nossos retiros de fim-de-semana para recarregar as energias. São sempre fantásticos e fazem com que tudo o resto valha a pena. Gosto muito de vocês, de coração cheio! Um beijinho à baby Íris, o mais recente membro que veio acrescentar muito amor e carinho a este grupo.

E um obrigado aos “Lourenses” pelos nossos encontros sempre divertidos e por me fazerem sentir sempre incluída.

Por último, mas não menos importante, quero agradecer à minha família.

Ao meu pai e à minha mãe que me tornaram na pessoa que sou hoje. Que trabalharam imenso para me proporcionarem a melhor educação. Que apoiaram as minhas decisões. E que me ensinaram que nunca é tarde para mudarmos de rumo para seguirmos os nossos sonhos! Tenho um orgulho imenso em vocês. Não tenho como agradecer tudo o que fizeram por mim, mas espero estar sempre a altura das vossas expectativas. Amo-vos aos dois.

Aos meus tios e primos, que apesar não perceberem o que faço e acharem que trabalho com peixinhos com três olhos, sempre mostraram preocupação e carinho, e muitos chocolates.

Dedico ainda esta tese à minha avó, que onde quer que esteja, sempre quis o melhor para mim.

E ao João, que é sempre a melhor parte do meu dia. Obrigada por teres estado incansavelmente ao meu lado nesta longa reta final, por me levantares e dares energia para continuar e por me pores um sorriso na cara quando eu mais precisava. Obrigada por tudo!

Trabalho realizado ao abrigo da Bolsa (SFRH/BD/130272/2017), com o apoio da FCT (Fundação para a Ciência e a Tecnologia), do FSE (Fundo Social Europeu) e do POCH (Programa Operacional Capital Humano).

Abstract

Bilaterian animals, such as humans, are characterized by an external roughly mirror symmetry along the left – right axis that covers a pronounced internal asymmetric arrangement of the thoracic and abdominal organs. While external symmetry has been associated with health and beauty standards, the internal asymmetry may rely more on efficiency and functionality of the different physiological systems. The left – right asymmetry of visceral organs is established early on during embryonic development within a transient and specialized structure, commonly referred to as the left – right organizer (LRO).

The LROs appear in many shapes and sizes, depending on the species, but a common feature in some vertebrates is the requirement of motile cilia. The movement of these tiny hair-like protrusions generate a directional fluid flow, that scales with the cube of cilia length, in order to become capable of triggering a differentiated response on the left side of the LRO. Such flow-dependent response involves Pkd2 channel activation and calcium signaling that subsequently drive the left sided expression of the Nodal signaling cascade.

Nodal is a secreted protein that translates the asymmetries established at the LRO to the rest of the embryo, through the lateral plate mesoderm. As embryonic development evolves, at specific time points and locations along the anterior – posterior axis, Nodal induces the expression of genes involved in the formation of the heart, brain, gut and its derivatives, modulating the lateralization of these organs.

With this work, we dedicated our efforts to understanding a few molecular and cellular steps missing in the establishment of the left – right axis within the LRO. In the Chapter 2, we explored how the fluid flow is sensed by the LRO cells. Between the two hypotheses in the field, one based on mechanosensing and other on chemosensing properties of the flow, we found that the number of extracellular vesicles is too low and variable to transport sufficient and efficiently a sidedness molecular signal towards the left sided LRO cells. Moreover, pharmacological impairment of distinct endocytic pathways did not impact on heart laterality arrangement.

We also found out an upstream regulator of Notch signaling, *syntenin-a*, involved in the cell fate decision between motile and immotile cilia. We showed that *syntenin-a* loss-of-function severely affected the left – right axis development. By downregulating the levels of *syntenin-a*, Notch signaling is activated increasing the expression of *her12* and resulting in a higher number of immotile cilia, in concordance with our previous published data. We next described a potential molecular switch, downstream of Notch signaling, composed by the Rabconnectin complex. As this complex is known to promote V-ATPase assembly and consequently its activity, we inhibited the V-ATPase activity and we observed an increase in the number of motile cilia. Thus, suggesting that the link between Notch signaling and motile – immotile cilia ratio is through the modulation of pH.

Lastly, in Chapter 3, we focused on the impact of ciliary dysfunction in the epithelial respiratory cells. We characterized the distribution pattern of several ciliary proteins in two siblings harboring a primary ciliary dyskinesia causing mutation on *Zmynd10* gene. Recent studies showed that ZMYND10 is one of the cytoplasmatic factors responsible for stabilizing and driving axonemal dynein arm assembly. We showed here that outer and inner axonemal dyneins, that become mostly absent from the ciliary axoneme in *Zmynd10* mutant respiratory ciliated cells, can sometimes enter the proximal part of the cilium. These results suggest that

to a low extent the dynein arms can still assemble and be transported into the cilium in the absence of ZMYND10, thus opening an opportunity for small-molecule therapies that promote protein stability in primary ciliary dyskinesia disease management.

Key-words: left – right organizer, extracellular vesicles, viscosity, ciliary motility, primary ciliary dyskinesia, ZMYND10

Resumo

Os animais bilaterais, como os humanos, são caracterizados por uma simetria externa ao longo do eixo esquerda – direita que cobre um arranjo interno pronunciadamente assimétrico dos órgãos torácicos e abdominais. Enquanto a simetria externa tem sido associada a padrões de saúde e beleza, a assimetria interna pode depender maioritariamente da eficiência e funcionalidade da montagem dos diferentes sistemas fisiológicos. Esta assimetria esquerda – direita dos órgãos viscerais é estabelecida durante o desenvolvimento embrionário dentro de uma estrutura transiente e especializada, normalmente conhecida por organizador esquerda – direita.

Os organizadores esquerda – direita aparecem em várias formas e tamanhos, dependendo da espécie, mas uma característica comum em alguns dos vertebrados é a existência de cílios. Os cílios são organelos compostos por microtúbulos que são projetados da superfície da célula. E estes podem ser móveis ou imóveis dependendo da presença ou ausência de proteínas motoras, as dineínas do axonema, que geram energia suficiente para mover o cílio. No caso do organizador esquerda – direita, os dois tipos de cílios estão presentes e desempenham funções distintas: os cílios móveis promovem um fluxo direcional do fluido existente no lúmen dos organizadores, cuja velocidade é proporcional ao cubo do comprimento ciliar, e os cílios imóveis são potencialmente responsáveis por detetar esse mesmo fluxo. Por conseguinte, a deteção do fluxo desencadeia uma resposta assimétrica nas células do lado esquerdo do organizador esquerda – direita, que é dependente do canal de cálcio Pkd2 localizado nos cílios. Assim, os iões de cálcio entram pelo cílio e ativam a libertação de mais iões dos organelos internos, o que resulta numa onda de cálcio propagada pela célula que, por sua vez, é necessária para iniciar uma cascada molecular de sinalização composta por Nodal e os seus inibidores.

Nodal é um factor secretado da família TGF-β inicialmente expresso em redor do organizador esquerda-direita de forma simétrica. Um dos seus antagonistas expresso no organizador, Dand5, impede a propagação precoce e simétrica de Nodal para a placa lateral da mesoderme. Contudo, a onda de cálcio que se forma nas células do organizador promove a degradação de *dand5*, tornando-se assim o primeiro gene assimetricamente expresso e libertando Nodal da sua repressão especificamente no lado esquerdo do organizador. Consequentemente, Nodal é capaz de ativar a sua própria expressão na placa lateral da mesoderme do lado esquerdo e a expressão de um segundo inibidor, *lefty1*, na linha mediana, de forma a impedir que Nodal ative a sua expressão no lado direito.

À medida que o desenvolvimento embrionário evolui, Nodal propaga-se pela mesoderme ao longo do eixo anterior - posterior, que em estadios e regiões específicas, leva à expressão de genes envolvidos na formação do coração, cérebro, fígado, pâncreas, entre outros, modulando a lateralização destes órgãos.

Este campo da biologia do desenvolvimento tem evoluído bastante ao longo dos últimos anos, contudo algumas questões continuam em aberto. A forma como o fluxo é detetado pelas células do organizador esquerda – direita é uma delas. Historicamente, o campo está dividido em torno de duas hipóteses principais – o modelo quimiossensor e o modelo mecanossensor.

Por um lado, o modelo quimiossensor propõe que o fluxo serve para transportar vesículas e moléculas sinalizadoras para o lado esquerdo, onde serão internalizadas pelas células do organizador. Por outro lado, o modelo mecanossensor baseia-se na força hidrodinâmica que

o fluxo exerce sobre os cílios imóveis. Com este projeto de doutoramento pretendemos fornecer novos dados do mecanismo biofísico impulsionado pelo fluxo usando o organizador esquerda – direita do peixe-zebra como modelo animal. Inicialmente, dedicámo-nos a inspecionar as características moleculares das células do organizador e o conteúdo de fluído para inferir sobre as possíveis contribuições do modelo quimiosensor na deteção do fluxo de fluidos pelo canal Pkd2. Para tal, gerámos uma linha transgénica para quantificar e permitir o rastreamento de vesículas extracelulares dentro do lúmen do organizador e usámos uma nova configuração de micromanipulação para modificar o conteúdo do fluido do organizador. Os nossos resultados mostram que o número de vesículas extracelulares detetadas é muito baixo e variável para transportar um sinal molecular de lateralidade de forma eficiente para as células do organizador do lado esquerdo. Adicionalmente, a inibição farmacológica de vias endocíticas distintas não teve impacto na lateralidade do coração.

De seguida, analisámos a regulação do número de cílios móveis e imóveis no organizador esquerda – direita. No peixe zebra, todos os cílios têm a ultra estrutura necessária para se moverem, contudo, apenas alguns cílios se tornam móveis. O nosso grupo tinha anteriormente descoberto que a decisão entre móvel e imóvel é feita pela via de sinalização de Notch. Com este trabalho, nós identificámos novos moduladores a montante e efetores a jusante da sinalização de Notch envolvidos neste processo. Mostrámos que a perda de função da *syntenin-a* afeta severamente o desenvolvimento do eixo esquerda – direita, uma vez que ativa a sinalização de Notch e a expressão do seu gene alvo, *her12*, o que resulta num número maior de cílios imóveis e por conseguinte num fluxo do fluído menor. Também descrevemos um potencial botão molecular, a jusante da sinalização de Notch, composto pelo complexo Rabconnectin. Uma vez que este complexo é conhecido por promover a montagem da V-ATPase e consequentemente sua atividade, inibimos a atividade da V-ATPase e observámos um aumento do número de cílios móveis. Assim, sugerimos que a ligação entre a sinalização de Notch e a proporção de cílios móveis – imóveis se dá através da modulação do pH.

Por fim, no Capítulo 3, focámo-nos no impacto da disfunção ciliar nas células epiteliais respiratórias. Caracterizámos o padrão de distribuição de várias proteínas ciliares em dois irmãos portadores de discinésia ciliar primária causada por uma mutação no gene *Zmynd10*. Estudos recentes mostram que ZMYND10 é um dos fatores citoplasmáticos responsáveis por estabilizar e conduzir a montagem do braço de dineína que constituí o axonema do cílio móvel. Mostrámos aqui que as dineínas externas e internas do axonema, que se tornam principalmente ausentes do cílio em células respiratórias mutadas no gene *Zmynd10*, podem, no entanto, entrar na parte proximal do cílio. Estes resultados sugerem que uma pequena porção dos braços de dineína conseguem ser montados e transportados para o cílio na ausência de ZMYND10, abrindo assim uma oportunidade para terapias com pequenas moléculas que promovam a estabilidade de proteínas na gestão do tratamento da doença de discinésia ciliar primária.

List of publications

During the course of this PhD project, I have contributed to the following publications:

Kuhns, S., Seixas, C., Pestana, S., Tavares, B., Nogueira, R., Jacinto, R., Ramalho, J. S., Simpson, J. C., Andersen, J. S., Echard, A., Lopes, S. S., Barral, D. C., & Blacque, O. E. (2019). Rab 35 controls cilium length , function and membrane composition. *EMBO Reports*, *20*(10), e47625. https://doi.org/10.15252/embr.201847625

Jacinto, R., Sampaio, P., Roxo-Rosa, M., Pestana, S., & Lopes, S. S. (2021). Pkd2 Affects Cilia Length and Impacts LR Flow Dynamics and Dand5. *Frontiers in Cell and Developmental Biology*, *9*, 624531. https://doi.org/10.3389/fcell.2021.624531

Oliveira, I., Jacinto, R., Pestana, S., Nolasco, F., Calado, J., Lopes, S. S., & Roxo-rosa, M. (2021). Zebrafish Model as a Screen to Prevent Cyst Inflation in Autosomal Dominant Polycystic Kidney Disease. *International Journal of Molecular Sciences*, *22*(16), 9013. https://doi.org/10.3390/ijms22169013

Pinto, A. L., Rasteiro, M., Bota, C., Pestana, S., Sampaio, P., Hogg, C., Burgoyne, T., & Lopes, S. S. (2021). Zebrafish motile cilia as a model for primary ciliary dyskinesia. *International Journal of Molecular Sciences*, *22*(16), 8361. https://doi.org/10.3390/ijms22168361

Part of the work shown in here is included in the following article published in the BioRxiv:

Sampaio, P., Pestana, S., Guerrero, A., Telley, I. A., Smith, D. J., & Lopes, S. S. (2022). Fluid manipulations uncover mechanosensation for zebrafish left-right establishment during one-hour time interval. *BioRxiv*, 2022.04.21.489023. https://doi.org/10.1101/2022.04.21.489023

List of abbreviations

3'-UTR – three prime untranslated region

ActRIIB – serine/threonine kinase type II

ALIX – ALG-2 interacting protein X

ALK4 – serine/threonine kinase type I

AP – anterior-posterior axis

ATP – adenosine triphosphate

Ca^{2+} – calcium

CaMK-II – type II multifunctional Ca^{2+}/Calmodulin-dependent protein kinase

cAMP – cyclic adenosine monophosphate

CBF – ciliary beat frequency

CBP – ciliary beat pattern

CFTR – cystic fibrosis transmembrane conductance regulator

cGMP – cyclic guanosine monophosphate

CHD – congenital heart disease

Dand5 – DAN Domain BMP Antagonist family member 5

DFCs – dorsal forerunner cells

Dnah – dynein axonemal heavy chain

DV – dorsal-ventral axis

ER – endoplasmic reticulum

ESCRT – endosomal sorting complexes required for transport

EVs – extracellular vesicles

FGF – fibroblast growth factor

Foxj1a – forehead-domain-containing transcription factor

Gdf-1 – growth/differentiation factor-1

H^+/K^+-ATPase – hydrogen/potassium proton pump gene

her12 – hairy-related 12

HVMA – high-speed video microscopy analysis

ICOs – intraciliary calcium oscillations

IDA – inner dynein arm

IF – immunofluorescence

IFT – intraflagellar transport

ILVs – intraluminal vesicles

KV – Kupffer's vesicle

LPM – lateral plate mesoderm

LR – left-right

Lrd – left/right dynein

LRO – left-right organizer

MLCK – myosin-light chain kinase

mRNA – messenger ribonucleic acid

MVB – multivesicular body

NECD – notch extracellular domain

NICD – notch intracellular domain

nNO – nasal nitric oxide

Ntl – T-box transcription factor a, no tail

NVP – nodal vesicular parcels

ODA – outer dynein arm

ODA-DC – outer dynein arm docking complex

PCD – primary ciliary dyskinesia

PCP – planar cell polarity

PKD – polycystic kidney disease

RA – retinoic acid

ROCK 1 – Rho-associated protein kinase 1

ryr3 – ryanodine receptor 3

SELI – self-enhancement and lateral-inhibition

Shh – Sonic hedgehog

Sqt – Nodal related gene squint gene

Ss – somite stage

TEM – transmission electron microscopy

TGF-β – transforming growth factor beta

TRP – transient receptor potential cation channel

List of Figures

List of Supplementary Figures

List of Supplementary Movies

List of Tables

CHAPTER 1.
INTRODUCTION

"If the Lord Almighty had consulted me before embarking on creation
thus, I should have recommended something simpler."
– Attributed to Alfonso the Wise (13th century)

1. INTRODUCTION

The main characters of this story are the cilia.

Even though they are one of the oldest known cell organelles, it took over three hundred years to be recognized as fundamental in orchestrating many of the sensory and signaling events of the cell.

Its first appearance was in 1675, under Antoni van Leeuwenhoek's lens, who described it as "little feet, which were moved very nimbly" (Leewenhoeck, 1677). Since then, cilia have received a lot of attention mostly focused on its motility, the only hypothesized function at that time.

It was only in 1898, that Karl Wilhelm Zimmermann first recognized primary cilia in mammals. While working from fixed samples, Zimmermann was not able to infer cilia motility, but not only he correctly predicted the sensory role of primary cilia as he proposed that kidney tubule cilia worked as flow sensors (Zimmermann, 1898). This was successfully experimentally demonstrated by Praetorius and Spring, showing that bending one cilium led to an influx of intracellular calcium and a calcium wave that spread through the nearby cells (Praetorius & Spring, 2001).

Even with constant technical advances, studying primary cilia was not easy due to its small size and poor resolution, and so the cilia field went through some dark ages, being classified as a vestigial organelle by many investigators (reviewed by Bloodgood, 2018).

The re-birth of primary cilia was pushed by the development of transmission electron microscopy (TEM) and technical advances in light microscopy, molecular biology and genetics. The increased number of animal models, such as *Chlamydomonas*, *Caenorhabditis* and the mouse model, also helped (reviewed by Ostrowski et al., 2011).

Since then, we have been living in a Golden Age for cilia. We now know that cilia are involved in a myriad of biological processes and, when defective, in an ever-expanding list of human disorders, showing how crucial it is to better understand this field.

One of such disorders is primary ciliary dyskinesia (PCD), a heterogeneous group of inherited autosomal-recessive disorders of motile cilia. PCD is characterized by chronic airway infections, infertility and, in 50% of cases, laterality defects. This randomization of the left – right asymmetry derives from the malfunctioning of motile cilia within the left – right organizer (LRO), during embryogenesis. Motile cilia are responsible for generating a directional flow that triggers the correct genetic cascade signaling involved in the establishment of visceral organs

position. However, with sensory functions being discovered for motile cilia, the possibility of LRO cilia having other functions is still under debate (Kamura et al., 2011; Ferreira et al., 2017).

Thus, in this dissertation I will investigate how motility and potential sensory functions of LRO cilia could contribute to the establishment of the left – right axis and how ciliary motility is regulated both in the embryonic LRO and in the respiratory epithelium of PCD patients.

1.1. CILIA BIOLOGY

1.1.1. Motile and immotile cilia

Cilia are highly complex hair-like structures that protrude from the membrane of almost every human cell and are evolutionarily conserved across the eukaryotic kingdom. In general, the cilium elongates nine doublets of microtubules to form the cytoskeleton core, called axoneme, from the nine triplets of microtubules present in the basal body, a modified mother centriole that anchors the cilium to the apical cell surface (reviewed by Ishikawa & Marshall, 2011).

The microtubules are composed of α and β tubulin heterodimers that form a complete 13 protofilaments A-tubule and an incomplete 10 protofilaments B-tubule. The doublet is highly stable, even under significant stress during rapid ciliary beating, allowing cilia to be both actively bendable and sturdy (reviewed by Ichikawa et al., 2017).

The axoneme is ensheathed by a membrane that despite being continuous with the plasma membrane, exhibits a distinctive lipidic and protein composition. The identity of the ciliary membrane is maintained by different diffusion barriers at the cilia base (Verheya & Yang, 2016) and allows the cilium to function as a hub for signaling pathways (reviewed by Satir & Christensen, 2007).

The basic ultrastructure of the ciliary axoneme contains the ring of nine outer doublets of microtubules, in a called “9 + 0” configuration. Moreover, given the multitude of existing cilia, others can have additional two microtubule singlets placed in the middle of the nine microtubules ring, referred to as the “9 + 2” configuration, and may also have molecular motors and radial projections.

During ciliogenesis, ciliary proteins are selectively imported and transported through the cilium by the intraflagellar transport (IFT). Using large macromolecular IFT trains, this system provides ciliary cargo transport from the cell body towards the tip of the cilium (anterograde transport) or from the ciliary tip back to the basal body and the cell (retrograde transport),

powered by the molecular motors kinesin-2 and dynein-2 respectively (Cole et al., 1998; Pazour et al., 1998). Therefore, this molecular motor-driven system is responsible not only for the assembly and elongation of cilia, but also for the maintenance of ciliary length, through different rates of transport of the ciliary building blocks (reviewed by Wang et al., 2021). Additionally, IFT plays an important role in cilia function through the transport of mechanosensory and chemosensory proteins, as well as motility-associated appendages (Bhogaraju et al., 2013).

Hence, depending on its function, cilia are divided into two groups: primary and motile cilia. The primary cilia, also known as sensory cilia, are found on most cells in the human body as a single cilium per cell. Their shape, length and disposition across the cell can differ from one tissue to another, but primary cilia are generally described as non-motile cilia with a “9 + 0” axonemal organization devoid of motor components (Singla & Reiter, 2006). Some exceptions exist, like the kinocilia of hair cells that have an axonemal “9 + 2” conformation and an incomplete motor complex, which is not sufficient to induce motility (Kikuchi et al., 1989) and the primary cilia of olfactory sensory neurons that have an axonemal “9 + 2” conformation with a complete absence of the motor complex (Menco, 1984).

Primary cilia selectively incorporate specific receptors and ion channels at the ciliary membrane and high concentrations of protein transporters and signaling effectors within the axoneme. This specialized microenvironment allows the cilium to perceive stimuli from the extracellular space and convey that signaling information to the cell to regulate diverse cellular processes, including cell migration, differentiation, cell division and apoptosis, during development, organ function homeostasis and diseases. A diverse array of stimuli has been linked to the primary cilium, such as odorants, light, fluid shear stress, pressure and signaling molecules (reviewed by Berbari et al., 2009). Moreover, many signaling pathways are involved with cilia, including Hedgehog (Huangfu et al., 2003), Wnt (Otto et al., 2003; Corbit et al., 2008) and Notch signaling (Ezratty et al., 2011; Leitch et al., 2014), among others. Unsurprisingly, mutations that affect cilia give rise to broad phenotypically-overlapping pathologies, affecting embryonic development as well as postnatal life (reviewed by Fliegauf et al., 2007).

In contrast to primary cilia, only a few differentiated cell types develop highly specialized cilia that can move. Multiple motile cilia arise from the apical surface membrane of respiratory epithelial cells, fallopian duct epithelial cells and ependymal cells from the ventricles of the brain. These cilia beat in a synchronous fashion within and between neighborhood cells and play a critical role in fluid and particle transport to clear the mucus from the lungs, to move the egg through the reproductive system and to circulate the cerebrospinal fluid within the brain. Additionally, single specialized motile cilia protrude from the embryonic LRO cells, in order to

regulate the directional fluid flow necessary for the establishment of the left – right axis. Single cilium or flagella also protrude from spermatozoa, to promote gamete cell locomotion through the female reproductive tract (reviewed by Lee & Ostrowski, 2021). In addition to these roles, motile cilia can have concomitantly sensory functions. For instance, in human airway epithelial cilia, bitter taste receptors detect noxious compounds and elicit a ciliary beat frequency response to eliminate those compounds from the lungs (Shah et al., 2009). Whereas in mouse oviduct cilia, progesterone receptor and estrogen receptor are known to detect sex hormones (Teilmann et al., 2006), and calcium permeable cation channels are present and thought to mediate oviduct function (Teilmann et al., 2005).

With a few exceptions like the mouse LRO ciliated cells that have a “9 + 0” axonemal configuration, motile cilia are characterized by a “9 + 2” axonemal structure and the presence of motility associated appendages. These appendages form a complex and conserved structure of axonemal dyneins, radial spokes and nexin links (Ishikawa, 2017).

The axonemal dyneins are large multiprotein complexes from the family of ATPase motor proteins that can be divided into outer dynein arms (ODA), that extend from the peripheral side of the A-tubule from each microtubule doublet facing the ciliary membrane, and inner dynein arms (IDA), that extend from the central side of the A-tubule facing the central pair apparatus. The ODAs are composed of heavy-chains (400–500 kDa), intermediate chains (45–140 kDa) and light chains (8–28 kDa) and contain the AAA+ head domain that allows the chemical energy of adenosine triphosphate (ATP) binding and hydrolysis conversion into mechanical force (reviewed by King, 2016). By generating force, ODAs drive transient binding and sliding of neighboring microtubule doublets and, therefore, ciliary bending. The continuous beating is promoted by the synchronous switch between active and inactive dyneins, asymmetrically distributed, along the entire axoneme (Lin & Nicastro, 2018). ODA heavy chains can be further classified into subtype 1, which are located in the most proximal part of the ciliary axoneme; subtype 2, located in the distal part of the axoneme (Fliegauf et al., 2005) and subtype 3, located throughout the entire axoneme (Whitfield et al., 2019).

On the other hand, IDAs are smaller protein complexes mostly involved in the initiation of an asymmetric ciliary bending, controlling the amplitude and shape of microtubule movement, in order to create a distinct ciliary wave pattern (Kamiya et al., 1991; Yamamoto et al., 2021).

Before being incorporated into the axoneme, dynein arms are pre-assembled and stabilized in the cytoplasm by the chaperones and co-chaperones dynein axonemal assembly factors, and then transported to the cilium during ciliogenesis. ODAs need additionally an ODA docking complex that facilitates its binding to the microtubules (Owa et al., 2014).

Besides dyneins, motile cilia present linking components such as the nexin-dynein regulatory complex (N-DRC), the radial spokes and the central-pair projections. The N-DRC connects adjacent outer doublet microtubules to each other (Oda et al., 2013), whereas the radial spokes and the central pair-projections connect the outer doublet microtubules to the central pair microtubules (Goodenough & Heuser, 1985). Collectively, these structures not only modulate dynein motors spatial and temporal inhibition, but also regulate microtubules alignment and sliding activity, and consequently, the direction and propagation of ciliary movement .

The distribution of motility associated appendages throughout the ciliary axoneme is repeated every 96 nm and determined by the CCDC39 and CCDC40 molecular ruler complex. Moreover, this complex provides well-defined docking sites for individual IDAs along the repeat (Oda et al., 2014).

Overall, more than 400 proteins have been identified to be involved in motile cilia assembly, structure and function (Pazour et al., 2005; Blackburn et al., 2017). Such diversity can also be appreciated by the different movements that characterize each type of motile cilia.

In motile multiciliated cells, like the human respiratory epithelial cells, each cilium shows a two active parts planar motion, characterized by a power stroke and a recovery stroke (Figure 1.1 A) (reviewed by Satir et al., 2014). During the power stroke, the cilium moves perpendicular to the cell surface to generate fluid forward propulsion, while during the recovery stroke, the cilium bends and swings backwards more parallel to the cell surface, avoiding interference with the fluid transport. Hence, the two asymmetric strokes produce a unidirectional fluid flow. Whereas looking into these cilia within the tissue context, each cilium beats in a phase-shifted manner with its neighbors along the power stroke axis and in a synchronous manner with its neighbors in the perpendicular axis (Sanderson & Sleigh, 1981). This generates a metachronal wave that propels bulk mucus transport, also known as mucociliary clearance, without increasing the energetic burden on each cilium (Elgeti & Gompper, 2013).

On the other hand, in motile monociliated cells, as sperm, the flagella move in a periodic wave-like beat with a helical pattern, in order to propel a unidirectional swimming motion (Figure 1.1 B). This is achieved by a one-sided flagellar rolling stroke around the swimming axis coupled with a pulsating head spinning around the sperm's longitudinal axis, which rolls the sperm to beat equally on all sides (Gadêlha et al., 2021). Asymmetric and unilateral position of ion channels along the flagellum ensure fast signal transduction, ultimately regulating sperm waveform torsion (Miller et al., 2018)

Additionally, in monociliated LRO cells, cilia move in a circular motion (Figure 1.1 C and D) (Nonaka et al., 1998, 2005; Kramer-Zucker et al., 2005; Okada et al., 2005; Schweickert et

al., 2007). Interestingly, in the zebrafish LRO, although all cilia appear to have a normal motile "9 + 2" axonemal configuration showing a rotational movement (Kramer-Zucker et al., 2005; Tavares et al., 2017), some cilia randomly distributed around the organizer were described as "wobbling" due to its double ciliary beat frequency, and consequently, irregular movement pattern (Sampaio et al., 2014). On the contrary, in the mouse and medaka fish LROs, circular motion cilia have a "9 + 0" axonemal configuration with both outer and inner dyneins arms present (Nonaka et al., 1998; Takeda et al., 1999; Okada et al., 2005). Moreover, in the mouse LRO, cilia with a "9 + 2" ultrastructure were also seen, but in a much lower density and randomly distributed around the organizer (Caspary et al., 2007; Odate et al., 2016). Physiological significance for these scarce singular cilia with different ultrastructure, present both in zebrafish and in mice, has not been found so far.

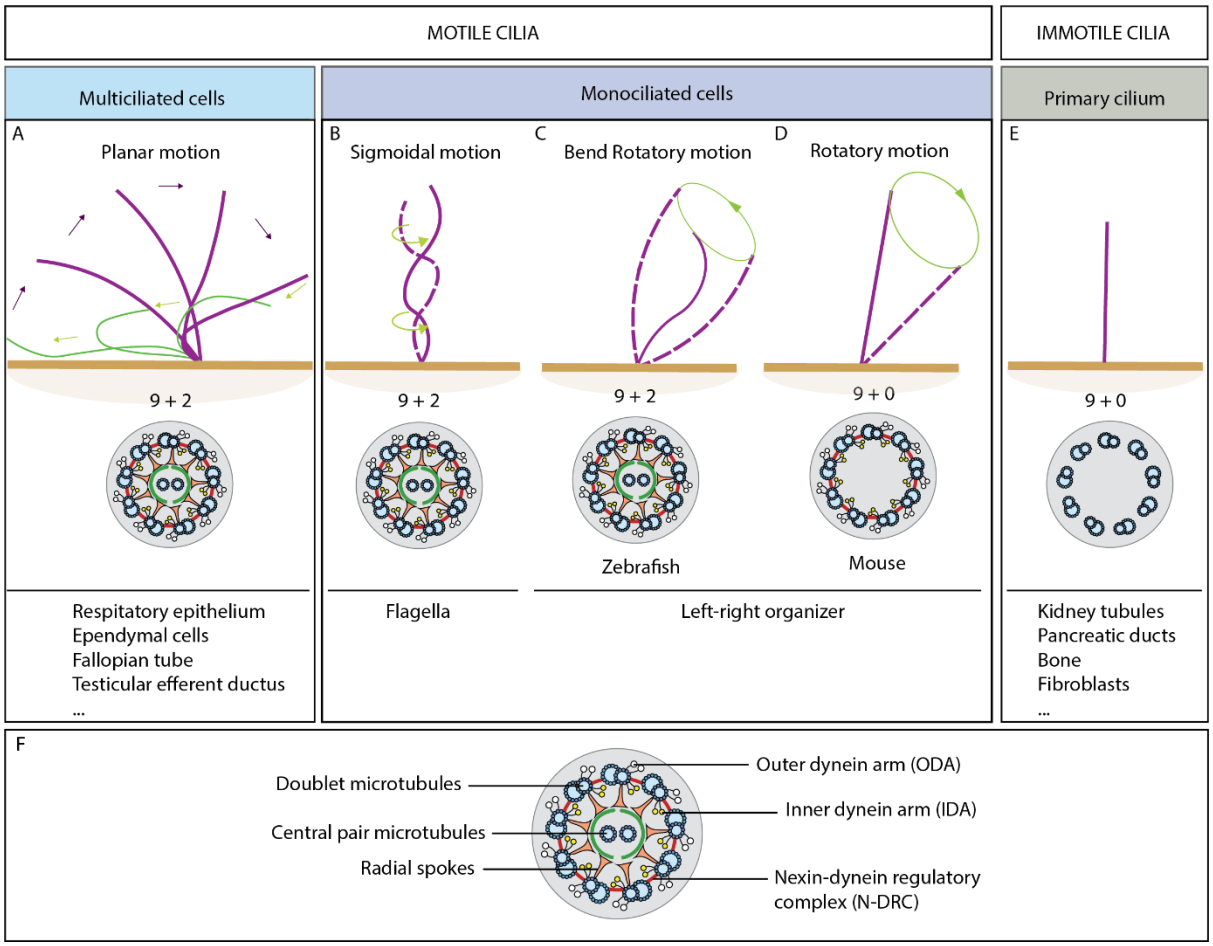

Figure 1.1: Cilia characterization.
Cilia can be classified into two main groups: the motile and the immotile cilia. (A) Representation of a single motile cilium from a multiciliated cell. Multiple cilia have a "9 + 2" ultrastructure pattern and a synchronized waveform motion, with an effective power stroke (purple arrows) and a recovery stroke (green arrows). These cilia are present in different tissues as the respiratory epithelium, ependymal cells from brain ventricles and both female and male reproductive tracts, in order to generate a directional fluid flow. (B) Representation of a single motile cilium or flagellum that protrudes from the spermatozoa. While having the same "9 + 2" ultrastructure pattern, this cilium has a sigmoidal motion that generates a propulsive force capable of moving the sperm through the medium. (C) Representation of single motile cilium with a bended and rotatory motion, present in the left-right organizer of the zebrafish embryo ("9 + 2" ultrastructure pattern). (D) Representation of single

motile cilium with a stiff rotatory motion, present in the left-right organizer of the mouse embryo ("9 + 0" ultrastructure pattern). Both LRO cilia rotate in a clockwise fashion when viewed from the apical side of the cell, in zebrafish, and from the ventral side, in mouse. (E) Representation of an immotile cilium with a "9 + 0" ultrastructure pattern that acts as primary or sensory cilia in multiple organs of the body. (F) Transversal view of cilia structure and main components. The ultrastructure pattern refers to the nine microtubule doublets and to the presence or absence of a central microtubule pair.

It should be noted that the circular motion is yet different between species. While zebrafish LRO cilia bend simultaneously with the rotatory movement (Sampaio et al., 2014; Pintado et al., 2017) (Figure 1.1 C), mouse cilia are stiffer, resulting in a straight conical movement (Okada et al., 2005).

Generally, LRO motile cilia are responsible for generating a transient fluid flow to initiate an asymmetric activation of a genetic cascade signaling that guides asymmetric morphogenesis of emerging internal organs. Besides rotational movement, cilia tilt and cilia length are crucial to produce the optimal directional fluid flow. Cilia rotate in a clockwise direction when viewed from the ventral side in the mouse LRO and from the apical side of cells in the zebrafish LRO (Nonaka et al., 2005; Okada et al., 2005; Okabe et al., 2008). This directional rotation is caused by a chiral asymmetry of microtubules and dynein arms arrangement within the cilium (Hilfinger & Julicher, 2008). Cilia tilt is given by the polarization of the basal body, that in response to non-canonical Wnt/planar cell polarity (PCP) signaling is gradually shifted towards the posterior side of the cell (reviewed by Shiratori & Hamada, 2006). Cilia length can also have a major impact on fluid flow production, by influencing the ciliary beat amplitude and, consequently ciliary beat frequency (Pintado et al., 2017). Several signaling pathways have been involved in cilia length control, such as FGF pathway (Neugebauer et al., 2009), Notch pathway (Lopes et al., 2010) and mTOR pathway (Yuan et al., 2011).

Therefore, motility-associated appendages increase cilia complexity, from motor-proteins assembly in the cytoplasm, proper chirality and spacing of motility unit along the cilium length (Figure 1.1 E), to the management of cilia length, apical polarization in the cell, beat frequency and movement pattern.

Regarding ciliary motility, experiments using isolated cilia from *Chlamydomonas* with detergent-removed ciliary membrane, showed motility re-activation in the presence of exogenous substrates and cofactors (nucleotides, ATP, metals) (Satir, 1980). Such molecules regulate specialized dyneins, ATP/ADP-generating enzymes (nucleoside diphosphate kinases), many phosphatases (PP1 and PP2) and kinases (PKA and PKC) and reduction/oxidation (redox) system associated proteins (Price & Sisson, 2019). These experiments revealed not only that the axoneme contains all components and macromolecules necessary for ciliary bending, but also that it can produce a behavioral

response to second messengers. Thus, uncoupling some ciliary motility triggers and further increasing the level of complexity of motile cilia regulation.

1.1.2. Cilia motility regulation

Although much progress has been made in the cilia field, the mechanisms underlying ciliary beating are still debatable. How spontaneous beating or changes in the cilia beat frequency and waveforms in response to signaling cascades occur are yet not well understood. These signaling pathways, in turn, can be activated by specific receptors located at the ciliary membrane or from elsewhere in the cell.

Cilia motility function relies on elevated levels of energy-demanding activity, fueled by the power released from ATP hydrolysis performed by the dyneins heavy chains along the entire axoneme. Since ATP consumption is proportional to cilia beat frequency, ATP supply must be efficiently delivered to sustain cilia intense activity and avoid cilia fatigue (Chen et al., 2015). Mitochondria are densely present in the apical surface of the cell in close proximity to the basal body, and subsequently to the ciliary axoneme (Pack et al., 1980). Thus, they are in a fine position to provide ATP to the cilium.

On the other hand, the major source of ATP in mammalian sperm cells is glycolysis. Several glycolytic enzymes and glucose transporters were found anchored around the flagellum axoneme and in the principal piece membrane, respectively. These molecules can incorporate glucose into the ciliary lumen and locally catabolize it into ATP, leading to the hyperactivation of motility necessary for sperm locomotion through the oviduct (Eddy et al., 2003).

Thus, intracellular ATP is sufficient to govern inherent and spontaneous ciliary beating, whereas ciliary beat frequency can be modulated by the second messenger cyclic adenosine monophosphate (cAMP), cyclic guanosine monophosphate (cGMP) and calcium (Ca^{2+}) (Ma et al., 2002).

Regarding the second messenger cAMP, the major sources are the adenylyl cyclases, that can be activated dependent or independently of increased concentrations of intracellular Ca^{2+}. Once produced, cAMP acts as a co-factor and activates the axonemal anchored protein kinase A (PKA) (Kultgen et al., 2002). The target of cAMP-dependent phosphorylation was first identified in the *Paramecium* ciliary axonemes, an ODA light chain p29. Functionally, phosphorylation of p29 mediates a switch from slow to the fast microtubule sliding velocity, increasing the ciliary beat frequency and therefore the swimming speed of *Paramecium*

(Hamasaki et al., 1991). An orthologous target of PKA was also found in mammalian airway cilia (Salathe et al., 1993).

On the other hand, the mechanism by which the cGMP signaling and cGMP-dependent protein kinase (PKG) regulates ciliary beat frequency remains unclear (Salathe, 2007).

Regarding the Ca^{2+} signaling, between different organisms, it has been involved in ciliary or flagellar waveform changes, rotation or reversal of ciliary or flagellar beating direction, beating arrest and beat frequency regulation (reviewed by Inaba, 2015). Studies from *Chlamydomonas* flagella showed several calcium binding proteins anchored to the axoneme. Some examples are ODA-DC3, a subunit of the ODA docking complex; LC4, an ODA light chain; centrin, a component of some inner-arm dyneins and calmodulin-binding proteins associated with radial spokes and central appendages. Once within the ciliary axoneme and depending on its concentration, calcium can bind to these calcium sensors and promote conformational changes in order to catalyze microtubule sliding and consequently increase beat frequency and/or change the waveform (reviewed by DiPetrillo & Smith, 2009).

In mammalians, however, changes in intraciliary Ca^{2+} are most frequently associated with changes in ciliary beat frequency, showing a linear relationship (Girard & Kennedy, 1986; Benedetto et al., 1991; Lansley et al., 1992; Schmid & Salathe, 2011).

Intraciliary calcium increase can occur through the release of calcium from intracellular stores, or it can be transported from the extracellular environment by ion channels present in the ciliary membrane. One example of such ion channels is CatSper, exclusively expressed in the principal piece of spermatozoa, this chemosensory calcium channel orchestrates capacitation, chemotaxis, hyperactivation and acrosome reaction. In turn, CatSper is pH-sensitive and sex hormone-sensitive (reviewed by Rahban & Nef, 2020).

The oviduct tract and airway epithelial cells also express calcium channels, such as the transient receptor potential cation channel subfamily V member 4 (TRP4) known to modulate ciliary beat frequency (Teilmann et al., 2005; Lorenzo et al., 2008), and the transient receptor potential family polycystin-2 (PKD2), to regulate ciliary motility (as proposed by Jain et al., 2012).

Besides concentration and spatial distribution, calcium signaling can also be triggered based on dynamic frequencies. Interestingly, for the previously mentioned calcium channels, calcium ion currents were found to be constitutively active in CatSper-expressed sperm cells (Kirichok et al., 2006), whereas Pkd2 channels were shown to produce consecutive calcium waves in order to induce a cellular response (Takao et al., 2013; Yuan et al., 2015; Mizuno et al., 2020).

Crosstalk between the three second messengers can also happen as, for instance, calcium signaling has been shown to regulate adenylyl cyclases and phosphodiesterases that in turn control cAMP production. Regarding what triggers these messengers to induce ciliary beat frequency variations, it includes extracellular ATP, acethylcholine (Lipson et al., 1997) and redox state changes (Price & Sisson, 2019). Additionally other signaling pathways have been described to completely abolish ciliary motility such as pH alterations (Sutto et al., 2004) and Notch signaling (Boskovski et al., 2013; Tavares et al., 2017).

pH balance plays an important role in organ homeostasis, by shaping the biochemical reactions that support cellular functions. The intracellular pH in most living cells is tightly buffered between 7.0 and 7.4, however airway epithelial cells have been shown to have a distinctive region of the cytoplasm, in the vicinity of ciliary membrane, prone to pH variations and largely controlled by extracellular pH (Lemberskiy-kuzin et al., 2008). Elevation of extracellular pH has little impact on cytoplasmic pH but lead to the alkalinization of the ciliary membrane and to a faster ciliary beating, whereas intracellular acidification attenuates ciliary movement (Clary-Meinesz et al., 1998; Sutto et al., 2004). It has been proposed that increased pH near cilia can alter calcium and calmodulin binding constants, facilitating its complex formation and thereby stimulating ciliary beating (Lemberskiy-kuzin et al., 2008).

Similarly, mammalian sperm cells are kept in a quiescent state at the epididymis lumen, a V-ATPase dependently acidic environment (Pietrement et al., 2006), whereas their optimal pH environment for motility is between 7.2 and 8.2, observed within the female genital tract (Zhou et al., 2015). The V-ATPase is a vacuolar proton (H^+) pump essential to maintain proper acidification of intracellular organelles, such as secretory granules, endosomes and lysosomes, and, when expressed at the apical membrane, establish acidification of extracellular compartments, such as the epididymis lumen (reviewed by Toei et al., 2010). When the sperm cells are transferred to an alkaline environment, it triggers the calcium channel Catsper, to increase calcium influx and consequently, inducing hyperactivated motility (Kirichok et al., 2006).

A known pathway involved in regulating motile and immotile cilia is Notch signaling (Boskovski et al., 2013; Tavares et al., 2017). Notch signaling is essentially composed by the following core proteins: the Notch ligands, Delta or Jagged, that are expressed on the signal-dispatching cell and Notch receptors expressed in the signal-receiving cell (Figure 1.2) (reviewed by Hori et al., 2013).

Notch ligands are transmembrane proteins with an extracellular domain required for Notch receptor binding. These proteins are ubiquitylated by E3 Neuralized and Mindbomb ligases, promoting its endocytosis, to either activate the ligand or regulate its accumulation at the cell

surface (reviewed by D'Souza et al., 2010). In addition, most ligands have a C-terminal PDZ motif that promotes interaction with scaffolding proteins in building functional protein complexes to facilitate signaling or determine protein localization (Pintar et al., 2007). Once at the plasma membrane, Notch ligands can bind to Notch receptors of adjacent cells.

Notch receptors, on the other hand, are composed of a Notch extracellular domain (NECD), required for ligand interaction; a regulatory region, which prevents access to the S2 cleavage site in the absence of ligand and a Notch intracellular domain (NICD), required for transcriptional activation of downstream targets (reviewed by Kopan & Ilagan, 2009). In addition, during synthesis and secretion, these proteins are subjected to the post-translational modifications, such as O-glycosylation, O-fucosylation and O-GlcNAc addition, which are crucial for proper Notch folding and activity (Rana & Haltiwanger, 2011). Upon ligand-receptor engagement, the signal-dispatching cell undergoes a second endocytosis event that generates a pulling force to expose the regulatory domain of Notch receptor. By this time, Notch receptor suffers a serie of proteolytic cleavages, first a S2 cleavage by ADAM metalloprotease and then a S3 cleavage by γ-secretase complex, to release from the membrane the NECD-ligand complex to the signal-sending cell and the NICD to the cytoplasm of the signal-receiving cell (reviewed by Seib & Klein, 2021).

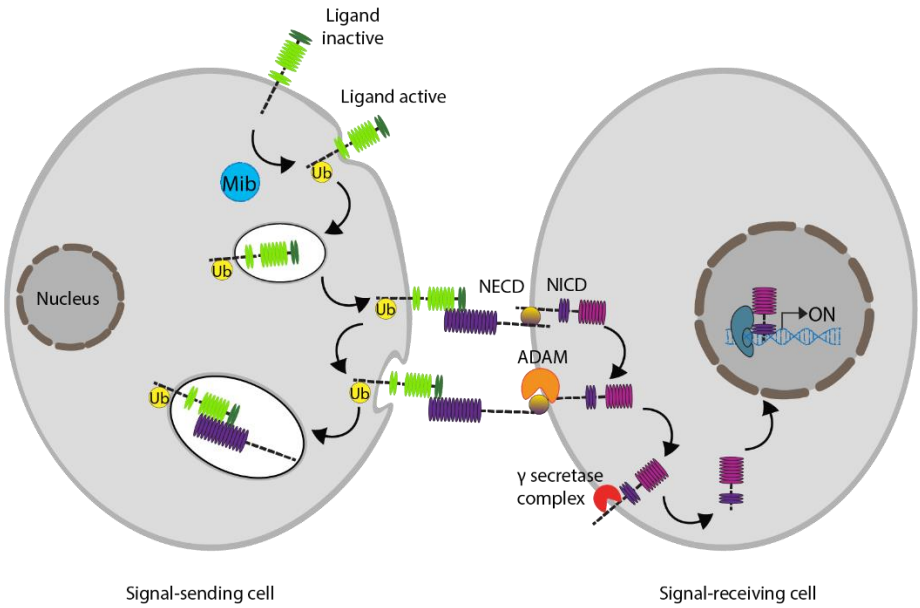

Figure 1.2: Schematic representation of Notch signaling pathway.
Signal-sending cells express Notch ligands (green) at the plasma membrane, which are activated dependent on ubiquitination (Ub) and endocytosis triggered by E3 Neuralized and Mindbomb (Mib, blue) ligases. Upon recycling to the plasma membrane, Notch ligands are now able to bind to Notch receptors (purple) located at the plasma membrane of signal-receiving cells. Ligand-receptor engagement allows a second endocytosis event, from the signal-sending cell, which generates a pulling force to expose the regulatory domain (brown) of Notch receptor, that is then cleaved by ADAM metalloprotease (orange) releasing the Notch extracellular domain (NECD). Notch receptor is further cleaved by the γ-secretase complex (red) releasing Notch intracellular domain (NICD) to the cytoplasm of the signal-receiving cell. NICD is translocated to the nucleus where it promotes gene expression of downstream targets.

The released NICD is translocated to the nucleus, where it forms a transcriptional complex with nuclear factors, such as the DNA-binding protein CSL (CBF/RBP in mammals, Suppressor of Hairless in *Drosophila* and LAG-1 in C. *elegans*), the co-activator Mastermind and others transcription activation mediators, to drive the expression of Notch downstream target genes (reviewed by Bray, 2006). Notch signaling and, therefore, its target genes, have been involved in a variety of developmental and physiological processes, such as cell-fate decisions, proliferation, apoptosis and cancer.

In *Xenopus* and zebrafish LRO ciliated cells, Notch signaling regulates the ratio of motile and immotile cilia without affecting the total cilia number. Upregulation of Notch signaling by overexpression of *Xenopus* and zebrafish *nicd* led to a decrease of motile cilia number, while downregulation of Notch signaling by using zebrafish *deltaD* mutants had the opposite effect (Boskovski et al., 2013; Tavares et al., 2017).

Furthermore, new genes are being discovered to have an effect on ciliary motility and beat frequency, such as *AGR3*, an endoplasmic reticulum disulfide isomerase (Bonser et al., 2015); *CFAP43*, a FOXJ1 downstream target (Rachev et al., 2020); and *PACRG*, which is regulated by a Parkinson's disease associated protein (Wilson et al., 2010). This will further help to uncover new mechanisms that regulate cilia motility and the implications of ciliary dysfunction on disease pathogenesis.

In this work I will further explore how regulation of motile – immotile cilia ratio, both in the embryonic LRO and the respiratory epithelium, links to primary ciliary dyskinesia syndrome.

1.2. PRIMARY CILIARY DYSKINESIA

Defects in motile cilia result in primary ciliary dyskinesia (PCD), a heterogenous ciliopathy mainly characterized phenotypically by chronic respiratory symptoms, associated with defects in laterality establishment of internal organs, fertility and brain development.

PCD was first reported in 1904 by AK Siewert, who associated bronchiectasis with *situs inversus totalis* (Siewert, 1903), a complete reversal of the internal organs condition, followed by Manes Kartagener that further included sinusitis in this syndrome (Kartagener, 1933). Years later, Afzelius found lack of dynein arms in sperm flagella and respiratory epithelial cilia from PCD patients, providing the first biological evidence of motile ciliary dysfunction as an etiology for PCD (Afzelius, 1976).

We now know that PCD is commonly an autosomal recessive hereditary disease, but X-chromosomal recessive inheritance (Vervoort et al., 2002; Budny et al., 2006; Paff et al., 2017) and *de novo* autosomal dominant mutations (Wallmeier et al., 2019) have also been described (reviewed by Horani et al., 2016). PCD incidence is estimated to be around 1:10 000 live births, however it is highly variable between countries and worldwide accepted as underreported since milder cases may not get diagnosed (Rubbo & Lucas, 2017).

PCD genes can be divided into three groups. The first group encompasses genes involved in ciliary axoneme structure, including ODAs, IDAs, microtubule inner proteins, N-DRC, central apparatus and radial spokes, that when mutated can lead to absence of each structural component or microtubule disorganization. The second group involves the cytoplasmic dynein axonemal assembly factors, responsible for pre-assembly and maturation of dynein arms, that when mutated can lead to the absence of both ODAs and IDAs. The third group comprises genes involved in multiciliogenesis, *MCIDAS*, *CCNO* and *FOXJ1*, where mutations in this type of genes lead to absence or reduced generation of multiple motile cilia. Altogether, mutations in nearly 50 different genes have been associated with PCD (Wallmeier et al., 2020).

Regarding the effect of such mutations in cilia morphology and function, a range of abnormalities have been described from reduced cilia number (Boon, Smits, et al., 2014) or shorter length (Chivukula et al., 2020), circular ciliary beating pattern (Stannard et al., 2004; Castleman et al., 2008) to hyperkinetic motion (Schwabe et al., 2008; Horani et al., 2013; Bustamante-marin et al., 2019) and partial or complete absence of ciliary beating (Raidt et al., 2014). Ultimately affecting cilia capability of driving effective fluid flow transport or sperm locomotion.

The impact of cilia motility dysfunction within the airway epithelium can be observed soon after birth, as 80% of PCD newborns have neonatal respiratory distress. Without proper mucociliary clearance, it is speculated that, during the transition from liquid to air breathing, newborns' distal airways are obstructed by mucus. This would explain the often-observed symptoms as decreased lung inflation and lobar collapse, and consequently respiratory distress with requirement to supplemental oxygen (Mullowney et al., 2014). From an early age, PCD patients develop wet and productive cough, recurrent nasal congestion, and chronic sinusitis. Recurrent bronchitis and pneumonia, due to opportunistic colonization of bacterial agents, ultimately lead to deterioration of lung function and obstructive lung disease, corrosion of lung structure and development of bronchiectasis. Additionally, recurrent ear infections and middle ear diffusion can also happen, increasing the chances of developing hearing loss and speech delay (Leigh et al., 2016).

In absence of effective treatment, PCD respiratory symptoms management relies on limiting lung disease progression through a healthy life-style, exercise and physiotherapy to stimulate cough and mucus clearance; endoscopic sinus surgery and broad-spectrum antibiotics to eradicate common respiratory pathogens. Lung transplantation is sometimes performed for end-stage respiratory failure. Therefore, PCD patients should be regularly followed up by specialists to access and monitor their pulmonary function (Lucas et al., 2014). Up to now, no drugs have been developed specifically to manage PCD, notwithstanding that a double-blind, randomized, placebo-controlled phase III clinical trial on the efficacy and safety of azithromycin maintenance therapy in PCD showed a high tolerability and a significant lower rate of respiratory exacerbations in the azithromycin-treated group (Kobbernagel et al., 2020).

Ciliary motility impairment in the human embryonic LRO leads to the randomization of internal organ position along the left – right axis. Therefore, 50% of PCD patients have normal organ placement, called *situs solitus*, while the other 50% have laterality defects. Furthermore, the majority of these defects, about 40%, are classified as *situs inversus totalis*, a complete mirror image arrangement, and the remaining cases, as *situs ambiguous*, the common name to summarize the broad spectrum of abnormal organ arrangements that can occur between *situs solitus* and *situs inversus* (Shapiro et al., 2014). Additionally, PCD patients can also have congenital heart disease (CHD). Although CHD could be found in every *situs* related group, abnormal *situs* was considered a risk factor for CHD (Kennedy et al., 2007; Best et al., 2019).

Even though, the majority of PCD genes have been associated with laterality defects, there are some exceptions, such as *CCNO* and *MCIDAS* (Boon, Wallmeier, et al., 2014; Wallmeier et al., 2014), which play a specific role in multiciliogenesis cells, or genes coding for central pair and radial spoke-related proteins (Olbrich et al., 2012; Knowles et al., 2014; Best et al., 2019), supporting the hypothesis that human LRO cilia have an axonemal “9 + 0” conformation.

Motile ciliary dysfunction can also affect male and female fertility. Sperm flagella and motile cilia are highly conserved, therefore PCD patients often show reduced or absent sperm motility and, consequently infertility. On the other hand, in cases where genetic conservation is not observed between the two organelles, PCD males with mutations on those genes can father children without assisted reproduction (reviewed by Sironen et al., 2020). Recently, it was found that motile cilia in the efferent ducts can also be responsible for male infertility even when sperm motility is normal (Aprea et al., 2021). Female infertility is thought to be caused by ciliary dysfunction of the fallopian tube in transporting the oocyte to the uterus (Halbert et al., 1997). Yet, recent studies have shown that 38.9% of PCD females had spontaneously conceived despite having seriously impaired ciliary motility (Raidt et al., 2015; Vanaken et al.,

2017). This advocates that PCD causes increased risk of subfertility, rather than complete infertility, and/or muscle contraction of fallopian tubes could compensate for the lack of ciliary motility.

Lastly, ciliary dysfunction can have an impact on brain development, by affecting motile ependymal cilia, and consequently lead to hydrocephalus. This phenomenon is more often reported for mutations affecting multiciliogenesis-related genes, such as *MCIDAS*, *CCNO* and *FOXJ1* (Boon, Wallmeier, et al., 2014; Amirav et al., 2016; Wallmeier et al., 2019).

1.2.1. PCD diagnosis

One of the major problems in PCD relies on diagnosing patients, and as soon as possible, in order to minimize their general morbidity (Kuehni et al., 2010; Sommer et al., 2011). Since PCD is a rare disease, it is not surprising that there is a widespread lack of awareness about the disease and lack of specialized diagnostic facilities with experienced technicians (Strippoli et al., 2012; Behan, Galvin, et al., 2016).

Additionally, as the most prevalent PCD symptoms are not specific, some patients may not even get a referral for testing. Although, the European respiratory society has developed a few recommendations on patient referrals (Barbato et al., 2009), PCD management is still highly variable within and between countries, mostly dependent on region, size of the center and the country's general government expenditure on health (Strippoli et al., 2012).

Different predictive tools were developed to further help clinicians determine the likelihood of a patient having PCD and consequently, refer them to a PCD center (Djakow et al., 2012; Behan, Dimitrov, et al., 2016; Leigh et al., 2016). These different questionnaires use medical data such as full-term pregnancy, neonatal respiratory distress, admission to neonatal intensive care unit, early-onset wet cough, early-onset rhinitis, laterality defects, congenital heart defects and chronic ear or hearing symptoms, to calculate a numeric score. The higher the score, the more likely a patient is to have PCD. Clinical index (CI) (Djakow et al., 2012), Primary CiliARy DyskinesiA Rule (PICADAR) (Behan, Dimitrov, et al., 2016) and North America criteria defined clinical features (NA-CDCF) (Leigh et al., 2016) are some examples of such tools that share similar sensitivity and specificity. Any of these tools can be implemented in health centers, being CI the easiest to establish since it does not require any specific examination, relying only on the patient's history (Martinů et al., 2021).

Regarding PCD diagnosis, there is no "gold standard" test. Therefore, European respiratory society recommends a combination of PCD-specific tests, including nasal nitric oxide (nNO)

measurements, transmission electron microscopy (TEM) assessment, high-speed video microscopy analysis (HVMA), immunofluorescence (IF) labeling and genetic screens, and an algorithm for diagnostic testing (Lucas et al., 2017; Dalrymple & Kenia, 2019). In addition, diagnostic PCD tests require high-priced sophisticated equipment and experienced clinicians and scientists to analyze and interpret results, thus diagnosis should only be performed in specialized centers.

nNO concentration, measured by sampling gas from one nostril, has been extensively used in PCD diagnosis. Although absolute values of nNO slightly fluctuate with the type of analyzer, sampling method and patient's age, they are consistently lower in PCD patients than in healthy individuals, by a yet unknown mechanism (Collins et al., 2014). nNO measurements should be performed in a chemiluminescence analyzer with velum closure maneuver, to avoid contamination by lower airway gases (Lucas et al., 2017). Nevertheless, tidal breathing procedures are widely accepted for young children that struggle to do proper velum closure (Marthin & Nielsen, 2013).

Noteworthy, while nNO measurements have a good sensitivity and specificity, around 10% of patients harboring mutations in specific PCD-associated genes show normal nNO levels (Marthin & Nielsen, 2011; Shapiro et al., 2020).

On the other hand, visualization of ciliary ultrastructure by TEM was once considered the "gold standard" diagnostic technique for PCD. TEM can be performed on nasal or bronchial brush biopsies ultrathin sectioned and cilia can then be visualized under a final magnification of x60 000 lens (Papon et al., 2010). Normally, more than 50 axonemes of individual cilia per patient should be analyzed for proper sample coverage (Shoemark et al., 2020).

Typical hallmarks of abnormal cilia include lack of ODAs; lack of simultaneously ODAs and IDAs; lack of IDAs with microtubular disorganization and lack, single or misplacement of central pair with microtubular transposition (Leigh et al., 2016). Having into account and excluding from analysis the secondary ciliary dyskinesia changes, as swollen ciliary membranes, extra-tubules, microtubular defects and compound cilia, that are caused by PCD distinct respiratory infections and inflammation (Dixon & Shoemark, 2017), typical abnormal ciliary ultrastructure depicted by TEM are 99% specifically related to PCD. However, different systematic reviews have reported that around 30% of PCD patients exhibit either no ultrastructure defects or subtle abnormalities that can be easily neglected (Boon, Smits, et al., 2014; Kouis et al., 2017). Intermittent defects can also be missed when insufficient numbers of cilia are analyzed (Lucas et al., 2017).

Another PCD diagnostic test relies on the direct assessment of ciliary function by high-speed video microscopy analysis (HVMA). Ciliated cells from nasal, or less used bronchial, brush

biopsies can be recorded at high-speed (from 120 to 500 frames per second) and then cilia movement can be analyzed in slow-motion replays and characterized by its ciliary beat frequency (CBF) and ciliary beat pattern (CBP) (Lucas et al., 2017). CBF is measured either manually through ciliary movement kymographs or automatically using fast Fourier transformed softwares, such as CiliarMove (Sampaio et al., 2021), whereas CBP is mostly assessed manually.

Particular CBFs have been linked to specific ultrastructural defects or genotypes. For instance, a complete ciliary immotility and a very reduced ciliary movement, with minimal residual beating phenotypes were observed in PCD patients with mutated-genes affecting both ODA/IDA and only ODAs, respectively. Increased CBFs, on the other hand, were found in *CCDC39* and *CCDC40* mutations, and in some *DNAH11* variants (Raidt et al., 2014).

Likewise, CBP has shown a high degree of genotype-phenotype correlation (Chilvers et al., 2003). Normally, the ciliary beat cycle is characterized by a strong beating stroke followed by a recovery stroke, whereas PCD patients have been described by harboring similar strokes, static cilia, stiff beating, flickering, reduced bending or reduced amplitude and some with abnormal circular motion. Quantification of each pattern proportion was shown to be particularly helpful in distinguishing ODA/IDA defects, ODA defects, IDA and microtubular disorganization defects, central pair defects and normal ultrastructure PCD groups (Blanchon et al., 2020).

Altogether, it was shown that HVMA has an excellent sensitivity and specificity by ones (Jackson et al., 2016), but the lack of standard methods, the variability among healthy individuals and the risk of observer bias, lead to CBF measurements not being recommended by others (Shapiro et al., 2016). For example, CBF and CBP change in a temperature-dependent manner (Reula et al., 2021), and different centers have reported ciliary function measurements either at 37ºC, 25ºC or room temperature (Chilvers et al., 2003; Raidt et al., 2014; Blanchon et al., 2020). This could be particularly challenging in generating comparable data. Moreover, it strengthens the necessity of each diagnostic center has a record of the CBF range for its own healthy control population.

Moving towards standardization, recently some recommendations have been proposed to further increase HVMA power in PCD diagnosis and, possibly, in other research areas (Dalrymple & Kenia, 2019; Kempeneers et al., 2019).

Of note, in cases of reduced generation of multiple cilia PCD, where the visualization of reduced numbers of motile respiratory cilia is conspicuous by TEM and HVMA, it is often mis-interpreted as poor quality sampling. Both TEM and HVMA accuracy can be improved by repeating the analysis on air-liquid interface cultures from biopsied cells (Lucas et al., 2017).

As epithelial cells regrow and differentiate in a sterile environment, not only secondary defects from respiratory infections or inflammation normalize but also PCD derived defects remain, including the reduced generation of multiple cilia PCD defects (Wallmeier et al., 2014).

Since 2005, immunofluorescence (IF) microscopy analysis has been applied to the PCD research field (Fliegauf et al., 2005), but validation studies to infer about the accuracy and limitations of this technique as a diagnostic tool are still a few.

Conceptually, the use of specific fluorescent tagged antibodies in the respiratory epithelial cells allows to detect and localize ciliary proteins, within the cell and along the length of the ciliary axoneme, by fluorescent or confocal microscopy. Absence or mis-localization of such proteins can confirm the diagnosis of PCD (Dougherty et al., 2016), but sometimes may reflect the downstream abnormalities, rather than the mutated protein (Dougherty et al., 2020).

A combined panel of antibodies against the ciliary proteins DNAH5 (an outer arm dynein), DNALI1 (an inner arm dynein), GAS8 (a nexin-link regulatory complex protein) and RSPH9 (a radial spoke component) was shown to be sufficient to identify ciliary defects in 88% of individuals suspected of having PCD. This panel covers the major ultrastructure defects and end products of multiple gene defects, but still missed 12% of PCD cases, that later after genotyping, revealed to be mutated-genes with normal ultrastructure by TEM (Shoemark et al., 2017).

Although at the time of this study, IF showed a similar accuracy as TEM, sensitivity will increase facing the growing number of validated antibodies and possible combinations. Recently, 21 commercially available antibodies were validated, including 10 against proteins whose defects in the ciliary ultrastructure cannot be easily recognized by TEM, and more await validation (Liu et al., 2020). In addition, IF analysis is less expensive and easier to implement on a diagnostic center, has a shorter time of sample processing and analyzing, and requires fewer ciliated cells to achieve a definitive result when compared with TEM (Shoemark et al., 2017). Thus, even IF analysis is not being recommended as a routinely PCD diagnostic test by European guidelines, it represents a good alternative to other tests, when these are not readily available (Lucas et al., 2017; Dalrymple & Kenia, 2019). On the other hand, IF analysis limitations stem from the observations that different pathogenic variants of the same gene can lead to the correct assembly of those proteins within the ciliary axoneme, showing a normal pattern by IF, and therefore resulting in false-negatives (Dougherty et al., 2016).

A confirmatory diagnosis can be given by a genetic test showing a homozygous or compound heterozygous mutations (autosomal recessive PCD), a heterozygous mutation (autosomal dominant FOXJ1 PCD) or a hemizygous mutation (X-linked PCD), previously reported as PCD-causing variants. However, even after sequencing all known PCD genes, a causative

mutation will not be found in 20 - 30% of individuals with clinical manifestations compatible with PCD (Marshall et al., 2015).

Nevertheless, the American thoracic society recommends the use of extended genetic panels for PCD diagnosis in patients with strong clinical phenotype (Shapiro et al., 2018). Genetic results can often be difficult to interpret due to the high number of variants of unknown significance, therefore detected mutations should be confirmed by Sanger sequencing, correlated with the phenotype assessed by any other PCD diagnostic test, and checked for parents' segregation (Lucas et al., 2017).

Latest advances in genetic approaches, such as in the whole-exome sequencing technique, have improved its technical complexity and time efficiency while it allows discovering new PCD-causing genes (Horani et al., 2012) and building data on candidate genes for further validation (Wheway et al., 2021).

In summary, although PCD tests showed high specificity and sensitivity, when performed one of these techniques alone, 10 to 30% of PCD cases will remain misdiagnosed (Jackson et al., 2016). Therefore, PCD patients require a disease-specific comprehensive multidisciplinary management approach and current recommendations accept a positive diagnosis based on a suggestive clinical background combined with at least two abnormal diagnostic results on the other PCD tests (Lucas et al., 2017).

Once reached a positive PCD diagnosis, patients should be counseled regarding the outcome of the diagnostic tests and further assessed to investigate comorbidities and complications of PCD, such as an in-depth ear, nose and throat examination, pulmonary function follow-up, fertility and genetic counseling, and *situs ambiguous* related clinical important defects inspection (Shapiro et al., 2016).

While situs inversus appearance is well understood in light of the ciliary dysfunction on the LRO cells during the embryonic development of PCD patients, *situs ambiguous* with complex congenital intracardiac defects is not fully understood and, particularly, how left – right patterning is integrated and translated by the developing cardiovascular system needs further elucidation (Shapiro et al., 2014).

1.3. LEFT-RIGHT AXIS ESTABLISHMENT

The embryonic development represents a long and carefully regulated journey for a zygote to achieve a fully differentiated embryo containing all structures and internal organs needed for adulthood survival and reproduction. Positioning of such structures and organs, like the heart, gut, liver and brain, within the body plan relies on progressive symmetry breaking events such as the establishment of the anterior – posterior (AP), dorsal – ventral (DV) and left – right (LR) axes, to ultimately build a functional system. In fact, abnormal LR patterning leads to laterality defects in 1:10 000 human births, apart from the laterality defects that arise in PCD patients (Lin et al., 2014).

The main orchestrator of the LR axis patterning is the Nodal pathway, a left-sided determinant, conserved across the entire deuterostome tree of life, from vertebrates to primitive chordates and echinoderms, and in some protostomes, like snails and slugs (Blum et al., 2014; Blum & Ott, 2018). Within vertebrates, Nodal signaling has been extensively studied in chick, mouse, *Xenopus* and zebrafish (Levin et al., 1995; Collignon et al., 1996; Lustig et al., 1996; Long et al., 2003).

The Nodal gene encodes a secreted growth factor belonging to the transforming growth factor beta (TGF-β) family, that is initially expressed bilaterally around the left-right organizer (LRO), together with its co-ligand growth/differentiation factor-1 (Gdf-1) (Rankin et al., 2000). Gdf-1 binds directly to Nodal, allowing its secretion through the left side of the lateral plate mesoderm (LPM) and increasing its long-range activity (Tanaka et al., 2007). On the other hand, DAN Domain BMP Antagonist family member 5 (Dand5), a secreted Nodal inhibitor, is also expressed around the LRO, more intensively on the right side, and prevents Nodal spreading to the right sided LPM (Marques et al., 2004). Dand5 is also highly conserved within vertebrates, being previously known as *Cerberus-like2 (Cerl-2)* in mouse (Marques et al., 2004), *charon* in zebrafish (Hashimoto et al., 2004) and *Coco* in *Xenopus* (Vonica & Brivanlou, 2007).

Therefore, activated Nodal signaling on the left side of LRO, but not on the right side, is able to induce its own transcription by a self-enhancement and lateral-inhibition (SELI) system (Nakamura et al., 2006), converting this small difference at the LRO into a robust asymmetry of Nodal expression at the left side of the LPM (Brennan et al., 2002; Saijoh et al., 2003).

To exert its function, Nodal binds to its co-factor Cryptic, that facilitates their interaction and further activation of a transmembrane complex composed of serine/threonine kinase type I (ALK4) and type II (ActRIIB) activin receptors (Yeo & Whitman, 2001; Sakuma et al., 2002). Phosphorylation of ALK4, by activated ActRIIB, results in Smad2 phosphorylation. Consequently, Smad2 forms nuclear complexes with Smad4 and members of the FAST family of forkhead domain transcription factors to activate the expression of target genes (reviewed by Schier & Shen, 2000).

Noteworthy, AtcRIIB receptor is widely expressed through the embryo (Oh & Li, 1997), whereas Gdf-1 and Cryptic are expressed at the mouse's LRO and symmetrically in the LPM (Shen et al., 1997; Rankin et al., 2000), this means that both sides of LPM are competent to respond and induce Nodal signaling. Indeed, in mice *Dand5* mutants, in the absence of its inhibitor on the LRO's right side, 50% of the embryos showed a bilateral expression of Nodal at the LPM (Marques et al., 2004).

Regarding Nodal downstream target genes at the LPM, it includes *Nodal* itself, *Lefty1, Lefty2* and *Pitx2* (Shiratori et al., 2001; Whitman, 2001). Lefty genes encode for secreted feedback looped Nodal inhibitors, that exert their functions by competing for the ability to bind the co-factor Cryptic and also by blocking Nodal interaction with activin receptors (Sakuma et al., 2002; Chen & Shen, 2004). *Lefty1* is expressed in the midline, preventing Nodal diffusion and expression on the right side of LPM (Meno et al., 1998), while *Lefty2* is expressed on the left-sided LPM, adjacently or overlapping Nodal expression domains, preventing extended expression of Nodal and, consequently, bilateral expression of *Pitx2* (Meno et al., 2001). Together, Nodal and Lefty comprise a reaction – diffusion system to restrict the range and duration of Nodal signaling in the developing embryo (Müller et al., 2012). By the time that *Nodal* transient expression on the left side of LPM stops, homeobox transcription factor *Pitx2* expression persists and, later on, is localized to the left side of the primordial organs (Shiratori et al., 2001).

In summary, Nodal cascade signaling pathway plays a critical role in symmetry breaking of the LR axis. Interestingly, having symmetric signals that overall result in either bilateral expression or complete absence of Nodal in the LPM will give rise to different laterality defects. This happens because being a left-sided determinant means that cells that receive Nodal signals will adopt left-side morphology, whereas those that do not receive Nodal signals will adopt right-side morphology. Conversely, conditions where Nodal is bilaterally expressed in the LPM, such as in *Lefty1* and *Dand5* mutants, mice develop left pulmonary isomerism, meaning two left-side characterized lungs (mono-lobed lungs in mice) (Meno et al., 1998; Marques et al., 2004); whereas conditions lacking Nodal signaling in the LPM, such as in *Cryptic* and *ActIIB* mutants, mice develop right pulmonary isomerism, meaning two right-side characterized lungs (four-lobed lungs in mice) (Oh & Li, 1997; Yan et al., 1999), besides other laterality defects.

In humans, mutations in these genes have also been described, associated with LR laterality defects, such as in *LEFTY A* and *LEFTY B* (Kosaki et al., 1999), *CFC1 (CRYPTIC)* (Bamford et al., 2000), *GDF1* (Jin et al., 2017), *PITX2* (Franco et al., 2017), *DAND5* (Cristo et al., 2017), *NODAL, ACVR2B* and *SMAD2* (Li et al., 2019). However, mutations in Nodal signaling only account for 3% of all patients with isolated *situs ambiguous*. This could be explained by LR patterning being a very robust system in humans and maybe additional pathways playing a role in close interaction with Nodal signaling, or most Nodal signaling mutations may cause lethal developmental defects. This last hypothesis is supported by the other roles of Nodal signaling during embryonic development of vertebrates in AP axis patterning and positioning, neural tube formation and mesoderm induction (Schier & Shen, 2000; Whitman, 2001).

Nevertheless, human genotype – phenotype correlation reinforces the importance of Nodal cascade signaling the LR axis establishment and its conservation across vertebrates.

Next, I will describe the early processes of symmetry breaking, prior to Nodal signaling, in mouse and zebrafish embryos separately, as clear differences will appear between the two animal models.

1.3.1. Early left-right symmetry breaking events in the mouse embryo

While the first reports of human cases having *situs inversus* date back to 17-18th century (Baillie, 1789) and the first etiology theories were raised around the fetus turning direction regarding the umbilical cord (Cleveland, 1926), it was only in 1976, with Afzelius correlating the absence of ciliary dynein arms with *situs inversus* in PCD patients, that the first description of, a yet to discover, embryonic left-right organizer (LRO) harboring motile cilia was made (Afzelius, 1976).

Nearly 20 years later, Sulik published the first extensive study on the development of the LRO, the node in mouse, unaware of its function (Sulik et al., 1994). The node is a transient organ that is fully formed around the late bud (LB) stage and the early headfold (EHF) stage, located between the anterior notochord and the primitive streak in the ventral midline of the embryo (Sulik et al., 1994). It is composed by approximately 250 columnar epithelial cells, referred to as the pit cells, displaced in a cup and concave arrangement elongated along the AP axis, where each cell exhibits a single motile cilium on their apical surface (Sulik et al., 1994; Nonaka et al., 1998; Yamanaka et al., 2007). On the other hand, surrounding the node in a horseshoe-shaped ring, the majority of cells, referred to as the crown cells, harbors a single immotile cilium (Bellomo et al., 1996; Lee & Anderson, 2008). On its ventral surface, the node is covered by the Reichert's membrane, producing a small and contained extraembryonic liquid-filled space.

By the same time that *Nodal* was identified in mice (Zhou et al., 1994) and found to be asymmetrically expressed at the node and at the LPM (Collignon et al., 1996; Lowe et al., 1996), *Lefty2* was found asymmetrically expressed at the LPM (Meno et al., 1998).

As pieces of the LR patterning puzzle were being put together, several mouse mutants led to major contributions by showing experimentally the link between ciliary motility and LR patterning.

The *situs inversus viscerum (iv/iv)* mouse mutant was known to have a 50% incidence of *situs inversus* (Hummel & Chapman, 1956; Layton, 1976). These mice harbor a single mutation on the *left/right dynein* gene, *Lrd*, currently known as *dynein axonemal heavy chain 11 (Dnah11),* that normally is expressed at the pit cells of the node and, at adulthood, in other ciliated tissues (Supp et al., 1997; McGrath et al., 2003). It was then shown that this mutation led to a complete absence of ciliary motility and consequently, lack of nodal flow and mis-expression of *Lefty2* at the right side of LPM in 50% of the embryos, which correlated with the *situs inversus* phenotype (Meno et al., 1996; Okada et al., 1999). A targeted deletion of the ATP binding domain necessary for the motor function of *Lrd/Dnah11* was used to confirm the *iv* mutant results by showing similar phenotypes (Supp et al., 1999).

As for the *inversion of embryonic turning (inv/inv)* mouse mutant, that have a partial deletion of *Inversin* gene, it was found to develop *situs inversus* in all homozygous mutants (Yokoyama et al., 1993; Mochizuki et al., 1998; Morgan et al., 1998). This mutation resulted in a complete or partial absence of motility in half of nodal cilia and therefore, a much slower and disorganized fluid flow and, later on, in a complete reversal of *Nodal* and *Lefty2* expression patterns at the LPM (Collignon et al., 1996; Lowe et al., 1996; Meno et al., 1996; Okada et al., 1999, 2005). Moreover, *inv* mutants showed a deformed node's structure and 20% of cilia tilted incorrectly towards the anterior side, meaning that the phase and directionality of the effective stroke were reversed, advocating for the importance of LRO shape and cilia

polarization to develop a proper flow (Okada et al., 1999, 2005). Later on, some phenotypic variability was found across different *inv* mutants, depending on the mice strain background (Oki et al., 2009).

On the other hand, *Kif3A* and *Kif3B* mouse mutants showed either bilateral or absent expression of *Lefty2* at the LPM and, later on, a randomization of the LR position of the heart (Nonaka et al., 1998; Takeda et al., 1999). Kif3A and Kif3B are two molecular microtubule-dependent motors of the intraflagellar transport (IFT) system, that act as a complex, to promote flagellar and ciliary assembly and structure maintenance (Morris & Scholey, 1997; Cole et al., 1998). Indeed, Kif3A and Kif3B proteins were localized along the axoneme of nodal cilia and mutations on those led to a complete absence of mature cilia and, consequently, a lack of nodal flow (Nonaka et al., 1998; Takeda et al., 1999). Furthermore, these authors described that the leftward nodal flow was generated not only by ciliary motility but also by a clockwise beat pattern combined with a posteriorly tilt of nodal cilia (Nonaka et al., 1998, 2005). Ciliary tilt towards the posterior side ensures that the rightward recovery stroke passes closest to the surface, where it is more difficult to move fluid due to the cell surface resistance that retards the movement of the fluid and the cilium itself. Hence, avoiding a counterproductive rightward flow near the surface and increasing effectiveness of the leftward power stroke (Cartwright et al., 2004; Nonaka et al., 2005; Okada et al., 2005).

Thus, the observations taken from the *iv* and *inv* mouse mutants suggested that a normal nodal fluid flow is necessary for the correct expression pattern of the asymmetric gene cassette and the LR patterning and, by adding the observations from *Kif3A* and *Kif3B* mouse mutants, reinforced the importance of cilia in generating that optimal leftward fluid flow.

Lastly, mouse embryos at pre-somitic stages were cultured in a flow chamber and their membrane-removed nodes were exposed to a peristaltic pump-driven fluid. By applying an artificial fluid flow, Nonaka and colleagues showed that a rightward flow led to the reversal of the *Pitx2* expression pattern and, consequently, to the reversal of heart position. Moreover, leftward artificial flow was sufficient to rescue the laterality defects of *iv* mutants, which have immotile cilia (Nonaka et al., 2002). This work elegantly demonstrated that the leftward fluid flow is not only necessary but also sufficient to trigger the symmetry breaking for the correct placement of visceral organs in the developing embryo.

Studies of nodal flow dynamics showed that initially the leftward fluid flow is weak and locally generated in the node, at the early headfold stage, and then the net velocity increases until the flow becomes fully developed with a maximal global leftward directionality across the entire node, at 2 somite stage (ss) (Okada et al., 1999; Shinohara et al., 2012). This is most likely due to the gradual increase of motile cilia within the node cells, at the expense of immotile cilia (Yoshiba et al., 2012). Surprisingly and despite flow velocity increase, by using different concentrations of a nontoxic viscous methylcellulose to manipulate flow velocity, it was shown that the early and weak leftward fluid flow is enough to break the LR symmetry (Shinohara et al., 2012).

As for the mechanism by which the LRO cells are able to perceive the weak fluid flow directionality and transduce it into gene expression changes, it would remain debatable for many years.

1.3.2. Hypothesis for the symmetry breaking: Chemosensing or Mechanosensing

The first hypothesis for the determination of LR asymmetry came from Hirokawa's group, upon showing that the node of wild-type mouse embryos had a directional nodal flow towards the left side capable of propel fluorescent latex beads. They proposed that an unknown factor was secreted to the embryonic node where it was transported by the fluid flow and became concentrated on the left side of the node. This hypothesized gradient would allow more molecules of such a factor to bind to its receptors on the left side, reaching a threshold for the activation of the downstream cascade signaling (Nonaka et al., 1998; Takeda et al., 1999). Furthermore, by showing that in *iv* and *inv* mouse mutants, *Lefty2* expression starts one somite later, they proposed that in the perturbed nodal flow scenario, symmetry breaking was delayed due to a slower accumulation of the morphogen (Okada et al., 1999). At this point, as Sonic hedgehog (Shh), a molecule involved in short- and long-range interactions, was found to be required for LR determination in chick's node (Levin et al., 1995, 1997), Hirokawa's group wondered if Shh role could be conserved in mammalian embryos (Okada et al., 1999; Takeda et al., 1999).

Only in 2005, new contributions were made to this morphogen model by Tanaka's work revealing that fibroblast growth factor (FGF) signaling was able to promote the release of small extracellular vesicles, called nodal vesicular parcels (NVP), carrying Shh and retinoic acid (RA). By time-lapse microscopy, they imaged membranous NVPs protruding from the microvilli of all regions of the ventral node, being carried by nodal leftward current and then fragmented by cilia on the left side of the node. Cracking NVPs would release its content near the apical membrane of the crown immotile ciliated cells and consequently trigger an intracellular calcium wave from the node towards the LPM. Moreover, they observed more NVPs in *Kif3A* mutants that do not have cilia, reinforcing the role of cilia in facilitating the fragmentation of NVPs (Tanaka et al., 2005) (Figure 1.3 A).

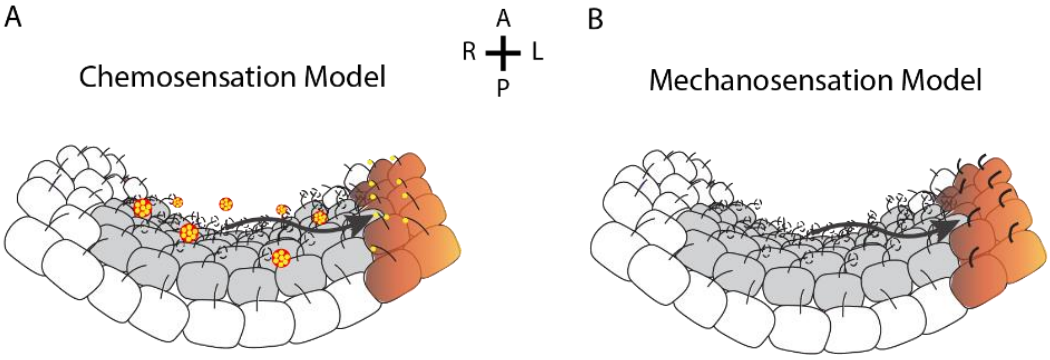

Figure 1.3: Current models for the initial LR asymmetry breaking in the mouse node.
(A) Chemosensation model is based on the morphogen-containing vesicle hypothesis proposed by Tanaka et al, after they observed nodal vesicular parcels (NVP, red) being transported by the fluid flow towards the left side of the node. Upon hitting the cilia or the cell wall, NVP would release its content (yellow) triggering an asymmetric calcium wave on the left node crown cells (brown). (B) Mechanosensation model is based on the "two cilia" hypothesis and proposes that the immotile cilia of crown cells are able to sense the fluid flow generated by the motile cilia in the pit cells. The leftwards flow would bend the immotile cilia from the left side of the node, triggering an increase of calcium signal (highlighted in brown) in a *Pkd2*-dependent mechanism.
A, anterior. P, posterior. L, left. R, right.

Further mathematical modeling supports that both morphogens and NVPs released in a symmetric fashion into the cavity of the node would lead to a concentration gradient, with more particles on the left side, while assuming that the morphogen or NVPs are rapidly degraded or inactive after its release to avoid diffusion-induced uniform distribution throughout the node (Cartwright et al., 2004, 2007; Gallagher & Smith, 2020).

However, simulations regarding NVPs rupture upon impact with cilia or with the cell surface found that it was impossible to occur, due to biophysical properties, namely viscosity, of the nodal fluid (Cartwright et al., 2007). Additionally, visualization of NVPs has not been replicated and further genetic analysis of *Shh* and *RA* mutants did not provide convincing support of their roles as nodal flow morphogens (Zhang et al., 2001; Vermot & Pourquié, 2005).

On the other hand, before proposing the morphogen model, Okada and colleagues first considered that the flow itself could physically induce a mechanical response in crown cells (Okada et al., 1999). But it took a few years until a model based on ciliary mechanosensation for the initiation of LR asymmetry appeared (Figure 1.3 B).

The major evidence for the mechanosensory function of cilia came from the *Pkd2* mouse mutant, that had autosomal polycystic kidney disease and laterality defects, including randomization of organ arrangement, with right pulmonary isomerism in most embryos, absence of *Nodal* and *Lefty2* expression at the LPM and abnormal expression pattern of *Pitx2* (Wu et al., 2000; Pennekamp et al., 2002). Thus, suggesting that *Pkd2* would have a role upstream of the Nodal cascade signaling.

Following on kidney studies, PKD2, polycystin-2, was shown to function as a monovalent cation-selective channel (transient receptor potential polycystic channel, TRPP2) with high permeability to calcium and to interact with PKD1, polycystin-1, a putative mechanosensory receptor (Hanaoka et al., 2000; González-Perrett et al., 2001; Retailleau & Duprat, 2014). The PKD1-PKD2 complex, localized at the kidney primary cilia, is responsible for detecting variations in the urine flow that are then transduced into the activation of PKD2 and consequently, into an increase of intracellular calcium (Pazour et al., 2002; Nauli et al., 2003, 2006). Additionally, intracellular calcium waves were observed upon micropipette-driven bending of renal cilia (Praetorius & Spring, 2001), supporting the role of cilia as a flow sensor and the role of PKD1-PKD2 complex as a flow mechanotransducer.

Whereas on LR field, Pkd2 was found to be ubiquitously localized, including in every nodal cell and its cilium, in contrast to Lrd/Dnah11 that was present only in a centrally located subset of cilia from the node, in the pit cells. By video microscopy analysis, presence and absence of Lrd/Dnah11 was correlated with motile and immotile cilia in mice. These two types of cilia were then proposed to have distinct roles in LR initiation: motile cilia from the pit cells would be

responsible for generating the asymmetrical nodal flow and immotile cilia from the peripheral crown cells would have the sensory function of perceiving that flow. This was called the 'two-cilia model' (McGrath et al., 2003). Consistent with this hypothesis, calcium transients were observed at the left margin of the node and sometimes at a wider region of the left sided endoderm. Asymmetric perinodal calcium signal was absent in *Lrd*/*Dnah11* and *Pkd2* mouse mutants, supporting that those motile cilia were necessary to generate the leftward fluid flow, which in turn was being sensed by Pkd2, leading into an increase in intracellular calcium on the left side of the node (McGrath et al., 2003; Tabin & Vogan, 2003).

Evidence for immotile cilia responsiveness to the fluid flow came from Yoshiba's work, who elegantly showed, by restoring cilia formation specifically in the crown cells of an overall lacking cilia *Kif3A* mouse mutant, that embryos were able to respond to artificial fluid flow, based on *Pitx2* expression pattern (Yoshiba et al., 2012).

Further analysis of *Pkd2* mouse mutant also showed that re-introduction of *Pkd2* wild-type gene expression in the crown cells, and more specifically a *Pkd2* variant capable to localize to the cilium were able to rescue the left sided expression of *Nodal* and *Pitx2*, whereas re-introduction of *Pkd2* expression in the pit cells or a *Pkd2* variant incapable to localize to the cilium when expressed in crown cells were both inept of restoring the Nodal cascade signaling. Thus, confirming that the role of immotile cilia from mice crown cells in the LR determination is dependent on *Pkd2* localization within those cilia (Yoshiba et al., 2012).

Unexpectedly, *Pkd1* mouse mutants develop progressive polycystic kidney disease but do not show any laterality defects, which later correlated with its absence from the node (Wu et al., 2000; Karcher et al., 2005), raising the hypothesis that *Pkd2* could have another partner in the LRO. In fact, the *Pkd1* paralogue, *polycystic kidney disease 1-like 1 (Pkd1l1),* was found to be expressed in nodal cells and to physically interact with Pkd2 (Field et al., 2011). Moreover, *Pkd1l1* mouse mutants, whose node's structure, cilia morphology and motility were comparable to controls, showed a reliably absence of symmetry breaking processes, including symmetric expression of *Dand5* and *Nodal* at the node and absence of *Nodal*, *Lefty2* and *Pitx2* at the LPM and *Lefty1* at the midline. *Pkd1l1* mutants did not exhibit kidney developmental defects, consistent with polycystic kidney disease, thus supporting a role of Pkd1l1 as Pkd2 partner restricted to the LR axis establishment (Field et al., 2011; Grimes et al., 2016). Similar results were observed in *pkd1l1* medaka fish mutants (Kamura et al., 2011), arguing for a conserved role across vertebrates. Of note, *PKD1L1* mutations have also been found in humans associated with laterality defects and congenital heart malformations (Vetrini et al., 2016; Antony et al., 2022).

The role of Pkd1l1-Pkd2 complexes at the LRO suggests that cilia function as mechanosensors of the leftward fluid flow. However, analysis of fluid flow strength suggests that it is too weak to efficiently deflect cilia and activate the polycystic complex, while flow directionality is perceived equally in both sides of the node, as cilia from the right and the left side will experience a similar flow emerging from the right side, causing a deflection towards the left. Thus, considering that the mechanical property of the flow that triggers LR asymmetry initiation is yet missing, both morphogen and 'two-cilia' hypotheses remain open (Omori et al., 2018; Gallagher & Smith, 2020).

1.3.3. Left-right genetic signaling cascade

Independently of the role of the fluid flow at the LRO, either as being a mechanical force inducer or a chemical signal transporter, it remains as the first LR asymmetric phenomenon in the developing embryo. Prior to that, both sides of the embryo had developed equally, including within the node.

About the early headfold stage, as the node is fully formed and cilia start to beat, *Nodal* and *Dand5* are expressed symmetrically in a horse-shoe shaped pattern around the mouse node. Additionally, *Nodal* begins to be expressed at the left side of the LPM, around 4 ss, and progressively increases its expression pattern towards the anterior side until 8 ss, in contrast to *Dand5* expression, which is restricted to the node (Collignon et al., 1996; Lowe et al., 1996; Marques et al., 2004). Additionally, it was shown that, at the node, these gene expression patterns undergo some changes, whereas *Dand5* is downregulated on the left side and becomes strongly expressed on the right side, at the late headfold stage, subsequently and in an opposite trend, *Nodal* becomes strongly expressed on the left side of the mouse node, at 2 ss (Marques et al., 2004; Kawasumi et al., 2011). Since Dand5 belongs to a family of secreted inhibitors of TGF-β proteins, it has been suggested that it antagonizes Nodal activity on the right side of the node, to prevent additional Nodal cascade signaling activation on the right side of the LPM. In fact, several pieces of data seem to corroborate this hypothesis.

First, analysis of *Dand5* mouse mutants revealed that 50% of the embryos had bilateral expression of *Nodal* at the LPM and, consequently, bilateral expression of its downstream target genes *Lefty2* and *Pitx2* at the LPM, whereas *Lefty1* expression at the midline remain unchanged. Moreover, 10% of the embryos showed a right sided expression pattern of *Nodal*, *Lefty2* and *Pitx2* on the LPM. This fairly correlates with the 60% of mutant animals that showed either left pulmonary isomerism, thoracic *situs inversus*, *situs ambiguous* of the abdominal organs and cardiovascular malformations. Moreover, removal of one copy of *Nodal* from these

mutants, *Dand5*$^{-/-}$;*Nodal*$^{+/-}$ mice, alleviated the number of embryos with laterality defects, when comparing with their siblings *Dand5*$^{-/-}$;*Nodal*$^{+/+}$ (Marques et al., 2004).

Second, analysis of *Pkd2* mouse mutants showed that the expression pattern of *Dand5* was predominantly symmetric around the node and *Nodal* expression was absent from the LPM (Pennekamp et al., 2002; Yoshiba et al., 2012). Whereas in *Pkd2*$^{-/-}$;*Dand5*$^{-/-}$ double mutants, *Nodal* is no longer repressed by its inhibitor and the expression pattern becomes randomized at the LPM, a phenotype partially resembling *Dand5* mutants (Yoshiba et al., 2012).

Lastly, co-injections of mouse *Nodal* and *Dand5* mRNAs into the animal pole of *Xenopus* embryos showed a complete blockage of Nodal downstream targets expression, which was bypassed when a constitutively active form of a Nodal receptor was added (Marques et al., 2004). Collectively, these studies argue that Dand5 truly antagonizes Nodal, most likely by physical binding in the extracellular space.

The data from *Pkd2* mouse mutants also suggests that *Dand5* is the downstream target of Pkd2-dependent calcium signaling (Yoshiba et al., 2012). In fact, calcium oscillations were observed first symmetrically distributed around the node at the early headfold stage and then, at higher frequencies on the left side of the peripheral node from late headfold stage onwards. In *Pkd2* mutants, calcium signals were overall reduced and symmetrically around the node (Takao et al., 2013). The presence of calcium signals oscillating at early stages suggests that not only calcium distribution but also calcium frequencies may be important for the LR asymmetry breaking. However, the molecular mechanism by which calcium signaling leads to the degradation of *Dand5* mRNA remains unclear.

On the other hand, manipulations of *Dand5* mRNA sequence had revealed that its flow-dependent downregulation is determined post-transcriptionally through its three prime untranslated region (3'-UTR). After *Dand5* degradation is triggered by the leftward fluid flow, an inhibitory feedback loop with *Wnt3a*, which is asymmetrically expressed on the left side of the node, further decreases *Dand5* on that side, in order to sustain the LR asymmetries (Nakamura et al., 2012). Moreover, *Wnt3a, Dand5, Nodal* and *Gdf-1* expressions were abolished from the node upon inhibiting Notch signaling, suggesting that this pathway induces a synchronized expression of the LR asymmetry related genes as a set (Krebs et al., 2003; Raya et al., 2003; Kitajima et al., 2013).

In summary, *Wnt3a, Dand5, Nodal, Gdf-1* and *Pkd2* are firstly symmetrically expressed around the embryonic mouse node (Figure 1.4 A). Cilia start to move generating a leftward fluid flow, that by a mechano or a chemosensory mechanism, is necessary and sufficient to trigger a Pkd2-dependent calcium signal on the left side of the node. This signal, by a yet uncovered mechanism, will trigger a left-sided *Dand5* mRNA degradation, further sustained by Wnt3a

(Figure 1.4 B). Downregulation of the Nodal antagonist allows increased Nodal activation of phosphorylated Smad2 on the left side of the node and subsequent induction of the Nodal cassette signaling genes on the left side of the LPM (Figure 1.4 C and D). On the right side of the node, Dand5 continuously inhibits Nodal, to maintain these LR asymmetries (Figure 1.4 B, C and D).

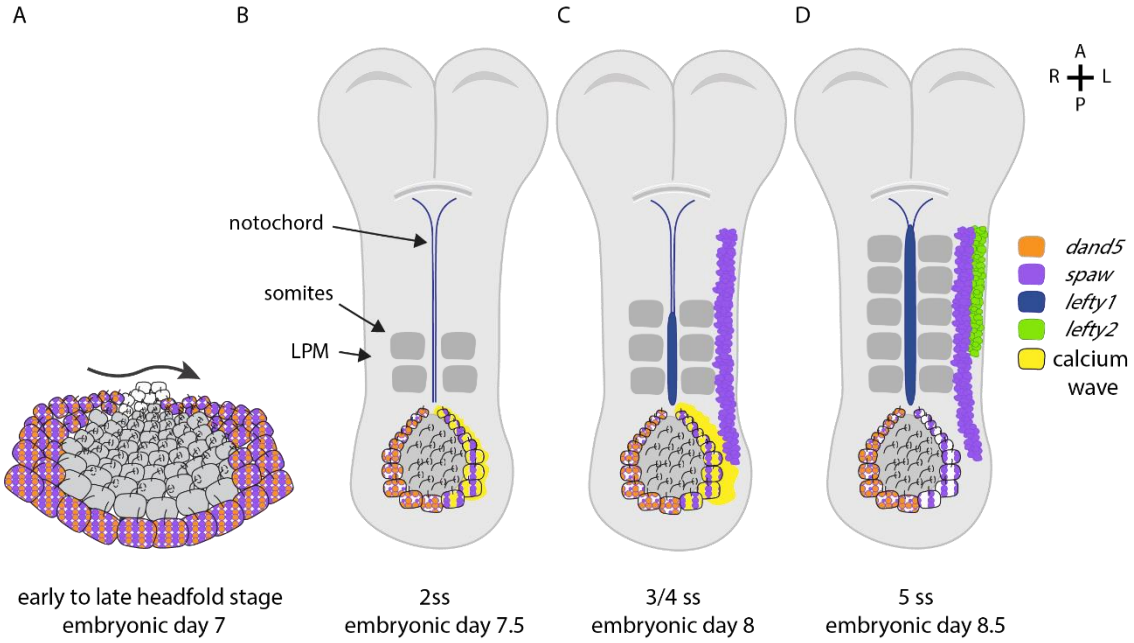

Figure 1.4: Left-right patterning in the mouse embryo.
(A) The mouse node has a ventral cup shape composed by pit cells at the center (grey cells) harboring motile cilia and by the crown cells (colored cells) that have immotile cilia. Crown cells express both *Dand5* and *Nodal* transcripts symmetrically around the node. Motile cilia generate a leftward fluid flow that reaches its maximal velocity at 2-3 ss. (B) By 2ss, fluid flow has triggered a calcium wave on the left side of node, ultimately leading to the degradation of *Dand5* transcripts. (C) In the absence of its inhibitor, *Dand5*, Nodal activates its own transcription on the left side of the lateral plate mesoderm and its antagonist *Lefty1* in the notochord. Such a midline barrier prevents Nodal to travel to the right side of the embryo and induce its own expression in the right lateral plate mesoderm. (D) By 5 ss, Nodal propagated through lateral plate mesoderm towards the anterior pole of the embryo, concomitantly with *Lefty2* expression activation in the left sided lateral plate mesoderm. *Nodal* and *Lefty1* expressions are robustly expressed until 6 ss. Ss: somite stage. LPM: lateral plate mesoderm. A: anterior. P: posterior. L: left. R: right.

1.3.4. Left-right axis establishment in the zebrafish embryo

The first phenomenon associated with the LR axis establishment in the zebrafish embryo is a hydrogen/potassium flux at the cleavage stages. Although symmetrically distributed, inhibition of H^+/K^+-ATPase proton pump led to the randomization of *nodal* and *pitx2* expression pattern at the LPM, without affecting LRO cilia distribution or size, nor fluid flow (Kawakami et al.,

2005). Similar roles for H^+/K^+-ATPase pump were seen in other vertebrates, such as chick and *Xenopus*, associated with a potential activation of Notch signaling and subsequently *Nodal* expression in the LRO (Levin et al., 2002; Raya et al., 2004; Hibino et al., 2006), however the underlying mechanism in zebrafish is poorly understood.

It is understandable, nevertheless, that defects in the development of a proper LRO and in the setting of the necessary symmetric expression pattern of the LR related genes will have similar faulty laterality phenotypes as the ones caused by defects occurring after the LR asymmetry is established, for instance, in the Nodal cascade signaling.

In zebrafish, the embryonic LRO is named Kupffer's vesicle (KV) and presents a characteristic spherical fluid-filled structure enclosed by a ciliated curved epithelium, transiently located at the ventral side of tailbud between 2-3 ss and 20 ss (Cooper & D'Amico, 1996; Essner et al., 2005). The KV cells derive from a subset of the dorsal surface epithelial cells at the dorsal margin of the embryo that, rather than involuting with the rest of the tissue at the beginning of gastrulation, they ingress towards the distal edge and convert into deep mesenchymal-type cells, that due to its position are called as dorsal forerunner cells (DFCs) (Figure 1.5 A) (Cooper & D'Amico, 1996; Melby et al., 1996). Such ingression movements are dependent on Nodal signaling (Oteiza et al., 2008).

During epiboly stages, around 20 to 30 DFCs progressively cluster and migrate ahead of the dorsal margin attached to the overlying surface epithelium towards the vegetal pole. The number of DFCs was found to be highly variable between embryos and small reductions in progenitor cell number increase the likelihood of developing a defective KV (Moreno-Ayala et al., 2021). Therefore, to ensure that all progenitors reach the site of terminal differentiation in a sufficient number, DFCs cluster formation and organization is tightly controlled by E-cadherin mediated cell-cell adhesion (Oteiza et al., 2010; Pulgar et al., 2021). FGF signaling was found to increase *e-cadherin* in the DFCs adherent junctions by a positive feedback loop dependent on *canopy1* and, subsequent induction of the FGF mediator *tbx16*, a T-box transcription factor (Amack et al., 2007; Matsui et al., 2011; Arrington et al., 2013). Another mechanism known to regulate cell adhesion is the planar cell polarity (PCP) signaling and, in fact, downregulation of the non-canonical Wnt/PCP signaling of *princkle1a* alone or combined with *wnt11* reduce adhesion forces between DFCs, through *e-cadherin*, impairing its convergence and integration into a cluster and, consequently, leading to an abnormal KV morphogenesis (Oteiza et al., 2010). Non-canonical Wnt signaling is also thought to inhibit canonical Wnt signaling in order to maintain DFCs clustering through migration. Inhibition of calcium signaling for 20 minutes during epiboly stages or knockdown of *naked cuticle 1* (*nkd1*), a Wnt antagonist, lead to an increase in β-catenin translocation to the nucleus and consequently activation of β-catenin

downstream targets, individual DFCs scattered nearby the DFCs cluster and reduced KV size and cilia number. *Nkd1* mediates β-catenin activity through downregulation of *disheveled,* a component of β-catenin degradation complex, whereas if *nkd1* acts downstream or in parallel with calcium release is yet to be established (Schneider et al., 2008, 2010).

While clustering and migrating towards the vegetal pole, DFCs also undergo mitotic division. Some studies have shown that inhibiting V-ATPase activity during epiboly stages reduced DFCs proliferation rate, most likely due to a dysregulation of proton flux and cytoplasmic pH (Gokey et al., 2015), while others have been shown that blocking Wnt signaling transiently or specifically in the DFCs lead to reduced number of KV cells (Caron et al., 2012; Zhang et al., 2012). More recently, it was shown that the Hippo pathway is, in fact, the upstream signaling regulating DFCs proliferation, where loss of function of different transcription factors and co-factors of this pathway reduced the mitotic rate and, in tandem, Yap gain of function resulted in larger KVs with higher number of cells (Fillatre et al., 2019).

Interestingly, DFCs proliferation defects are often accompanied by shorter cilia in KV cells. This was found to be regulated by a chemokine signaling, composed with the *cxcl12b* ligand and the *cxcr4a* DFCs specific receptor, that links cell cycle progression and cilia formation. Upon activation of cyclin-dependent kinases, the cell cycle is accelerated to promote DFCs proliferation while *foxj1a* is phosphorylated in order to avoid its degradation and, consequently increase its cytoplasmic levels for further support in cilia initiation and elongation (Liu et al., 2019). *Foxj1a* is a well-known forkhead-domain containing transcription factor that activates the transcriptional program for motile cilia production, such as the motility genes *dnah7* and *dnah9,* within the zebrafish KV cells (Stubbs et al., 2008; Yu et al., 2008; Caron et al., 2012; Choksi et al., 2014).

Hence, defects in DFCs clustering, proliferation and migration can lead to insufficient numbers of cells to accomplish a proper KV, compromising its structure, volume, cilia number and cilia length, in a way it can no longer establish a reliable LR patterning (Amack et al., 2007; Oteiza et al., 2008, 2010; Schneider et al., 2008; Zhang et al., 2012; Gokey et al., 2015; Moreno-Ayala et al., 2021)

By this early developmental time, from epiboly to bud, DFCs are regulated by Nodal related gene *squint* (*sqt*) and the T-box transcription factor *tbxa* (*no tail, ntl,* homologous to mouse *brachyury*), that drive the expression of the complex network necessary for the further steps of DFCs mesenchymal to epithelial transition, KV lumen formation, ciliary motor proteins expression and LR-related genes expression in the KV cells (Melby et al., 1996; Amack & Yost, 2004; Bisgrove et al., 2005; Essner et al., 2005; Amack et al., 2007; Gourronc et al., 2007).

At bud stage, as DFCs undergo one last mitotic division, the cytokinetic bridges and midbodies remain in the cells and are translocated to the center of the cluster, as focal points of the future lumen formation site, and give rise to a three-dimensional rosette like structure (Figure 1.5 B) (Rathbun et al., 2020). Concomitantly, DFCs start to establish apicobasal polarity by expressing *tight junction protein 1a (tjp1a)* and *claudin 5a (cldn5a)* at the apical focal points and *e-cadherin* at the basal membranes, that will work together to firmly seal the KV during lumen formation and expansion, avoiding any fluid leakage (Oteiza et al., 2008; Tay et al., 2013; Kim et al., 2017).

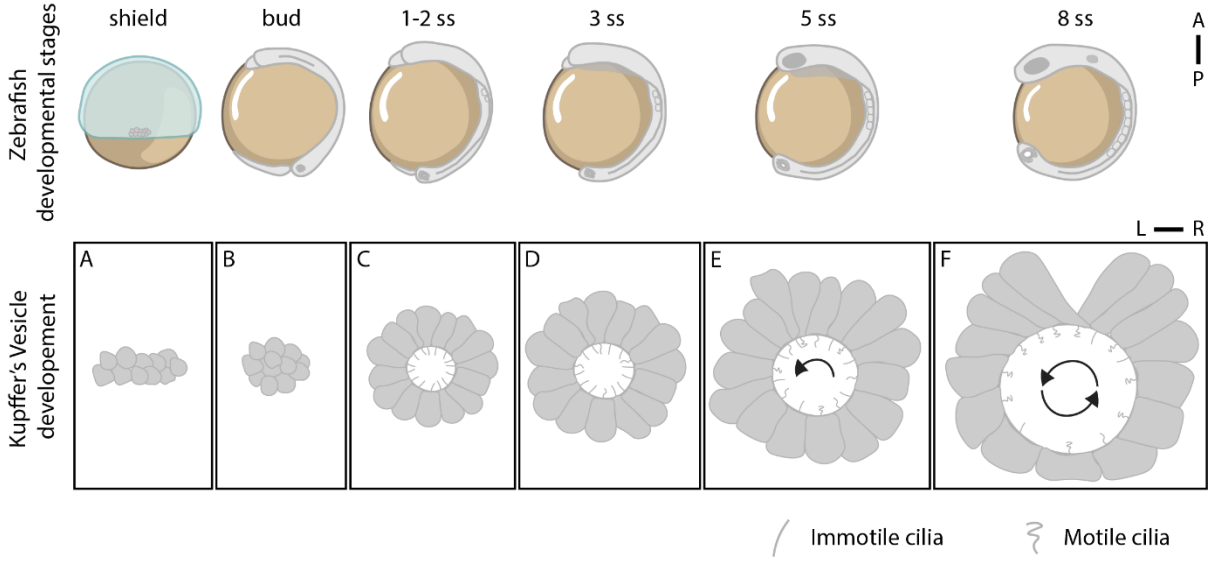

Figure 1.5: Kupffer's Vesicle development.
(A) At the shield stage, on the dorsal side of the embryo, a non-involuting endocytic marginal cells cluster gives rise to the dorsal forerunner cells (DFCs) that remain at the border of blastoderm margin. (B) At bud stage, DFCs have generated a cluster that collectively migrated towards the vegetal pole, underwent cell division and formed a rosette-like epithelial structure with a single focal foci at the center. (C) Between 1 and 2 ss, a small extracellular lumen is formed at the apical center concomitantly with ciliogenesis. One cilium protrudes from every KV cell and ciliary motility is acquired progressively. (D) At 3ss, only 25% of cilia are motile producing a weak flow. (E) At 5ss, 70% of cilia move and are capable of producing a homogeneous counterclockwise fluid flow. (F) By 8ss, KV cells have undergone cell shape remodeling, with more elongated compacted cells at the anterior region and wider at the posterior region, resulting in asymmetric distribution of cilia along the AP axis with a higher cilia density at the anterior side. Together with cilia motility continuously increasing, the directional fluid flow acquires its characteristic velocity and heterogeneous pattern, presenting a faster flow at the anterior quadrant of the KV. KV: Kupffer's Vesicle. Ss: somite stage. A: anterior. P: posterior. L: left. R: right.

KV lumen formation is a rapid and dynamic process that starts at 1 ss and expands until 8 ss, mostly dependent on fluid secretion and cellular morphological rearrangements (Figure 1.5 C, D, E and F) (Navis & Bagnat, 2015). Firstly, intracellular trafficking of vacuolar-like structures to the apical surface of KV cells, mediated by the unconventional *myosin 1d*, *myo1d*, delivers intracellular liquid directly into the lumen (Saydmohammed et al., 2018). In parallel, Rab11 positive vesicles travel through the cytokinetic bridges towards the KV center to deliver the

cystic fibrosis transmembrane conductance regulator (*Cftr*) to the apical membrane (Rathbun et al., 2020). CFTR is the main driving force for liquid secretion and by regulating the transport of chloride into the lumen, the channel promotes a luminal electrochemical gradient of sodium that pushes the movement of water through the tissue into the lumen. In fact, lack of *Cftr* activity, in the zebrafish embryo, blocks KV lumen inflation and randomizes LR patterning and, conversely, pharmacological stimulation of *Cftr* results in KV lumen expansion (Navis et al., 2013; Compagnon et al., 2014; Roxo-Rosa et al., 2015). This further supports the necessity of a minimum size threshold for a functional KV, nevertheless increased sizes can also result in defective KV morphogenesis and LR abnormalities (Compagnon et al., 2014; Gokey et al., 2016). In agreement, studies have shown that cells must have a preventive lumen over-inflation mechanism. In KV cells, Pkd2-dependent calcium increase in the cytoplasm seem to maintain the basal intracellular levels of cAMP required for the normal rate of Cftr activity, whereas in the absence of Pkd2, intracellular levels of cAMP increase and drive overstimulation of Cftr (Roxo-Rosa et al., 2015; Oliveira et al., 2021). A similar mechanism was observed in *pkd2* mouse mutants during kidney cysts development (Walker et al., 2019).

Secondly, cellular rearrangements of the KV occur between 4 ss and 6ss, becoming asymmetrically distributed along with the AP axis (Figure 1.5 D, E and F) (Kreiling et al., 2007; Okabe et al., 2008). KV cells from the anterior side show an increase in its volume and height, becoming larger and elongated, in contrast to the KV cells from the posterior side that show a decrease in its volume and length and an increase in width, resulting in shorter and wider cells (Wang et al., 2011; Roxo-Rosa et al., 2015; Dasgupta et al., 2018). This leads to a tight packing of ciliated cells into the anterior dorsal side and it has been shown to be dependent on *Rho kinase 2a* protein, Rock2b and *non-muscle myosin II* functions, two regulators of the actomyosin cytoskeleton. By downregulating *rock2b* or blocking Myosin II activity, KV remodeling was impaired and cells remained symmetrically distributed along the AP axis, leading to an abnormal counterclockwise flow and consequently to a randomization of LR patterning. Of note, these manipulations did not affect the KV lumen expansion nor the ciliary length (Wang et al., 2011, 2012). These authors further proposed, based on mathematical simulations, that Rock2b-Myosin II pathway regulates cell contractility and cell adhesion, to induce enough cell-cell tension to drive KV remodeling (Wang et al., 2012).

On the other hand, KV re-shape was also seen to be dependent on the lumen expansion. By interfering with Cftr activity, asymmetrical cell distribution was abrogated (Compagnon et al., 2014; Dasgupta et al., 2018). Supporting this, Compagnon and colleagues found an extracellular matrix (ECM) accumulation of *laminin γ1* and *fibronectin-1*, triggered by the adjacent notochord. This local source of ECM components, at the interface of KV anterior region and notochord, would help to specifically constrain the anterior sided cells in response

to KV lumen inflation, whereas the posterior sided cells would undergo apical expansion (Compagnon et al., 2014).

More recently, it has also been pointed out that the strong AP movements of the tailbud tissue surrounding the KV could produce sufficient viscoelastic drag forces to drive changes in KV architecture (Erdemci-tandogan et al., 2018; Sanematsu et al., 2021).

Concomitantly with KV maturation, each cell grows a monocilia from its apical surface that progressively increase in length (Oteiza et al., 2008). This process is tightly regulated by different transcription factors, such as *foxj1a* and *ntl* (Essner et al., 2005; Stubbs et al., 2008; Choksi et al., 2014), ciliary proteins (Essner et al., 2005; Kramer-Zucker et al., 2005; Pintado et al., 2017), lipid production regulators (Sarmah et al., 2007; Jászai et al., 2020), cellular trafficking mediators (Kuhns et al., 2019) and signaling pathways, such as FGF (Neugebauer et al., 2009), Wnt (Caron et al., 2012) and Notch (Lopes et al., 2010), among others proteins. Together these proteins ensure the KV cilia achieve the correct length for optimal fluid flow generation within the lumen as flow varies exponentially with cilia length, within certain limits, by the power of 3 (Pintado et al., 2017).

Additionally, ciliary motility is also acquired gradually during KV maturation (Figure 1.4 D, E and F) (Yuan et al., 2015; Ferreira et al., 2017; Tavares et al., 2017). Although KV cilia seem to share the same ultrastructure of “9 + 2” configuration with the necessary machinery to beat, they all start as immotile. Tavares and colleagues found that the motility switch is regulated by Notch signaling. Thus, increasing Notch signaling by overexpression of *nicd (notch intracellular domain)* led to a decrease in motile cilia number, while decreasing Notch signaling, using Notch ligand mutants such as, zebrafish *deltaD* and *deltaD*;*deltaC* double mutants, had the opposite effect, increasing the number of motile cilia, both manipulations without affecting the total cilia number (Sampaio et al., 2014; Tavares et al., 2017). Furthermore, this pathway was found to be at least partially mediated by *hairy-related 12* gene, *her12*, a homologue of the mammalian *HES5* that belongs to a family of transcription repressors. However, the full molecular mechanism by which Notch signaling or Her12 control cilia motility is still unknown.

Regulation of motile – immotile cilia ratio and spatial distribution, by Notch signaling, is conserved in *Xenopus* LRO ciliated cells, mediated by Notch receptor-1 glycosylation via the action of N-acetylgalactosamine-type O-glycosylation enzyme Galnt11. Similarly to zebrafish, downregulation of *notch1* or *galnt11* led to an increase in motile cilia number, whereas overexpression of *nicd* led to a decrease in motility, resulting in defective LR patterning in both cases (Boskovski et al., 2013; Tavares et al., 2017). Moreover, GALNT11 protein was found to be enriched in crown cells of the mouse LRO and *GALNT11* copy number variations were

found in humans associated with *situs ambiguous,* suggesting a conserved role of Notch signaling across vertebrate LROs (Fakhro et al., 2011; Boskovski et al., 2013).

Thus, ciliary length and motility play crucial roles in the establishment of the KV fluid motion, however it is not enough to drive a directional flow. As in mouse, zebrafish LRO cilia are also tilted, but due to the complexity of KV 3D architecture the correct cilia orientation has been inconsistent, being reported as posteriorly tilted (Kramer-Zucker et al., 2005; Borovina et al., 2010), dorsal tilted (Supatto et al., 2008) or a mix of the two depending on cell location (Okabe et al., 2008). More recently, Ferreira and colleagues analyzed the KV cilia tilt in 3D live embryos and found that they exhibit a meridional tilt towards the dorsal pole of the zebrafish KV, meaning that all motile cilia, independently of its location within the KV, can contribute to the flow directionality (Ferreira et al., 2017). This orientation makes the rightward fraction of the cilium motion to pass closest to the epithelial surface of the cell, where the viscous drag forces are greater, in opposition to the leftward motion that passes farther the cell surface. Consequently, the rightward movement forms the recovery stroke, producing a slow average flow velocity, and the leftward movement results in the power stroke, that efficiently generates a strong fluid flow motion towards the left side of the KV and above the cilia tips (Supatto & Vermot, 2011).

The molecular mechanism that sets cilia orientation is regulated by the PCP pathway, where *VANGL planar cell polarity protein 2 (vangl2)* and *myosin 1d (myo1d)* have opposing activities to polarize the basal body docking at the apical membrane of the zebrafish KV cilia (Borovina et al., 2010; Juan et al., 2018). Similar PCP signaling contributions to cilia orientation were observed in mice (Hashimoto et al., 2010; Song et al., 2010) and in *Xenopus* (Park et al., 2006, 2008). Additionally, other components involved in ciliary motility, such as *cilia and flagella associated protein 298 (cfap298* or *c21orf59)*, also modulate KV cilia orientation via the PCP signaling (Jaffe et al., 2016).

As a result, the cilia orientation promotes a fluid flow counterclockwise direction by 4 ss and the KV remodeling promotes a higher density of cilia on the anterior side, which leads to a corresponding stronger local flow by the 5 ss. At the beginning, the average global flow velocity is low and then progressively increases with the length and number of motile cilia that arise during KV maturation (Sampaio et al., 2014; Montenegro-Johnson et al., 2016; Ferreira et al., 2017; Tavares et al., 2017).

1.3.5. Hypothesis for flow sensing mechanism in a more complex LRO

Motile cilia and directional fluid flow are well established to play critical functions in the LR patterning of both mouse and zebrafish. However, due to discrepancies in the anatomy of zebrafish LRO and consequently a more complex swirling motion of KV fluid flow, it is possible that flow sensing mechanisms may slightly operate differently in these two species. In fact, in mouse LRO where cilia numbers around about 200-300, as few as 2 cilia are enough to drive symmetry breaking of LR axis (Shinohara et al., 2012), in contrast to zebrafish, that have between 40 and 60 KV cilia in total and a minimum threshold of 30 was shown to be necessary to define the LR axis, where still 10% of the embryos would fail to achieve *situs solitus* (Sampaio et al., 2014; Moreno-Ayala et al., 2021). The variability of cilia number between zebrafish embryos suggests that it may not be under evolutionary pressure and the KV may be more of a biasing than robust organizer, accomplishing normal *situs* most of the times (Smith et al., 2014).

Several theoretical and mathematical simulations have been used to find the best model, between the biochemical gradient towards the left side and flow direction-dependent physical stimulus, that try to explain the underlying mechanism of symmetry breaking within the zebrafish LRO environment (Smith et al., 2012; Sampaio et al., 2014; Montenegro-Johnson et al., 2016; Ferreira et al., 2017; Smith et al., 2019; Solowiej-Wedderburn et al., 2019; Cartwright et al., 2020).

Advocating for a mechanosensory mechanism, Sampaio and colleagues found that locally generated flow was predictive of organ *situs*. By downregulating *dynein axonemal heavy chain 7, dnah7*, and selecting embryos that showed only a few motile cilia clustered together specifically on one side or the other of the KV, they observed that local flow on the left side resulted in left sided hearts, whereas local flow on the right side resulted in right sided hearts (Sampaio et al., 2014). However, numerical calculated flow amplitudes from live imaged cilia were found to be highly variable between embryos and without a bias between left and right sides (Ferreira et al., 2017).

As for the chemosensory mechanism in the KV, only predictions were made either using morphogens or vesicles, similarly to what was done in the mouse node (Cartwright et al., 2020). Montenegro-Johnson, Ferreira and colleagues proposed that a signaling molecule was secreted from the anterior side, transported towards the left side by the fluid flow and accumulated in a time-dependent manner on the left sided KV cells, thereby generating a LR differential concentration capable of breaking symmetry (Montenegro-Johnson et al., 2016; Ferreira et al., 2017). It was calculated that a morphogen size between 2 and 10 nm would

correctly establish the LR asymmetric distribution in more than 95% of the simulations, without the need of having an anterior cluster of ciliated cells (Ferreira et al., 2017).

In parallel, Solowiej-Wedderburn and colleagues suggested that the KV anterior side, due to its high density of motile cilia, may actually induce shear stress-dependent exocytosis of extracellular vesicles that would carry the morphogen inside. Given that KV fluid flow is governed by the low Reynolds number, which implies completely negligible inertial effects over viscosity, bigger vesicles would behavior similarly to the morphogens, with the exception that by having a greater mass, they would have lower diffusion rates (Solowiej-Wedderburn et al., 2019). Although this piece of work is entirely theoretical, it is compatible with viable shear stress values observed in flow sensing human vascular endothelial cells (Baratchi et al., 2014, 2016).

Thus, I will next shed some light into the extracellular vesicles that may potentially be involved in zebrafish LR symmetry breaking.

1.3.6. Extracellular vesicles

The extracellular vesicles (EVs) comprise a heterogenous group of membrane enclosed structures, containing cytosol from the delivering cell and loaded with proteins, nucleic acids, lipids and other biomolecules, that are secreted from a wide variety of cells across prokaryotes and eukaryotes (Sager & Palade, 1957; Chatterjee et al., 1959; De, 1959; Sotelo & Porter, 1959; Takeo et al., 1973). First thought to function as a waste disposal mechanism, EVs are now well-known to play diverse roles in cellular communications, providing a mechanism to transmit cargo in high concentrations, unaffected by diffusion or dilution, and therefore, mediating both cellular homeostasis and pathological conditions. Additionally, EVs offer cargo protection against degradation by RNases and proteases during its delivery process and encode the molecular information needed for targeting specific recipient cells (reviewed by Colombo et al., 2014; Woith et al., 2019).

EVs can be generally divided into three main groups: apoptotic bodies, microvesicles and exosomes, based on their physical properties, content, size and nature, although some characteristics may be interchangeable among the groups depending on the cell type from which they derive (Figure 1.6) (reviewed by György et al., 2011; Bazzan et al., 2021).

The apoptotic bodies are relatively large vesicles between 500 nm and 5 µm, highly variable in structure and composition, that result from the programmed cell clearance process, apoptosis (Hristov et al., 2004; Kakarla et al., 2020). During this process, the plasma

membrane deforms into blebs and generates membrane protrusions, driven by cytoskeleton collapse and increased hydrostatic pressure, leading to the final steps of fragmentation and vesicles release. Blebbing formation is mediated by Rho-associated protein kinase 1 (ROCK1) and myosin-light chain kinase (MLCK) by increasing actomyosin contraction (Mills et al., 1998; Aoki et al., 2020). Once the apoptotic bodies are formed, the most typical features are characterized by the externalization of phosphatidylserine (PS) to the vesicle surface and consequently the increase of Annexin V, a phospholipid-binding protein, at the membrane, whereas the cytosol contains biomolecules from the dying cell (Segawa et al., 2014). Both PS and Annexin V accumulation are widely used as specific apoptotic body markers (Engeland et al., 1998). Upon release, these vesicles can be either cleared by phagocytes, to avoid cytotoxic substance leakage into surrounding tissues or engulfed by target cells to promote compensatory proliferation, differentiation and regeneration (reviewed by Battistelli & Falcieri, 2020; Li et al., 2020).

Similarly, the microvesicles are also generated by the outward budding and fission of the plasma membrane but of non-apoptotic cells, mainly of platelet, erythrocyte, leukocyte, and endothelial origin (reviewed by Tricarico et al., 2017). Microvesicle production is triggered by ATP stimulation and an increase in intracellular calcium that activates the protease Calpain, which consequently detaches the membrane from the intracellular cytoskeleton, ultimately leading in a few seconds to a range of vesicles between 50 nm and 1 μm in diameter (Pasquet et al., 1996; Mallick et al., 2015). Upon stimulation, lipids, cell surface receptors, cytosolic proteins anchored to the plasma membrane and other cargoes selectively accumulate at the budding site (Alexy et al., 2014; Cocucci & Meldolesi, 2015). This process was found to be dependent on lipid rafts, Ras-related GTPase 22a (Rab22a), vesicle-associated membrane protein 3 (VAMP3) and Ras-related GTPase ADP-ribosylation factor 6 (ARF6) (Muralidharan-Chari et al., 2009; Wang et al., 2014; Clancy et al., 2015). In turn, protein accumulation and specific lipid translocation between the leaflets of the membrane cause physical curvature and membrane bending. Concomitantly, ARF6 mediates MLCK activation and ARF1 mediates ROCK signaling pathway which together promote actomyosin contractility to drive membrane budding and fission (Cocucci et al., 2009; Muralidharan-Chari et al., 2009). Complete abscission of microvesicles can also involve the tumor susceptibility gene 101 (TSG101), a component of the endosomal sorting complexes required for transport (ESCRT)-I complex, the adaptor arrestin domain-containing protein 1 (ARRDC1) and the ATPase activity of vacuolar protein sorting-associated protein 4 (VPS4) that catalyze the final pinch-off from the membranes (Nabhan et al., 2012).

Some of these sorting machineries and intracellular mechanisms can also play a role in exosome biogenesis in a distinct location within the cell. From the progressive maturation of

endosomes in the cytoplasm from early to late endosomes, results a multivesicular body (MVB) that by inward budding of the membrane becomes filled with intraluminal vesicles (ILVs). The fusion of the MVB either with the lysosome or the plasma membrane, can drive content degradation or ILVs secretion, respectively. Once in the extracellular space, ILVs are called exosomes (reviewed by György et al., 2011; Colombo et al., 2014).

Assembly of ILVs can generally be divided into three pathways: one fully dependent on the endosomal sorting complexes required for transport (ESCRT) complex, another dependent on Syndecan-Syntenin-Alix complex and a third dependent on ceramide synthesis (Niel et al., 2018).

In the canonical ESCRT pathway, ESCRT-0 recruits and binds several ubiquitinated cargoes to small membrane domains within the MVB, ESCRT-I and II initiate local membrane invagination and ESCRT-III polymerizes around the neck of the bud and cleaves the membrane (Juan & Fürthauer, 2017). Additionally, by hydrolyzing ATP, the VPS4 is responsible for generating energy to depolymerize the ESCRT-III complex releasing the ILV inside the MVB (Scott et al., 2005).

On the other hand, Syndecans are cell surface proteoglycans that act as co-receptors and help recruiting specific cargo to the ILVs through its heparan sulfate chains, whereas Syntenin is a PDZ-domain cytoplasmic adaptor (Grootjans et al., 2000). Together, Syndecan and Syntenin, form a tricomplex with Alix (ALG-2 interacting protein X), in order to sequester and stabilize the ESCRT-III complex (Baietti et al., 2012). Therefore, Syndecan-Syntenin-Alix complex functions as a differential exosomal cargo hub while driving the budding of ILVs through the canonical ESCRT pathway (reviewed by Friand et al., 2015).

Lastly, the third pathway is ESCRT-independent and requires generation of ceramide by neural type II sphingomyelinase (nSMase) activity, which hydrolyses sphingomyelin to ceramide (Niel et al., 2018). The full mechanism is poorly understood, but ceramide could generate membrane subdomains and membrane budding or be metabolized to sphingosine 1-phosphate (S1P) to activate S1P-receptor, that appears to be essential for cargo sorting into exosomal ILVs and MVB maturation (Kajimoto et al., 2013).

Thus, ILV production is complex, with different pathways that can act in parallel or sequentially to recruit specific cargoes, depending on cellular signals and pathological stimuli, originating different subpopulations of ILVs and consequently exosomes.

Once the ILVs are formed, the MVBs are transported along actin and tubulin microtubules, associated with molecular motors – dyneins, kinesins and myosins – that are mediated by a few molecular switches, such as the GTPases Rab11, Rab27a, Rab27b and Rab35 (Savina

et al., 2002; Hsu et al., 2010; Ostrowski et al., 2010). However, the exact molecular mechanism performed by these key factors of endo- and exocytic vesicular trafficking will depend on the cell type and steady vs stimulation state. During membrane fusion, several soluble N-ethylmaleimide-sensitive factor attachment protein receptors (SNAREs), tethering factors, Rabs and other Ras GTPases interact to overcome the energy barriers and facilitate fusion, releasing the exosomes (reviewed by Hessvik & Llorente, 2018).

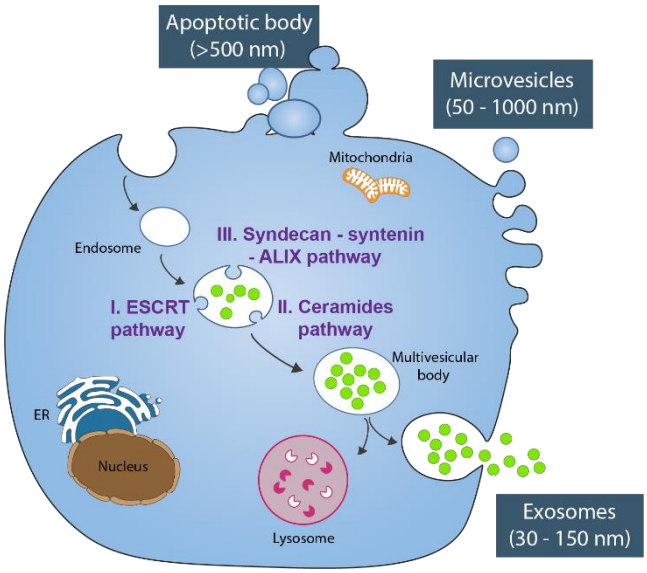

Figure 1.6: Extracellular vesicle biogenesis.
Extracellular vesicles can be divided into three main groups: apoptotic bodies, microvesicles and exosomes, depending on their size and nature. Apoptotic bodies and microvesicles arise from the plasma membrane outward budding, whereas exosomes form through the endocytic pathway as intraluminal vesicles (green). Intraluminal vesicle biogenesis can occur via three pathways: one dependent on the endosomal sorting complexes required for transport (ESCRT) complex, a second dependent on Syndecan-Syntenin-Alix complex and a third dependent on ceramide synthesis. Upon fusion between the multivesicular body and plasma membrane, the exosomes are released to the extracellular space.

Other molecules closely involved in EV production are the tetraspanins, a protein superfamily that promotes clustering and interaction between a large variety of transmembrane and cytosolic signaling proteins, forming membrane subdomains that act as signaling platforms. Tetraspanin CD9, CD81, CD63 and CD82 antigens are most often highly concentrated in exosomes, being used as exosomal markers, but recycling to the plasma membrane can drive its localization to microvesicles as well. Due to its function, tetraspanins have been implicated in EV biogenesis, cargo selection, targeting and uptake, contributing to the heterogeneity of EV subpopulations (Andreu & Yáñez-Mó, 2014).

Upon release, exosomes and microvesicles reach local or distant recipient cells and deliver their content to exert functional responses and promote phenotypic changes that will affect

cell physiological or pathological status (Iraci et al., 2016). Regarding the molecular mechanisms involved in EV internalization, these are not consensual and seem to be dependent on the proteins and glycoproteins expressed at the surface of EVs as well as at the recipient cell. Several studies showed evidence for the contribution of different endocytic pathways, including clathrin- and caveolin-dependent endocytosis, macropinocytosis, phagocytosis, lipid raft mediated uptake and membrane fusion (reviewed by Raposo & Stoorvogel, 2013; Mulcahy et al., 2014; Kwok et al., 2021). Although EVs can adopt different routes to enter the cell, a recent study showed that it relies on a low yield process, where only 1% of EVs were internalized *per* hour and from those only 30% were capable of releasing their content within the cytoplasm (Bonsergent et al., 2021). This low yield process can be overcome, for instance, by a highly sensitive mechanism for acute spatio-temporal changes or signal amplification mechanisms. Nevertheless, studies about the minimum amount of EVs and/or cargo molecules needed for triggering cellular phenotypes are still missing.

The whole EV pathway can be further regulated and activated by specific intracellular signals dependent on the cell type, mostly associated with increased cellular stress such as hypoxia, inhibition of autophagy, increased intracellular calcium, increased cAMP signaling, inactivation of V-ATPase, histamine-mediate GPCR activation and retinoic acid signaling (Savina et al., 2003; Edgar et al., 2016; Verweij et al., 2016; Lin et al., 2021; Ferreira et al., 2022). Additionally, mechanical stress was also shown to increase EV secretion and modulate its microRNA content, contributing for muscle and bone homeostatic communication (Miyazaki et al., 1996; Takafuji et al., 2021).

Thus, secretion of morphogen-containing EVs by mechanical shear stress could in principle occur within the zebrafish LRO from the anterior side. EVs would then be transported by the leftward fluid flow and internalized by the left sided cells. Within these cells, the morphogen would be released to the cytosol and trigger *dand5* mRNA degradation, necessary for symmetry breaking. This model would resolve the link between the strong flow on the anterior side, where increased shear stress would promote EV secretion, and the *dand5* gene expression degradation on the left side of the KV.

1.3.7. Left-right signaling cascade after symmetry breaking in zebrafish

As development progresses and the KV flow builds up, the expression of the LR related genes is set in motion within the KV and in its surroundings.

Similarly to mouse embryos, zebrafish LR axis patterning relies on one Nodal-related gene, *southpaw* (*spaw*) and on its potent antagonist, *dand5.* Their expression starts at 4 – 5 ss,

where d*and5* presents a horse-shoe pattern in KV, and *spaw* shows as two separated domains symmetrically located around the KV (Figure 1.7 A). These expression domains do not overlap and remain until late somitogenesis (Long et al., 2003; Hashimoto et al., 2004; Lopes et al., 2010). Furthermore, they are both independently regulated by Nodal-related gene *sqt* and the T-box transcription factor *ntl,* which in turn also activates *pkd2* and *dnah9* expression in the KV, respectively (Hashimoto et al., 2004; Bisgrove et al., 2005; Essner et al., 2005; Gourronc et al., 2007). Suggesting that *sqt* and *ntl* are master regulators of LR necessary genes.

Moreover, compelling evidence supports that *dand5* expression is also regulated by Notch signaling, likewise in mice (Kitajima et al., 2013). Firstly, *dand5* sequence harbors three CSL/RBP-J (DNA binding partners of Notch) binding sites and secondly, inhibiting Notch signaling, either by pharmacological antagonists or using Notch ligand *deltaD* mutants, showed a strong reduction in *dand5* mRNA production (Gourronc et al., 2007; Lopes et al., 2010).

After *dand5* symmetrical expression is well established, the leftward fluid flow reaches its threshold to induce symmetry breaking in a Pkd2-mediated sensing mechanism, that ultimately leads to the downregulation of *dand5* on the left side of the KV around 8 ss. Hence, *dand5* becomes the first gene asymmetrically expressed along the LR axis (Lopes et al., 2010). Whereas, in the absence of the *pkd2* channel, *dand5* remained symmetric, causing a randomization of Nodal cascade signaling genes at the LPM and organ *situs* defects (Bisgrove et al., 2005; Schottenfeld et al., 2007; Jacinto et al., 2021).

However, *pkd2* is expressed in DFCs much earlier and persists widely spread across early somite stages, suggesting other roles besides mediating flow response (Schottenfeld et al., 2007; England et al., 2017). In fact, zebrafish *pkd2* mutants and morphants (embryos injected with morpholinos that block protein translation and consequently lead to its knockdown) show architectural defects, increased volume and reduced ciliary length within the KV (Roxo-Rosa et al., 2015; Jacinto et al., 2021). Early phenotypes regarding LRO specification, structure and cilia were also observed in *pkd2* knockdown in *Xenopus* (Vick et al., 2018). Additionally, targeting *pkd2* knockdown specifically to the DFCs partially rescue whole-embryo *pkd2* knockdown laterality defects, suggesting that Pkd2 may also contribute to the LR establishment through other tissues (Bisgrove et al., 2005; Jacinto et al., 2021). During early somitogenesis, *pkd2* knockdown was also demonstrated to suppress cytosolic calcium signals and block further activation of type II multifunctional calcium/calmodulin-dependent protein kinase (CaMK-II) (Francescatto et al., 2010; Yuan et al., 2015).

Yuan and colleagues have shown that baseline intraciliary calcium oscillations (ICOs) were present as soon as the bud stage and peaked at the onset of ciliary motility, between 1 and 4

ss, mostly on the anterior-left quadrant of the KV. Subsequently, increased cilia-to-cytosolic calcium waves were observed and, between 5 and 9 ss, cytosolic calcium waves were stably propagated through to the left mesendodermal tissue surrounding the KV. This temporal sequence of calcium events suggests that not only ciliary calcium influx is needed to break the symmetry but also that accumulation of ICOs is required to achieve a robust cytosolic signal on the KV left side. Similarly to *pkd2* knockdown, buffering calcium at the KV cilia by overexpressing the calcium-binding protein parvalbumin, impaired ICOs and suppressed mesendodermal cytosolic calcium waves, leading to defects in *dand5* asymmetric expression and heart position (Yuan et al., 2015).

Furthermore, a few years before Yuan's publication, CaMK-II was found to be a crucial effector of Pkd2 (Francescatto et al., 2010; Rothschild et al., 2011). Time course experiments suggested that prolonged calcium stimulation activates transiently CaMK-II activity, by showing a weak expression of phosphorylated CaMK-II around the KV in a bilaterally fashion, between 3 ss and 6 ss, that later became increasingly restricted to the left KV cells and occasionally seen at the anterior KV cells. Concomitantly, *pkd2* knockdown reduced the levels of active CaMK-II, and CaMK-II gene knockdown resulted in randomization of *spaw* expression pattern at the LPM and consequently laterality defects (Francescatto et al., 2010). Thus, impaired KV calcium signals, reduced the number of KV cells expressing active CaMK-II and randomized organ position.

Moreover, upon knockdown of *ryanodine receptor 3*, *ryr3,* which in normal conditions is responsible for calcium outflow from the endoplasmic reticulum (ER), also randomized organ *situs* (Jurynec et al., 2008; Francescatto et al., 2010). Interestingly, overexpression of a human *PKD2* variant unable to go the cilium and mostly confined in the ER was found to rescue more efficiently the laterality defects of zebrafish *pkd2* morphants, than when overexpressing a wildtype *PKD2* or a variant unable to travel to the ER (Fu et al., 2008).

These data suggest that, upon fluid flow stimulation, ciliary membrane Pkd2 plays a major role initiating ICOs, whereas Pkd2 and Ryr3 channels, located at the ER membrane, are involved in signal amplification transforming a small ciliary calcium signal into a large cytoplasmatic calcium signal. This mechanism is retained in renal cells (Jin et al., 2014).

Calcium sensing mechanism through ciliary membrane Pkd2 is particularly mediated by its partner Pkd1l1 in mouse and medaka LROs (Field et al., 2011; Kamura et al., 2011; Grimes et al., 2016). Likewise, zebrafish *pkd1l1* is expressed in the KV from early bud stage throughout somitogenesis (England et al., 2017) and located at the cilium (Roxo-Rosa & Lopes, 2019). However, functional studies about Pkd1l1 contribution to the LR axis establishment in zebrafish embryos are still missing.

Thus, calcium signaling mediated by Pkd2 and its associates convey the fluid information from the KV lumen through the KV lining cells until the surrounding mesendodermal tissue. Within the KV cells, calcium is postulated to downregulate *dand5* in a microRNA dependent mechanism, as *dand5* mRNA remains symmetric and stably expressed by an increased period of time in zebrafish mutants for *dicer1,* the enzyme catalyzing the final step of microRNA biosynthesis (Maerker et al., 2021). Whereas within the mesendodermal tissue, the role of calcium is largely unknown.

Downregulation of *dand5* expression at the KV left sided cells, at 8 ss, is thought to derepress Spaw protein on the left side of the LPM, as it can be observed that *spaw* expression domains remain symmetrically at the KV vicinity while *spaw* signal is activated on the left side of the LPM. On the right side, Dand5 is continuously expressed and thereby is thought to bind to Spaw by physical interaction, most likely in the extracellular space, inhibiting it from travelling to the right sided LPM (Figure 1.7 B) (Long et al., 2003; Hashimoto et al., 2004; Montague et al., 2018). In fact, *dand5* mutants and morphants show a precocious initiation of *spaw* expression at both sides of the LPM, revealing that *spaw* wave is initiated stochastically and *dand5* is not only responsible for a laterality instructive signal, but also controls the appropriate timing for *spaw* propagation to the LPM (Hashimoto et al., 2004; Wang & Yost, 2008; Montague et al., 2018). Additionally, another secreted Nodal inhibitor, *lefty1*, is firstly induced at the posterior midline by BMP signaling to regulate Spaw spatially and temporally around the KV region, contributing for the molecular clock that dictates *spaw* initiation (Figure 1.7 C) (Wang & Yost, 2008; Smith et al., 2011; Montague et al., 2018).

On the other hand, *spaw* mutants and morphants fail to express *spaw* at the left sided LPM, while *spaw* expression around the KV is maintained, confirming that Spaw protein originated from the KV vicinity is required for inducing *spaw* mRNA expression at the LPM and that posterior-to-anterior wave is enhanced by a positive feedback loop (Long et al., 2003; Noel et al., 2013; Montague et al., 2018).

Spaw transference to the LPM is further enhanced by binding to its co-factor *growth differentiation factor 3, gdf-3,* expressed at the dorsal tailbud region and both sides of LPM (Peterson et al., 2013; Pelliccia et al., 2017; Montague et al., 2018), and by activating its EGF-CFC co-receptor *one-eyed pinhead, oep,* expressed at the midline and bilaterally at the LPM (Zhang et al., 1998; Yan et al., 1999). Thus, the long-range Spaw signal can be converted to a local range activator, as it can only induce its own expression in Gdf-3 and Oep-positive LPM cells. Similarly to the mouse, Nodal activates Oep receptors which result in phosphorylation of Smad2 transcription factor. Activated Smad2 forms a complex with Smad4 and the oligomer is translocated to the nucleus, where it additionally associates with other

transcription factors such as FoxH1. In fact, zebrafish foxH1 expression is very similar to other Nodal components, as at the onset of somitogenesis, it is detected in the midline, LPM and in the anterior dorsal neuroectoderm (Pogoda et al., 2000). Nuclear translocation of these transcriptional factors positively activates the expression of *spaw*, its antagonists *lefty1* and *lefty2* and the transcription factor *pitx2* through the posterior-anterior axis (Figure 1.7 D) (Long et al., 2003; Noel et al., 2013; Montague et al., 2018).

Lefty1 is expressed at the midline and shows a higher effective diffusion coefficient when compared to Nodal genes, supporting a reaction-diffusion model to the regulation of Nodal signaling in the LPM, where *lefty1* plays a critical role in regulating spaw propagation speed and shutting down the pathway at the appropriate time (Wang & Yost, 2008; Müller et al., 2012; Montague et al., 2018).

Lefty2 is expressed on the left side of the primordium heart field and accounts for the "anterior barrier", preventing Spaw from signaling across the anterior limit of the midline and propagate towards the posterior side on the right sided LPM (Lenhart et al., 2011). Additionally, a BMP signaling dependent "posterior barrier" plays a role in zebrafish, preventing Spaw from spreading through the posterior left LPM towards the right side (Lenhart et al., 2011).

Thus, these different molecular barriers allow dynamic buffering of slight fluctuations in Nodal signaling, in order to achieve reliable organ laterality patterns in the presence of endogenous genetic challenges (Rogers et al., 2017).

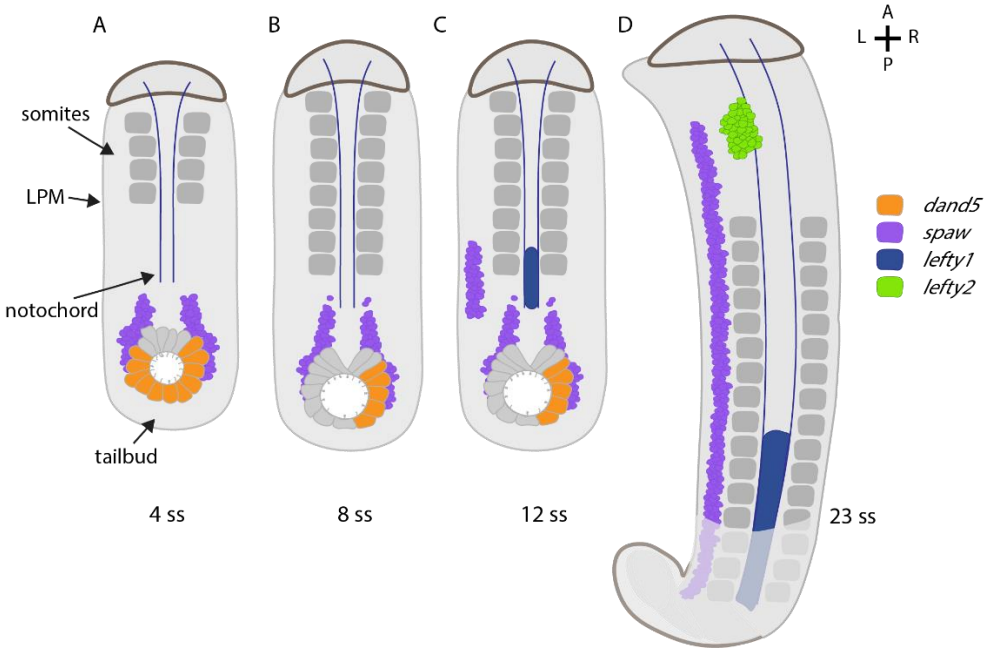

Figure 1.7: Left-right patterning in the zebrafish embryo.
(A) Around 4 ss, *dand5* is firstly expressed bilaterally in a subset of KV cells and perinodal *spaw* transcripts normally appear on two domains dorsally localized to the KV, which is robustly maintained until 10-12 ss. (B) By 8 ss, fluid flow has triggered a calcium wave on the left side of KV, ultimately leading to the degradation of *dand5*

transcripts. (C) In the absence of its inhibitor, *dand5*, Spaw activates its own transcription on the left side of the lateral plate mesoderm and its antagonist *lefty1* in the notochord. Such midline barrier prevents Spaw from travelling to the right side of the embryo and inducing its own expression in the right lateral plate mesoderm. (D) By 23 ss, Spaw propagated through lateral plate mesoderm towards the anterior pole of the embryo, where it activated *lefty2* expression in the heart field. KV: Kupffer's Vesicle. Ss: somite stage. A: anterior. P: posterior. L: left. R: right.

Nodal-induced *pitx2* expression was found on the left sided dorsal diencephalon, where it regulates brain asymmetry (Liang et al., 2000; Garric et al., 2014) and on the left sided LPM, where it persists way longer than *spaw* and it was thought to be responsible for mediating asymmetric organ morphogenesis (Essner et al., 2000). However, *pitx2* mutants and morphants lack LR asymmetry abnormalities in the heart and gut and show several defects in eye, craniofacial and tooth development, resembling Axenfeld-Rieger syndrome (ARS) observed in humans harboring *PITX2* mutations, that derive from *pitx2* expression on early stages at the prechordal plate (Essner et al., 2000; Liu & Semina, 2012; Ji et al., 2016). Although ARS has never been reported in association with laterality abnormalities, congenital heart defects (CHDs) were particularly linked with another ARS-related *FOXC1* mutations (Gripp et al., 2013). Interestingly, a recent study showed that *foxc1a* and *foxc1b* double zebrafish mutants have cardiac and gut *situs* problems, associated with a Nodal-independent absence of *lefty2* expression at the heart field, besides the ARS associated phenotypes (Chrystal et al., 2021). ARS is caused by heterozygous mutations in *PITX2* and, therefore it is plausible that homozygous mutations may not be compatible with life as well as *pitx2* zebrafish mutants may not have a complex enough cardiac system to correctly evaluate all phenotypes of CHDs. Additional studies are necessary to unravel this PITX2 conundrum and confirm the putative role of FOXC1 in the LR axis patterning.

Moreover, *ELOVL fatty acid elongase 6 (elovl6)* gene, that lies next to *pitx2* on chromosome 14, was found to be asymmetrically expressed on the left side LPM, similarly to *pitx2* expression domain, in a Nodal-dependent manner (Ji et al., 2016). This opens the possibility of new pathways involved in the LR patterning to be discovered.

By the time of *spaw* expression on the left side LPM, the cardiac progenitor cell clusters are located on each side at the posterior half of the anterior LPM. Subsequently, the two cardiac fields migrate to the midline and fuse into a morphological symmetric cardiac cone, already expressing *lefty2* on the left side (Baker et al., 2008). Nodal signals induce higher migration velocity and directionality of the left sided cardiomyocytes towards the anterior and left axes when comparing with the right sided progenitors, generating a heart tube displaced on the left side of the embryo, named heart jogging (Campos-baptista et al., 2008). Asymmetrical cellular migration is further sustained by a crosstalk with BMP signaling from the right side of the

embryo (Lenhart et al., 2013). Jogging is followed by heart looping, where the two poles of the tube rotate in opposing directions, regarding the longitudinal axis, resulting in a dextral S-shaped heart. Twisting of the heart was found to be dependent on intrinsic mechanisms driven by the transcription factor *tbx5a* as well as extrinsic mechanisms as non-autonomous BMP dependent activation of *paired related homeobox 1a (prrx1a)* gene, that encodes an epithelial to mesenchymal transition inducer at the LPM, slightly increased on the right side (Ocaña et al., 2017; Tessadori et al., 2021). Concomitantly, the heart aligns the inflow and outflow tracts, cardiac chambers and the atrioventricular canal, in order to establish a functional heart.

Therefore, heart jogging is highly sensitive to Nodal signaling, whereas the heart looping is mediated by heart-intrinsic chirality. In fact, *spaw* null mutants with hearts that jog to the right side, only developed into sinistral looping in half of the cases, while hearts that jogged to the left side always preceded a dextral looping. Moreover, explanted hearts cultured in the absence of Nodal signaling mostly preserved their own chiral looping (Noel et al., 2013). This further supports that heart jogging acts as a looping mediator, independently of Nodal signaling, increasing its robustness (Grimes et al., 2020).

On the other hand, gut, liver and pancreas positions arise from the endodermal gut looping at the midline in a particular region of the AP axis. LPM from both sides starts to migrate autonomously towards the midline, where Nodal signal on the left side triggers a LPM movement from the dorsal side of the endoderm, in contrast to the right sided LPM that moves from the ventrolateral side of the endoderm (Horne-Badovinac et al., 2003). This asymmetric migration results in the displacement of the endodermal gut to the left side. Furthermore, extracellular matrix (ECM) remodeling, dependent on the transcription factor *heart and neural crest derivatives expressed transcript 2, hand2,* and its downstream targets *laminin* and *matrix metalloproteinases,* are also required for the asymmetric LPM cell movement to occur (Yin et al., 2010). However, the mechanism by which Nodal signaling regulates ECM during gut lopping is poorly understood.

By the time that Nodal cascade signaling is well established in the LPM and ready to induce asymmetric morphogenesis, KV collapses and cells are incorporated into mesodermal tissues such as the notochord, the somites and the tail mesenchyme and subsequently are transdifferentiated into mature cell types according to their location (Cooper & D'Amico, 1996; Melby et al., 1996; Keda et al., 2022).

Taking all together, LR axis establishment and progressive patterning throughout embryonic development have been extensively studied in the last years with many prestigious laboratories contributing to advances in the field. Still, several gaps remain to be covered to fulfill this puzzle.

1.4. AIMS

In this first Chapter I tried to cover the bibliography from the oldest to the more recent information regarding the LR axis. From the early stages of the LRO formation and the pivotal role of cilia, passing by the controversial fluid flow triggered mechanism and the conserved Nodal genetic cassette, to the impact of all these mechanisms to PCD patients. In summary, I hope to have alerted to the difficulties but also the importance of studying the LR field in detail.

Cilia-driven fluid flow within the LRO is necessary and sufficient to induce a Pkd2-dependent calcium influx on the left side, that consequently triggers several sequential changes in gene expression throughout the entire embryo with high impact on the asymmetric morphogenesis of the future adult organs. Having such a critical function, fluid flow dynamics has been scrutinized by biologists, mathematicians and physics, however a consensus for the flow-sensing mechanism has not been reached yet. Therefore, with this study I intended to provide new clues of the biophysical mechanism driven by the flow using the zebrafish LRO as the animal model of choice. In the first part of Chapter 2, I engaged in inspecting the molecular characteristics of LRO cells and LRO fluid content to infer possible implications on fluid flow dynamics and Pkd2-sensing mechanism. I generated a transgenic line to quantify and allow the tracking of extracellular vesicles within the LRO's lumen and I used a novel micromanipulation setup to manipulate the content of the LRO's fluid. In collaboration with Pedro Sampaio (a former PhD student in the lab), we could identify that LR symmetry breaking relies on fluid flow dynamics and its physical properties. Namely, we found that viscosity has a huge impact on *dand5* expression pattern and later on heart *situs*.

Historically, motile cilia functions were restricted to the generation of fluid movement, whereas immotile cilia were thought to play important roles in sensing the environment and orchestrating cellular responses accordingly. Being associated with a characteristic ultrastructure, these two types of cilia were considered completely different from each other with non-interchangeable functions. Within the zebrafish KV, all cilia have an axonemal "9 + 2" conformation and harbor motility appendages, however by live imaging we determined that several cilia remain immotile throughout the development of the LRO and the establishment of the symmetry breaking event. We have previously found that Notch signaling manipulations alter the immotile cilia number, at the expenses of the motile cilia. Therefore, with this study I intended to assess the contribution of Notch signaling as a molecular switch for ciliary motility. In the second part of Chapter 2, I used knockdown and rescue studies of *syntenin-a*, an adaptor protein which was characterized to modulate membrane traffic of Notch ligand DeltaD, and consequently evaluated the impact of Notch signaling on ciliary motility by live imaging

microscopy. I identified upstream modulators and downstream effectors of Notch signaling that contribute for the fate decision between motile and immotile status of the KV cilia.

Ultimately, any defect in motile cilia will have an impact on the organism, leading to Primary Ciliary Dyskinesia in humans. As many genes are involved in PCD etiology and clinical symptoms are most of the times not specific, PCD diagnosis is complex and requires the complementary use of multidisciplinary techniques, such as nasal nitric oxide (nNO) measurements, high-speed video microscopy analysis (HSVMA), transmission electron microscopy (TEM) analysis, ciliary protein immunofluorescence (IF) labelling and genetic screening. In Portugal, PCD data is scarce and diagnosis was mostly achieved by TEM. Our laboratory recently published for the first time the normal ranges of ciliary beat frequency using HVMA within the Portuguese community, by analyzing a healthy Portuguese control group. Furthermore, we identified the genetic variants prevalent in Portugal for a PCD patient group and performed genotype – phenotype correlations using HVMA results. With my study, I intended to further implement IF diagnostic studies in the laboratory for better PCD diagnosis on a daily basis, since it represents a less costly alternative for resource-limited countries, where TEM is not readily available. In Chapter 3, I extensively characterized two siblings previously diagnosed with PCD, confirmed by genetic screen, using the IF method. We could infer that IF results are accurate and sensitive to intrinsic patient variability. Moreover, IF has the potential to be used not only as a diagnosis method but also in PCD clinical research.

In the last Chapter 4, the main findings described in the previous chapters are discussed in light of the current literature, pinpointing the most relevant contributions for the long-standing questions of the LR research field and PCD clinical investigation in Portugal.

1.5. REFERENCES

Afzelius, B. a. (1976). A human syndrome caused by immotile cilia. *Science*, *193*(4250), 317–319. https://doi.org/10.1126/science.1084576

Alexy, T., Rooney, K., Weber, M., Gray, W. D., & Searles, C. D. (2014). TNF-α alters the release and transfer of microparticle-encapsulated miRNAs from endothelial cells. *Physiological Genomics*, *46*(22), 833–840. https://doi.org/10.1152/physiolgenomics.00079.2014

Amack, J. D., Wang, X., & Yost, H. J. (2007). Two T-box genes play independent and cooperative roles to regulate morphogenesis of ciliated Kupffer ' s vesicle in zebrafish. *Developmental Biology*, *310*(2), 196–210. https://doi.org/10.1016/j.ydbio.2007.05.039

Amack, J. D., & Yost, H. J. (2004). The T Box Transcription Factor No Tail in Ciliated Cells Controls Zebrafish Left-Right Asymmetry. *Current Biology*, *14*(8), 685–690. https://doi.org/10.1016/j

Amirav, I., Wallmeier, J., Loges, N. T., Menchen, T., Pennekamp, P., Mussaffi, H., Abitbul, R., Avital, A., Bentur, L., Dougherty, G. W., Nael, E., Lavie, M., Olbrich, H., Werner, C., Kintner, C., Omran, H., & Israeli PCD Consortium Investigators. (2016). Systematic Analysis of CCNO Variants in a Defined Population : Implications for Clinical Phenotype and. *Human Mutation*, *37*(4), 396–405. https://doi.org/10.1002/humu.22957

Andreu, Z., & Yáñez-Mó, M. (2014). Tetraspanins in extracellular vesicle formation and function. *Frontiers in Immunology*, *5*(SEP), 1–12. https://doi.org/10.3389/fimmu.2014.00442

Antony, D., Gulec Yilmaz, E., Gezdirici, A., Slagter, L., Bakey, Z., Bornaun, H., Tanidir, I. C., Van Dinh, T., Brunner, H. G., Walentek, P., Arnold, S. J., Backofen, R., & Schmidts, M. (2022). Spectrum of Genetic Variants in a Cohort of 37 Laterality Defect Cases. *Frontiers in Genetics*, *13*, 861236. https://doi.org/10.3389/fgene.2022.861236

Aoki, K., Satoi, S., Harada, S., Uchida, S., Iwasa, Y., & Ikenouchi, J. (2020). Coordinated changes in cell membrane and cytoplasm during maturation of apoptotic bleb. *Molecular Biology of the Cell*, *31*(8), 833–844. https://doi.org/10.1091/mbc.E19-12-0691

Aprea, I., Nöthe-Menchen, T., Dougherty, G. W., Raidt, J., Loges, N. T., Kaiser, T., Wallmeier, J., Olbrich, H., Strünker, T., Kliesch, S., Pennekamp, P., & Omran, H. (2021). Motility of efferent duct cilia aids passage of sperm cells through the male reproductive system. *Molecular Human Reproduction*, *27*(3), gaab009. https://doi.org/10.1093/molehr/gaab009

Arrington, C. B., Peterson, A. G., & Joseph Yost, H. (2013). Sdc2 and Tbx16 regulate Fgf2-dependent epithelial cell morphogenesis in the ciliated organ of asymmetry. *Development (Cambridge, England)*, *140*(19), 4102–4109. https://doi.org/10.1242/dev.096933

Baietti, M. F., Zhang, Z., Mortier, E., Melchior, A., Degeest, G., Geeraerts, A., Ivarsson, Y., Depoortere, F., Coomans, C., Vermeiren, E., Zimmermann, P., & David, G. (2012). Syndecan-syntenin-ALIX regulates the biogenesis of exosomes. *Nature Cell Biology*, *14*(7), 677–685. https://doi.org/10.1038/ncb2502

Baillie, M. (1789). An Account of a Remarkable Transposition of the Viscera in the Human Body. *The London Medical Journal*, *10*(Pt 2), 178–197.

Baker, K., Holtzman, N. G., & Burdine, R. D. (2008). Direct and indirect roles for Nodal signaling in two axis conversions during asymmetric morphogenesis of the zebrafish heart. *Proceedings of the National Academy of Sciences of the United States of America*, *105*(37), 13924–13929. https://doi.org/10.1073/pnas.0802159105

Bamford, R. N., Roessler, E., Burdine, R. D., Umay, S., Cruz, J., Splitt, M., Towbin, J., Bowers, P., Marino, B., Schier, A. F., Shen, M. M., Muenke, M., & Casey, B. (2000). Loss-of-function mutations in the EGF-CFC gene CFC1 are associated with human left-right laterality defects. *Nature Genetics*, *26*(3), 365–369. https://doi.org/10.1038/81695

Baratchi, S., Almazi, J. G., Darby, W., Arnan, F. J. T., & Peter, M. (2016). Shear stress mediates exocytosis of functional TRPV4 channels in endothelial cells. *Cellular and Molecular Life Sciences : CMLS*, *73*(3), 649–666. https://doi.org/10.1007/s00018-015-2018-8

Baratchi, S., Tovar-Lopez, F. J., Khoshmanesh, K., Grace, M. S., Darby, W., Almazi, J., Mitchell, A., & McIntyre, P. (2014). Examination of the role of transient receptor potential vanilloid type 4 in endothelial responses to shear forces. *Biomicrofluidics*, *8*(4), 044117. https://doi.org/10.1063/1.4893272

Barbato, A., Frischer, T., Kuehni, C. E., Snijders, D., Azevedo, I., Baktai, G., Bartoloni, L., Eber, E., Escribano, A., Haarman, E., Hesselmar, B., Hogg, C., Jorissen, M., Lucas, J., Nielsen, K. G., O'Callaghan, C., Omran, H., Pohunek, P., Strippoli, M. P. F., & Bush, A. (2009). Primary ciliary dyskinesia: A consensus statement on diagnostic and treatment approaches in children. *The European Respiratory Journal*, *34*(6), 1264–1276. https://doi.org/10.1183/09031936.00176608

Battistelli, M., & Falcieri, E. (2020). Apoptotic Bodies: Particular Extracellular Vesicles Involved in Intercellular Communication. *Biology*, *9*(1), 21. https://doi.org/10.3390/biology9010021

Bazzan, E., Tin, M., Casara, A., Biondini, D., Semenzato, U., Cocconcelli, E., Balestro, E., Damin, M., Radu, C. M., Turato, G., Baraldo, S., Simioni, P., Spagnolo, P., Saetta, M., & Cosio, M. G. (2021). Critical Review of the Evolution of Extracellular Vesicles' Knowledge: From 1946 to Today. *International Journal of Molecular Sciences*, *22*(12), 6417. https://doi.org/10.3390/ijms22126417

Behan, L., Dimitrov, B., Kuehni, C., Hogg, C., CArrol, M., Evans, H., Goutaki, M., Harris, A., Packham, S., Walker, W., & Lucas, J. (2016). PICADAR: A diagnostic predictive tool for primary ciliary dyskinesia. *The European Respiratory Journal*, *47*(4), 1103–1112. https://doi.org/10.1183/13993003.01551-2015

Behan, L., Galvin, A. D., Rubbo, B., Masefield, S., Copeland, F., Manion, M., Rindlisbacher, B., Redfern, B., & Lucas, J. S. (2016). Diagnosing primary ciliary dyskinesia: An international patient perspective. *The European Respiratory Journal*, *48*(4), 1096–1107. https://doi.org/10.1183/13993003.02018-2015

Bellomo, D., Lander, A., Harragan, L., & Brown, N. A. (1996). Cell proliferation in mammalian gastrulation: The ventral node and notochord are relatively quiescent. *Developmental Dynamics : An Official Publication of the American Association of Anatomists*, *205*(4), 471–485. https://doi.org/10.1002/(SICI)1097-0177(199604)205:4<471::AID-AJA10>3.0.CO;2-4

Berbari, N. F., O'Connor, A. K., Haycraft, C. J., & Yoder, B. K. (2009). The Primary Cilium as a Complex Signaling Center. *Current Biology*, *19*(13), R526–R535. https://doi.org/10.1016/j.cub.2009.05.025

Best, S., Shoemark, A., Rubbo, B., Patel, M. P., Fassad, M. R., Dixon, M., Rogers, A. V, Hirst, R. A.,

Rutman, A., Ollosson, S., Jackson, C. L., Goggin, P., Thomas, S., Pengelly, R., Cullup, T., Pissaridou, E., Hayward, J., Onoufriadis, A., Callaghan, C. O., … Hogg, C. (2019). Risk factors for situs defects and congenital heart disease in primary ciliary dyskinesia. *Thorax*, *74*(2), 203–205. https://doi.org/10.1136/thoraxjnl-2018-212104

Bhogaraju, S., Engel, B. D., & Lorentzen, E. (2013). Intraflagellar transport complex structure and cargo interactions. *Cilia*, *2*(1), 10. https://doi.org/10.1186/2046-2530-2-10

Bisgrove, B. W., Snarr, B. S., Emrazian, A., & Yost, H. J. (2005). Polaris and Polycystin-2 in dorsal forerunner cells and Kupffer's vesicle are required for specification of the zebrafish left-right axis. *Developmental Biology*, *287*(2), 274–288. https://doi.org/10.1016/j.ydbio.2005.08.047

Blackburn, K., Bustamante, X., Yin, W., Goshe, M. B., & Ostrowski, L. E. (2017). Quantitative Proteomic Analysis of Human Airway Cilia Identifies Previously Uncharacterized Proteins of High Abundance. *Journal of Proteome Research*, *16*(4), 1579–1592. https://doi.org/10.1021/acs.jproteome.6b00972.Quantitative

Blanchon, S., Legendre, M., Bottier, M., Tamalet, A., Montantin, G., Collot, N., Faucon, C., Dastot, F., Copin, B., Clement, A., Filoche, M., Coste, A., Amselem, S., Escudier, E., Papon, J.-F., & Louis, B. (2020). Deep phenotyping , including quantitative ciliary beating parameters , and extensive genotyping in primary ciliary dyskinesia. *Journal of Medical Genetics*, *57*(4), 237–244. https://doi.org/10.1136/jmedgenet-2019-106424

Bloodgood, R. A. (2018). From Central to Rudimentary to Primary: The History of an Underappreciated Organelle Whose Time Has Come. The Primary Cilium. In *Methods in Cell Biology: VOLUME 94* (First edit, Vol. 94). Elsevier. https://doi.org/10.1016/S0091-679X(08)94001-2

Blum, M., Feistel, K., Thumberger, T., & Schweickert, A. (2014). The evolution and conservation of left-right patterning mechanisms. *Development*, *141*(8), 1603–1613. https://doi.org/10.1242/dev.100560

Blum, M., & Ott, T. (2018). Animal left–right asymmetry. *Current Biology*, *28*(7), R301–R304. https://doi.org/10.1016/j.cub.2018.02.073

Bonser, L. R., Schroeder, B. W., Ostrin, L. A., Baumlin, N., Olson, J. L., Salathe, M., & Erle, D. J. (2015). The Endoplasmic Reticulum Resident Protein AGR3 Required for Regulation of Ciliary Beat Frequency in the Airway. *American Journal of Respiratory Cell and Molecular Biology*, *53*(4), 536–543. https://doi.org/10.1165/rcmb.2014-0318OC

Bonsergent, E., Grisard, E., Buchrieser, J., Schwartz, O., Théry, C., & Lavieu, G. (2021). Quantitative characterization of extracellular vesicle uptake and content delivery within mammalian cells. *Nature Communications*, *12*(1), 1864. https://doi.org/10.1038/s41467-021-22126-y

Boon, M., Smits, A., Cuppens, H., Jaspers, M., Proesmans, M., Dupont, L. J., Vermeulen, F. L., Daele, S. Van, Malfroot, A., Godding, V., Jorissen, M., & Boeck, K. De. (2014). Primary ciliary dyskinesia : critical evaluation of clinical symptoms and diagnosis in patients with normal and abnormal ultrastructure. *Orphanet Journal of Rare Diseases*, *9*, 11. https://doi.org/10.1186/1750-1172-9-11

Boon, M., Wallmeier, J., Ma, L., Loges, N. T., Jaspers, M., Olbrich, H., Dougherty, G. W., Raidt, J., Werner, C., Amirav, I., Hevroni, A., Abitbul, R., Avital, A., Soferman, R., Wessels, M., Callaghan, C. O., Chung, E. M. K., Rutman, A., Hirst, R. A., … Omran, H. (2014). MCIDAS mutations result in a mucociliary

clearance disorder with reduced generation of multiple motile cilia. *Nature Communications*, *5*, 4418. https://doi.org/10.1038/ncomms5418

Borovina, A., Superina, S., Voskas, D., & Ciruna, B. (2010). Vangl2 directs the posterior tilting and asymmetric localization of motile primary cilia. *Nature Cell Biology*, *12*(4), 407–412. https://doi.org/10.1038/ncb2042

Boskovski, M. T., Yuan, S., Pedersen, N. B., & Goth, C. K. (2013). The Heterotaxy gene, GALNT11, glycosylates Notch to orchestrate cilia type and laterality. *Nature*, *504*(7480), 456–459. https://doi.org/10.1038/nature12723.The

Bray, S. J. (2006). Notch signalling: A simple pathway becomes complex. *Nature Reviews Molecular Cell Biology*, *7*(9), 678–689. https://doi.org/10.1038/nrm2009

Brennan, J., Norris, D. P., & Robertson, E. J. (2002). Nodal activity in the node governs left-right asymmetry. *Genes and Development*, *16*(18), 2339–2344. https://doi.org/10.1101/gad.1016202

Budny, B., Chen, W., Omran, H., Fliegauf, M., Tzschach, A., Wisniewska, M., Jensen, L. R., Raynaud, M., Shoichet, S. A., Badura, M., Ste, V., Anna, L., & Ropers, H. (2006). A novel X-linked recessive mental retardation syndrome comprising macrocephaly and ciliary dysfunction is allelic to oral – facial – digital type I syndrome. *Human Genetics*, *120*(2), 171–178. https://doi.org/10.1007/s00439-006-0210-5

Bustamante-marin, X. M., Yin, W., Sears, P. R., Werner, M. E., Brotslaw, E. J., Mitchell, B. J., Jania, C. M., Zeman, K. L., Rogers, T. D., Herring, L. E., Refabe, L., Thomas, L., Amselem, S., Escudier, E., Legendre, M., Grubb, B. R., Knowles, M. R., Zariwala, M. A., & Ostrowski, L. E. (2019). Lack of GAS2L2 Causes PCD by Impairing Cilia Orientation and Mucociliary Clearance. *American Journal of Human Genetics*, *104*(2), 229–245. https://doi.org/10.1016/j.ajhg.2018.12.009

Campos-baptista, M. I. M. De, Holtzman, N. G., Yelon, D., & Schier, A. F. (2008). Nodal signaling promotes the speed and directional movement of cardiomyocytes in zebrafish. *Developmental Dynamics : An Official Publication of the American Association of Anatomists*, *237*(12), 3624–3633. https://doi.org/10.1002/dvdy.21777.Nodal

Caron, A., Xu, X., & Lin, X. (2012). Wnt/Beta-catenin signaling directly regulates Foxj1 expression and ciliogenesis in zebrafish Kupffer's vesicle. *Development (Cambridge, England)*, *139*(3), 514–524. https://doi.org/10.1242/dev.071746

Cartwright, J. H. E., Piro, N., Piro, O., & Tuval, I. (2007). Embryonic nodal flow and the dynamics of nodal vesicular parcels. *Journal of the Royal Society, Interface*, *4*(12), 49–55. https://doi.org/10.1098/rsif.2006.0155

Cartwright, J. H. E., Piro, O., & Tuval, I. (2004). Fluid-dynamical basis of the embryonic development of left – right asymmetry in vertebrates. *Proceedings of the National Academy of Sciences of the United States of America*, *101*(19), 7234–7239. https://doi.org/10.1073/pnas.0402001101

Cartwright, J. H. E., Piro, O., & Tuval, I. (2020). Chemosensing versus mechanosensing in nodal and Kupffer's vesicle cilia and in other left-right organizer organs. *Philosophical Transactions of the Royal Society B: Biological Sciences*, *375*(1792). https://doi.org/10.1098/rstb.2019.0566

Caspary, T., Larkins, C. E., & Anderson, K. V. (2007). The Graded Response to Sonic Hedgehog Depends on Cilia Architecture. *Developmental Cell*, *12*(5), 767–778.

https://doi.org/10.1016/j.devcel.2007.03.004

Castleman, V. H., Romio, L., Chodhari, R., Hirst, R. A., de Castro, S. C. P., Parker, K. A., Ybot-Gonzalez, P., Emes, R. D., Wilson, S. W., Wallis, C., Johnson, C. A., Herrera, R. J., Rutman, A., Dixon, M., Shoemark, A., Bush, A., Hogg, C., Gardiner, R. M., Reish, O., … Mitchison, H. M. (2008). Mutations in radial spoke head protein genes RSPH9 and RSPH4A cause primary ciliary dyskinesia with central-microtubular-pair abnormalities. *The American Journal of Human Genetics*, *84*(2), 197–209. https://doi.org/10.1016/j.ajhg.2009.01.011

Chatterjee, K. R., Das Gupta, N. N., & De, M. L. (1959). Electron microscopic observations on the morphology of Mycobacterium leprae. *Experimental Cell Research*, *18*, 521–527. https://doi.org/10.1016/0014-4827(59)90317-9

Chen, C., & Shen, M. (2004). Two Modes by which Lefty Proteins Inhibit Nodal Signaling. *Current Biology*, *14*(7), 618–624. https://doi.org/10.1016/j

Chen, D. T. N., Heymann, M., Fraden, S., Nicastro, D., & Dogic, Z. (2015). ATP Consumption of Eukaryotic Flagella Measured at a Single-Cell Level. *Biophysical Journal*, *109*(12), 2562–2573. https://doi.org/10.1016/j.bpj.2015.11.003

Chilvers, M. A., Rutman, A., & O'Callaghan, C. (2003). Ciliary beat pattern is associated with specific ultrastructural defects in primary ciliary dyskinesia. *The Journal of Allergy and Clinical Immunology*, *112*(3), 518–524. https://doi.org/10.1016/S0091-6749(03)01799-8

Chivukula, R. R., Montoro, D. T., Leung, H. M., Yang, J., Shamseldin, H. E., Taylor, M. S., Dougherty, G. W., Zariwala, M. A., Carson, J., Daniels, M. L. A., Sears, P. R., Black, K. E., Hariri, L. P., Almogarri, I., Frenkel, E. M., Vinarsky, V., Omran, H., Knowles, M. R., Tearney, G., … Sabatini, D. M. (2020). A human ciliopathy reveals essential functions for NEK10 in airway mucociliary clearance. *Nature Medicine*, *26*(2), 300. https://doi.org/10.1038/s41591-019-0730-x

Choksi, S. P., Babu, D., Lau, D., Yu, X., & Roy, S. (2014). Systematic discovery of novel ciliary genes through functional genomics in the zebrafish. *Development (Cambridge, England)*, *141*(17), 3410–3419. https://doi.org/10.1242/dev.108209

Chrystal, P. W., French, C. R., Jean, F., Havrylov, S., Baarle, S. Van, Peturson, A., Xu, P., Crump, J. G., Pilgrim, D. B., Lehmann, O. J., & Waskiewicz, A. J. (2021). The Axenfeld – Rieger Syndrome Gene FOXC1 Contributes to Left – Right Patterning. *Genes*, *12*(2), 170. https://doi.org/10.3390/genes12020170

Clancy, J. W., Sedgwick, A., Rosse, C., Muralidharan-chari, V., Raposo, G., Method, M., Chavrier, P., & Souza-schorey, C. D. (2015). Regulated delivery of molecular cargo to invasive tumour-derived microvesicles. *Nature Communications*, *6*, 6919. https://doi.org/10.1038/ncomms7919

Clary-Meinesz, C., Mouroux, J., Cosson, J., Huitorel, P., & Blaive, B. (1998). Influence of external pH on ciliary beat frequency in human bronchi and bronchioles. *The European Respiratory Journal*, *11*(2), 330–333. https://doi.org/10.1183/09031936.98.11020330

Cleveland, M. (1926). Situs inversus viscerum. *Archives of Surgery*, *13*(3), 343.

Cocucci, E., & Meldolesi, J. (2015). Ectosomes and exosomes : shedding the confusion between extracellular vesicles. *Trends in Cell Biology*, *25*(6), 364–372. https://doi.org/10.1016/j.tcb.2015.01.004

Cocucci, E., Racchetti, G., & Meldolesi, J. (2009). Shedding microvesicles : artefacts no more. *Trends in Cell Biology*, *19*(2), 43–51. https://doi.org/10.1016/j.tcb.2008.11.003

Cole, D., Diener, D., Himelblau, A., Beech, P., Fuster, J., & Rosenbaum, J. (1998). Chlamydomonas kinesin-II-dependent intraflagellar transport (IFT): IFT particles contain proteins required for ciliary assembly in Caenorhabditis elegans sensory neurons. *The Journal of Cell Biology*, *141*(4), 993–1008. https://doi.org/10.1083/jcb.141.4.993

Collignon, J., Varlet, I., & Robertson, E. J. (1996). Relationship between asymmetric nodal expression and the direction of embryonic turning. *Nature*, *381*(6578), 155–158. https://doi.org/10.1038/381155a0

Collins, S. A., Gove, K., Walker, W., & Lucas, J. S. A. (2014). Nasal nitric oxide screening for primary ciliary dyskinesia: Systematic review and meta-analysis. *The European Respiratory Journal*, *44*(6), 1589–1599. https://doi.org/10.1183/09031936.00088614

Colombo, M., Raposo, G., & Théry, C. (2014). Biogenesis , Secretion , and Intercellular Interactions of Exosomes and Other Extracellular Vesicles. *Annual Review of Cell and Developmental Biology*, *30*(1), 255–289. https://doi.org/10.1146/annurev-cellbio-101512-122326

Compagnon, J., Barone, V., Rajshekar, S., Kottmeier, R., Pranjic-Ferscha, K., Behrndt, M., & Heisenberg, C.-P. (2014). The Notochord Breaks Bilateral Symmetry by Controlling Cell Shapes in the Zebrafish Laterality Organ. *Developmental Cell*, *31*(6), 774–783. https://doi.org/10.1016/j.devcel.2014.11.003

Cooper, M. S., & D'Amico, L. A. (1996). A cluster of noninvoluting endocytic cells at the margin of the zebrafish blastoderm marks the site of embryonic shield formation. *Developmental Biology*, *180*(1), 184–198. https://doi.org/10.1006/dbio.1996.0294

Corbit, K. C., Shyer, A. E., Dowdle, W. E., Gaulden, J., Singla, V., & Reiter, J. F. (2008). Kif3a constrains β-catenin-dependent Wnt signalling through dual ciliary and non-ciliary mechanisms. *Nature Cell Biology*, *10*(1), 70–76. https://doi.org/10.1038/ncb1670

Cristo, F., Inácio, J. M., Almeida, S. De, Mendes, P., Martins, D. S., Maio, J., Anjos, R., & Belo, J. A. (2017). Functional study of DAND5 variant in patients with Congenital Heart Disease and laterality defects. *BMC Medical Genetics*, *18*(1), 77. https://doi.org/10.1186/s12881-017-0444-1

D'Souza, B., Meloty-Kapella, L., & Weinmaster, G. (2010). Canonical and non-canonical notch ligands. *Current Topics in Developmental Biology*, *92*(C), 73–129. https://doi.org/10.1016/S0070-2153(10)92003-6

Dalrymple, R. A., & Kenia, P. (2019). European Respiratory Society guidelines for the diagnosis of primary ciliary dyskinesia: A guideline review. *Archives of Disease in Childhood: Education and Practice Edition*, *104*(5), 265–269. https://doi.org/10.1136/archdischild-2017-312902

Dasgupta, A., Merkel, M., Clark, M. J., Jacob, A. E., Dawson, J. E., Manning, M. L., & Amack, J. D. (2018). Cell volume changes contribute to epithelial morphogenesis in zebrafish Kupffer's vesicle. *ELife*, *7*, e30963. https://doi.org/10.7554/eLife.30963

De, S. N. (1959). Enterotoxicity of bacteria-free culture-filtrate of Vibrio cholerae. *Nature*, *183*(4674), 1533–1534. https://doi.org/10.1038/1831533a0

Di Benedetto, G., Magnus, C. J., Gray, P. T., & Mehta, A. (1991). Calcium regulation of ciliary beat frequency in human respiratory epithelium in vitro. *The Journal of Physiology*, *439*, 103–113. https://doi.org/10.1113/jphysiol.1991.sp018659

DiPetrillo, C., & Smith, E. (2009). Calcium regulation of ciliary motility analysis of axonemal calcium-binding proteins. In *Methods in cell biology* (First edit, Vol. 92, Issue 08). Elsevier. https://doi.org/10.1016/S0091-679X(08)92011-2

Dixon, M., & Shoemark, A. (2017). Secondary defects detected by transmission electron microscopy in primary ciliary dyskinesia diagnostics. *Ultrastructural Pathology*, *41*(6), 390–398. https://doi.org/10.1080/01913123.2017.1365990

Djakow, J., Rozehnalova, E., Havlisova, M., Svobodova, T., & Pohunek, P. (2012). Clinical index to evaluate the risk of primary ciliary dyskinesia in children. *European Respiratory Journal*, *40*(Suppl. 56), 2844.

Dougherty, G. W., Loges, N. T., Klinkenbusch, J. A., Olbrich, H., Pennekamp, P., Menchen, T., Raidt, J., Wallmeier, J., Werner, C., Westermann, C., Ruckert, C., Mirra, V., Hjeij, R., Memari, Y., Durbin, R., Kolb-kokocinski, A., Praveen, K., Kashef, M. A., Kashef, S., … Omran, H. (2016). DNAH11 Localization in the Proximal Region of Respiratory Cilia Defines Distinct Outer Dynein Arm Complexes. *American Journal of Respiratory Cell and Molecular Biology*, *55*(2), 213–224. https://doi.org/10.1165/rcmb.2015-0353OC

Dougherty, G. W., Olbrich, H., Hjeij, R., Loges, N. T., Amirav, I., Philipsen, M. C., Marthin, J. K., Nielsen, K. G., Sutharsan, S., Raidt, J., Werner, C., Pennekamp, P., Dworniczak, B., & Omran, H. (2020). SPEF2- and HYDIN -Mutant Cilia Lack the Central Pair – associated Protein SPEF2 , Aiding Primary Ciliary Dyskinesia Diagnostics. *American Journal of Respiratory Cell and Molecular Biology*, *62*(3), 382–396. https://doi.org/10.1165/rcmb.2019-0086OC

Eddy, E. M., Toshimori, K., & O'Brien, D. A. (2003). Fibrous sheath of mammalian spermatozoa. *Microscopy Research and Technique*, *61*(1), 103–115. https://doi.org/10.1002/jemt.10320

Edgar, J. R., Manna, P. T., Nishimura, S., Banting, G., & Robinson, M. S. (2016). Tetherin is an exosomal tether. *ELife*, *5*, e17180. https://doi.org/10.7554/eLife.17180

Elgeti, J., & Gompper, G. (2013). Emergence of metachronal waves in cilia arrays. *Proceedings of the National Academy of Sciences of the United States of America*, *110*(12), 4470–4475. https://doi.org/10.1073/pnas.1218869110

Engeland, M. van, Nieland, L. J., Ramaekers, F. C., Schutte, B., & Reutelingsperger, C. P. (1998). Annexin V-affinity assay: a review on an apoptosis detection system based on phosphatidylserine exposure. *Cytometry*, *31*(1), 1–9. https://doi.org/10.1002/(sici)1097-0320(19980101)31:1<1::aid-cyto1>3.0.co;2-r

England, S. J., Campbell, P. C., Banerjee, S., & Swanson, A. J. (2017). Identification and Expression Analysis of the Complete Family of Zebrafish pkd Genes. *Frontiers in Cell and Developmental Biology*, *5*, 5. https://doi.org/10.3389/fcell.2017.00005

Erdemci-tandogan, G., Clark, M. J., Amack, J. D., & Manning, M. L. (2018). Tissue Flow Induces Cell Shape Changes During Organogenesis. *Biophysical Journal*, *115*(11), 2259–2270.

https://doi.org/10.1016/j.bpj.2018.10.028

Essner, J. J., Amack, J. D., Nyholm, M. K., Harris, E. B., & Yost, H. J. (2005). Kupffer's vesicle is a ciliated organ of asymmetry in the zebrafish embryo that initiates left-right development of the brain, heart and gut. *Development (Cambridge, England*, *132*(6), 1247–1260. https://doi.org/10.1242/dev.01663

Essner, J. J., Branford, W. W., Zhang, J., & Yost, H. J. (2000). Mesendoderm and left-right brain , heart and gut development are differentially regulated by pitx2 isoforms. *Development (Cambridge, England)*, *127*(5), 1081–1093. https://doi.org/10.1242/dev.127.5.1081

Ezratty, E., Stokes, N., Chai, S., Shah, A., Williams, S., & Fuchs, E. (2011). A role for the primary cilium in Notch signaling and epidermal differentiation during skin development. *Cell*, *145*(7), 1129–1141. https://doi.org/10.1016/j.cell.2011.05.030.A

Fakhro, K. a, Choi, M., Ware, S. M., Belmont, J. W., Towbin, J. a, Lifton, R. P., Khokha, M. K., & Brueckner, M. (2011). Rare copy number variations in congenital heart disease patients identify unique genes in left-right patterning. *Proceedings of the National Academy of Sciences of the United States of America*, *108*(7), 2915–2920. https://doi.org/10.1073/pnas.1019645108

Ferreira, J. V., Da Rosa Soares, A., Ramalho, J., Carvalho, C. M., Cardoso, M. H., Pintado, P., Carvalho, A. S., Beck, H. C., Matthiesen, R., Zuzarte, M., Girao, H., Van Niel, G., & Pereira, P. (2022). LAMP2A regulates the loading of proteins into exosomes. *Science Advances*, *8*(12), eabm1140. https://doi.org/10.1126/sciadv.abm1140

Ferreira, R. R., Vilfan, A., Jülicher, F., Supatto, W., & Vermot, J. (2017). Physical limits of flow sensing in the left-right organizer. *ELife*, *6*, e25078. https://doi.org/10.7554/eLife.25078

Field, S., Riley, K.-L., Grimes, D. T., Hilton, H., Simon, M., Powles-Glover, N., Siggers, P., Bogani, D., Greenfield, A., & Norris, D. P. (2011). Pkd1l1 establishes left-right asymmetry and physically interacts with Pkd2. *Development (Cambridge, England)*, *138*(6), 1131–1142. https://doi.org/10.1242/dev.058149

Fillatre, J., Fauny, J., Fels, J. A., Li, C., Goll, M., Thisse, C., & Thisse, B. (2019). TEADs, Yap, Taz, Vgll4s transcription factors control the establishment of Left-Right asymmetry in zebrafish. *ELife*, *8*, e45241. https://doi.org/10.7554/eLife.45241

Fliegauf, M., Benzing, T., & Omran, H. (2007). When cilia go bad: cilia defects and ciliopathies. *Nature Reviews. Molecular Cell Biology*, *8*(11), 880–893. https://doi.org/10.1038/nrm2278

Fliegauf, M., Olbrich, H., Horvath, J., Wildhaber, J. H., Zariwala, M. A., Kennedy, M., Knowles, M. R., & Omran, H. (2005). Mislocalization of DNAH5 and DNAH9 in Respiratory Cells from Patients with Primary Ciliary Dyskinesia. *American Journal of Respiratory and Critical Care Medicine*, *171*(12), 1343–1349. https://doi.org/10.1164/rccm.200411-1583OC

Francescatto, L., Rothschild, S. C., Myers, A. L., & Tombes, R. M. (2010). The activation of membrane targeted CaMK-II in the zebrafish Kupffer's vesicle is required for left-right asymmetry. *Development (Cambridge, England)*, *137*(16), 2753–2762. https://doi.org/10.1242/dev.049627

Franco, D., Sedmera, D., &, & Lozano-Velasco, E. (2017). Multiple Roles of Pitx2 in Cardiac Development and Disease. *Journal of Cardiovascular Development and Disease*, *4*(4), 16. https://doi.org/10.3390/jcdd4040016

Friand, V., David, G., & Zimmermann, P. (2015). Syntenin and syndecan in the biogenesis of exosomes. *Biology of the Cell*, *107*(10), 331–341. https://doi.org/10.1111/boc.201500010

Fu, X., Wang, Y., Schetle, N., Gao, H., Pütz, M., von Gersdorff, G., Walz, G., & Kramer-Zucker, A. G. (2008). The subcellular localization of TRPP2 modulates its function. *Journal of the American Society of Nephrology: JASN*, *19*(7), 1342–1351. https://doi.org/10.1681/ASN.2007070730

Gadêlha, H., Hernández-Herrera, P., Montoya, F., Darszon, A., & Corkidi, G. (2021). Retraction of the Research Article: "Human sperm uses asymmetric and anisotropic flagellar controls to regulate swimming symmetry and cell steering. *Science Advances*, *7*(21), eaau9116. https://doi.org/10.1126/sciadv.aau9116

Gallagher, M. T., & Smith, D. J. (2020). Simulations of particle tracking in the oligociliated mouse node and implications for left-right symmetry breaking mechanics. *Philosophical Transactions of the Royal Society of London. Series B, Biological Sciences*, *375*(1792), 20190161. https://doi.org/10.1098/rstb.2019.0161

Garric, L., Ronsin, B., Roussigné, M., Booton, S., Gamse, J. T., Dufourcq, P., & Blader, P. (2014). Pitx2c ensures habenular asymmetry by restricting parapineal cell number. *Development (Cambridge, England)*, *141*(7), 1572–1579. https://doi.org/10.1242/dev.100305

Girard, P. R., & Kennedy, J. R. (1986). Calcium regulation of ciliary activity in rabbit tracheal epithelial explants and outgrowth. *European Journal of Cell Biology*, *40*(2), 203–209.

Gokey, J. J., Dasgupta, A., Amack, J. D., & Medical, U. (2015). The V-ATPase accessory protein Atp6ap1b mediates dorsal forerunner cell proliferation and left-right asymmetry in zebrafish. *Developmental Biology*, *407*(1), 115–130. https://doi.org/10.1016/j.ydbio.2015.08.002.The

Gokey, J. J., Ji, Y., Tay, H. G., Litts, B., & Amack, J. D. (2016). Kupffer's vesicle size threshold for robust left-right patterning of the zebrafish embryo. *Developmental Dynamics : An Official Publication of the American Association of Anatomists*, *245*(1), 22–33. https://doi.org/10.1002/dvdy.24355

González-Perrett, S., Kim, K., Ibarra, C., Damiano, A. E., Zotta, E., Batelli, M., Harris, P. C., Reisin, I. L., Arnaout, M. A., & Cantiello, H. F. (2001). Polycystin-2 , the protein mutated in autosomal dominant polycystic kidney disease (ADPKD), is a Ca 2 ⁒ -permeable nonselective cation channel. *Proceedings of the National Academy of Sciences of the United States of America*, *98*(3), 1182–1187. https://doi.org/10.1073/pnas.98.3.1182

Goodenough, U. W., & Heuser, J. E. (1985). Substructure of Inner Dynein Arms , Radial Spokes , and the Central Pair / Projection Complex of Cilia and Flagella. *The Journal of Cell Biology*, *100*(6), 2008–2018. https://doi.org/10.1083/jcb.100.6.2008

Gourronc, F., Ahmad, N., Nedza, N., Eggleston, T., & Rebagliati, M. (2007). Nodal Activity Around Kupffer's Vesicle Depends on the T-Box Transcription Factors Notail and Spadetail and on Notch Signaling. *Developmental Dynamics : An Official Publication of the American Association of Anatomists*, *236*(8), 2131–2146. https://doi.org/10.1002/dvdy.21249

Grimes, D. T., Keynton, J. L., Buenavista, M. T., Jin, X., Patel, S. H., Kyosuke, S., Vibert, J., Williams, D. J., Hamada, H., Hussain, R., Nauli, S. M., & Norris, D. P. (2016). Genetic Analysis Reveals a Hierarchy of Interactions between Polycystin- Encoding Genes and Genes Controlling Cilia Function during Left-

Right Determination. *PLoS Genetics*, *12*(6), e1006070. https://doi.org/10.1371/journal.pgen.1006070

Grimes, D. T., Patterson, V. L., Luna-arvizu, G., Schottenfeld-roames, J., Irons, Z. H., & Burdine, R. D. (2020). Left-right asymmetric heart jogging increases the robustness of dextral heart looping in zebrafish. *Developmental Biology*, *459*(2), 79–86. https://doi.org/10.1016/j.ydbio.2019.11.012

Gripp, K. W., Hopkins, E., Jenny, K., Thacker, D., & Salvin, J. (2013). Cardiac Anomalies in Axenfeld – Rieger Syndrome Due to a Novel FOXC1 Mutation. *American Journal of Medical Genetics. Part A*, *161A*(1), 114–119. https://doi.org/10.1002/ajmg.a.35697

Grootjans, J. J., Reekmans, G., Ceulemans, H., & David, G. (2000). Syntenin-syndecan binding requires syndecan-synteny and the co-operation of both PDZ domains of syntenin. *The Journal of Biological Chemistry*, *275*(26), 19933–19941. https://doi.org/10.1074/jbc.M002459200

György, B., Szabó, T. G., Pásztói, M., Pál, Z., Misják, P., Aradi, B., László, V., Pállinger, E., Pap, E., Kittel, A., Nagy, G., Falus, A., & Buzás, E. I. (2011). Membrane vesicles , current state-of-the-art : emerging role of extracellular vesicles. *Cellular and Molecular Life Sciences : CMLS*, *68*(16), 2667–2688. https://doi.org/10.1007/s00018-011-0689-3

Halbert, S. A., Patton, D. L., Zarutskie, P. W., & Soules, M. R. (1997). Function and structure of cilia in the Fallopian tube of an infertile woman with Kartagener's syndrome. *Human Reproduction (Oxford, England)*, *12*(1), 55–58. https://doi.org/10.1093/humrep/12.1.55

Hamasaki, T., Barkalow, K., Richmond, J., & Satir, P. (1991). cAMP-stimulated phosphorylation of an axonemal polypeptide that copurifies with the 22S dynein arm regulates microtubule translocation velocity and swimming speed in Paramecium. *Proceedings of the National Academy of Sciences of the United States of America*, *88*(18), 7918–7922. https://doi.org/10.1073/pnas.88.18.7918

Hanaoka, K., Qian, F., Boletta, A., Bhunia, A. K., Piontek, K., Tsiokas, L., Sukhatme, V. P., Guggino, W. B., & Germino, G. G. (2000). Co-assembly of polycystin-1 and -2 produces unique cation-permeable currents. *Nature*, *408*(6815), 990–994. https://doi.org/10.1038/35050128

Hashimoto, H., Rebagliati, M., Ahmad, N., Muraoka, O., Kurokawa, T., Hibi, M., & Suzuki, T. (2004). The Cerberus/Dan-family protein Charon is a negative regulator of Nodal signaling during left-right patterning in zebrafish. *Development (Cambridge, England)*, *131*(8), 1741–1753. https://doi.org/10.1242/dev.01070

Hashimoto, M., Shinohara, K., Wang, J., Ikeuchi, S., Yoshiba, S., Meno, C., Nonaka, S., Takada, S., Hatta, K., Wynshaw-boris, A., & Hamada, H. (2010). Planar polarization of node cells determines the rotational axis of node cilia. *Nature Cell Biology*, *12*(2), 170–176. https://doi.org/10.1038/ncb2020

Hessvik, N. P., & Llorente, A. (2018). Current knowledge on exosome biogenesis and release. *Cellular and Molecular Life Sciences : CMLS*, *75*(2), 193–208. https://doi.org/10.1007/s00018-017-2595-9

Hibino, T., Ishii, Y., Levin, M., & Nishino, A. (2006). Ion flow regulates left – right asymmetry in sea urchin development. *Development Genes and Evolution*, *216*(5), 265–276. https://doi.org/10.1007/s00427-005-0051-6

Hilfinger, A., & Julicher, F. (2008). The chirality of ciliary beats. *Physical Biology*, *5*(1), 016003. https://doi.org/10.1088/1478-3975/5/1/016003

Horani, A., Brody, S. L., Ferkol, T. W., Shoseyov, D., Wasserman, M. G., Ta-shma, A., Wilson, K. S., Bayly, P. V, Amirav, I., Cohen-cymberknoh, M., Dutcher, S. K., Elpeleg, O., & Kerem, E. (2013). CCDC65 Mutation Causes Primary Ciliary Dyskinesia with Normal Ultrastructure and Hyperkinetic Cilia. *PloS One*, *8*(8), e72299. https://doi.org/10.1371/journal.pone.0072299

Horani, A., Druley, T. E., Zariwala, M. A., Patel, A. C., Levinson, B. T., Arendonk, L. G. Van, Thornton, K. C., Giacalone, J. C., Albee, A. J., Wilson, K. S., Turner, E. H., Nickerson, D. A., Shendure, J., Bayly, P. V, Leigh, M. W., Knowles, M. R., Brody, S. L., Dutcher, S. K., & Ferkol, T. W. (2012). Whole-Exome Capture and Sequencing Identifies HEATR2 Mutation as a Cause of Primary Ciliary Dyskinesia. *The American Journal of Human Genetics*, *91*(4), 685–693. https://doi.org/10.1016/j.ajhg.2012.08.022

Horani, A., Ferkol, T. W., Dutcher, S., & Brody, S. L. (2016). Genetics and biology of primary ciliary dyskinesia. *Paediatric Respiratory Reviews*, *18*, 18–24. https://doi.org/10.1016/bs.mcb.2015.01.016.Observing

Hori, K., Sen, A., & Artavanis-Tsakonas, S. (2013). Notch signaling at a glance. *Journal of Cell Science*, *126*(10), 2135–2140. https://doi.org/10.1242/jcs.127308

Horne-Badovinac, S., Rebagliati, M., & Stainier, D. Y. (2003). A Cellular Framework for Gut-Looping Morphogenesis in Zebrafish. *Science (New York, N.Y.)*, *302*(5645), 662–665. https://doi.org/10.1126/science.1085397

Hristov, M., Erl, W., Linder, S., & Weber, P. C. (2004). Apoptotic bodies from endothelial cells enhance the number and initiate the differentiation of human endothelial progenitor cells in vitro. *Blood*, *104*(9), 2761–2766. https://doi.org/10.1182/blood-2003-10-3614.Supported

Hsu, C., Morohashi, Y., Yoshimura, S., Manrique-hoyos, N., Jung, S., Lauterbach, M. A., Bakhti, M., Grønborg, M., Möbius, W., Rhee, J., Barr, F. A., & Simons, M. (2010). Regulation of exosome secretion by Rab35 and its GTPase-activating proteins TBC1D10A–C. *The Journal of Cell Biology*, *189*(2), 223–232. https://doi.org/10.1083/jcb.200911018

Huangfu, D., Liu, A., Rakeman, A. S., & Murcia, N. S. (2003). Hedgehog signalling in the mouse requires intraflagellar transport proteins. *Nature*, *426*(6962), 83–87. https://doi.org/10.1038/nature02080.1.

Hummel, K. P., & Chapman, D. (1956). Situs viscerum inversus. *Mouse News Lett*, *14*, 21.

Ichikawa, M., Liu, D., Kastritis, P. L., Basu, K., Hsu, T. C., Yang, S., & Bui, K. H. (2017). Subnanometre-resolution structure of the doublet microtubule reveals new classes of microtubule- associated proteins. *Nature Communications*, *8*(15035), 1–12. https://doi.org/10.1038/ncomms15035

Inaba, K. (2015). Calcium sensors of ciliary outer arm dynein: functions and phylogenetic considerations for eukaryotic evolution. *Cilia*, *4*, 6. https://doi.org/10.1186/s13630-015-0015-z

Iraci, N., Leonardi, T., Gessler, F., & Vega, B. (2016). Focus on Extracellular Vesicles : Physiological Role and Signalling Properties of Extracellular Membrane Vesicles. *International Journal of Molecular Sciences*, *17*(2), 171. https://doi.org/10.3390/ijms17020171

Ishikawa, H., & Marshall, W. F. (2011). Ciliogenesis: building the cell's antenna. *Nature Reviews. Molecular Cell Biology*, *12*(4), 222–234. https://doi.org/10.1038/nrm3085

Ishikawa, T. (2017). Axoneme structure from motile cilia. *Cold Spring Harbor Perspectives in Biology*,

9(1), a028076. https://doi.org/10.1101/cshperspect.a028076

Jacinto, R., Sampaio, P., Roxo-Rosa, M., Pestana, S., & Lopes, S. S. (2021). Pkd2 Affects Cilia Length and Impacts LR Flow Dynamics and Dand5. *Frontiers in Cell and Developmental Biology*, *9*, 624531. https://doi.org/10.3389/fcell.2021.624531

Jackson, C. L., Behan, L., Collins, S. A., Goggin, P. M., Adam, E. C., Coles, J. L., Evans, H. J., Harris, A., Lackie, P., Packham, S., Page, A., Thompson, J., Walker, W. T., Kuehni, C., & Lucas, J. S. (2016). Accuracy of diagnostic testing in primary ciliary dyskinesia. *The European Respiratory Journal*, *47*(3), 837–848. https://doi.org/10.1183/13993003.00749-2015

Jaffe, K. M., Grimes, D. T., Schottenfeld-Roames, J., Werner, M. E., Ku, T. S. J., Kim, S. K., Pelliccia, J. L., Morante, N. F. C., Mitchell, B. J., & Burdine, R. D. (2016). C21orf59/kurly Controls Both Cilia Motility and Polarization. *Cell Reports*, *14*(8), 1841–1849. https://doi.org/10.1016/j.celrep.2016.01.069

Jain, R., Javidan-Nejad, C., Alexander-Brett, J., Horani, A., Cabellon, M. C., Walter, M. J., & Brody, S. L. (2012). Sensory functions of motile cilia and implication for bronchiectasis. *Frontiers in Bioscience (Scholar Edition)*, *4*(3), 1088–1098. https://doi.org/10.2741/S320

Jászai, J., Thamm, K., Karbanová, X. J., Janich, P., Fargeas, C. A., Huttner, W. B., & Corbeil, D. (2020). Prominins control ciliary length throughout the animal kingdom : New lessons from human prominin-1 and zebrafish prominin-3. *The Journal of Biological Chemistry*, *295*(18), 6007–6022. https://doi.org/10.1074/jbc.RA119.011253

Ji, Y., Buel, S. M., & Amack, J. D. (2016). Mutations in zebrafish pitx2 model congenital malformations in Axenfeld-Rieger syndrome but do not disrupt left-right placement of visceral organs. *Developmental Biology*, *416*(1), 69–81. https://doi.org/10.1016/j.ydbio.2016.06.010

Jin, S. C., Homsy, J., Zaidi, S., Lu, Q., Morton, S., Depalma, S. R., Zeng, X., Qi, H., Chang, W., Sierant, M. C., Hung, W., Haider, S., Zhang, J., Knight, J., Bjornson, R. D., Castaldi, C., Tikhonoa, I. R., Bilguvar, K., Mane, S. M., … Brueckner, M. (2017). Contribution of rare inherited and de novo variants in 2,871 congenital heart disease probands. *Nature Publishing Group*, *49*(11), 1593–1601. https://doi.org/10.1038/ng.3970

Jin, X., Mohieldin, A. M., Muntean, B. S., Green, J. A., Shah, J. V, Mykytyn, K., & Nauli, S. M. (2014). Cilioplasm is a cellular compartment for calcium signaling in response to mechanical and chemical stimuli. *Cellular and Molecular Life Sciences : CMLS*, *71*(11), 2165–2178. https://doi.org/10.1007/s00018-013-1483-1

Juan, T., & Fürthauer, M. (2017). Biogenesis and function of ESCRT-dependent extracellular vesicles. *Seminars in Cell and Developmental Biology*, *74*, 66–77. https://doi.org/10.1016/j.semcdb.2017.08.022

Juan, T., Géminard, C., Coutelis, J. B., Cerezo, D., Polès, S., Noselli, S., & Fürthauer, M. (2018). Myosin1D is an evolutionarily conserved regulator of animal left-right asymmetry. *Nature Communications*, *9*(1). https://doi.org/10.1038/s41467-018-04284-8

Jurynec, M. J., Xia, R., Mackrill, J. J., Gunther, D., Crawford, T., Flanigan, K. M., Abramson, J. J., Howard, M. T., & Grunwald, D. J. (2008). Selenoprotein N is required for ryanodine receptor calcium release channel activity in human and zebrafish muscle. *Proceedings of the National Academy of Sciences of*

the United States of America, *105*(34), 12485–12490. https://doi.org/10.1073/pnas.0806015105

Kajimoto, T., Okada, T., Miya, S., Zhang, L., & Nakamura, S. (2013). Ongoing activation of sphingosine 1-phosphate receptors mediates maturation of exosomal multivesicular endosomes. *Nature Communications*, *4*, 2712. https://doi.org/10.1038/ncomms3712

Kakarla, R., Hur, J., Kim, Y. J., Kim, J., & Chwae, Y. (2020). Apoptotic cell-derived exosomes : messages from dying cells. *Experimental & Molecular Medicine*, *52*(1), 1–6. https://doi.org/10.1038/s12276-019-0362-8

Kamiya, R., Kurimoto, E., & Muto, E. (1991). Two types of Chlamydomonas flagellar mutants missing different components of inner-arm dynein. *The Journal of Cell Biology*, *112*(3), 441–447. https://doi.org/10.1083/jcb.112.3.441

Kamura, K., Kobayashi, D., Uehara, Y., Koshida, S., Iijima, N., Kudo, A., Yokoyama, T., & Takeda, H. (2011). Pkd1l1 complexes with Pkd2 on motile cilia and functions to establish the left-right axis. *Development (Cambridge, England)*, *138*(6), 1121–1129. https://doi.org/10.1242/dev.058271

Karcher, C., Fischer, A., Schweickert, A., Bitzer, E., Horie, S., Witzgall, R., & Blum, M. (2005). Lack of a laterality phenotype in Pkd1 knock-out embryos correlates with absence of polycystin-1 in nodal cilia. *Differentiation; Research in Biological Diversity*, *73*(8), 425–432. https://doi.org/10.1111/j.1432-0436.2005.00048.x

Kartagener, M. (1933). Zur Pathogenese der Bronchiektasien. Bronchiektasien bei situs inversus viscerum. *Beitr Klin Tuberk*, *83*, 489–501.

Kawakami, Y., Raya, A., Raya, R. M., Rodríguez-Esteban, C., & Izpisúa Belmonte, J. C. (2005). Retinoic acid signalling links left – right asymmetric patterning and bilaterally symmetric somitogenesis in the zebrafish embryo. *Nature*, *435*(7039), 165–171. https://doi.org/10.1038/nature03512

Kawasumi, A., Nakamura, T., Iwai, N., Yashiro, K., Saijoh, Y., Belo, J. A., Shiratori, H., & Hamada, H. (2011). Left-right asymmetry in the level of active Nodal protein produced in the node is translated into left-right asymmetry in the lateral plate of mouse embryos. *Developmental Biology*, *353*(2), 321–330. https://doi.org/10.1016/j.ydbio.2011.03.009

Keda, T., Inamori, K., Kawanishi, T., & Takeda, H. (2022). Reemployment of Kupffer's vesicle cells into axial and paraxial mesoderm via transdifferentiation. *Development, Growth & Differentiation*, *64*(3), 163–177. https://doi.org/10.1111/dgd.12774

Kempeneers, C., Seaton, C., Garcia Espinosa, B., & Chilvers, M. A. (2019). Ciliary functional analysis : Beating a path towards standardization. *Pediatric Pulmonology*, *54*(10), 1627–1638. https://doi.org/10.1002/ppul.24439

Kennedy, M. P., Omran, H., Leigh, M. W., Dell, S., Morgan, L., Molina, P. L., Robinson, B. V, Minnix, S. L., Olbrich, H., Severin, T., Ahrens, P., Lange, L., Morillas, H. N., Noone, P. G., Zariwala, M. A., & Knowles, M. R. (2007). Congenital Heart Disease and Other Heterotaxic Defects in a Large Cohort of Patients With Primary Ciliary Dyskinesia. *Circulation*, *115*, 2814–2821. https://doi.org/10.1161/CIRCULATIONAHA.106.649038

Kikuchi, T., Takasaka, T., Tonosaki, A., & Watanabe, H. (1989). Fine Structure of Guinea Pig Vestibular Kinocilium. *Acta Oto-Laryngologica*, *108*(1–2), 26–30. https://doi.org/10.3109/00016488909107388

Kim, J., Bae, S., Lee, H. S., Park, J., & Kim, K. (2017). Claudin5a is required for proper inflation of Kupffer ' s vesicle lumen and organ laterality. *PloS One*, *12*(8), e0182047. https://doi.org/10.1371/journal.pone.0182047

King, S. M. (2016). Axonemal Dynein Arms. *Cold Spring Harbor Perspectives in Biology*, *8*(11), a028100. https://doi.org/10.1101/cshperspect.a028100

Kirichok, Y., Navarro, B., & Clapham, D. E. (2006). Whole-cell patch-clamp measurements of spermatozoa reveal an alkaline-activated Ca2+ channel. *Nature*, *439*, 737–740. https://doi.org/10.1038/nature04417

Kitajima, K., Oki, S., Ohkawa, Y., Sumi, T., & Meno, C. (2013). Wnt signaling regulates left – right axis formation in the node of mouse embryos. *Developmental Biology*, *380*(2), 222–232. https://doi.org/10.1016/j.ydbio.2013.05.011

Knowles, M. R., Ostrowski, L. E., Leigh, M. W., Sears, P. R., Davis, S. D., Wolf, W. E., Hazucha, M. J., Carson, J. L., Olivier, K. N., Sagel, S. D., Rosenfeld, M., Ferkol, T. W., Dell, S. D., Milla, C. E., Randell, S. H., Yin, W., Sannuti, A., Metjian, H. M., Noone, P. G., … Zariwala, M. A. (2014). Mutations in RSPH1 Cause Primary Ciliary Dyskinesia with a Unique Clinical and Ciliary Phenotype. *American Journal of Respiratory and Critical Care Medicine*, *189*(6), 707–717. https://doi.org/10.1164/rccm.201311-2047OC

Kobbernagel, H. E., Buchvald, F. F., Haarman, E. G., Casaulta, C., Collins, S. A., Hogg, C., Kuehni, C. E., Lucas, J. S., Moser, C. E., Quittner, A. L., Raidt, J., Rosthøj, S., Sørensen, A. L., Thomsen, K., Werner, C., Omran, H., & Nielsen, K. G. (2020). Efficacy and safety of azithromycin maintenance therapy in primary ciliary dyskinesia (BESTCILIA): a multicentre , double-blind , randomised , placebo-controlled phase 3 trial. *The Lancet. Respiratory Medicine*, *8*(5), 493–505. https://doi.org/10.1016/S2213-2600(20)30058-8

Kopan, R., & Ilagan, M. X. G. (2009). The Canonical Notch Signaling Pathway: Unfolding the Activation Mechanism. *Cell*, *137*(2), 216–233. https://doi.org/10.1016/j.cell.2009.03.045

Kosaki, K., Bassi, M. T., Kosaki, R., Lewin, M., Belmont, J., Schauer, G., & Casey, B. (1999). Characterization and Mutation Analysis of Human LEFTY A and LEFTY B , Homologues of Murine Genes Implicated in Left-Right Axis Development. *American Journal of Human Genetics*, *64*(3), 712–721. https://doi.org/10.1086/302289

Kouis, P., Yiallouros, P. K., Middleton, N., Evans, J. S., Kyriacou, K., & Papatheodorou, S. (2017). Prevalence of primary ciliary dyskinesia in consecutive referrals of suspect cases and the transmission electron microscopy detection rate: a systematic review and meta-analysis. *Pediatric Research*, *81*(3), 398–405. https://doi.org/10.1038/pr.2016.263

Kramer-Zucker, A. G., Olale, F., Haycraft, C. J., Yoder, B. K., Schier, A. F., & Drummond, I. A. (2005). Cilia-driven fluid flow in the zebrafish pronephros, brain and Kupffer's vesicle is required for normal organogenesis. *Development (Cambridge, England)*, *132*(8), 1907–1921. https://doi.org/10.1242/dev.01772

Krebs, L. T., Iwai, N., Nonaka, S., Welsh, I. C., Lan, Y., Jiang, R., Saijoh, Y., Brien, T. P. O., Hamada, H., & Gridley, T. (2003). Notch signaling regulates left – right asymmetry determination by inducing Nodal expression. *Genes & Development*, *17*(10), 1207–1212. https://doi.org/10.1101/gad.1084703.(3)

Kreiling, J. A., Prabhat, Williams, G., & Creton, R. (2007). Analysis of Kupffer's vesicle in zebrafish embryos using a cave automated virtual environment. *Developmental Dynamics : An Official Publication of the American Association of Anatomists*, *236*(7), 1963–1969. https://doi.org/10.1002/dvdy.21191

Kuehni, C. E., Frischer, T., Strippoli, M. P., Maurer, E., Bush, A., Nielsen, K. G., Escribano, A., Lucas, J. S., Yiallouros, P., Omran, H., Eber, E., O'Callaghan, C., Snijders, D., & Barbato, A. (2010). Factors influencing age at diagnosis of primary ciliary dyskinesia in European children. *The European Respiratory Journal*, *36*(6), 1248–1258. https://doi.org/10.1183/09031936.00001010

Kuhns, S., Seixas, C., Pestana, S., Tavares, B., Nogueira, R., Jacinto, R., Ramalho, J. S., Simpson, J. C., Andersen, J. S., Echard, A., Lopes, S. S., Barral, D. C., & Blacque, O. E. (2019). Rab 35 controls cilium length , function and membrane composition. *EMBO Reports*, *20*(10), e47625. https://doi.org/10.15252/embr.201847625

Kultgen, P. L., Byrd, S. K., Ostrowski, L. E., & Milgram, S. L. (2002). Characterization of an A-Kinase Anchoring Protein in Human Ciliary Axonemes. *Molecular Biology of the Cell*, *13*, 4156–4166. https://doi.org/10.1091/mbc.E02

Kwok, Z. H., Wang, C., & Jin, Y. (2021). Extracellular vesicle transportation and uptake by recipient cells: A critical process to regulate human diseases. *Processes (Basel, Switzerland)*, *9*(2), 273. https://doi.org/10.3390/pr9020273

Lansley, A. B., Sanderson, M. J., & Dirksen, E. R. (1992). Control of the beat cycle of respiratory tract cilia by Ca2+ and cAMP. *The American Journal of Physiology*, *263*(2 Pt 1), L232-42. https://doi.org/10.1152/ajplung.1992.263.2.L232

Layton, W. M. (1976). Random determination of a developmental process: reversal of normal visceral asymmetry in the mouse. *The Journal of Heredity*, *67*(6), 336–338. https://doi.org/10.1093/oxfordjournals.jhered.a108749

Lee, J., & Anderson, K. (2008). Morphogenesis of the Node and Notochord : The Cellular Basis for the Establishment and Maintenance of Left – Right Asymmetry in the Mouse. *Developmental Dynamics : An Official Publication of the American Association of Anatomists*, *237*(12), 3464–3476. https://doi.org/10.1002/dvdy.21598

Lee, L., & Ostrowski, L. E. (2021). Motile cilia genetics and cell biology : big results from little mice. *Cellular and Molecular Life Sciences*, *78*(3), 769–797. https://doi.org/10.1007/s00018-020-03633-5

Leewenhoeck, A. Van. (1677). Observations, communicated to the publisher by Mr. Antony van Leewenhoeck, in a dutch letter of the 9th Octob. *Philosophical Transactions of the Royal Society of London*, *12*(133).

Leigh, M. W., Ferkol, T. W., Davis, S. D., Lee, H., Rosenfeld, M., Dell, S. D., Sagel, S. D., Milla, C., Olivier, K. N., Sullivan, K. M., Zariwala, M. A., Pittman, J. E., Shapiro, A., Carson, J. L., Krischer, J., Hazucha, M. J., & Knowles, M. R. (2016). Clinical Features and Associated Likelihood of Primary Ciliary Dyskinesia in Children and Adolescents. *Annals of the American Thoracic Society*, *13*(8), 1305–1313. https://doi.org/10.1513/AnnalsATS.201511-748OC

Leitch, C. C., Lodh, S., Prieto-Echagüe, V., Badano, J. L., & Zaghloul, N. A. (2014). Basal body proteins

regulate Notch signaling through endosomal trafficking. *Journal of Cell Science*, *127*(Pt 11), 2407–2419. https://doi.org/10.1242/jcs.130344

Lemberskiy-kuzin, L., Fainshtein, M., Fridman, P., Passwell, E., Braiman, A., & Priel, Z. (2008). Localized cytosolic alkalization and its functional impact in ciliary cells. *Biochimica et Biophysica Acta (BBA) - Molecular Cell Research*, *1783*(6), 1102–1110. https://doi.org/10.1016/j.bbamcr.2008.02.005

Lenhart, K. F., Holtzman, N. G., Williams, J. R., & Burdine, R. D. (2013). Integration of Nodal and BMP Signals in the Heart Requires FoxH1 to Create Left – Right Differences in Cell Migration Rates That Direct Cardiac Asymmetry. *PLoS Genetics*, *9*(1), e1003109. https://doi.org/10.1371/journal.pgen.1003109

Lenhart, K. F., Lin, S.-Y., Titus, T. A., Postlethwait, J. H., & Burdine, R. D. (2011). Two additional midline barriers function with midline lefty1 expression to maintain asymmetric Nodal signaling during left-right axis specification in zebrafish. *Development (Cambridge, England)*, *138*(20), 4405–4410. https://doi.org/10.1242/dev.071092

Levin, M., Johnson, R. L., Stern, C. D., Kuehn, M., & Tabin, C. (1995). Determining Left-Right Asymmetry in Chick Embryogenesis. *Cell*, *82*(5), 803–814. https://doi.org/10.1016/0092-8674(95)90477-8

Levin, M., Pagan, S., Roberts, D. J., Cooke, J., Kuehn, M. R., & Tabin, C. J. (1997). Left/Right Patterning Signals and the Independent Regulation of Different Aspects of Situs in the Chick Embryo. *Developmental Biology*, *189*(1), 57–67. https://doi.org/10.1006/dbio.1997.8662

Levin, M., Thorlin, T., Robinson, K. R., Nogi, T., & Mercola, M. (2002). Asymmetries in H+/K+-ATPase and Cell Membrane Potentials Comprise a Very Early Step in Left-Right Patterning. *Cell*, *111*(1), 77–89. https://doi.org/10.1016/s0092-8674(02)00939-x

Li, A. H., Hanchard, N. A., Azamian, M., Alessandro, L. C. A. D., Coban-akdemir, Z., Lopez, K. N., Hall, N. J., Dickerson, H., Nicosia, A., Fernbach, S., Boone, P. M., Gambin, T., Karaca, E., Gu, S., Yuan, B., Jhangiani, S. N., Doddapaneni, H., Hu, J., Dinh, H., … Belmont, J. W. (2019). Genetic architecture of laterality defects revealed by whole exome sequencing. *European Journal of Human Genetics*, *27*(4), 563–573. https://doi.org/10.1038/s41431-018-0307-z

Li, M., Liao, L., Tian, W., & Gregory, C. (2020). Extracellular Vesicles Derived From Apoptotic Cells : An Essential Link Between Death and Regeneration. *Frontiers in Cell and Developmental Biology*, *8*, 573511. https://doi.org/10.3389/fcell.2020.573511

Liang, J. O., Etheridge, A., Hantsoo, L., Rubinstein, A. L., & Nowak, S. J. (2000). Asymmetric Nodal signaling in the zebrafish diencephalon positions the pineal organ. *Development (Cambridge, England)*, *127*(23), 5101–5112. https://doi.org/10.1242/dev.127.23.5101

Lin, J., & Nicastro, D. (2018). Asymmetric distribution and spatial switching of dynein activity generates ciliary motility. *Science*, *360*(6387), 1–29. https://doi.org/10.1126/science.aar1968.Asymmetric

Lin, Krikov, S., Riehle-Colarusso, T., Frías, J., Belmont, J., Anderka, M., Geva, T., Getz, K., & Botto, L. (2014). Laterality defects in the national birth defects prevention study (1998-2007): Birth prevalence and descriptive epidemiology. *American Journal of Medical Genetics. Part A*, *164*(10), 2581–2591. https://doi.org/10.1002/ajmg.a.36695

Lin, Y. W., Nhieu, J., Wei, C. W., Lin, Y. L., Kagechika, H., & Wei, L. N. (2021). Regulation of exosome

secretion by cellular retinoic acid binding protein 1 contributes to systemic anti-inflammation. *Cell Communication and Signaling*, *19*(1), 69. https://doi.org/10.1186/s12964-021-00751-w

Lipson, E. J., Ivonnet, P. I., Lipson, E. J., Ivonnet, P. I., & Bookman, J. (1997). Muscarinic signaling in ciliated tracheal epithelial cells : dual effects on Ca2 + and ciliary beating. *The American Journal of Physiology*, *272*(2 Pt 1), L301–L310. https://doi.org/10.1152/ajplung.1997.272.2.L301

Liu, J., Zhu, C., Ning, G., Yang, L., Cao, Y., & Id, S. H. (2019). Chemokine signaling links cell-cycle progression and cilia formation for left – right symmetry breaking. *PLoS Biology*, *17*(8), e3000203. https://doi.org/10.1371/journal.pbio.3000203

Liu, Y., & Semina, E. V. (2012). pitx2 Deficiency Results in Abnormal Ocular and Craniofacial Development in Zebrafish. *PloS One*, *7*(1), e30896. https://doi.org/10.1371/journal.pone.0030896

Liu, Z., Nguyen, Q. P. H., Guan, Q., Albulescu, A., Erdman, L., Mahdaviyeh, Y., Kang, J., Ouyang, H., Hegele, R. G., Moraes, T., Goldenberg, A., Dell, S. D., & Mennella, V. (2020). A quantitative super-resolution imaging toolbox for diagnosis of motile ciliopathies. *Science Translational Medicine*, *12*(535), eaay0071. https://doi.org/10.1126/scitranslmed.aay0071

Long, S., Ahmad, N., & Rebagliati, M. (2003). The zebrafish nodal-related gene southpaw is required for visceral and diencephalic left-right asymmetry. *Development (Cambridge, England)*, *130*(11), 2303–2316. https://doi.org/10.1242/dev.00436

Lopes, S. S., Lourenço, R., Pacheco, L., Moreno, N., Kreiling, J., & Saúde, L. (2010). Notch signalling regulates left-right asymmetry through ciliary length control. *Development (Cambridge, England)*, *137*(21), 3625–3632. https://doi.org/10.1242/dev.054452

Lorenzo, I. M., Liedtke, W., Sanderson, M. J., & Valverde, M. A. (2008). TRPV4 channel participates in receptor-operated calcium entry and ciliary beat frequency regulation in mouse airway epithelial cells. *Proceedings of the National Academy of Sciences of the United States of America*, *105*(34), 12611–12616. https://doi.org/10.1073/pnas.0803970105

Lowe, L. A., Supp, D. M., Sampath, K., Yokoyama, T., Wright, C. V., Potter, S. S., Overbeek, P., & Kuehn, M. R. (1996). Conserved left-right asymmetry of nodal expression and alterations in murine situs inversus. *Nature*, *381*(6578), 158–161. https://doi.org/10.1038/381158a0

Lucas, J. S., Barbato, A., Collins, S. A., Goutaki, M., Behan, L., Caudri, D., Dell, S., Eber, E., Escudier, E., Hirst, R. A., Hogg, C., Jorissen, M., Latzin, P., Legendre, M., Leigh, M. W., Midulla, F., Nielsen, K. G., Omran, H., Papon, J. F., … Kuehni, C. E. (2017). European Respiratory Society guidelines for the diagnosis of primary ciliary dyskinesia. *The European Respiratory Journal*, *49*(1), 1601090. https://doi.org/10.1183/13993003.01090-2016

Lucas, J. S., Burgess, A., Mitchison, H. M., Moya, E., Williamson, M., & Hogg, C. (2014). Diagnosis and management of primary ciliary dyskinesia. *Archives of Disease in Childhood*, *99*(9), 850–856. https://doi.org/10.1136/archdischild-2013-304831

Lustig, K. D., Kroll, K., Sun, E., Ramos, R., Elmendorf, H., & Kirschner, M. W. (1996). A Xenopus nodal-related gene that acts in synergy with noggin to induce complete secondary axis and notochord formation. *Development (Cambridge, England)*, *122*(10), 3275–3282. https://doi.org/10.1242/dev.122.10.3275

Ma, W., Silberberg, S. D., & Priel, Z. (2002). Distinct axonemal processes underlie spontaneous and stimulated airway ciliary activity. *Journal of General Physiology*, *120*(6), 875–885. https://doi.org/10.1085/jgp.20028695

Maerker, M., Getwan, M., Dowdle, M. E., McSheene, J. C., Gonzalez, V., Pelliccia, J. L., Hamilton, D. S., Yartseva, V., Vejnar, C., Tingler, M., Minegishi, K., Vick, P., Giraldez, A. J., Hamada, H., Burdine, R. D., Sheets, M. D., Blum, M., & Schweickert, A. (2021). Bicc1 and Dicer regulate left-right patterning through post-transcriptional control of the Nodal inhibitor Dand5. *Nature Communications*, *12*(1), 1–15. https://doi.org/10.1038/s41467-021-25464-z

Mallick, R. L., Kumari, S., Singh, N., Sonkar, V. K., & Dash, D. (2015). Cell Calcium Prion protein fragment (106 – 126) induces prothrombotic state by raising platelet intracellular calcium and microparticle release. *Cell Calcium*, *57*(4), 300–311. https://doi.org/10.1016/j.ceca.2015.02.002

Marques, S., Borges, A. C., Silva, A. C., Freitas, S., Cordenonsi, M., & Belo, J. A. (2004). The activity of the Nodal antagonist Cerl-2 in the mouse node is required for correct L/R body axis. *Genes & Development*, *18*(19), 2342–2347. https://doi.org/10.1101/gad.306504.2342

Marshall, C. R., Scherer, S. W., Zariwala, M. A., Lau, L., Paton, T. A., Stockley, T., Jobling, R. K., Ray, P. N., Knowles, M. R., Consortium, F. C., Hall, D. A., Dell, S. D., & Kim, R. H. (2015). Whole-Exome Sequencing and Targeted Copy Number Analysis in Primary Ciliary Dyskinesia. *G3: Genes, Genomes, Genetics*, *5*(8), 1775–1781. https://doi.org/10.1534/g3.115.019851

Marthin, J., & Nielsen, K. (2011). Choice of nasal nitric oxide technique as first-line test for primary ciliary dyskinesia. *The European Respiratory Journal*, *37*(3), 559–565. https://doi.org/10.1183/09031936.00032610

Marthin, J., & Nielsen, K. (2013). Hand-Held Tidal Breathing Nasal Nitric Oxide Measurement - A Promising Targeted Case-Finding Tool for the Diagnosis of Primary Ciliary Dyskinesia. *PLoS ONE*, *8*(2), e57262. https://doi.org/10.1371/journal.pone.0057262

Martinů, V., Bořek-Dohalská, L., Varényiová, Ž., Uhlík, J., Čapek, V., Pohunek, P., & Koucký, V. (2021). Evaluation of a clinical index as a predictive tool for primary ciliary dyskinesia. *Diagnostics*, *11*, 1088. https://doi.org/10.3390/diagnostics11061088

Matsui, T., Thitamadee, S., Murata, T., Kakinuma, H., Nabetani, T., & Hirabayashi, Y. (2011). Canopy1, a positive feedback regulator of FGF signaling , controls progenitor cell clustering during Kupffer ' s vesicle organogenesis. *Proceedings of the National Academy of Sciences of the United States of America*, *108*(24), 9881–9886. https://doi.org/10.1073/pnas.1017248108

McGrath, J., Somlo, S., Makova, S., Tian, X., & Brueckner, M. (2003). Two populations of node monocilia initiate left-right asymmetry in the mouse. *Cell*, *114*(1), 61–73. https://doi.org/10.1016/S0092-8674(03)00511-7

Melby, A. E., Warga, R. M., & Kimmel, C. B. (1996). Specification of cell fates at the dorsal margin of the zebrafish gastrula. *Development (Cambridge, England)*, *122*(7), 2225–2237. https://doi.org/10.1242/dev.122.7.2225

Menco, B. P. M. (1984). Ciliated and microvillous structures of rat olfactory and nasal respiratory epithelia A study using ultra-rapid cryo-fixation followed by freeze-substitution or freeze-etching. *Cell*

and Tissue Research, *235*(2), 225–241. https://doi.org/10.1007/BF00217846

Meno, C., Saijoh, Y., Fujii, H., Ikeda, M., Yokoyama, T., Yokoyama, M., Toyoda, Y., & Hamada, H. (1996). Left-right asymmetric expression of the TGF beta-family member lefty in mouse embryos. *Nature*, *381*(6578), 151–155. https://doi.org/10.1038/381151a0

Meno, C., Shimono, A., Saijoh, Y., Yashiro, K., Mochida, K., Ohishi, S., Noji, S., Kondoh, H., & Hamada, H. (1998). lefty-1 Is Required for Left-Right Determination as a Regulator of lefty-2 and nodal. *Cell*, *94*(3), 287–297. https://doi.org/10.1016/s0092-8674(00)81472-5

Meno, C., Takeuchi, J., Sakuma, R., Koshiba-takeuchi, K., Ohishi, S., Saijoh, Y., Miyazaki, J., Dijke, P., Ogura, T., & Hamada, H. (2001). Diffusion of Nodal Signaling Activity in the Absence of the Feedback Inhibitor Lefty2. *Developmental Cell*, *1*(1), 127–138. https://doi.org/10.1016/s1534-5807(01)00006-5

Miller, M. R., Kenny, S. J., Mannowetz, N., Mansell, S. A., Wojcik, M., Mendoza, S., Zucker, R. S., Xu, K., & Lishko, P. V. (2018). Asymmetrically Positioned Flagellar Control Units Regulate Human Sperm Rotation. *Cell Reports*, *24*(10), 2606–2613. https://doi.org/10.1016/j.celrep.2018.08.016

Mills, J. C., Stone, N. L., Erhardt, J., & Pittman, R. N. (1998). Apoptotic membrane blebbing is regulated by myosin light chain phosphorylation. *The Journal of Cell Biology*, *140*(3), 627–636. https://doi.org/10.1083/jcb.140.3.627

Miyazaki, Y., Nomura, S., Miyake, T., Kagawa, H., Kitada, C., Taniguchi, H., Komiyama, Y., Fujimura, Y., Ikeda, Y., & Fukuhara, S. (1996). High shear stress can initiate both platelet aggregation and shedding of procoagulant containing microparticles. *Blood*, *88*(9), 3456–3464. https://doi.org/10.1182/blood.v88.9.3456.bloodjournal8893456

Mizuno, K., Shiozawa, K., Katoh, T. A., Minegishi, K., Ide, T., Ikawa, Y., Nishimura, H., Takaoka, K., Itabashi, T., Iwane, A. H., Nakai, J., Shiratori, H., & Hamada, H. (2020). Role of Ca2+ transients at the node of the mouse embryo in breaking of left-right symmetry. *Science Advances*, *6*(30). https://doi.org/10.1126/sciadv.aba1195

Mochizuki, T., Saijoh, Y., Tsuchiya, K., Shirayoshi, Y., Takai, S., Taya, C., Yonekawa, H., Yamada, K., Nihei, H., Nakatsuji, N., Overbeek, P. A., Hamada, H., & Yokoyama, T. (1998). Cloning of inv, a gene that controls left/right asymmetry and kidney development. *Nature*, *395*(6698), 177–181. https://doi.org/10.1038/26006

Montague, T. G., Gagnon, J. A., & Schier, A. F. (2018). Conserved regulation of nodal-mediated left-right patterning in zebrafish and mouse. *Development (Cambridge, England)*, *145*(24), dev171090. https://doi.org/10.1242/dev.171090

Montenegro-Johnson, T. D., Baker, D. I., Smith, D. J., & Lopes, S. S. (2016). Three-dimensional flow in Kupffer's Vesicle. *Journal of Mathematical Biology*, *73*(3), 705–725. https://doi.org/10.1007/s00285-016-0967-7

Moreno-Ayala, R., Olivares-Chauvet, P., Schäfer, R., & Junker, J. P. (2021). Variability of an Early Developmental Cell Population Underlies Stochastic Laterality Defects. *Cell Reports*, *34*(2), 108606. https://doi.org/10.1016/j.celrep.2020.108606

Morgan, D., Turnpenny, L., Goodship, J., Dai, W., Majumder, K., Matthews, L., Gardner, A., Schuster, G., Vien, L., Harrison, W., Elder, F. F. B., Penman-splitt, M., Overbeek, P., & Strachan, T. (1998).

Inversin, a novel gene in the vertebrate left-right axis pathway , is partially deleted in the inv mouse. *Nature Genetics*, *20*(2), 149–156. https://doi.org/10.1038/2450

Morris, R. L., & Scholey, J. M. (1997). Heterotrimeric kinesin-II is required for the assembly of motile 9+2 ciliary axonemes on sea urchin embryos. *The Journal of Cell Biology*, *138*(5), 1009–1022. https://doi.org/10.1083/jcb.138.5.1009

Mulcahy, L. A., Pink, R. C., & Carter, D. R. F. (2014). Routes and mechanisms of extracellular vesicle uptake. *Journal of Extracellular Vesicles*, *3*, 10.3402/jev.v3.24641. https://doi.org/10.3402/jev.v3.24641

Müller, P., Rogers, K. W., Jordan, B. M., Lee, J. S., Robson, D., Ramanathan, S., & Schier, A. F. (2012). Differential Diffusivity of Nodal and Lefty Underlies a Reaction-Diffusion Patterning System. *Science (New York, N.Y.)*, *336*(6082), 721–724. https://doi.org/10.1126/science.1221920

Mullowney, T., Manson, D., Kim, R., Stephens, D., Shah, V., & Dell, S. (2014). Primary Ciliary Dyskinesia and Neonatal Respiratory Distress. *Pediatrics*, *134*(6), 1160–1166. https://doi.org/10.1542/peds.2014-0808

Muralidharan-Chari, V., Clancy, J., Plou, C., Romao, M., Chavrier, P., Raposo, G., & D'Souza-Schorey, C. (2009). ARF6-regulated shedding of tumor cell-derived plasma membrane microvesicles. *Current Biology : CB*, *19*(22), 1875–1885. https://doi.org/10.1016/j.cub.2009.09.059.ARF6-regulated

Nabhan, J. F., Hu, R., Oh, R. S., Cohen, S. N., & Lu, Q. (2012). Formation and release of arrestin domain-containing protein 1-mediated microvesicles (ARMMs) at plasma membrane by recruitment of TSG101 protein. *Proceedings of the National Academy of Sciences of the United States of America*, *109*(11), 4146–4151. https://doi.org/10.1073/pnas.1200448109

Nakamura, T., Mine, N., Nakaguchi, E., Mochizuki, A., Yamamoto, M., Yashiro, K., Meno, C., & Hamada, H. (2006). Generation of Robust Left-Right Asymmetry in the Mouse Embryo Requires a Self-Enhancement and Lateral-Inhibition System. *Developmental Cell*, *11*(4), 495–504. https://doi.org/10.1016/j.devcel.2006.08.002

Nakamura, T., Saito, D., Kawasumi, A., Shinohara, K., Asai, Y., Takaoka, K., Dong, F., Takamatsu, A., Belo, J. A., Mochizuki, A., & Hamada, H. (2012). Fluid flow and interlinked feedback loops establish left-right asymmetric decay of Cerl2 mRNA. *Nature Communications*, *3*, 1322. https://doi.org/10.1038/ncomms2319

Nauli, S. M., Alenghat, F. J., Luo, Y., Williams, E., Vassilev, P., Li, X., Elia, A. E. H., Lu, W., Brown, E. M., Quinn, S. J., Ingber, D. E., & Zhou, J. (2003). Polycystins 1 and 2 mediate mechanosensation in the primary cilium of kidney cells. *Nature Genetics*, *33*(2), 129–137. https://doi.org/10.1038/ng1076

Nauli, S. M., Rossetti, S., Kolb, R. J., Alenghat, F. J., Consugar, M. B., Harris, P. C., Ingber, D. E., Loghman-adham, M., & Zhou, J. (2006). Loss of Polycystin-1 in Human Cyst-Lining Epithelia Leads to Ciliary Dysfunction. *Journal of the American Society of Nephrology : JASN*, *17*(4), 1015–1025. https://doi.org/10.1681/ASN.2005080830

Navis, A., & Bagnat, M. (2015). Developing pressures: fluid forces driving morphogenesis. *Current Opinion in Genetics & Development*, *32*, 24–30. https://doi.org/10.1016/j.gde.2015.01.010.Developing

Navis, A., Marjoram, L., & Bagnat, M. (2013). Cftr controls lumen expansion and function of Kupffer's vesicle in zebrafish. *Development (Cambridge, England)*, *140*(8), 1703–1712. https://doi.org/10.1242/dev.091819

Neugebauer, J. M., Amack, J. D., Peterson, A. G., Bisgrove, B. W., & Yost, H. J. (2009). FGF signalling during embryo development regulates cilia length in diverse epithelia. *Nature*, *458*(7238), 651–654. https://doi.org/10.1038/nature07753

Niel, G. Van, Angelo, G. D., & Raposo, G. (2018). Shedding light on the cell biology of extracellular vesicles. *Nature Reviews. Molecular Cell Biology*, *19*(4), 213–228. https://doi.org/10.1038/nrm.2017.125

Noel, E., Verhoeven, M., Lagendijk, A. K., Tessadori, F., Smith, K., Noe, E. S., Choorapoikayil, S., Hertog, J. Den, & Bakkers, J. (2013). A Nodal-independent and tissue-intrinsic mechanism controls heart-looping chirality. *Nature Communications*, *4*, 2754. https://doi.org/10.1038/ncomms3754

Nonaka, S., Shiratori, H., Saijoh, Y., & Hamada, H. (2002). Determination of left-right patterning of the mouse embryo by artificial nodal flow. *Nature*, *418*(6893), 96–99. https://doi.org/10.1038/nature00849

Nonaka, S., Tanaka, Y., Okada, Y., Takeda, S., Harada, A., Kanai, Y., Kido, M., & Hirokawa, N. (1998). Randomization of left-right asymmetry due to loss of nodal cilia generating leftward flow of extraembryonic fluid in mice lacking KIF3B motor protein. *Cell*, *95*(6), 829–837. https://doi.org/10.1016/S0092-8674(00)81705-5

Nonaka, S., Yoshiba, S., Watanabe, D., Ikeuchi, S., & Goto, T. (2005). De Novo Formation of Left – Right Asymmetry by Posterior Tilt of Nodal Cilia. *PLoS Biology*, *3*(8). https://doi.org/10.1371/journal.pbio.0030268

Ocaña, O. H., Coskun, H., Minguillón, C., Murawala, P., Tanaka, E. M., Galcerán, J., Muñoz-chápuli, R., & Nieto, M. A. (2017). A right-handed signalling pathway drives heart looping in vertebrates. *Nature*, *549*(7670), 86–90. https://doi.org/10.1038/nature23454

Oda, T., Yagi, T., & Yanagisawa, H. (2013). Identification of the Outer-Inner Dynein Linker as a Hub Controller for Axonemal Dynein Activities. *Current Biology*, *23*(8), 656–664. https://doi.org/10.1016/j.cub.2013.03.028

Oda, T., Yanagisawa, H., Kamiya, R., & Kikkawa, M. (2014). A molecular ruler determines the repeat length in eukaryotic cilia and flagella. *Science (New York, N.Y.)*, *346*(6211), 857–860. https://doi.org/10.1126/science.1260214

Odate, T., Takeda, S., Narita, K., & Kawahara, T. (2016). 9 + 0 and 9 + 2 cilia are randomly dispersed in the mouse node. *Microscopy (Oxford, England)*, *65*(2), 119–126. https://doi.org/10.1093/jmicro/dfv352

Oh, S. P., & Li, E. (1997). The signaling pathway mediated by the type IIB activin receptor controls axial patterning and lateral asymmetry in the mouse. *Genes & Development*, *11*(14), 1812–1826. https://doi.org/10.1101/gad.11.14.1812

Okabe, N., Xu, B., & Burdine, R. D. (2008). Fluid dynamics in zebrafish Kuppfer's vesicle. *Developmental Dynamics : An Official Publication of the American Association of Anatomists*, *237*(12), 3602–3612.

https://doi.org/10.1002/dvdy.21730.Fluid

Okada, Y., Nonaka, S., Tanaka, Y., Saijoh, Y., Hamada, H., & Hirokawa, N. (1999). Abnormal nodal flow precedes situs inversus in iv and inv mice. *Molecular Cell*, *4*(4), 459–468. https://doi.org/10.1016/S1097-2765(00)80197-5

Okada, Y., Takeda, S., Tanaka, Y., Belmonte, J. C. I., & Hirokawa, N. (2005). Mechanism of nodal flow: A conserved symmetry breaking event in left-right axis determination. *Cell*, *121*(4), 633–644. https://doi.org/10.1016/j.cell.2005.04.008

Oki, S., Kitajima, K., Marques, S., Belo, J. A., Yokoyama, T., Hamada, H., & Meno, C. (2009). Reversal of left-right asymmetry induced by aberrant Nodal signaling in the node of mouse embryos. *Development (Cambridge, England)*, *136*(23), 3917–3925. https://doi.org/10.1242/dev.039305

Olbrich, H., Schmidts, M., Werner, C., Onoufriadis, A., Loges, N. T., Raidt, J., Banki, N. F., Shoemark, A., Burgoyne, T., Al Turki, S., Hurles, M. E., Köhler, G., Schroeder, J., Nürnberg, G., Nürnberg, P., Chung, E. M. K., Reinhardt, R., Marthin, J. K., Nielsen, K. G., … Omran, H. (2012). Recessive HYDIN mutations cause primary ciliary dyskinesia without randomization of left-right body asymmetry. *American Journal of Human Genetics*, *91*(4), 672–684. https://doi.org/10.1016/j.ajhg.2012.08.016

Oliveira, I., Jacinto, R., Pestana, S., Nolasco, F., Calado, J., Lopes, S. S., & Roxo-rosa, M. (2021). Zebrafish Model as a Screen to Prevent Cyst Inflation in Autosomal Dominant Polycystic Kidney Disease. *International Journal of Molecular Sciences*, *22*(16), 9013. https://doi.org/10.3390/ijms22169013

Omori, T., Winter, K., Shinohara, K., Hamada, H., & Ishikawa, T. (2018). Simulation of the nodal flow of mutant embryos with a small number of cilia : comparison of mechanosensing and vesicle transport hypotheses. *Royal Society Open Science*, *5*(8), 180601. https://doi.org/10.1038/ncomms1624

Ostrowski, L. E., Dutcher, S. K., & Lo, C. W. (2011). Cilia and models for studying structure and function. *Proceedings of the American Thoracic Society*, *8*(5), 423–429. https://doi.org/10.1513/pats.201103-027SD

Ostrowski, M., Carmo, N. B., Krumeich, S., Fanget, I., Raposo, G., Savina, A., Moita, C. F., Schauer, K., Hume, A. N., Freitas, R. P., Goud, B., Benaroch, P., Hacohen, N., Fukuda, M., Desnos, C., Seabra, M. C., Darchen, F., Amigorena, S., Moita, L. F., & Thery, C. (2010). Rab27a and Rab27b control different steps of the exosome secretion pathway. *Nature Cell Biology*, *12*(1), 19–30. https://doi.org/10.1038/ncb2000

Oteiza, P., Köppen, M., Concha, M. L., & Heisenberg, C. P. (2008). Origin and shaping of the laterality organ in zebrafish. *Development (Cambridge, England)*, *135*(16), 2807–2813. https://doi.org/10.1242/dev.022228

Oteiza, P., Köppen, M., Krieg, M., Pulgar, E., Farias, C., Melo, C., Preibisch, S., Müller, D., Tada, M., Hartel, S., Heisenberg, C. P., & Concha, M. L. (2010). Planar cell polarity signalling regulates cell adhesion properties in progenitors of the zebrafish laterality organ. *Development (Cambridge, England)*, *137*(20), 3459–3468. https://doi.org/10.1242/dev.049981

Otto, E. A., Schermer, B., Obara, T., O'Toole, J. F., Hiller, K. S., Mueller, A. M., Ruf, R. G., Hoefele, J., Beekmann, F., Landau, D., Foreman, J. W., Goodship, J. A., Strachan, T., Kispert, A., Wolf, M. T., Gagnadoux, M. F., Nivet, H., Antignac, C., Walz, G., … Hildebrandt, F. (2003). Mutations in INVS

encoding inversin cause nephronophthisis type 2, linking renal cystic disease to the function of primary cilia and left-right axis determination. *Nature Genetics*, *34*(4), 413–420. https://doi.org/10.1038/ng1217

Owa, M., Furuta, A., Usukura, J., Arisaka, F., King, S. M., Witman, G. B., Kamiya, R., & Wakabayashi, K. (2014). Cooperative binding of the outer arm-docking complex underlies the regular arrangement of outer arm dynein in the axoneme. *Proceedings of the National Academy of Sciences of the United States of America*, *111*(26), 9461–9466. https://doi.org/10.1073/pnas.1403101111

Pack, R. J., A-ugaily, L. H., Morris, G., & Widdicombe, J. G. (1980). The Distribution and Structure of Cells in the Tracheal Epithelium of the Mouse. *Cell and Tissue Research*, *208*(1), 65–84. https://doi.org/10.1007/BF00234174

Paff, T., Loges, N. T., Aprea, I., Wu, K., Bakey, Z., Haarman, E. G., Daniels, J. M. A., Sistermans, E. A., Bogunovic, N., Dougherty, G. W., Matter, A., Olbrich, H., Werner, C., Pals, G., Ho, I. M., Schmidts, M., Omran, H., & Micha, D. (2017). Mutations in PIH1D3 Cause X-Linked Primary Ciliary Dyskinesia with Outer and Inner Dynein Arm Defects. *American Journal of Human Genetics*, *100*(1), 160–168. https://doi.org/10.1016/j.ajhg.2016.11.019

Papon, J. F., Coste, A., Roudot-Thoraval, F., Boucherat, M., Roger, G., Tamalet, A., Vojtek, A. M., Amselem, S., & Escudier, E. (2010). A 20-year experience of electron microscopy in the diagnosis of primary ciliary dyskinesia. *The European Respiratory Journal*, *35*(5), 1057–1063. https://doi.org/10.1183/09031936.00046209

Park, T. J., Haigo, S. L., & Wallingford, J. B. (2006). Ciliogenesis defects in embryos lacking inturned or fuzzy function are associated with failure of planar cell polarity and Hedgehog signaling. *Nature Genetics*, *38*(3), 303–311. https://doi.org/10.1038/ng1753

Park, T. J., Mitchell, B. J., Abitua, P. B., Kintner, C., & John, B. W. (2008). Dishevelled controls apical docking and planar polarization of basal bodies in ciliated epithelial cells. *Nature Genetics*, *40*(7), 871–879. https://doi.org/10.1038/ng.104.Dishevelled

Pasquet, J., Dachary-prigent, J., & Nurden, A. T. (1996). Calcium influx is a determining factor of calpain activation and microparticle formation in platelets. *European Journal of Biochemistry*, *239*(3), 647–654. https://doi.org/10.1111/j.1432-1033.1996.0647u.x

Pazour, Agrin, N., Leszyk, J., & Witman, G. (2005). Proteomic analysis of a eukaryotic cilium. *The Journal of Cell Biology*, *170*(1), 103–113. https://doi.org/10.1083/jcb.200504008

Pazour, G. J., San Agustin, J. T., Follit, J. A., Rosenbaum, J. L., & Witman, G. B. (2002). Polycystin-2 localizes to kidney cilia and the ciliary level is elevated in orpk mice with polycystic kidney disease. *Current Biology : CB*, *12*(11), 378–380. https://doi.org/10.1016/s0960-9822(02)00877-1

Pazour, G. J., Wilkerson, C. G., & Witman, G. B. (1998). A dynein light chain is essential for the retrograde particle movement of intraflagellar transport (IFT). *The Journal of Cell Biology*, *141*(4), 979–992. https://doi.org/10.1083/jcb.141.4.979

Pelliccia, J. L., Jindal, G. A., & Burdine, R. D. (2017). Gdf3 is required for robust Nodal signaling during germ layer formation and left-right patterning. *ELife*, *6*, e28635. https://doi.org/10.7554/eLife.28635

Pennekamp, P., Karcher, C., Fischer, A., Schweickert, A., Skryabin, B., Horst, J., Blum, M., & Dworniczak,

B. (2002). The ion channel polycystin-2 is required for left-right axis determination in mice. *Current Biology*, *12*(11), 938–943. https://doi.org/10.1016/S0960-9822(02)00869-2

Peterson, A. G., Wang, X., & Yost, H. J. (2013). Dvr1 transfers left – right asymmetric signals from Kupffer's vesicle to lateral plate mesoderm in zebrafish. *Developmental Biology*, *382*(1), 198–208. https://doi.org/10.1016/j.ydbio.2013.06.011

Pietrement, C., Silva, N. Da, Mckee, M., Marshansky, V., Brown, D., & Futai, M. (2006). Distinct Expression Patterns of Different Subunit Isoforms of the V-ATPase in the Rat Epididymis 1. *Biology of Reproduction*, *74*(1), 185–194. https://doi.org/10.1095/biolreprod.105.043752

Pintado, P., Sampaio, P., Tavares, B., Smith, D. J., & Lopes, S. S. (2017). Dynamics of cilia length in left – right development. *Royal Society Open Science*, *4*(3), 161102. http://dx.doi.org/10.1098/rsos.161102

Pintar, A., De Biasio, A., Popovic, M., Ivanova, N., & Pongor, S. (2007). The intracellular region of Notch ligands: does the tail make the difference? *Biology Direct*, *2*, 1–13. https://doi.org/10.1186/1745-6150-2-19

Pogoda, H., Solnica-krezel, L., Driever, W., & Meyer, D. (2000). The zebrafish forkhead transcription factor FoxH1 / Fast1 is a modulator of Nodal signaling required for organizer formation. *Current Biology : CB*, *10*(17), 1041–1049. https://doi.org/10.1016/s0960-9822(00)00669-2

Praetorius, H. A., & Spring, K. R. (2001). Bending the MDCK Cell Primary Cilium Increases Intracellular Calcium. *The Journal of Membrane Biology*, *184*(1), 71–79. https://doi.org/10.1007/s00232-001-0075-4

Price, M. E., & Sisson, J. H. (2019). Redox regulation of motile cilia in airway disease. *Redox Biology*, *27*, 101146. https://doi.org/10.1016/j.redox.2019.101146

Pulgar, E., Schwayer, C., Guerrero, N., López, L., & Concha, M. L. (2021). Apical contacts stemming from incomplete delamination guide progenitor cell allocation through a dragging mechanism. *ELife*, *10*, e66483. https://doi.org/10.7554/eLife.66483

Rachev, E., Schuster-gossler, K., Fuhl, F., Ott, T., Tveriakhina, L., Beckers, A., Hegermann, J., Boldt, K., Mai, M., Kremmer, E., Uef, M., Blum, M., & Gossler, A. (2020). CFAP43 modulates ciliary beating in mouse and Xenopus. *Developmental Biology*, *459*(2), 109–125. https://doi.org/10.1016/j.ydbio.2019.12.010

Rahban, R., & Nef, S. (2020). CatSper: The complex main gate of calcium entry in mammalian spermatozoa. *Molecular and Cellular Endocrinology*, *518*(April), 110951. https://doi.org/10.1016/j.mce.2020.110951

Raidt, J., Wallmeier, J., Hjeij, R., Onnebrink, G., Pennekamp, P., Loges, N. T., Olbrich, H., Ha, K., Dougherty, G. W., Omran, H., & Werner, C. (2014). Ciliary beat pattern and frequency in genetic variants of primary ciliary dyskinesia. *The European Respiratory Journal*, *44*(6), 1579–1588. https://doi.org/10.1183/09031936.00052014

Raidt, J., Werner, C., Menchen, T., Dougherty, G. W., Olbrich, H., Loges, N. T., Schmitz, R., Pennekamp, P., & Omran, H. (2015). Ciliary function and motor protein composition of human fallopian tubes. *Human Reproduction (Oxford, England)*, *30*(12), 2871–2880. https://doi.org/10.1093/humrep/dev227

Rana, N. A., & Haltiwanger, R. S. (2011). Fringe benefits: Functional and structural impacts of O-glycosylation on the extracellular domain of Notch receptors. *Current Opinion in Structural Biology*, *21*(5), 583–589. https://doi.org/10.1016/j.sbi.2011.08.008

Rankin, C. T., Bunton, T., Lawler, A. M., & Lee, S. (2000). Regulation of left-right patterning in mice by growth / differentiation factor-1. *Nature Genetics*, *24*(3), 262–265. https://doi.org/10.1038/73472

Raposo, G., & Stoorvogel, W. (2013). Extracellular vesicles: Exosomes, microvesicles, and friends. *The Journal of Cell Biology*, *200*(4), 373–383. https://doi.org/10.1083/jcb.201211138

Rathbun, L. I., Colicino, E. G., Manikas, J., Connell, J. O., Krishnan, N., Reilly, N. S., Coyne, S., Garrastegui, A., Freshour, J., Santra, P., Manning, M. L., Amack, J. D., & Hehnly, H. (2020). Cytokinetic bridge triggers de novo lumen formation in vivo. *Nature Communications*, *11*(1), 1269. https://doi.org/10.1038/s41467-020-15002-8

Raya, A., Kawakami, Y., Rodriguez-Esteban, C., Buscher, D., Koth, C. M., Itoh, T., Morita, M., Raya, R. M., Dubova, I., Bessa, J. G., de la Pompa, J. L., & Izpisua Belmonte, J. C. (2003). Notch activity induces Nodal expression and mediates the establishment of left – right asymmetry in vertebrate embryos. *Genes & Development*, *17*(10), 1213–1218. https://doi.org/10.1101/gad.1084403.GENES

Raya, A., Kawakami, Y., Rodríguez-Esteban, C., Ibañes, M., Rasskin-Gutman, D., Rodríguez-León, J., Büscher, D., Feijó, J. A., & Izpisúa Belmonte, J. C. (2004). Notch activity acts as a sensor for extracellular calcium during vertebrate left – right determination. *Nature*, *427*(6970), 121–128. https://doi.org/10.1038/nature02190

Retailleau, K., & Duprat, F. (2014). Polycystins and partners: proposed role in mechanosensitivity. *The Journal of Physiology*, *592*(12), 2453–2471. https://doi.org/10.1113/jphysiol.2014.271346

Reula, A., Pitarch-fabregat, J., Milara, J., Cortijo, J., Mata-roig, M., Milian, L., & Armengot, M. (2021). High-Speed Video Microscopy for Primary Ciliary Dyskinesia Diagnosis: A Study of Ciliary Motility Variations with Time and Temperature. *Diagnostics (Basel, Switzerland)*, *11*(7), 1301. https://doi.org/10.3390/diagnostics11071301

Rogers, K. W., Lord, N. D., Gagnon, J. A., Pauli, A., Zimmerman, S., Aksel, D. C., Reyon, D., & Tsai, S. Q. (2017). Nodal patterning without Lefty inhibitory feedback is functional but fragile. *ELife*, *6*, e28785. https://doi.org/10.7554/eLife.28785

Rothschild, S. C., Francescatto, L., Drummond, I. A., & Tombes, R. M. (2011). CaMK-II is a PKD2 target that promotes pronephric kidney development and stabilizes cilia. *Development (Cambridge, England)*, *138*(16), 3387–3397. https://doi.org/10.1242/dev.066340

Roxo-Rosa, M., Jacinto, R., Sampaio, P., & Lopes, S. S. (2015). The zebrafish Kupffer's vesicle as a model system for the molecular mechanisms by which the lack of Polycystin-2 leads to stimulation of CFTR. *Biology Open*, *4*(11), 1356–1366. https://doi.org/10.1242/bio.014076

Roxo-Rosa, M., & Lopes, S. S. (2019). The Zebrafish Kupffer's Vesicle: A Special Organ in a Model Organism to Study Human Diseases. *In Zebrafish in Biomedical Research. IntechOpen*. https://doi.org/10.5772/intechopen.88266%0D

Rubbo, B., & Lucas, J. S. (2017). Clinical care for primary ciliary dyskinesia : current challenges and future directions. *European Respiratory Review : An Official Journal of the European Respiratory*

Society, *26*(145), 170023. https://doi.org/10.1183/16000617.0023-2017

Sager, R., & Palade, G. E. (1957). Structure and development of the chloroplast in Chlamydomonas. I. The normal green cell. *The Journal of Biophysical and Biochemical Cytology*, *3*(3), 463–488. https://doi.org/10.1083/jcb.3.3.463

Saijoh, Y., Oki, S., Ohishi, S., & Hamada, H. (2003). Left – right patterning of the mouse lateral plate requires Nodal produced in the node. *Developmental Biology*, *256*(1), 160–172. https://doi.org/10.1016/S0012-1606(02)00121-5

Sakuma, R., Ohnishi, Y., Meno, C., Fujii, H., Juan, H., Takeuchi, J., Ogura, T., Li, E., Miyazono, K., & Hamada, H. (2002). Inhibition of Nodal signalling by Lefty mediated through interaction with common receptors and efficient diffusion. *Genes to Cells : Devoted to Molecular & Cellular Mechanisms*, *7*(4), 401–412. https://doi.org/10.1046/j.1365-2443.2002.00528.x

Salathe, M. (2007). Regulation of mammalian ciliary beating. *Annual Review of Physiology*, *69*, 401–422. https://doi.org/10.1146/annurev.physiol.69.040705.141253

Salathe, M., Pratt, M. M., & Wanner, A. (1993). Cyclic AMP-dependent phosphorylation of a 26 kD axonemal protein in ovine cilia isolated from small tissue pieces. *American Journal of Respiratory Cell and Molecular Biology*, *9*(3), 306–314. https://doi.org/10.1165/ajrcmb/9.3.306

Sampaio, P., da Silva, M. F., Vale, I., Roxo-Rosa, M., Pinto, A., Constant, C., Pereira, L., Quintão, C. M., & Lopes, S. S. (2021). CiliarMove: new software for evaluating ciliary beat frequency helps find novel mutations by a Portuguese multidisciplinary team on primary ciliary dyskinesia. *ERJ Open Research*, *7*(1), 00792–02020. https://doi.org/10.1183/23120541.00792-2020

Sampaio, P., Ferreira, R. R., Guerrero, A., Pintado, P., Tavares, B., Amaro, J., Smith, A. A., Montenegro-Johnson, T., Smith, D. J., & Lopes, S. S. (2014). Left-Right Organizer Flow Dynamics: How Much Cilia Activity Reliably Yields Laterality? *Developmental Cell*, *29*(6), 716–728. https://doi.org/10.1016/j.devcel.2014.04.030

Sanderson, M. J., & Sleigh, M. A. (1981). Ciliary activity of cultured rabbit tracheal epithelium: beat pattern and metachrony. *Journal of Cell Science*, *47*, 331–347. https://doi.org/10.1242/jcs.47.1.331

Sanematsu, P. C., Erdemci-tandogan, G., Patel, H., Retzlaff, E. M., Amack, D., & Manning, M. L. (2021). 3D viscoelastic drag forces contribute to cell shape changes during organogenesis in the zebrafish embryo. *Cells & Development*, *168*, 203718. https://doi.org/10.1016/j.cdev.2021.203718

Sarmah, B., Winfrey, V. P., Olson, G. E., Appel, B., & Wente, S. R. (2007). A role for the inositol kinase Ipk1 in ciliary beating and length maintenance. *Proceedings of the National Academy of Sciences of the United States of America*, *104*(50), 19843–19848. https://doi.org/10.1073/pnas.0706934104

Satir, P. (1980). Structural Basis of Ciliary Movement. *Environmental Health Perspectives*, *35*, 77–82. https://doi.org/10.1289/ehp.803577

Satir, P., & Christensen, S. T. (2007). Overview of structure and function of mammalian cilia. *Annual Review of Physiology*, *69*, 377–400. https://doi.org/10.1146/annurev.physiol.69.040705.141236

Satir, P., Heuser, T., & Sale, W. S. (2014). A Structural Basis for How Motile Cilia Beat. *BioScience*, *64*(12), 1073–1083. https://doi.org/10.1093/biosci/biu180

Savina, A., Furlán, M., Vidal, M., & Colombo, M. I. (2003). Exosome release is regulated by a calcium-dependent mechanism in K562 cells. *Journal of Biological Chemistry*, *278*(22), 20083–20090. https://doi.org/10.1074/jbc.M301642200

Savina, A., Vidal, M., & Colombo, M. I. (2002). The exosome pathway in K562 cells is regulated by Rab11. *Journal of Cell Science*, *115*(Pt 12), 2505–2515. https://doi.org/10.1242/jcs.115.12.2505

Saydmohammed, M., Yagi, H., Calderon, M., Clark, M. J., Feinstein, T., Sun, M., Stolz, D. B., Watkins, S. C., Amack, J. D., Lo, C. W., & Tsang, M. (2018). Vertebrate myosin 1d regulates left–right organizer morphogenesis and laterality. *Nature Communications*, *9*(1), 1–11. https://doi.org/10.1038/s41467-018-05866-2

Schier, A. F., & Shen, M. M. (2000). Nodal signalling in vertebrate development. *Nature*, *403*(6768), 385–389. https://doi.org/10.1038/35000126

Schmid, A., & Salathe, M. (2011). Ciliary beat co-ordination by calcium. *Biology of the Cell*, *103*(4), 159–169. https://doi.org/10.1042/bc20100120

Schneider, I., Houston, D. W., Rebagliati, M. R., & Slusarski, D. C. (2008). Calcium fluxes in dorsal forerunner cells antagonize beta-catenin and alter left-right patterning. *Development (Cambridge, England)*, *135*(1), 75–84. https://doi.org/10.1242/dev.004713

Schneider, I., Schneider, P. N., Derry, S. W., Lin, S., Barton, L. J., Westfall, T., & Slusarski, D. C. (2010). Zebrafish Nkd1 promotes Dvl degradation and is required for left-right patterning. *Developmental Biology*, *348*(1), 22–33. https://doi.org/10.1016/j.ydbio.2010.08.040

Schottenfeld, J., Sullivan-Brown, J., & Burdine, R. D. (2007). Zebrafish curly up encodes a Pkd2 ortholog that restricts left-side-specific expression of southpaw. *Development (Cambridge, England)*, *134*(8), 1605–1615. https://doi.org/10.1242/dev.02827

Schwabe, G. C., Hoffmann, Ã. K., Loges, N. T., Birker, D., Rossier, C., Santi, M. M. De, Olbrich, H., Fliegauf, M., Failly, M., Liebers, U., Collura, M., Gaedicke, G., Mundlos, S., Wahn, U., Blouin, J., Niggemann, B., Omran, H., Antonarakis, S. E., & Bartoloni, L. (2008). Primary Ciliary Dyskinesia Associated With Normal Axoneme Ultrastructure Is Caused by DNAH11 Mutations. *Human Mutation*, *29*(2), 289–298. https://doi.org/10.1002/humu

Schweickert, A., Weber, T., Beyer, T., Vick, P., Bogusch, S., Feistel, K., & Blum, M. (2007). Cilia-Driven Leftward Flow Determines Laterality in Xenopus. *Current Biology*, *17*(1), 60–66. https://doi.org/10.1016/j.cub.2006.10.067

Scott, A., Gaspar, J., Stuchell-Brereton, M. D., Alam, S. L., Skalicky, J. J., & Sundquist, W. I. (2005). Structure and ESCRT-III protein interactions of the MIT domain of human VPS4A. *Proceedings of the National Academy of Sciences of the United States of America*, *102*(39), 13813–13818. https://doi.org/10.1073/pnas.0502165102

Segawa, K., Kurata, S., Yanagihashi, Y., Brummelkamp, T. R., Matsuda, F., & Nagata, S. (2014). Caspase-mediated cleavage of phospholipid flippase for apoptotic phosphatidylserine exposure. *Science (New York, N.Y.)*, *344*(6188), 1164–1168. https://doi.org/10.1126/science.1252809

Seib, E., & Klein, T. (2021). The role of ligand endocytosis in notch signalling. *Biology of the Cell*, *113*, 401–418. https://doi.org/10.1111/boc.202100009

Shah, A. S., Ben-shahar, Y., Moninger, T. O., Kline, J. N., & Welsh, M. J. (2009). Motile Cilia of Human Airway Epithelia Are Chemosensory. *Science (New York, N.Y.)*, *325*(5944), 1131–1134. https://doi.org/10.1126/science.1173869.Motile

Shapiro, A., Davis, S. D., Leigh, M. W., Knowles, M. R., Lavergne, V., & Ferkol, T. (2020). Limitations of nasal nitric oxide testing in primary ciliary dyskinesia. *American Journal of Respiratory and Critical Care Medicine*, *202*(3), 476–477. https://doi.org/10.1164/rccm.202003-0835LE

Shapiro, A., Davis, S. D., Polineni, D., Manion, M., Rosenfeld, M., Dell, S. D., Chilvers, M. A., Ferkol, T. W., Zariwala, M. A., Sagel, S. D., Josephson, M., Morgan, L., Yilmaz, O., Olivier, K. N., Milla, C., Pittman, J. E., Leigh Anne Daniels, M., Jones, M. H., Janahi, I. A., … Lavergne, V. (2018). Diagnosis of primary ciliary dyskinesia: An official American thoracic society clinical practice guideline. *American Journal of Respiratory and Critical Care Medicine*, *197*(12), e24–e39. https://doi.org/10.1164/rccm.201805-0819ST

Shapiro, A., Davis, S., Ferkol, T., Dell, S., Rosenfeld, M., Olivier, K. N., Sagel, S. D., Milla, C., Zariwala, M. A., Wolf, W., Carson, J. L., Hazucha, M. J., Burns, K., Robinson, B., Knowles, M. R., Leigh, M. W., & Consortium, G. D. of M. C. (2014). Laterality Defects Other Than Situs Inversus Totalis in Primary Ciliary Dyskinesia Insights Into Situs Ambiguus and Heterotaxy. *Chest*, *146*(5), 1176–1186. https://doi.org/10.1378/chest.13-1704

Shapiro, A., Zariwala, M. A., Ferkol, T., Davis, S. D., Sagel, S. D., Dell, S. D., Rosenfeld, M., Olivier, K. N., Milla, C., Daniel, S. J., Kimple, A. J., Manion, M., Knowles, M. R., & Leigh, M. W. (2016). Diagnosis, monitoring, and treatment of primary ciliary dyskinesia: PCD foundation consensus recommendations based on state of the art review. *Pediatric Pulmonology*, *51*(2), 115–132. https://doi.org/10.1002/ppul.23304

Shen, M. M., Wang, H., & Leder, P. (1997). A differential display strategy identifies Cryptic , a novel EGF-related gene expressed in the axial and lateral mesoderm during mouse gastrulation. *Development (Cambridge, England)*, *124*(2), 429–442. https://doi.org/10.1242/dev.124.2.429

Shinohara, K., Kawasumi, A., Takamatsu, A., Yoshiba, S., Botilde, Y., Motoyama, N., Reith, W., Durand, B., Shiratori, H., & Hamada, H. (2012). Two rotating cilia in the node cavity are sufficient to break left-right symmetry in the mouse embryo. *Nature Communications*, *3*, 622. https://doi.org/10.1038/ncomms1624

Shiratori, H., & Hamada, H. (2006). The left-right axis in the mouse : from origin to morphology. *Development (Cambridge, England)*, *133*(11), 2095–2104. https://doi.org/10.1242/dev.02384

Shiratori, H., Sakuma, R., Watanabe, M., Hashiguchi, H., Mochida, K., Sakai, Y., Nishino, J., Saijoh, Y., Whitman, M., & Hamada, H. (2001). Two-Step Regulation of Left – Right Asymmetric Expression of Pitx2 : Initiation by Nodal Signaling and Maintenance by Nkx2. *Molecular Cell*, *7*(1), 137–149. https://doi.org/10.1016/s1534-5807(01)00006-5

Shoemark, A., Boon, M., Brochhausen, C., Bukowy-Bieryllo, Z., de Santi, M. M., Goggin, P., Griffin, P., Hegele, R. G., Hirst, R. A., Leigh, M. W., Lupton, A., MacKenney, K., Omran, H., Pache, J. C., Pinto, A., Reinholt, F. P., Schroeder, J., Yiallouros, P., & Escudier, E. (2020). International consensus guideline for reporting transmission electron microscopy results in the diagnosis of Primary Ciliary Dyskinesia (BEAT PCD TEM Criteria). *The European Respiratory Journal*, *55*(4), 1900725.

https://doi.org/10.1183/13993003.00725-2019

Shoemark, A., Frost, E., Dixon, M., Ollosson, S., Kilpin, K., Patel, M., Scully, J., Rogers, A. V, Mitchison, H. M., Bush, A., & Hogg, C. (2017). Accuracy of Immuno fluorescence in the Diagnosis of Primary Ciliary Dyskinesia. *American Journal of Respiratory and Critical Care Medicine*, *196*(1), 94–101. https://doi.org/10.1164/rccm.201607-1351OC

Siewert, A. R. (1903). Ueber einen Fall von Bronchiectasis bei einem Patienten mit Situs viscerum inversus. *Berl. Klin. Wchnschr.*, *41*, 139–141.

Singla, V., & Reiter, J. F. (2006). The primary cilium as the cell's antenna: signaling at a sensory organelle. *Science*, *313*(5787), 629–633. https://doi.org/10.1126/science.1124534

Sironen, A., Shoemark, A., Patel, M., Loebinger, M. R., & Mitchison, H. M. (2020). Sperm defects in primary ciliary dyskinesia and related causes of male infertility. *Cellular and Molecular Life Sciences*, *77*(11), 2029–2048. https://doi.org/10.1007/s00018-019-03389-7

Smith, A. A., Johnson, T. D., Smith, D. J., & Blake, J. R. (2012). Symmetry breaking cilia-driven flow in the zebrafish embryo. *Journal of Fluid Mechanics*, *705*, 26–45. https://doi.org/10.1017/jfm.2012.117

Smith, D. J., Montenegro-johnson, T. D., & Lopes, S. S. (2019). Symmetry-Breaking Cilia-Driven Flow in Embryogenesis. *Annual Review of Fluid Mechanics*, *51*, 105–128. https://doi.org/10.1146/annurev-fluid-010518- 040231

Smith, D., Montenegro-Johnson, T., & Lopes, S. (2014). Organized chaos in Kupffer's vesicle: How a heterogeneous structure achieves consistent left-right patterning. *Bioarchitecture*, *4*(3), 119–125. https://doi.org/10.4161/19490992.2014.956593

Smith, K., Noël, E., Thurlings, I., Rehmann, H., Chocron, S., & Bakkers, J. (2011). Bmp and Nodal independently regulate lefty1 expression to maintain unilateral Nodal activity during left-right axis specification in zebrafish. *PLoS Genetics*, *7*(9), e1002289. https://doi.org/10.1371/journal.pgen.1002289

Solowiej-Wedderburn, J., Smith, D. J., Lopes, S. S., & Montenegro-johnson, T. D. (2019). Wall stress enhanced exocytosis of extracellular vesicles as a possible mechanism of left-right symmetry-breaking in vertebrate development. *Journal of Theoretical Biology*, *460*, 220–226. https://doi.org/10.1016/j.jtbi.2018.10.015

Sommer, J. U., Schäfer, K., Omran, H., Olbrich, H., Wallmeier, J., Blum, A., Hörmann, K., & Stuck, B. A. (2011). ENT manifestations in patients with primary ciliary dyskinesia: Prevalence and significance of otorhinolaryngologic co-morbidities. *European Archives of Oto-Rhino-Laryngology : Official Journal of the European Federation of Oto-Rhino-Laryngological Societies (EUFOS) : Affiliated with the German Society for Oto-Rhino-Laryngology - Head and Neck Surgery*, *268*(3), 383–388. https://doi.org/10.1007/s00405-010-1341-9

Song, H., Hu, J., Chen, W., Elliott, G., Andre, P., Gao, B., & Yang, Y. (2010). Planar cell polarity breaks bilateral symmetry by controlling ciliary positioning. *Nature*, *466*(7304), 378–382. https://doi.org/10.1038/nature09129.Planar

Sotelo, J. R., & Porter, K. R. (1959). An electron microscope study of the rat ovum. *The Journal of Biophysical and Biochemical Cytology*, *5*(2), 327–342. https://doi.org/10.1083/jcb.5.2.327

Stannard, W., Rutman, A., Wallis, C., & O'Callaghan, C. (2004). Central microtubular agenesis causing primary ciliary dyskinesia. *American Journal of Respiratory and Critical Care Medicine*, *169*(5), 634–637. https://doi.org/10.1164/rccm.200306-782OC

Strippoli, M. P. F., Frischer, T., Barbato, A., Snijders, D., Maurer, E., Lucas, J. S. A., Eber, E., Karadag, B., Pohunek, P., Zivkovic, Z., Escribano, A., O'callaghan, C., Bush, A., & Kuehni, C. E. (2012). Management of primary ciliary dyskinesia in European children: Recommendations and clinical practice. *European Respiratory Journal*, *39*(6), 1482–1491. https://doi.org/10.1183/09031936.00073911

Stubbs, J. L., Oishi, I., Izpisúa Belmonte, J. C., & Kintner, C. (2008). The forkhead protein Foxj1 specifies node-like cilia in Xenopus and zebrafish embryos. *Nature Genetics*, *40*(12), 1454–1460. https://doi.org/10.1038/ng.267

Sulik, K., Dehart, D. B., Iangaki, T., Carson, J. L., Vrablic, T., Gesteland, K., & Schoenwolf, G. C. (1994). Morphogenesis of the murine node and notochordal plate. *Developmental Dynamics : An Official Publication of the American Association of Anatomists*, *201*(3), 260–278. https://doi.org/10.1002/aja.1002010309

Supatto, W., Fraser, S. E., & Vermot, J. (2008). An All-Optical Approach for Probing Microscopic Flows in Living Embryos. *Biophysical Journal*, *95*(4), L29–L31. https://doi.org/10.1529/biophysj.108.137786

Supatto, W., & Vermot, J. (2011). From Cilia Hydrodynamics to Zebrafish Embryonic Development. In *Current topics in developmental biology* (1st ed., Vol. 95). Elsevier Inc. https://doi.org/10.1016/B978-0-12-385065-2.00002-5

Supp, D. M., Brueckner, M., Kuehn, M. R., Witte, D. P., Lowe, L. A., Mcgrath, J., Corrales, J., & Potter, S. S. (1999). Targeted deletion of the ATP binding domain of left-right dynein confirms its role in specifying development of left-right asymmetries. *Development (Cambridge, England)*, *126*(23), 5495–5504. https://doi.org/10.1242/dev.126.23.5495

Supp, D. M., Witte, D. P., Potter, S. S., & Brueckner, M. (1997). Mutation of an axonemal dynein affects left–right asymmetry in inversus viscerum mice. *Nature*, *389*(6654), 963–966. https://doi.org/10.1097/MPG.0b013e3181a15ae8.Screening

Sutto, Z., Conner, G. E., & Salathe, M. (2004). Regulation of human airway ciliary beat frequency by intracellular pH. *The Journal of Physiology*, *560*(Pt2), 519–532. https://doi.org/10.1113/jphysiol.2004.068171

Tabin, C. J., & Vogan, K. J. (2003). A two-cilia model for vertebrate left-right axis specification. *Genes & Development*, *17*(1), 1–6. https://doi.org/10.1101/gad.1053803

Takafuji, Y., Tatsumi, K., Kawao, N., Okada, K., Muratani, M., & Kaji, H. (2021). Effects of fluid flow shear stress to mouse muscle cells on the bone actions of muscle cell-derived extracellular vesicless. *PLoS ONE*, *16*(5), e0250741. https://doi.org/10.1371/journal.pone.0250741

Takao, D., Nemoto, T., Abe, T., Kiyonari, H., Kajiura-kobayashi, H., Shiratori, H., & Nonaka, S. (2013). Asymmetric distribution of dynamic calcium signals in the node of mouse embryo during left – right axis formation. *Developmental Biology*, *376*(1), 23–30. https://doi.org/10.1016/j.ydbio.2013.01.018

Takeda, S., Yonekawa, Y., Tanaka, Y., Okada, Y., Nonaka, S., & Hirokawa, N. (1999). Left-right asymmetry and kinesin superfamily protein KIF3a: New insights in determination of laterality and

mesoderm induction by KIF3A(-/-) mice analysis. *The Journal of Cell Biology*, *145*(4), 825–836. https://doi.org/10.1083/jcb.145.4.825

Takeo, K., Uesaka, I., Uehira, K., & Nishiura, M. (1973). Fine structure of Cryptococcus neoformans grown in vitro as observed by freeze-etching. *Journal of Bacteriology*, *113*(3), 1442–1448. https://doi.org/10.1128/jb.113.3.1442-1448.1973

Tanaka, C., Sakuma, R., Nakamura, T., Hamada, H., & Saijoh, Y. (2007). Long-range action of Nodal requires interaction with GDF1. *Genes & Development*, *21*(24), 3272–3282. https://doi.org/10.1101/gad.1623907.expression

Tanaka, Y., Okada, Y., & Hirokawa, N. (2005). FGF-induced vesicular release of Sonic hedgehog and retinoic acid in leftward nodal flow is critical for left-right determination. *Nature*, *435*(7039), 172–177. https://doi.org/10.1038/nature03494

Tavares, B., Jacinto, R., Sampaio, P., Pestana, S., Pinto, A., Vaz, A., Roxo-Rosa, M., Gardner, R., Lopes, T., Schilling, B., Henry, I., Saúde, L., & Lopes, S. S. (2017). Notch/Her12 signalling modulates, motile/immotile cilia ratio downstream of Foxj1a in zebrafish left-right organizer. *ELife*, *6*, e25165. https://doi.org/10.7554/eLife.25165

Tay, H. G., Schulze, S. K., Compagnon, J., Foley, F. C., Heisenberg, C., Yost, H. J., Abdelilah-seyfried, S., & Amack, J. D. (2013). Lethal giant larvae 2 regulates development of the ciliated organ Kupffer's vesicle. *Development (Cambridge, England)*, *140*(7), 1550–1559. https://doi.org/10.1242/dev.087130

Teilmann, S., Byskov, A. G., Pedersen, P. E. R. A., Wheatley, D. N., Pazour, G. J., & Christensen, S. T. (2005). Localization of Transient Receptor Potential Ion Channels in Primary and Motile Cilia of the Female Murine Reproductive Organs. *Molecular Reproduction and Development*, *71*(4), 444–452. https://doi.org/10.1002/mrd.20312

Teilmann, S., Clement, C. A., Thorup, J., & Byskov, A. G. (2006). Expression and localization of the progesterone receptor in mouse and human reproductive organs. *Journal of Endocrinology*, *191*(3), 525–535. https://doi.org/10.1677/joe.1.06565

Tessadori, F., Tsingos, E., Colizzi, E. S., Kruse, F., Brink, S. C. Van Den, Boogaard, M. Van Den, & Christoffels, V. M. (2021). Twisting of the zebrafish heart tube during cardiac looping is a tbx5 - dependent and tissue-intrinsic process. *ELife*, *10*, e61733. https://doi.org/10.7554/eLife.61733

Toei, M., Saum, R., & Forgac, M. (2010). Regulation and isoform function of the V-ATPases. *Biochemistry*, *49*(23), 4715–4723. https://doi.org/10.1021/bi100397s.Regulation

Tricarico, C., Clancy, J., & Souza-schorey, C. D. (2017). Biology and biogenesis of shed microvesicles. *Small GTPases*, *8*(4), 220–232. https://doi.org/10.1080/21541248.2016.1215283

Vanaken, G. J., Bassinet, L., Boon, M., Mani, R., Honoré, I., Papon, J.-F. P., Cuppens, H., Jaspers, M., Lorent, N., Coste, A., Escudier, E., Amselem, S., Maitre, B., Legendre, M., & Christin-Maitre, S. (2017). Infertility in an adult cohort with primary ciliary dyskinesia: phenotype–gene association. *The European Respiratory Journal*, *50*(6), 1750314. https://doi.org/10.1183/13993003.00314-2017

Verheya, K. J., & Yang, W. (2016). Permeability barriers for generating a unique ciliary protein and lipid composition. *Current Opinion in Cell Biology*, *41*, 109–116. https://doi.org/10.1016/j.ceb.2016.05.004.Permeability

Vermot, J., & Pourquié, O. (2005). Retinoic acid coordinates somitogenesis and left – right patterning in vertebrate embryos. *Nature*, *435*(7039), 215–220. https://doi.org/10.1038/nature03567.Published

Vervoort, R., Wright, A. F., & Bobrow, M. (2002). Mutations of RPGR in X-linked Retinitis Pigmentosa (RP3). *Human Mutation*, *19*(5), 486–500. https://doi.org/10.1002/humu.10057

Verweij, F., Bebelman, M., Jimenez, C., Vallejo, J., Janssen, H., Neefjes, J., Knol, J. C., Haas, R., Piersma, S., Baglio, S. R., Verhage, M., Middeldorp, J. M., Zomer, A., Rheenen, J. Van, Coppolino, M., Hurbain, I., Raposo, G., Smit, M., Toonen, R., … Pegtel, D. M. (2016). Quantifying exosome secretion from single cells reveals a modulatory role for GPCR signaling. *The Journal of Cell Biology*, *217*(3), 1129–1142. https://doi.org/10.1083/jcb.201703206

Vetrini, F., D'Alessandro, L. C. A., Akdemir, Z. C., Braxton, A., Azamian, M. S., Eldomery, M. K., Miller, K., Kois, C., Sack, V., Shur, N., Rijhsinghani, A., Chandarana, J., Ding, Y., Holtzman, J., Jhangiani, S. N., Muzny, D. M., Gibbs, R. A., Eng, C. M., Hanchard, N. A., … Yang, Y. (2016). Bi-allelic Mutations in PKD1L1 Are Associated with Laterality Defects in Humans. *American Journal of Human Genetics*, *99*(4), 886–893. https://doi.org/10.1016/j.ajhg.2016.07.011

Vick, P., Kreis, J., Blum, M., Vick, P., Kreis, J., Schneider, I., Tingler, M., Getwan, M., Thumberger, T., Beyer, T., Schweickert, A., & Blum, M. (2018). An Early Function of Polycystin-2 for Left-Right Organizer Induction in Xenopus An Early Function of Polycystin-2 for Left-Right Organizer Induction in Xenopus. *IScience*, *2*, 76–85. https://doi.org/10.1016/j.isci.2018.03.011

Vonica, A., & Brivanlou, A. H. (2007). The left – right axis is regulated by the interplay of Coco , Xnr1 and derrière in Xenopus embryos. *Developmental Biology*, *303*(1), 281–294. https://doi.org/10.1016/j.ydbio.2006.09.039

Walker, R. V, Keynton, J. L., Grimes, D. T., Sreekumar, V., Williams, D. J., Esapa, C., Wu, D., Knight, M. M., & Norris, D. P. (2019). Ciliary exclusion of Polycystin-2 promotes kidney cystogenesis in an autosomal dominant polycystic kidney disease model. *Nature Communications*, *10*(1), 4072. https://doi.org/10.1038/s41467-019-12067-y

Wallmeier, J., Al-mutairi, D. A., Chen, C., Loges, N. T., Pennekamp, P., Menchen, T., Ma, L., Shamseldin, H. E., Olbrich, H., Dougherty, G. W., Werner, C., Alsabah, B. H., Köhler, G., Jaspers, M., Boon, M., Griese, M., Schmitt-grohé, S., Zimmermann, T., Koerner-rettberg, C., … Omran, H. (2014). Mutations in CCNO result in congenital mucociliary clearance disorder with reduced generation of multiple motile cilia. *Nature Genetics*, *46*(6), 646–651. https://doi.org/10.1038/ng.2961

Wallmeier, J., Frank, D., Shoemark, A., Nöthe-Menchen, T., Cindric, S., Olbrich, H., Loges, N. T., Aprea, I., Dougherty, G. W., Pennekamp, P., Kaiser, T., Mitchison, H. M., Hogg, C., Carr, S. B., Zariwala, M. A., Ferkol, T., Leigh, M. W., Davis, S. D., Atkinson, J., … Omran, H. (2019). De Novo Mutations in FOXJ1 Result in a Motile Ciliopathy with Hydrocephalus and Randomization of Left / Right Body Asymmetry. *American Journal of Human Genetics*, *105*(5), 1030–1039. https://doi.org/10.1016/j.ajhg.2019.09.022

Wallmeier, J., Nielsen, K. G., Kuehni, C. E., Lucas, J. S., Leigh, M. W., Zariwala, M. A., & Omran, H. (2020). Motile ciliopathies. *Nature Reviews Disease Primers*, *6*(1), 77. https://doi.org/10.1038/s41572-020-0209-6

Wang, G., Cadwallader, A. B., Jang, D. S., Tsang, M., Yost, H. J., & Amack, J. D. (2011). The Rho kinase rock2b establishes anteroposterior asymmetry of the ciliated Kupffer's vesicle in zebrafish.

Development (Cambridge, England), *138*(1), 45–54. https://doi.org/10.1242/dev.052985

Wang, G., Manning, M. L., & Amack, J. D. (2012). Regional cell shape changes control form and function of Kupffer's vesicle in the zebrafish embryo. *Developmental Biology*, *370*(1), 52–62. https://doi.org/10.1016/j.cmet.2012.08.002.

Wang, T., Gilkes, D. M., Takano, N., Xiang, L., Luo, W., Bishop, C. J., Chaturvedi, P., Green, J. J., & Semenza, G. L. (2014). Hypoxia-inducible factors and RAB22A mediate formation of microvesicles that stimulate breast cancer invasion and metastasis. *Proceedings of the National Academy of Sciences of the United States of America*, *111*(31), E3234–E3242. https://doi.org/10.1073/pnas.1410041111

Wang, W., Jack, B. M., Wang, H. H., Kavanaugh, M. A., Maser, R. L., & Tran, P. V. (2021). Intraflagellar Transport Proteins as Regulators of Primary Cilia Length. *Frontiers in Cell and Developmental Biology*, *9*, 661350. https://doi.org/10.3389/fcell.2021.661350

Wang, X., & Yost, H. J. (2008). Initiation and propagation of posterior to anterior (PA) waves in zebrafish left-right development. *Developmental Dynamics : An Official Publication of the American Association of Anatomists*, *237*(12), 3640–3647. https://doi.org/10.1002/dvdy.21771.Initiation

Wheway, G., Thomas, N. S., Carroll, M., Coles, J., Doherty, R., England, G., Goggin, P., Green, B., Harris, A., Hunt, D., Jackson, C. L., Lord, J., Mennella, V., Thompson, J., Walker, W. T., & Lucas, J. S. (2021). Whole genome sequencing in the diagnosis of primary ciliary dyskinesia. *BMC Medical Genomics*, *14*(2), 234. https://doi.org/10.1186/s12920-021-01084-w

Whitfield, M., Thomas, L., Bequignon, E., Schmitt, A., Stouvenel, L., Montantin, G., Tissier, S., Duquesnoy, P., Copin, B., Chantot, S., Whitfield, M., Thomas, L., Bequignon, E., Schmitt, A., & Stouvenel, L. (2019). Mutations in DNAH17 , Encoding a Sperm-Specific Axonemal Outer Dynein Arm Heavy Chain , Cause Isolated Male Infertility Due to Asthenozoospermia. *American Journal of Human Genetics*, *105*(1), 198–212. https://doi.org/10.1016/j.ajhg.2019.04.015

Whitman, M. (2001). Nodal Signaling in Early Vertebrate Embryos : Themes and Variations. *Developmental Cell*, *1*(5), 605–617. https://doi.org/10.1016/s1534-5807(01)00076-4

Wilson, G. R., Wang, H. X., Egan, G. F., Robinson, P. J., Delatycki, M. B., Bryan, M. K. O., & Lockhart, P. J. (2010). Deletion of the Parkin co-regulated gene causes defects in ependymal ciliary motility and hydrocephalus in the quaking viable mutant mouse. *Human Molecular Genetics*, *19*(8), 1593–1602. https://doi.org/10.1093/hmg/ddq031

Woith, E., Fuhrmann, G., & Melzig, M. (2019). Extracellular Vesicles — Connecting Kingdoms. *International Journal of Molecular Sciences*, *20*(22), 5695. https://doi.org/10.3390/ijms20225695

Wu, G., Markowitz, G. S., Li, L., Agati, V. D. D., Factor, S. M., Geng, L., Tibara, S., Tuchman, J., Cai, Y., Park, J. H., Adelsberg, J. Van, Jr, H. H., Kucherlapati, R., Edelmann, W., & Somlo, S. (2000). Cardiac defects and renal failure in mice with targeted mutations in Pkd2. *Nature Genetics*, *24*(1), 75–78. https://doi.org/10.1038/71724

Yamamoto, R., Sale, W. S., Hwang, J., Kon, T., & Sale, W. S. (2021). Composition and function of ciliary inner-dynein-arm subunits studied in Chlamydomonas reinhardtii. *Cytoskeleton (Hoboken, N.J.)*, *78*(3), 77–96. https://doi.org/10.1002/cm.21662

Yamanaka, Y., Tamplin, O. J., Beckers, A., Gossler, A., & Rossant, J. (2007). Live Imaging and Genetic

Analysis of Mouse Notochord Formation Reveals Regional Morphogenetic Mechanisms. *Developmental Cell*, *13*(6), 884–896. https://doi.org/10.1016/j.devcel.2007.10.016

Yan, Y., Gritsman, K., Ding, J., Burdine, R. D., Corrales, J. D., Price, S. M., Talbot, W. S., Schier, A. F., & Shen, M. M. (1999). Conserved requirement for EGF – CFC genes in vertebrate left – right axis formation. *Genes & Development*, *13*(19), 2527–2537. https://doi.org/10.1101/gad.13.19.2527

Yeo, C., & Whitman, M. (2001). Nodal Signals to Smads through Cripto-Dependent and Cripto-Independent Mechanisms. *Molecular Cell*, *7*(5), 949–957. https://doi.org/10.1016/s1097-2765(01)00249-0

Yin, C., Kikuchi, K., Poss, K. D., & Didier Y. R. Stainier. (2010). Hand2 regulates extracellular matrix remodeling essential for gut-looping morphogenesis in zebrafish. *Developmental Cell*, *18*(6), 973–984. https://doi.org/10.1016/j.devcel.2010.05.009.Hand2

Yokoyama, T., Copeland, N. G., Jenkins, N. A., Charles, A., Elder, F. F. B., Overbeek, P. A., Yokoyama, T., Copeland, N. G., Jenkins, N. A., Montgomery, C. A., Elder, F. F. B., & Overbeek, P. A. (1993). Reversal of Left-Right Asymmetry : A Situs Inversus Mutation. *Science (New York, N.Y.)*, *260*(5108), 679–682. https://doi.org/10.1126/science.8480178

Yoshiba, S., Shiratori, H., Kuo, I. Y., Kawasumi, A., Shinohara, K., Nonaka, S., Asai, Y., Sasaki, G., Belo, J. A., Sasaki, H., Nakai, J., Dworniczak, B., Ehrlich, B., Pennekamp, P., & Hamada, H. (2012). Cilia at the node of mouse embryos sense fluid flow for left-right determination via Pkd2. *Science (New York, N.Y.)*, *338*(6104), 226–231. https://doi.org/10.1038/nature13314.A

Yu, X., Ng, C. P., Habacher, H., & Roy, S. (2008). Foxj1 transcription factors are master regulators of the motile ciliogenic program. *Nature Genetics*, *40*(12), 1445–1453. https://doi.org/10.1038/ng.263

Yuan, S., Li, J., Diener, D. R., Choma, M. A., Rosenbaum, J. L., & Sun, Z. (2011). Target-of-rapamycin complex 1 (Torc1) signaling modulates cilia size and function through protein synthesis regulation. *Proceedings of the National Academy of Sciences of the United States of America*, *109*(6), 2021–2026. https://doi.org/10.1073/pnas.1112834109

Yuan, S., Zhao, L., Brueckner, M., & Sun, Z. (2015). Intraciliary Calcium Oscillations Initiate Vertebrate Left-Right Asymmetry. *Current Biology : CB*, *25*(5), 556–567. https://doi.org/10.1016/j.cub.2014.12.051

Zhang, J., Talbot, W. S., & Schier, A. F. (1998). Positional Cloning Identifies Zebrafish one-eyed pinhead as a Permissive EGF-Related Ligand Required during Gastrulation. *Cell*, *92*(2), 241–251. https://doi.org/10.1016/s0092-8674(00)80918-6

Zhang, M., Zhang, J., Lin, S.-C., & Meng, A. (2012). β-Catenin 1 and β-catenin 2 play similar and distinct roles in left-right asymmetric development of zebrafish embryos. *Development (Cambridge, England)*, *139*(11), 2009–2019. https://doi.org/10.1242/dev.074435

Zhang, X. M., Ramalho-Santos, M., & McMahon, A. P. (2001). Smoothened mutants reveal redundant roles for Shh and Ihh signaling including regulation of L/R asymmetry by the mouse node. *Cell*, *106*(2), 781–792. https://doi.org/10.1016/S0092-8674(01)00385-3

Zhou, J., Chen, L., Li, J., Li, H., Hong, Z., Xie, M., Chen, S., Yao, B., & Drevet, J. R. (2015). The semen pH affects sperm motility and capacitation. *PLoS ONE*, *10*(7), 1–15.

https://doi.org/10.1371/journal.pone.0132974

Zhou, X., Sasaki, H., Lowe, L., Hogan, B., & Kuehn, M. (1994). Nodal is a novel TGF-beta-like gene expressed in the mouse node during gastrulation. *Nature*, *361*(6412), 543–547. https://doi.org/10.1038/361543a0

Zimmermann, K. W. (1898). Beiträge zur Kenntniss einiger Drüsen und Epithelien. *Archiv Für Mikroskopische Anatomie*, *52*(3), 552–706. https://doi.org/10.1007/BF02975837

CHAPTER 2.
THE ROLE OF EXTRACELLULAR VESICLES IN THE LEFT – RIGHT ORGANIZER

2. INTRODUCTION

To our eyes, symmetry represents a certain sense of equilibrium, however nature often evolves to break it, showing across the different kingdoms of life several examples of asymmetry, which most probably accounted for an increase in evolutionary fitness throughout time (Blum & Ott, 2018).

In fact, asymmetric distribution of the visceral organs, such as the lungs, heart, brain, liver and spleen, along the left-right (LR) axis is well conserved in vertebrates. Developmental biology studies using mouse, zebrafish and *Xenopus* embryos show three common steps in the establishment of such LR pattern: firstly, the symmetry breaking occurs within a transient structure generally referred to as the left-right organizer (LRO) in a cilia-driven flow dependent manner; secondly, the asymmetric signal is transferred to the lateral plate mesoderm (LPM) from the posterior to the anterior side and thirdly, induction of *situs*-specific organogenesis (Hamada & Tam, 2014).

In zebrafish, the LR axis establishment starts in a fluid-filled transient structure present at the tailbud from 3 somite stage (ss) to 20 ss, called Kupffer's Vesicle (KV) (Essner et al., 2005; Kramer-Zucker et al., 2005). During gastrulation, a small population of KV precursor cells, named the dorsal forerunner cells (DFCs), escape from involution and migrate in the forefront of the dorsal margin towards the vegetal pole (Cooper & D'Amico, 1996; Oteiza et al., 2008). By the end of gastrulation, DFCs form a cell cluster and become epithelial. Subsequently, the cells form a rosette and secrete an extracellular fluid via *cystic fibrosis transmembrane conductance regulator (cftr)* chloride channel, present on the apical side of the cells, giving rise to the lumen of the differentiated KV (Navis et al., 2013; Roxo-Rosa et al., 2015). While KV lumen expands, each cell extends one single immotile cilium facing the lumen that gradually starts to acquire motility, generating a leftward fluid flow within the lumen (Yuan et al., 2015; Ferreira et al., 2017; Tavares et al., 2017).

Our previous work showed by transmitted electron microscopy and by live imaging with a fluorescent tagged *dnal1, a light chain outer dynein arm axonemal dynein motor*, expressed in zebrafish embryos, that all KV cilia when imaged had an ultrastructure characteristic of motile cilia with clearly visible dynein arms, both in motile and immotile cilia (Tavares et al., 2017). Moreover, all KV cells expressed *foxj1a*, the master transcription factor involved in building motile cilia. This finding suggested that all KV cilia are capable of moving while the ratio between motile and immotile cilia is actively regulated. In fact, downregulation of Notch signaling increased motile cilia number, while overexpression of Notch signaling had the opposite effect, without changing the total number of KV cilia and independently of *foxj1a*

(Sampaio et al., 2014; Tavares et al., 2017). Furthermore, we found that *hairy-related 12* gene, *her12*, a homologue of the mammalian *HES5* that belongs to a family of transcription repressors, proved to be a faithful Notch signaling readout and regulated ciliary motility, most likely by inhibiting the transcription of a yet unknown crucial motility switch (Tavares et al., 2017). Similarly, Notch signaling had been found to regulate motile – immotile cilia fate in the LRO of *Xenopus* (Boskovski et al., 2013).

Concomitantly, KV cells undergo region-specific morphological rearrangements, between 4 ss and 6 ss, driven by changes in actomyosin cytoskeleton contractility, cell-cell adhesions and extracellular matrix composition, which result in an asymmetrically distribution of ciliated cells, concentrated at the anterior side (Wang et al., 2011, 2012; Compagnon et al., 2014).

Thus, KV lumen expansion, ciliary length and motility and cell rearrangements are key to produce a fluid flow within the KV capable of breaking the asymmetry. Our lab has previously characterized the directionality and speed of the fluid flow, by following native particles inside the KV lumen using bright field microscopy. Around 3 ss, we observed a heterogeneous and slow fluid flow, in agreement with the low number of motile cilia found at that stage. As development progresses and the number of motile cilia increases, the fluid flow acquires a counterclockwise directionality and its velocity escalates (Yuan et al., 2015; Ferreira et al., 2017; Tavares et al., 2017). By the 8 ss, local hotspots of strong flow speed on the anterior and left sides were observed and correlated with *dand5* downregulation (Sampaio et al., 2014). Therefore, fluid flow maps were predictive of gene expression alterations and later of heart and liver positions. Although KV persists within the tailbud until 20 ss, its role in LR establishment is completed by 10 ss, as demonstrated by the normal asymmetric expression pattern of *lefty2* and *pitx2* and normal heart *situs*, upon KV lumen disruptions performed at 10 – 15 ss (Essner et al., 2005).

As in mouse (Marques et al., 2004) and *Xenopus* (Schweickert et al., 2010), *dand5* starts to be expressed symmetrically around the KV and, upon fluid flow stimulation, its expression decreases on the left side while remains strongly expressed on the right side, becoming the first LR asymmetric molecular marker (Lopes et al., 2010; Sampaio et al., 2014). Dand5 is a physical inhibitor of Nodal proteins and, consequently to its left sided degradation, Nodal repression is alleviated triggering a conserved left-sided asymmetric genetic cascade signaling, comprising *nodal*, *lefty2*, *pitx2* and *elovl6* genes, in the lateral plate mesoderm (LPM) (Long et al., 2003; Hashimoto et al., 2004; Ji et al., 2016; Montague et al., 2018). Nodal cassette signaling spreads throughout the entire left sided LPM towards the anterior side, where at different locations and developmental time points it regulates several organ-specific

target genes to induce the asymmetric development of the gut and its derivatives, heart and vasculature and brain, among others (Grimes & Burdine, 2017).

However, it remains unclear how the flow is sensed by the LRO cells and the subsequent molecular mechanism that elicits gene expression changes. Historically, the LR field has been divided around two main hypotheses for the flow-sensing mechanism – the chemosensory model and the mechanosensory model – but in the absence of satisfactory data towards one or the other, new assumptions have emerged.

The chemosensory model was first based on morphogens and then updated to morphogen carrying extracellular vesicles that would be release symmetrically across the mouse LRO to the lumen, transported by the directional fluid flow and accumulated on the left side, where its content would be released near the cell membranes, triggering an asymmetric intracellular calcium signal increase (Nonaka et al., 1998; Tanaka et al., 2005). Conversely, the mechanosensory model is based on the clear separation of motile and immotile cilia functions. Where motile cilia in the center of the mouse LRO are responsible for generating fluid flow and peripheral immotile cilia, by bending accordingly to the flow, are able to sense it and trigger an asymmetric influx of calcium on the left side through the Pkd1l1-Pkd2 complex (McGrath et al., 2003). *Pkd1l1* is a paralogue of the mechanosensor *polycystic kidney disease 1* gene, *Pkd1,* expressed in mouse and fish LROs (Field et al., 2011; Kamura et al., 2011; England et al., 2017; Roxo-Rosa & Lopes, 2019), and its activation is thought to open the transient receptor potential (TRP) cation channel, Pkd2, leading to the entrance of extracellular ions, mainly calcium ions, into the cell and subsequently to induce intracellular calcium waves (McGrath et al., 2003; Yuan et al., 2015). Restorage of Pkd2 specifically on the immotile cilia of peripheral crown cells rescued the Nodal cascade signaling defects of the *Pkd2* mouse mutant, supporting the mechanosensory model in the mouse LRO (Yoshiba et al., 2012).

Nevertheless, Pkd1l1 and Pkd2 are localized within all LRO cells raising the question of if and how motile cilia can sense the fluid flow movement and how peripheral cells can distinguish the directionality of the flow.

On the other hand, zebrafish LRO is architecturally more complex and motile and immotile cilia are not spatially distributed in different domains as in the mouse LRO. In fact, immotile cilia are randomly distributed around the KV (Tavares et al., 2017). Moreover, the average distance between two cilia is under 8 µm, which implies strong local flow perturbations generated by motile cilia around the immotile ones, making mechanosensing driven by the directionality of flow deflection unlikely (Supatto et al., 2008; Ferreira et al., 2017). We have previously suggested that different flow magnitudes could be distinguished, however numerical calculated flow profiles of single KVs showed a significant variability between

embryos, incompatible with the observed reliable LR axis establishment event (Sampaio et al., 2014; Smith et al., 2014; Ferreira et al., 2017). Additionally, Ferreira and colleagues reported that the number of immotile cilia is insufficient to perceive the flow. They showed that the calculated forces acting on one cilium are below the detection threshold of other mechanosensitive cilia and a robust symmetry breaking would occur with the accumulative forces sensed by at least 3 immotile cilia on each side, which were not observed in most of the KVs analyzed from 8 ss onwards (Ferreira et al., 2017). Nevertheless, immotile cilia number varies accordingly with the KV developmental stage, ranging between 73 – 67% at 4 ss and 16 – 10% at 8 ss (Yuan et al., 2015; Tavares et al., 2017). Hence, the mechanosensory model may still be considered in the zebrafish, depending on the precise timing at which the flow is perceived and the remaining immotile cilia number.

Controversially, Delling and colleagues argued that immotile cilia are not calcium-responsive mechanosensors by showing an absence of intracellular calcium increase in mouse LRO cells, upon 10 seconds of stimulation using either a physiological or a supraphysiological velocity fluid flow (Delling et al., 2016). However, this work was found to be performed under unsuitable medium conditions after Hamada's and Sun's groups showed left sided intraciliary calcium transients dependent on fluid flow and Pkd2, followed by cytoplasmatic calcium waves in both mouse and zebrafish LROs (Yuan et al., 2015; Mizuno et al., 2020).

Alternatively, motile cilia could sense their own movement, as resultant forces of ciliary beating acting on themselves are about 20 times higher than the forces produced by the directional fluid flow (Ferreira et al., 2017). Asymmetric cilia tilt and intrinsic orientation between the left and right side of the KV, towards the already established axes, could provide enough subcellular information for motile cilia to distinguish the yet to break LR axis (Ferreira et al., 2018, 2019). In fact, we showed that motile cilia increase beat frequency throughout the development of the KV, from 33 Hz at 3 – 4 ss to 37 Hz at 5 – 6 ss and 40 Hz at 7 – 8 ss, which can be suggestive of a ciliary beat frequency minimum threshold for a sensory system activation (Tavares et al., 2017).

More recently, the chemosensory model was revisited under zebrafish LRO scrutiny. Both signaling molecules and extracellular vesicles (EVs) containing such molecules were modeled to be secreted by the anterior sided cells, transported by the directional flow and accumulated on the left side (Ferreira et al., 2017; Solowiej-Wedderburn et al., 2019). Solowiej-Wedderburn estimated the wall shear stress caused by motile cilia motion at the membrane of KV cells and found it comparable to other systems such as the human vascular endothelial cells (Solowiej-Wedderburn et al., 2019). These cells play critical roles in maintenance of cardiovascular homeostasis by responding to the blood fluid flow with an exocytosis increased rate and a

TRP ion channel, TRPV4-dependent calcium influx (Baratchi et al., 2014, 2016). Based on this, Solowiej-Wedderburn hypothesized that the shear stress calculated for KV cells could be sufficient to enhance the release of extracellular vesicles and, concomitantly, strong anterior flow due to the cluster of motile cilia would induce higher rates of exocytosis in the anterior region (Solowiej-Wedderburn et al., 2019). Interestingly, observations from transmission electron microscopy suggested a site of active vesicular fusion within the cellular region in close proximity to the cilium (Kramer-Zucker et al., 2005). Moreover, Ferreira and colleagues also proposed a secretion region at the anterior side, as particles would firstly be transported towards the left, promoting a stronger signal on that side. Further mathematical simulations, using 9 - 14 ss fluid flow maps, also revealed that molecules above 2 nm are able to reach a reliable asymmetric distribution in a few seconds (Ferreira et al., 2017).

In summary, the complexity of the LROs, the hydrodynamics of the flow and the fast development of the events make the design of experiments to distinguish between the chemosensory and mechanosensory hypotheses very difficult to accomplish. As a result, there are compiling data, from the evolutionary – developmental biology and the mathematical modeling fields, that are compatible with either one of the models. On the other side, they both have limitations, the chemosensory of a morphogen or an extracellular vesicle-contained morphogen lack experimental evidence and replication, whereas the mechanosensory model implies a system with a sensitivity threshold of magnitude much lower than any other known equivalent system.

With the extracellular vesicle field emerging, due to the latest technological advances, it became clear that EVs play crucial functions in intercellular communication, instead of a simple cellular disposal mechanism. EVs role within the KV would explain the importance of the motile cilia cluster at the anterior side and, consequently, the strong local flow, and it would provide a mechanism to link the anterior region and the left side, where the downregulation of *dand5* occurs. Thus, making the chemosensory hypothesis very attractive in the zebrafish model.

The purpose of this work was to analyze the biophysical properties of the LRO cells and flow that would be needed to cope with the EV-based model. We generated a stable transgenic fish line expressing a fluorescent tagged CD63, a widely used EV marker, in order to quantify and track its dynamics within the KV lumen. Using live imaging assays, we observed that KV cells had very dynamic intracellular CD63 positive vesicles and that CD63 positive vesicles were observed within the KV lumen, being carried by the fluid flow current. Single EV quantification analysis revealed a significant variability in the number of EVs between embryos.

KV cells are known to have high secretory rates, as observed for the dynamic trafficking towards the apical side of fluid-filled vacuoles by the motor protein myosin 1d and Rab11 positive vesicles carrying CFTR molecules to the plasma membrane to drive KV inflation (Tay et al., 2013; Saydmohammed et al., 2018; Rathbun et al., 2020). In order to infer if symmetry breaking relies on EV secretion, we aimed to interfere with their generation, more specifically with the exosomes sub-type, and further investigate their potential function *in vivo*. Exosomes are formed through the endocytic pathway as intraluminal vesicles inside multivesicular bodies, that are then released to the extracellular space upon fusion of the multivesicular body with the plasma membrane (Niel et al., 2018). The Syndecan – Syntenin – Alix complex is involved in cargo binding and membrane inward invagination during intraluminal vesicles biogenesis and it was recently shown to be conserved in zebrafish (Verweij et al., 2019). We reasoned that if we inhibit the formation of intraluminal vesicles, less exosomes would be released to the KV lumen. Therefore, we performed KV specific *syntenin-a* knockdown and observed an impact on the LR related gene expression patterns and a randomization of the heart placement. We also found that downregulation of *syntenin-a* led to motile – immotile cilia ratio alterations in a Notch signaling dependent manner, which resulted in abnormal flow dynamics. Given the fact that we detected an extremely variable exosome number and the indirect effect of *syntenin-a* knockdown on flow dynamics, we conclude that the LR defects caused by *syntenin-a* reduction cannot be assigned exclusively to its putative role in promoting extracellular vesicle chemosensing.

Moreover, KV precursor cells have unique endocytic properties during gastrulation stages, shown by the high rate of membrane impermeant fluorescent dyes uptake when compared to the rest of the embryo (Cooper & D'Amico, 1996). To address if KV cells were also capable of endocytic function we took advantage of a new micromanipulation setup developed in the laboratory that allows for highly controlled KV fluid extraction and re-fill in live zebrafish embryos, to evaluate the role of fluid content in a spatiotemporally resolved manner. By diluting the KV fluid content with different fluorescent dyes and endocytic pharmacological inhibitors, we showed that KV cells continue to show some endocytic activity, but its inhibition does not seem to impact on the LR asymmetric organ morphogenesis.

Our results show that the number of extracellular vesicles within the KV fluid is too variable to induce a robust flow-sensing mechanism and that the endocytic events seem to occur symmetrically in KV cells, without a persistent bias between the left and right sides, therefore this process by itself cannot be a good indicator of the embryonic side. Although not fully disproven, the chemosensory model may not be a reliable approach for KV cells to detect the asymmetric cues of the fluid flow.

2.1. EXPERIMENTAL PROCEDURES

Fish husbandry and genetics

Zebrafish maintenance and breeding protocols were conducted according to standard procedures described in the zebrafish book by Westerfield (1995). Experimental protocols were approved and implemented in line with the Portuguese DGAV (Direção Geral de Alimentação e Veterinária) guidelines. Zebrafish embryos were raised at 25ºC or 28ºC in E3 embryo media (NaCl 5mM, KCl 0.17 mM, CaCl2 0.33 mM, MgSO4 0.33 mM) and staged according to age (hours post-fertilization, hpf), the number of somites and morphological features, as described elsewhere (Kimmel et al., 1995). Wild-type AB line, *Tg(sox17:GFP)*^{s870} (Chung & Stainier, 2008), *Tg(actb2:Lifeact-GFP)* (Behrndt et al., 2012) and *deltaD* ^{tr233} (Eeden et al., 1996) were used for this work. pUbi-CD63-pHluorin construct (a gift from Guillaume van Niel) was co-injected with *Tol2* transposase mRNA at the one-cell stage zebrafish embryos (Kwan et al., 2007). Once the embryos reached adulthood, they were outcrossed with a wild-type line and the GFP positive progeny was selected to generate a stable ubi:CD63-pHluorin transgenic line.

Injections of Morpholino oligonucleotides and/or mRNA

synta, *synta*bis and mismatch morpholinos (Lambaerts et al., 2012) were obtained from Gene Tools LLC (Philomath, USA) and diluted in 10,000 MW rhodamine-dextran solution (1:2; Sigma-Aldrich). To infer about *syntenin-a* knockdown specifically at the KV cells, the morpholinos were injected between 512 and 1,000 cell stages into the yolk, as previously described (Amack & Yost, 2004), at a dose of 6 ng per embryo.

The rhodamine lineage tracer allowed us to meticulously control the injection efficiency, by selecting the embryos positive for diffusion through the yolk cell and into DFCs (Amack and Yost, 2004) (Figure 2.8 B). 50 pg of zebrafish *syntenin-a* mRNA was injected in combination with *synta* MO for rescue experiments. To assess ciliary motility, 50 pg of *arl13b*-GFP mRNA was injected into one-cell staged embryos. Overexpression of *her12* was accomplished by injecting 50 pg of *her12* mRNA into 1 cell stage embryos. Injected embryos were allowed to develop to the proper stages to study KV cilia, expression patterns of different genes and organ *situs*.

Overexpression and *in situ* hybridization assays

Full length *syntenin-a* (ENSDARG00000012513), resistant for *synta* MO, construct was a gift from Pascale Zimmermann and it was cloned into a pCS2+ plasmid. Primer sequences used: *synta* forward 5'- TAAGCACTCGAGATGAGTCTATATCCATCGCTAG -3' and reverse 5'-TGCTTATACGTATCAGACCTCAGGCACAG -3'. PCR was performed using iProof™ High-Fidelity DNA Polymerase (Bio-rad). The amplified gene and plasmid were double digested and incubated overnight at 16ºC with DNA ligase T4 (NEB). DH5α competent *E. coli* were transformed with the ligation product and plated in LB Agar (Carl Roth) supplemented with 100 mg/mL of Ampicillin. Resistant colonies were screened by PCR using pCS2+ specific primers and positive colonies were sequenced to evaluate the quality of PCR amplification. A colony with correct sequence was grown on secondary culture and a high quality and concentrated plasmid was obtained using, according to the instructions of manufacture, a ZymoPURE™ plasmid Midiprep kit (Zymo Research). For *in vitro* capped mRNA production, both *syntenin-a* and *alr13b*-GFP (a gift from Helena Soares) plasmids were linearized and processed with mMESSAGE mMACHINE™ SP6 Transcription Kit (Invitrogen™ Ambion™). mRNAs were purified, quantified, aliquoted and stored at -80ºC. For *in situ* hybridization probes, *syntenin-a* plasmid was processed with T7 and SP6 RNA Polymerase (Promega), to produce antisense and sense probes respectively, and labelled with DIG (Roche). RNA probes were purified, quantified, diluted in 200uL of Hybridization Mix and stored at -20ºC.

In situ hybridization probes of *syndecan-2* (ENSDARG00000002731), *syndecan-3* (Gene ID: 337077), *syndecan-4* (ENSDARG00000059906) and *pdcd6ip* (ENSDARG00000025269) were amplified from wild-type zebrafish cDNA into pGem-Teasy vector (Promega) using the following primers: *syndecan-2* forward 5'-ATGAGGAACCTTTGGATGATTTTAACCCTC-3' and reverse 5'-TTATGCGTAAAACTCCTTGGTGGGAGC-3'; *syndecan-3* forward 5'-GCCTTACGATGATGAAGACTTCTACTCTGG-3' and reverse 5'-CCTTCGTCTTTCTTTTTCATCCGGTAGAC-3'; *syndecan-4* forward 5'-GATGTTGAAAGTTTACCTCATGTTGG-3' and reverse 5'-TCATGCGTAGATTTCTGTGGTTG-3' and *pdcd6ip* forward 5'-CAAAGAGAATCTGCCTAAGGACGTG-3' and reverse 5'-CTGAGACCTCAACACATTTACCACC-3'. PCRs were performed using NZYTaq II DNA Polymerase (NZYTech). The resulting amplicons and the vector were digested and incubated overnight at 16ºC with DNAligase T4 (NEB). DH5α competent *E. coli* were transformed with the ligation products and plated in LB Agar (Carl Roth) with 100 mg/mL of Ampicillin. Colonies were assessed by PCR using pGem-Teasy specific primers and positive colonies were sequenced to evaluate not only the integrity of PCR amplification but also the construct orientation within the vector. Colonies were further grown on secondary cultures and plasmids were purified using ZymoPURE™ plasmid Midiprep kit (Zymo Research). Linearized plasmids

were used to produce both sense and antisense *in situ* hybridization probes either with T7 or SP6 RNA Polymerases (Promega) and labelled with DIG (Roche). RNA probes were purified, quantified, diluted in 200uL of Hybridization Mix and stored at -20ºC.

RNA in situ hybridization and immunofluorescence

Whole-mount *in situ* hybridization for *syntenin-a*, *syndecan-2*, *syndecan-3*, *syndecan-4* and *pdcd6ip* were performed at 4 and 10 somite stage in wild-type embryos as described in Thisse Lab - In situ Hybridization Protocol 2010 update Zfin (https://goo.gl/XdcfCH). Digoxigenin RNA probes were synthesized from DNA templates of *dand5* and *spaw* (Hashimoto et al., 2004) and the whole-mount *in situ* hybridization was performed at 8 and 12 somite stage embryos as described elsewhere (Thisse & Thisse, 2008).

Images of whole-mount embryos were obtained on a Zeiss Z2 Widefield Microscope with Zeiss air EC Plan-Neofluar 5x (0.16 NA) and 10x (0.3 NA) lenses. Expression patterns of *dand5* and *spaw* were evaluated relatively to the KV position – left, right, bilateral, or absent.

dand5 in situ hybridizations were performed in 73 wild-type embryos, 35 mismatch MO^{DFCs}, 65 *synta* MO^{DFCs}, 15 *synta* MO^{DFCs} + 50 pg *synta* RNA^{DFCs} and 16 *synta*bis MO^{DFCs} to characterize *syntenin-a* knockdown phenotype and in 24 wild-type embryos, 6 ‘Danieau’s buffer dilution’ embryos and 12 ‘methylcellulose dilution’ embryos to evaluate the effect of KV fluid manipulation. *spaw in situ* hybridizations were performed in 8 wild-type embryos, 15 mismatch MO^{DFCs} and 19 *synta* MO^{DFCs}. Fisher’s exact test was used to compare the frequency of left-right defects between controls and manipulated embryos.

Whole-mount immunostaining was performed as described previously (Lopes et al., 2010). Antibodies used for immunostaining were anti-acetylated alpha-tubulin (1:400; ref.:T7451, Sigma or ref.:5335, Cell Signaling), anti-DeltaD (1:50; ref.: ab73331, Abcam), anti-V-ATPase V1 subunit A (1:200, ref.: A00938, GenScript), anti-TJP1 (1:200, ref.: HPA001636, Sigma), Alexa Fluor 488 (1:500; Invitrogen), Alexa Fluor 647 (1:500; Invitrogen) and Alexa Fluor 546 phalloidin (1:200, Invitrogen/molecular probes). Nuclei were stained with DAPI (1:500). Stacks of flat-mount embryos were acquired either on a laser scanning confocal microscope Zeiss LSM710 with an Olympus 40x water immersion lens (0.8 NA) or on an Airyscan laser scanning confocal microscope Zeiss LSM 980 with a 40x water immersion lens (1.2 NA).

Fluorescence activated cell sorting (FACS)

Tg(sox17:GFP) control embryos and injected with mismatch MO and *synta* MO embryos were allowed to develop overnight at 25ºC until 8 somite stage. The embryos were dechorionated with pronase E (2 mg/mL, Merck), washed extensively with E3 media and transferred into 2 mL eppendorfs. Cells were dissociated in 1 mL of CO2 independent medium (Gibco™) complemented with 0.5 mM EDTA by manual up and down pipetting with filter tips. Cells were centrifuged at room temperature for 3 minutes at 700 g. The supernatant was discarded and cells were resuspended in a new 1 mL of CO2 independent medium (Gibco™) complemented with 0.5 mM EDTA. The dissociation and centrifugation steps were performed 3 times, until the removed supernatant became translucent pink. Cells were then re-suspended in 300 µL of FACS buffer (5mM EDTA; 25mM HEPES pH 7.0; 1% inactivated fetal bovine serum; 1x PBS; filtered using a 0.2 µm acrodisc® syringe filter (Pall, Life Sciences)) and filtered with a 30 µm mesh. FACS was performed in a BD FACSAria™ III Cell Sorter (Becton Dickinson) with a sheath fluid pressure at 70 psi, by the facility technician. GFP high positive cells were selected, collected directly into 300 µL of QIAzol Lysis Reagent (Qiagen) and RNA extraction protocol was immediately performed. We collected three independent samples for control embryo, mismatch MO and *synta* MO injected embryos, each with around 15 000 cells per sample.

RNA isolation, cDNA synthesis and quantitative PCR

Total RNA was extracted with the RNeasy® micro kit (ref.: 74104, Qiagen) and cDNA was synthesized by reverse transcription using both oligo(dT)18 and random hexamer primers with the RevertAid First Strand cDNA Synthesis kit (ref.: K1622, Thermo Scientific™), both protocols were followed by the manufacturer's instructions. Real-time qPCR reactions using Roche SYBR Green I Master (ref.: 04887352001, Roche) were performed in a Roche LightCycler® 96 Real-Time PCR System. Three biological replicates were analysed for each gene and all the experiments were performed in triplicate. Results were analysed and RNA transcripts levels were normalized to the expression of the housekeeping ribosomal protein L13a (rpl13a) gene. The following primers were used: *rpl13a* forward 5'-TGACAAGAGAAAGCGCATGGTT-3' and reverse 5'-GCCTGGTACTTCCAGCCAACTT-3'; *dand5* forward 5′-CCGCAATCCTGACCCATAGCAA-3′ and reverse 5′-CTCCTCCGTTATGCGCTGTGTA-3′; *dnah7* forward 5'-CGTTGCCTCAGCTCAGAAGTGAAA-3' and reverse 5'-GTTTGGATCGGGCTCGCTGTAT-3'; *rbc3a* forward 5'-CAAGTGTGGCGTTGCAGATGGTGA-3' and reverse 5'-

TGGACTGTCCCGCTGTGGCG-3'; *deltaD* forward 5'-ACCGCAGCCGCGCGCCGGACT-3' and reverse 5'-TGTGGCTTCGCTCCTCTCAGAA-3'.

Live imaging of CD63 positive vesicles and actin dynamics in the zebrafish KV and Bafilomycin A1 treatment

Tg(CD63-pHluorin) and *Tg(actb2:Lifeact-GFP)* embryos were developed at 28ºC until 5 somite stage, then mounted in a 2% (w/v) agarose mold in glass-bottom Petri dish and covered with E3 medium. *Tg(CD63-pHluorin)* siblings were also treated at 3 somite stage with 100 nM Bafilomycin A1 for 1 hour before being immobilized in the 2% (w/v) agarose mold. Live imaging was performed in an airyscan laser scanning confocal microscope (Zeiss LSM 980) with a 40x water objective lens (1.2 NA) at room temperature or in a spinning disk laser confocal microscope (Andor Resolution XD) with a 60x water immersion objective (1.2 NA) at 28ºC. Time-lapses of the KV midplane of the embryos were acquired for one minute.

KV liquid manipulation

Wild-type embryos were developed until 5 somite stage and KV fluid manipulations were set under a 10x Plan DL air objective lens on a Nikon Eclipse Ti-U inverted microscope at 28ºC. Embryos were held individually from the anterior dorsal side of the body using a holding pipette while a second pipette was used to penetrate the KV from the posterior dorsal side. The pipettes were attached to CellTram's (CellTram Vario, FemtoJet, Eppendorf) and were controlled by a set of two motorized axis manipulators (MPC-385-2, Sutter Instruments). To dilute the KV fluid, the injection pipette was pre-filled with Danieau's solution 1x (58mM NaCl, 0.7mM KCl, 0.4mM MgSO4, 0.6 mM Ca(NO3)2, 5.0 mM HEPES pH 7.6) or Methylcellulose 1.5% (M0387, Sigma-Aldrich) diluted in 10,000 or 70,000 MW rhodamine-dextran solution (1:4; Sigma-Aldrich). Upon insertion of the injection pipette into the KV lumen, the vesicular fluid was aspirated, held for a few seconds inside the pipette to allow mixing and then the mixed solution was injected again into the KV until reaching the KV volume observed before the manipulation. Only embryos with rhodamine-positive KVs were selected for the experiment. Embryos were then mounted for fluid flow live imaging as described below. Afterwards, embryos were let to develop at 28°C and were later characterized according to *dand5* expression pattern or to heart laterality. KV fluid experiments were performed in: 10 embryos (70 kDa Rhodamine), 5 embryos (10 kDa Rhodamine), 28 embryos (methylcellulose), 21 embryos (Danieau's buffer), 20 embryos (DMSO), 12 embryos (chloroquine 200 µM), 10 embryos (chloroquine 400 µM), 9 embryos (chlorpromazine 10 µM),

3 embryos (chlorpromazine 50 µM), 7 embryos (amiloride 100 µM) and 3 embryos (EIPA 100 µM). In 6 embryos, the KV was punctured with the injection needle without applying suction. We named these embryos “Sham” and they were used as controls for the micromanipulation.

Live imaging of fluid flow and CBF measurements

Embryos injected with mismatch MO^{DFCs}, *synta* MO^{DFCs}, *synta* MO^{DFCs} + 50 pg *synta* RNA^{DFCs} and respective control siblings were developed overnight at 25ºC until 8 somite stage. In KV fluid dilution experiments, after the micromanipulation, the embryos were followed through development and stacks were acquired every 30 minutes between 6 and 8 somite stage.

Embryos were mounted with the dorsal roof of the KV facing the objective lens and the imaging was performed on an inverted transmission light microscope (Nikon Eclipse Ti-U) with a 100× oil immersion objective lens (1.30 NA) at room temperature. Bright field images were recorded with a FASTCAM MC2 camera (Photron Europe, Limited) controlled with PFV (Photron FASTCAM Viewer) software. Time lapses of native KV particles were filmed at 60 fps for 30 seconds and tracked using the ImageJ plugin MTrackJ as previously described (Sampaio et al., 2014). Ciliary movement was recorded at 500 fps for 2 seconds and cilia beat frequency was measured using the CiliarMove software (Pinto et al., 2021).

In section II, cilia beat frequency was analysed in 4 WT embryos (n=38 cilia), 4 mismatch MO^{DFCs} injected embryos (n=35 cilia) and 4 *synta* MO^{DFCs} injected embryos (n=38 cilia). Results were statistically analysed using the Kruskal-Wallis ANOVA test and a *post hoc* analysis with Dunn’s correction for multiple comparisons.

Angular flow velocity measurements

The flow speed and angular velocities were calculated by customized scripts in the program environment R (BioRxiv, Sampaio et al., 2022). In this flow dynamics studies, tracked points near the centre (corresponding to the interior half radius circle of the KV) were removed, as angular quantities are poorly defined along the axis of rotation, close to the centre of the KV. Therefore, KV flow measurements contemplate exclusively the near KV apical membrane circle, where the flow is more effective (Montenegro-Johnson et al., 2016). Angular velocity represents the effective circular flow magnitude of a particle moving between two consecutive time frames. The center of the KV was used as a reference point of a polar coordinate system in which angles are expressed in radians. Instantaneous angular velocity (rad/sec) was

calculated by dividing particle angle change by the time between consecutive image frames (0.2 seconds).

For the KV fluid dilution experiments, we successfully filmed 6 control embryos, 12 'Danieau's buffer dilution' embryos and 12 'Methylcellulose dilution' embryos. Results were analysed according to a linear mixed-effects model.

For the characterization of *syntenin-a* role in the LR establishment, a total of 7 wild-type embryos, 7 mismatch MO^{DFCs}, 8 *synta* MO^{DFCs} and 7 *synta* MO^{DFCs} + 50 pg *synta* RNA^{DFCs} injected embryos were imaged. Results were statistically analysed using the Kruskal-Wallis ANOVA test and a *post hoc* analysis with Dunn's correction for multiple comparisons.

Ciliary motility assay and Concanamycin A treatment

Embryos were firstly injected with 50 pg of *arl13b*-GFP mRNA at one cell stage, incubated at 28ºC for 2 hours and then injected with mismatch MO^{DFCs}, *synta* MO^{DFCs} or *synta* MO^{DFCs} + 50 pg *synta* RNA^{DFCs} between 512 and 1,000 cell stages. Once at 8 somite stage, $Rhodamine^{DFCs}$ positive embryos were mounted live in 2% (w/v) agarose mold and covered with E3 medium.

Embryos injected with 50 pg of *arl13b*-GFP mRNA at one cell stage were also allowed to develop at 28ºC until 3 somite stage and then incubated either with DMSO or Concanamycin A (200 nM). After 30 minutes, at 4 somite stage, embryos were mounted quickly in 2% (w/v) agarose mold and covered with E3 medium.

Live imaging of whole KVs was performed in a Zeiss LSM710 with an Olympus 40x water immersion lens (0.8 NA) at room temperature, scanned with z sections of 0.5 µm and an acquisition rate of 9.6 slices per minute (6.25 sec per slice) (Tavares et al., 2017). Stacks were reconstructed using Fiji and motile and immotile cilia identification was performed manually.

For the characterization of *syntenin-a* role in the LR establishment, a total of 23 *arl13b:GFP* RNA injected control embryos (n=869 cilia), 17 co-injected with mismatch MO^{DFCs} (n=754 cilia), 13 *synta* MO^{DFCs} (n=482 cilia) and 14 *synta* MO^{DFCs} + 50 pg *synta* RNA^{DFCs} injected (n=576 cilia) embryos were imaged. The one-way ANOVA test with Tukey's multiple comparisons *post hoc* analysis was performed to evaluate the distribution of motile and immotile cilia between the anterior and posterior halves of the KV, within treatments. While a Fisher test with Bonferroni correction was performed to compare the number of motile and immotile cilia between treatments.

To evaluate the effect of inhibiting V-ATPase activity on ciliary motility ratio, 5 control embryos (n=272 cilia), 3 DMSO incubated embryos (n=76 cilia) and 11 Concanamycin A incubated embryos (n=355 cilia) were analyzed with a Fisher test with Bonferroni correction.

Cilia number, 3D length measurements and anterior-posterior distribution

Embryos injected with mismatch MO^{DFCs}, *synta* MO^{DFCs} and respective control siblings were fixed at 8 somite stage in PFA 4% and processed for whole-mount immunostaining of acetylated alpha-tubulin as previously described (Lopes et al., 2010). Stacks were reconstructed using Fiji, cilia number and anterior-posterior distribution were analysed manually, and 3D cilia length was measured using the ImageJ plugin Simple Neurite Tracer (Longair et al., 2011).

The ciliary length was analysed in 8 WT embryos (n=461 cilia), 9 mismatch MO^{DFCs} injected embryos (n=358 cilia) and 10 *synta* MO^{DFCs} injected embryos (n=447 cilia). Results were statistically analysed by using the Welch's ANOVA test and a *post hoc* analysis with Dunnett's correction for multiple comparisons.

Fluorescence levels, area and KV volume measurements

Whole-KV scans at 8 somite stage or tailbud-midplane scan at bud stage for the immunolabelled DeltaD and Tjp1a proteins were analyzed and the fluorescent signal was measured and normalized using the semiautomated IMARIS software program. DeltaD protein profile was analysed in 8 control embryos and 6 synta MO^{DFCs} injected embryos at 8 ss and in 4 control embryos and 7 synta MO injected embryos at bud stage, while Tjp1a protein profile was analysed in 5 control embryos and 6 synta MO^{DFCs} injected embryos. Student's t-test with Welch's correction was used to compare the results.

For KV volume measurements, whole-KV scans of live imaged 20 *arl13b:GFP* RNA injected control embryos, 18 co-injected with mismatch MO^{DFCs}, 15 with *synta* MO^{DFCs} and 14 with *synta* MO^{DFCs} + 50 pg *synta* RNA^{DFCs} embryos were used. The KV lumen was delineated for each z-stack image, the luminal area was measured and the KV volume was calculated using the semiautomated IMARIS software program. The results were analysed by Kruskal-Wallis ANOVA test with Dunn's correction for multiple comparisons.

Heart *situs* evaluation

Heart jogging was assessed from the ventral side of 30 hpf embryos using a stereoscopic zoom microscope (SMZ745, Nikon Corporation). Scoring of the heart *situs* was evaluated relatively to the midline axis – left, right or central.

210 wild-type embryos, 27 mismatch MO^{DFCs}, 40 *synta* MO^{DFCs}, 20 *synta* MO^{DFCs} + 50 pg *synta* RNA^{DFCs} and 54 *synta*bis MO^{DFCs} injected embryos were evaluated for heart *situs* to characterize *syntenin-a* knockdown phenotype. Whereas 487 wild-type embryos, 21 embryos (Danieau's buffer), 28 embryos (methylcellulose), 20 embryos (DMSO), 12 embryos (chloroquine 200 µM), 10 embryos (chloroquine 400 µM), 9 embryos (chlorpromazine 10 µM), 3 embryos (chlorpromazine 50 µM), 7 embryos (amiloride 100 µM) and 3 embryos (EIPA 100 µM) were observed to evaluate the effect of KV fluid content manipulation. Fisher's exact test was used to compare the frequency of left-right defects between controls and manipulated embryos.

2.2. RESULTS

While the Nodal gene is the leftness signal widely conserved in the animal kingdom being present from radial symmetric animals to vertebrates, the symmetry breaking event has evolved from a simple chiral cellular arrangement during early cleavage divisions to the maturation of a complex ciliated structure for the sole reason of inducing Nodal expression (Blum et al., 2014; Blum & Ott, 2018). The motile cilia and subsequently the fluid flow are now at the heart of the LR axis establishment driving the latest questions within the field.

Here, we manipulated the KV fluid using a recently developed micromanipulation assay to address if its content is determinant for the flow-sensing mechanism carried by the surrounding cells (section I). Additionally, we performed knockdown experiments to manipulate Notch signaling in order to understand the mechanism behind the choice of motile versus immotile cilia, that is crucial for the generation of the optimal fluid flow (section II).

Section I – Testing the role of extracellular vesicles in the zebrafish embryo LRO

2.2.1. Kupffer's Vesicle fluid is composed of different extracellular vesicles

In order to understand if the chemosensory model could play a role in the zebrafish LR determination, we aimed to study the fluid content researching for extracellular vesicles (EVs) that could be responsible for the transportation of the sidedness molecule that triggers the asymmetric signaling cascade and, thus, driving the flow-sensing mechanism. During our previous studies regarding flow dynamics, we found the presence of a few native particles

within the KV lumen, by direct visualization through bright field microscopy, that allowed us to measure flow speed (Sampaio et al., 2014). Due to the variable and mostly high size of these native particles, they were considered as cellular debris. We later detected a lot more EVs, with variable size ranges, by performing transmission electron microscopy of wild-type (WT) zebrafish embryos at 8 ss (data not shown). This work was performed by Petra Pintado and Andreia Pinto from Susana Lopes lab. The difference between the two methods is due to the minimum threshold resolution, while we use a 100x lens for detection and tracking of native particles for flow dynamics, electron microscopy was performed at a magnification of 25 000x, allowing for the detection of small vesicles (Pinto et al., 2021). However, electron microscopy along with other techniques that require prior fixation of the samples may not reflect the native state of EVs as structural artifacts may occur due to dehydration and fixation.

Therefore, we decided to study EVs by live imaging using fluorescent tagged reporters, so we took advantage of a recently published construct validated in zebrafish (Verweij et al., 2019). CD63-pHluorin comprises a tetraspanin protein highly enriched in EV membranes cloned with a pH sensitive GFP variant, pHluorin, located in the first extracellular loop of CD63 (Verweij et al., 2016). Although the function of CD63 is largely unknown, as a tetraspanin, it is thought to interact with several molecules to regulate intracellular trafficking, signaling pathways and adhesion of exosomes to target cells (Pols & Klumperman, 2009). When injected into zebrafish embryos, CD63-pHluorin labelled single vesicles in the range of exosomes between 100 and 150 nm confirmed by immunogold labelling and nanoparticle tracking analysis (Verweij et al., 2019) suggesting that CD63-pHlourin is a suitable marker to visualize *in vivo* EVs in zebrafish.

We engineered a transgenic line to stably express CD63-pHluorin ubiquitously and by performing live imaging of 5 ss embryos we found an enrichment of fluorescence in the plasma membrane of KV cells (Figure 2.1 A). We focused on the KV midplane as it displays a maximum lumen area, comprises the preferential location to observe native particles and intercepts the flow vortex, being ideal for 2D studies (Sampaio et al., 2014). With this strategy, we detected for the first time in live CD63-pHluorin positive EVs inside the KV lumen being carried by the fluid flow (Figure 2.1 A', Supplementary Movie 2.1). We further attempted to increase the number of EVs inside the lumen by inhibiting the vacuolar H^+-ATPase, with Bafilomycin A1 (BafA), which elevates endosomal pH, decreasing the lysosomal degradation of multivesicular bodies and other endosomal components and consequently promoting exosomal secretion (Ferreira et al., 2022; Ortega et al., 2019). Incubation of *Tg(CD63-pHluorin)* embryos with 100 nM of BafA, for 1 hour prior to live imaging, showed an increased fluorescent signal within the KV cells, confirming the impairment of the lysosomal degradation (Figure 2.1 B), however no significant differences were observed regarding the number of EVs in the KV lumen (Figure 2.1 B').

Although zebrafish KV shows a variable number of cells and, as a result, different lumen sizes, the final outcome of LR, which is the correct organ position, is still accomplished in 90% of zebrafish larvae (Gokey et al., 2016; Moreno-Ayala et al., 2021). Therefore, we reasoned that the flow-sensing mechanism, here assessed by the EVs, should constitute a robust physical event. We then proposed to develop a reliable method to quantify and track EVs, but analysis of *Tg(CD63-pHluorin)* single vesicles, for stages ranging from 5 ss to 8 ss, revealed high levels of variability between embryos. While some embryos undoubtedly showed CD63-pHluorin positive EVs inside the KV lumen (n= 10 embryos), most embryos showed empty lumens or very low signal that could have been easily misinterpreted as background noise (n= 69 embryos) (Figure 2.1 C).

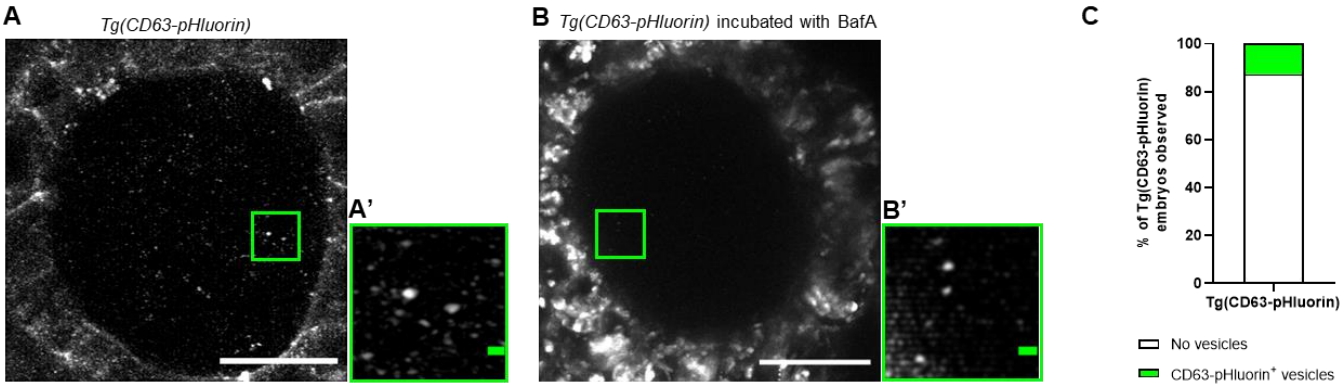

Figure 2.1: CD63-pHluorin positive vesicles were observed within the Kupffer's Vesicle lumen.
(A) Z-projection of a time lapse movie of a *Tg(CD63-pHluorin)* embryo with 5 ss (n= 10 embryos). (A') Higher magnification of CD63 positive vesicles found within the KV lumen of the embryo in A. (B) Z-projection of a time lapse movie of a *Tg(CD63-pHluorin)* embryo with 5 ss prior incubated with 100 µm Bafilomycin A1 (BafA) for 1 hour (n= 6 embryos). (B') Higher magnification of CD63 positive vesicles found within the KV lumen of the embryo in B.(C) Percentages of *Tg(CD63-pHluorin)* embryos observed with or without CD63-pHluorin positive vesicles in the KV lumen (n= 79 embryos). Embryos were imaged either using the spinning disk laser confocal microscopy (Andor Resolution XD) or the airyscan confocal microscopy Zeiss LSM 980. KV, Kupffer's Vesicle.; ss, somite stage. White and green scales represent 20 µm and 1 µm, respectively.

This could be due to technical issues, as most EVs may be under the limit of resolution. Detection limit for EVs can depend on the number of fluorescent molecules incorporated in the vesicles, the background fluorescence level within the KV lumen and/or the increased signal from surrounding tissues, such as the KV cells. Additionally, throughout development the KV fluid increases from 17 to 82 picoL in volume (Ferreira et al., 2017) and, concomitantly, migrates from 70 to 120 µm below the tail mesodermal cell layer. Meaning that the KV develops deep into the ventral side of the embryo, away from the microscope lens, which compromises the optimal distance for fluorescent signal detection. Lastly, we observed that CD63-pHluorin positive EVs adopted the speed of the flow, fluctuating between different focal planes of the KV lumen, increasing the difficulty of tracking them along the time-lapses.

Therefore, to validate the existence of EVs in all embryos a better method of detection is needed. Scanning the whole KV through high pressure freezing electron microscopy would avoid the classical structural anomalies observed in normal fixation for electron microscopy. A following step by immunogold labelling of CD63-pHluorin positive vesicles would fully confirm and characterize this sub-population of EVs. Moreover, other fluorescent tagged EV proteins could be tested, to find more markers, as EVs with different compositions can co-exist. Alternatively, performing mass-spectrometry of KV liquid would allow us to discriminate the biochemical signature. Unfortunately, obtaining enough KV liquid for such an experiment was not feasible, as KV fluid from thousands of embryos would be needed, and we did not pursue this task.

2.2.2. Cells from Kupffer's Vesicle maintain endocytic properties

Taking the low level of EV detection by fluorescent microscopy, we decided to tackle this issue by analyzing the biophysical properties of the KV cells necessary to cope with the uptake of EVs. Before developing into a mature KV, DFCs, the KV cell precursors, were described to be highly endocytic cells (Cooper & D'Amico, 1996). However, the endocytic profile of KV cells remains uncharacterized. For this purpose, we used a new setup established in the laboratory, initially developed to extract transiently the KV fluid without affecting its structure and preserving its function (Figure 2.2 A). With this setup, we reasoned that we could refill the KV after fluid extraction, replacing at least a part of its content. Hence, the KV liquid was extracted and diluted in approximately 1 µl of fluorescent tracers priorly loaded into the needle. After a few seconds, the resulting mixed liquid was re-injected into the KV until it reached the initial volume (Figure 2.2 B, Supplementary Movie 2.2). Fluorescent signal was contained inside the KV lumen with very low to no leakage into the surrounding tissues, confirming the successfulness of the procedure (Figure 2.2 C).

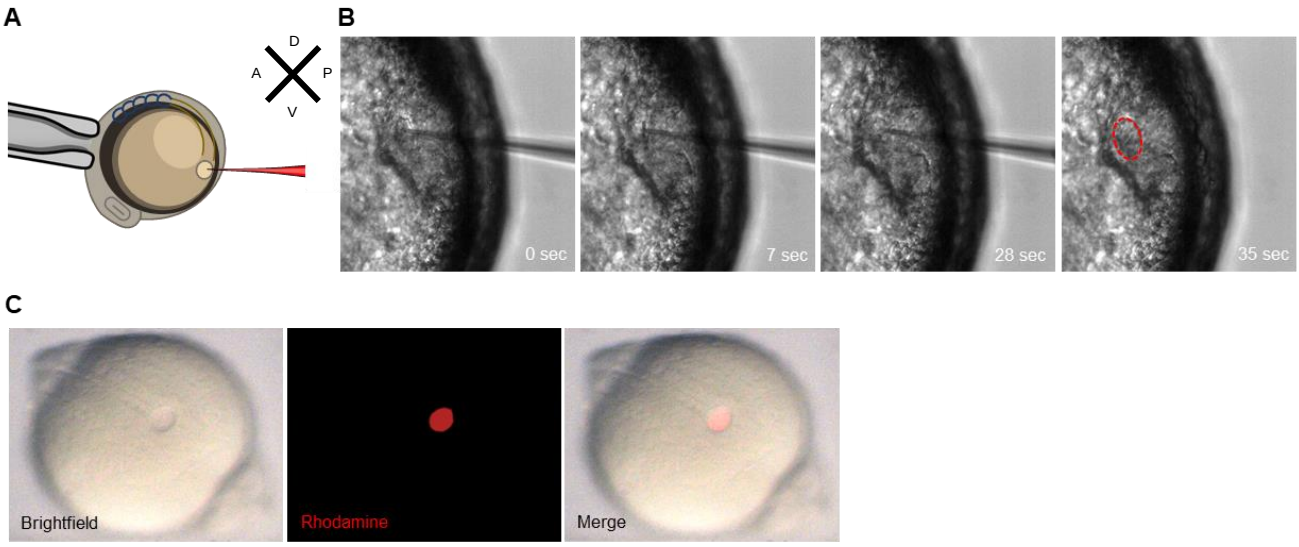

Figure 2.2: Kupffer's Vesicle fluid dilution procedure.
(A) Schematic representation of the micromanipulation setup that allows the partial replacement of the KV fluid throughout the zebrafish embryo development, showing the positioning of the holding pipette (on the left side) and the microinjection needle (on the right side) relatively to the embryo for KV lumen assessment. (B) Time-lapse of KV fluid dilution by microsurgery in a total of 35 seconds. Red dashed line delineates the final volume of the KV. (C) Rhodamine positive signal assessment from KV lumen to confirm the dilution procedure successfulness. KV, Kupffer's Vesicle; A, anterior; P, posterior; D, dorsal; V, ventral.

To analyze the capacity of KV cells to uptake the liquid and/or particles from the liquid, we replaced the KV fluid with two different molecular weight rhodamine-dextran tracers. Generally, cells have different strategies to incorporate extracellular fluid and molecules. Macropinocytosis is involved in bulk fluid internalization, independently of its content, through plasma membrane protrusions; whereas micropinocytosis is involved in small extracellular particles and molecules uptake, which is mediated by membrane-bound receptors and adaptors, as clathrin, dynamin and others (Doherty & McMahon, 2009). Therefore, internalization of extracellular molecules firstly depends on their size. Large molecules such as 70 kDa (kilo Dalton) fluorescent dextrans are predominantly engulfed by the non-selective fluid-phase macropinocytosis, while smaller molecules, such as 10 kDa fluorescent dextrans are generally internalized via clathrin- and dynamin-dependent endocytosis and macropinocytosis (Li et al., 2015).

Moreover, we have previously observed membrane protrusions at the apical side of the KV cells, by electron microscopy, resembling the actin driven ruffles that mediate macropinocytosis (data not shown). To confirm this phenomenon, we used a transgenic line that labels F-actin, *Tg(actb2:Lifeact-GFP)* and followed the KV cells between 5 ss and 8 ss (Figure 2.3 A). By live imaging, we detected actively dynamic F-actin protrusions at the plasma membrane of KV cells facing the lumen (Figure 2.3 A'), that formed sporadically and without

any specific bias towards a KV side. We then diluted the KV liquid of *Tg(actb2:Lifeact-GFP)* embryos with the 70 kDa rhodamine dextran containing solution to evaluate the ability of these actin protrusions to form macropinosomes that internalize liquid. We performed the tracer experiment at 5 ss and searched for rhodamine tracer internalization from 8 – 10 ss, when the first readout of flow, *dand5* mRNA, becomes visibly asymmetrically expressed on the right side (Lopes et al., 2010) and, presumably when the internalization of more EVs is no longer necessary. Results showed that manipulated embryos (n = 10) showed a strong fluorescent signal from the 70 kDa tracer contained within the KV lumen and almost no signal inside the KV cells (Figure 2.3 B) suggesting that macropinocytosis did not occur during this time window and most likely is not involved in the LR axis establishment.

Between 4 and 6 ss, KV cells suffer architectural changes, leading to the compaction of cells on the anterior-dorsal side, via Rock2b induced phosphorylation of Myosin II activity, that subsequently regulates cell contractility and cell adhesion (Wang et al., 2011, 2012). Therefore, it is plausible that our results showing F-actin protrusions may reflect the dynamic actin-myosin tensions occurring at the time.

Next, we replaced the KV fluid by the smaller molecular weight 10 kDa rhodamine dextran solution using the same setup as previously. Immediately after the dilution procedure, the fluorescent signal was confined to the lumen, as reported before (Figure 2.2 C), however, at 8 ss the rhodamine dextran was predominantly inside the KV cells distributed along the cytoplasm and clustered in small dots, resembling a vesicular labeling pattern (Figure 2.3 C).

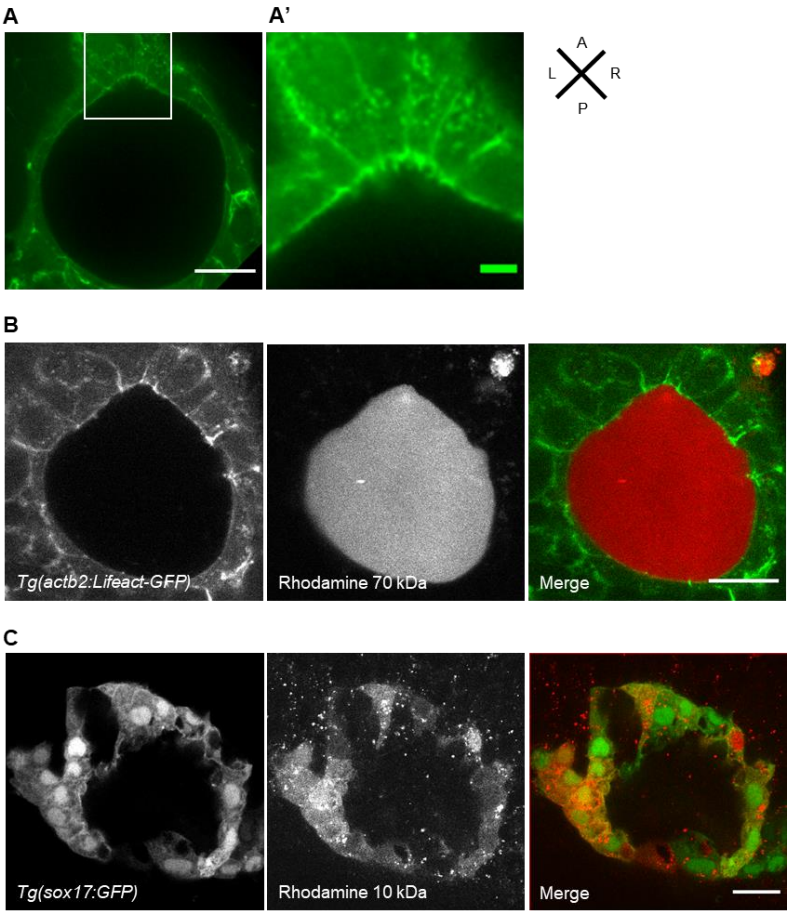

Figure 2.3: Kupffer's Vesicle cells are active endocytic cells.
(A) KV midplane of *Tg(actb2:Lifeact-GFP)* embryo at 5 ss showing actin protrusions at the anterior side (n= 13 embryos). Time-lapses of KVs were imaged using the spinning disk laser confocal microscopy (Andor Resolution XD). (A') Higher magnification of actin protrusions at the apical membrane of embryo A. (B) KV midplane of *Tg(actb2:Lifeact-GFP)* embryo injected with 70 kD Rhodamine at 5 ss and imaged at 8 – 10 ss (n= 10 embryos). Z-stack of whole KVs were imaged either using the laser scanning confocal microscopy Zeiss LSM 710 or airyscan Zeiss LSM 980. (C) KV midplane of *Tg(sox17:GFP)* embryo injected with 10 kDa Rhodamine at 5 ss and imaged at 8 – 10 ss (n= 5 embryos). White scale and green scale represent 20 µm and 5 µm, respectively. KV, Kupffer's Vesicle; ss, somite stage; A, anterior; P, posterior; L, left; R, right; kDa, kilo Dalton.

Our results showed that all KV cells are capable of endocytic function, as reported for their precursor cells. So, micropinocytosis, such as clathrin- and dynamin-dependent endocytosis, rather than macropinocytosis, may be active in the KV cells.

2.2.3. Inhibition of Kupffer's Vesicle fluid content internalization has no impact on LR axis establishment

Considering the chemosensory hypothesis predictions, EV release and uptake cycles would have to happen quickly in order to avoid mixing and diffusion and intermittent repetitively throughout the development of the KV to allow for a large and stable accumulation of EVs on

the left sided cells (Ferreira et al., 2017; Okada et al., 2005; Solowiej-Wedderburn et al., 2019). Moreover, particles transported by the KV fluid flow at its maximum speed perform a complete turn to the vesicle in about 15 seconds (Supatto et al., 2008). Therefore, we predicted that any interference with the internalization of the biochemical signal would have severe impacts on laterality.

Given the high precision and time resolution of our micromanipulation method to alter the KV fluid content locally, we proceeded with the injection of pharmacological antagonists to inhibit specifically KV cell endocytosis, avoiding any secondary effects that could occur by performing whole embryo bathing incubations. As a final redout of this assay, we let the embryos grow and looked at heart position after 30 hours post fertilization (hpf).

Amiloride and EIPA are both inhibitors of Na^+/H^+ exchanger pump, which impair the activation of GTPases at the vicinity of the plasma membrane that promote actin remodeling for dorsal ruffles development (Koivusalo et al., 2010). Therefore, they were used to test macropinocytosis and to control for toxicity effects upon pharmacological interference with KV cells. Chlorpromazine accumulates in the intracellular organelles and arrests clathrin and the key adaptor protein 2 within the endosomes, preventing their recycling to the plasma membrane and, consequently inhibiting the clathrin-mediated endocytosis pit formation (Wang et al., 1993). Thus, chlorpromazine was used for testing specifically clathrin-dependent endocytosis. Lastly, Chloroquine is a weak base that accumulates in the acidic compartments such as lysosomes and promotes pH increase, impairing endosomal function and indirectly inhibiting endocytosis (Ducharme & Farinotti, 1996). Hence, it was used as a general inhibitor of internalization processes.

Control groups contemplating either non manipulated embryos, innocuous Danieau's buffer (DB) injected embryos and EIPA vehicle control dimethylsulfoxide (DMSO) injected embryos, typically displayed the heart on the left side of the body (95.6%, 93.3% and 90% of the cases, respectively). Considering the embryos manipulated with endocytic inhibitors, none of treatments showed consistent defects in laterality of heart position (Fisher test with Bonferroni correction, p-value > 0.05) (Figure 2.4). KV fluid dilution with amiloride or EIPA showed a correct heart *situs* in all manipulated embryos, confirming that macropinocytosis does not occur in KV cells. Regarding dilution with Chlorpromazine, most of the embryos showed the heart on the left side even with higher concentrations (88% and 100% of the cases, respectively), suggesting that clathrin-dependent endocytosis is not involved in LR symmetry breaking. Lastly, dilution with a broader inhibitor of endocytosis, Chloroquine, showed 25% of embryos with laterality defects, but these results were no longer observed when used in higher

concentrations (0% of defective cases). Of note, with the selected panel, we could not fully infer on the role of ceramide and dynamin-dependent endocytosis.

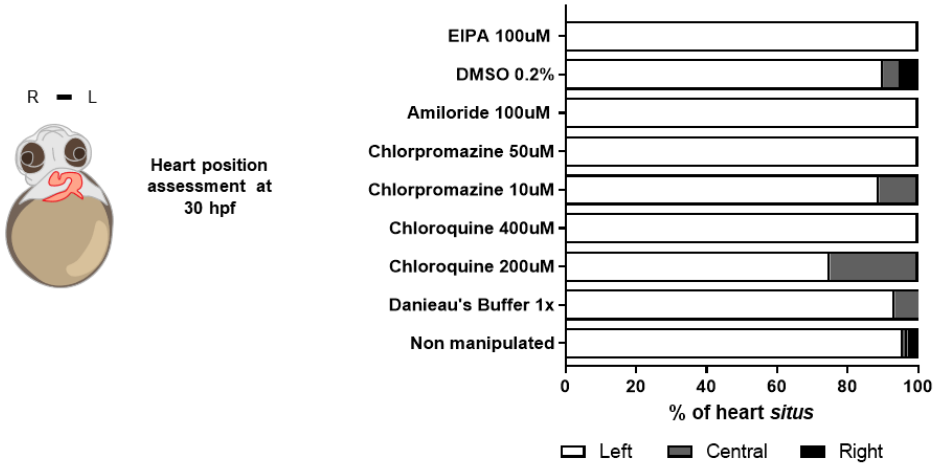

Figure 2.4: Inhibition of extracellular vesicles internalization does not affect left-right axis establishment. Heart position assessment at 30 hpf and scored for each control non manipulated embryos (n= 986 embryos) and manipulated embryos with control Danieau's buffer (n= 15 embryos), control DMSO (n= 20 embryos), chloroquine 200 µM (n= 12 embryos), chloroquine 400 µM (n= 10 embryos), chlorpromazine 10 µM (n= 9 embryos), chlorpromazine 50 µM (n= 3 embryos), amiloride 100 µM (n= 7 embryos) and EIPA 100 µM (n= 3 embryos). Hpf, hours post fertilization; L, left; R, right.

In summary, KV cells seem to actively internalize fluid content given the intracellular accumulation of 10 kDa rhodamine dextran tracer injected directly into the KV lumen. Our results showed that manipulated embryos did not develop robust LR defects by inhibiting multiple endocytic mechanisms with different concentrations, suggesting that symmetry breaking is independent of endocytic events and consequently, the observed internalization of 10 kDa rhodamine-dextran may reflect other cellular regulatory processes.

2.2.4. Increasing the Kupffer's Vesicle fluid viscosity severely affects the LR axis establishment

As inhibiting EV secretion did not affect LR development, we wanted to confirm that our experimental set up was sensitive enough to challenge the flow-sensing mechanism. Therefore, we diluted the KV fluid content in a methylcellulose solution (MC, viscosity ~1500 cP; water, viscosity 1 cP), as previously used in *Xenopus* and mouse (Schweickert et al., 2007; Shinohara et al., 2012). We reasoned that the overall contribution of fluid dynamics would be compromised by increasing fluid viscosity with methylcellulose.

The cilia-driven fluid flow is characterized by a laminar flow according to the Reynolds number (R_e), which by taking into account the diameter and flow speed scales, viscosity and density of the fluid, quantifies the ratio of inertial force to viscous force. The microscopic length scale of the cilia and the low velocity of the flow result in a low R_e of approximately < 10^{-2} and consequently the inertia effects can be neglected and viscous forces dominate, creating a laminar flow rather than turbulent (Supatto & Vermot, 2011; Montenegro-Johnson et al., 2016). Moreover, absence of inertia results in flow velocities proportional to the ciliary movement, which means that if a cilium stops beating, the flow speed decreases immediately (Supatto & Vermot, 2011).

In these studies, R_e was calculated based on water kinetic viscosity (Supatto & Vermot, 2011). We expected that within more viscous liquids, the same ciliary beating would be insufficient to apply enough force to achieve the same fluid flow velocity as in water-like fluids. Consequently, methylcellulose-driven slower fluid flow would result in a smaller defection of immotile cilia, affecting the mechanosensory mechanism.

On the other hand, at low R_e, flow mixing is mostly dependent on particle diffusion and chaotic advection produced by the ciliary movement, which is quantified by the Peclet number (P_e), using the characteristic diameter and velocity scales, as applied in R_e, and particle diffusion coefficient (Smith et al., 2007). Within the KV, chaotic advection results in vortical flows around the cilia (Supatto et al., 2008), however, its contribution for flow-sensing mechanism is unknown.

We reasoned that by increasing the fluid viscosity with methylcellulose and consequently lowering the flow velocity, particles would have more contact time within the fluid increasing the effect of diffusion (Bordbar et al., 2018). Thus, augmented particle diffusion would also impair the chemosensory mechanism.

To address how MC dilution and respective control DB dilution experiments affect fluid flow dynamics, we monitored flow physical properties after the procedure at 6 ss, 7 ss and 8 ss and proceeded to its analysis. Flow can be determined by tracking particles serving as fiduciary markers. We have previously established that the fluid flow speed is predictive of the LR patterning as well as specific local flow patterns are critical to break symmetry (Sampaio et al., 2014), such as the anterior hotspot of flow generated by the clustering of motile ciliated cells on the anterior-dorsal side of the KV (Compagnon et al., 2014; Tavares et al., 2017; Wang et al., 2011). Although local flow speed (velocity magnitude) is a useful measure for identifying regional flow patterns, it does not fully describe the directional material transport of the KV fluid (Ferreira et al., 2017; Juan et al., 2018). Thus, we determined the angular velocity at discrete locations as a proxy for the effective circular flow strength.

Angular velocity data from the many tracks obtained from the control group Sham and each dilution experiment were analyzed first dividing the KV in 8 radial sections and plotting the median angular velocity per section (Figure 2.5 A, B and C, Supplementary Movie 2.3 and 2.4).

To account for the hierarchical structure of the data with both within- and between-embryo variability in angular velocity tracks, linear mixed effects models were fitted to characterize how angular velocity varied across the KV and over time (Figure 2.5 E, F and G), incorporating somite stage, normalized LR and AP axis position and groups (Sham/ DB dilution/ MC dilution) as independent variables. Coefficient values can be interpreted as showing relative effect sizes and direction (Supplementary Table 2.1 for all p-values).

The linear mixed model for 'Sham' intervention and dilution experiments at 5 ss identified the following significant fixed (embryo-independent) effects:

(i) greater velocity in the anterior compared to the posterior region of the KV (p-value = 4.4e-142, coefficient 0.16 rad/s),

(ii) greater difference in flow between anterior and posterior following DB dilution (p-value = 0.0072, coefficient -0.021 rad/s) (Figure 2.5 E),

(iii) (at the significance level of 0.01) there is some evidence for any positive effect of DB dilution (e.g. in the anterior) receding over time (p-value = 0.010, coefficient - 0.013 rad/s/stage),

(iv) reduced difference in flow between anterior and posterior following MC dilution (p-value = 5.5e-14, coefficient -0.073 rad/s) (Figure 2.5 E),

(v) faster flow on the right compared with the left following MC dilution (but not DB dilution alone) (p-value = 0.0039, coefficient 0.026 rad/s) (Figure 2.5 F),

(vi) increased flow velocity over time (p-value = 5.6e-8, coefficient 0.021 rad/s/stage) and

(vii) a significant reduction of angular velocity following MC dilution (but not DB dilution alone) (p-value = 4.7e-4, coefficient -0.12 rad/s) (Figure 2.5 G).

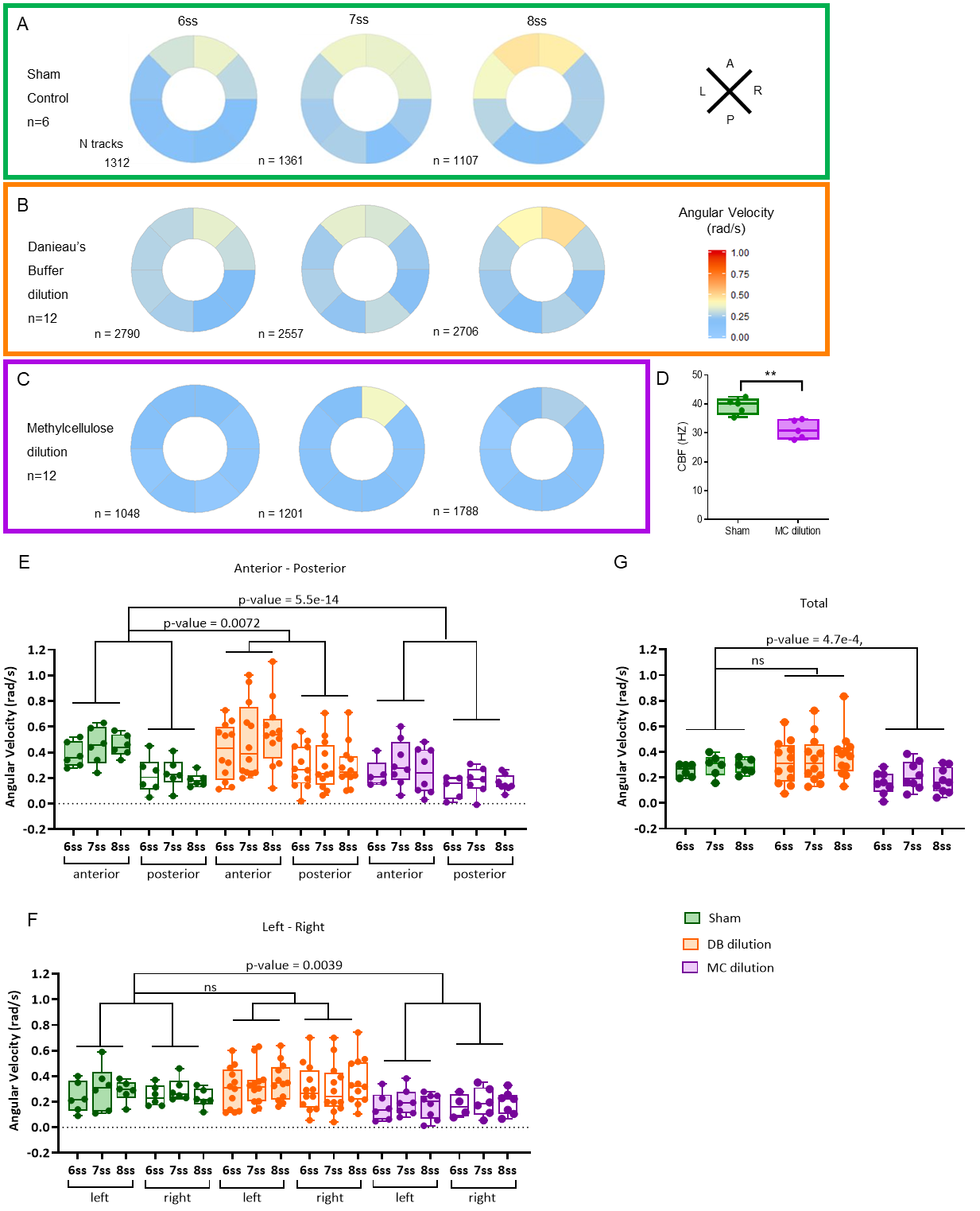

Figure 2.5: Kupffer's Vesicle flow dynamics is only affected when fluid dilution alters fluid viscosity.
(A-C) Angular velocity polar plots at 6ss, 7ss and 8ss for the three different groups (A) "Sham" control (n= 6 embryos), (B) "DB dilution" group (n= 12 embryos) and (C) "MC dilution" group (n= 12 embryos), after fluid extraction was performed at 5 ss; number of tracks refers to the number of particle trajectories identified for the quantifications and respective angular velocity plots. Colour code on polar plots refers to the median angular velocity for all pooled embryos. (E-G) Quantifications of angular velocities found for all tracks analyzed over time in (E) anterior and posterior quadrants, (F) left and right quadrants and (G) all KV. Dots contained in the bar plots correspond to median values per embryo. A statistical linear mixed model was applied (Supplementary Table 2.1 for all p-values). DB, Danieau's buffer; MC, methylcellulose; ss, somite stage.

In summary, KV fluid dilution with Danieau's buffer showed similar trends to the "Sham" control group, without significant differences, suggesting that this dilution experiment affected fluid content without perturbing flow dynamics for more than a few seconds. Interestingly, we observed major alterations on flow dynamics upon methylcellulose dilution into the KV lumen, disturbing local patterns of flow and decreasing the overall effectiveness of the flow throughout the recovery period.

In addition, we observed that dilution of KV fluid with MC significantly reduced cilia beat frequency (31.17 Hz ± 1.4; n = 50 cilia, 5 embryos) as compared to 'Sham' controls (39.29 Hz ± 1.2; n = 55 cilia; 5 embryos; Student's t-test with Welch's correction, p-value < 0.01) (Figure 2.5 D).

To further elucidate on how these two manipulations affect the LR axis patterning we assessed the expression pattern of *dand5*. This nodal antagonist is firstly expressed symmetrically around the KV and then, by the 8 ss, *dand5* is downregulated on the left side in response to optimal flow conditions (Lopes et al., 2010), turning into a predictive outcome for the internal organ lateralization. In WT embryos, the mainly right sided expression pattern of *dand5* was observed from 13 hpf onwards (corresponding to the 8 ss) (22/24 embryos, 91.7% of the cases). As expected, DB dilution alone showed *dand5* expression patterns on the right side comparable with WT results (5/6 embryos, 83.3% of the cases; Fisher test with Bonferroni correction, p-value > 0.05) (Figure 2.6 A). This indicates that a transient manipulation of the fluid content, without affecting its viscosity, does not impair the symmetry breaking mechanism of KV cells. Whereas the abnormal flow caused by MC dilution experiment resulted in more embryos displaying bilateral expression (7/12 embryos, 58% of the cases; Fisher test with Bonferroni correction, p-value < 0.001), reflecting either the lack of fluid flow dynamics or the lack of specific fluid content on induction of *dand5* degradation.

Moreover, consistent results for the same conditions were obtained later in development of heart placement, assessed at 30 hpf (Figure 2.6 B). WT embryos displayed normal left sided heart position (452/487 embryos, 92.8% of the cases), where manipulated embryos with DB dilution showed no significant differences when compared with control embryos (14/15 embryos, 93.3%; Fisher test with Bonferroni correction, p-value > 0.05) and manipulated embryos with MC dilution showed a significant reduction in the correct placement of the heart when compared to control embryos (7/16 embryos, 43.8% of the cases; Fisher test with Bonferroni correction, p-value < 0.0001).

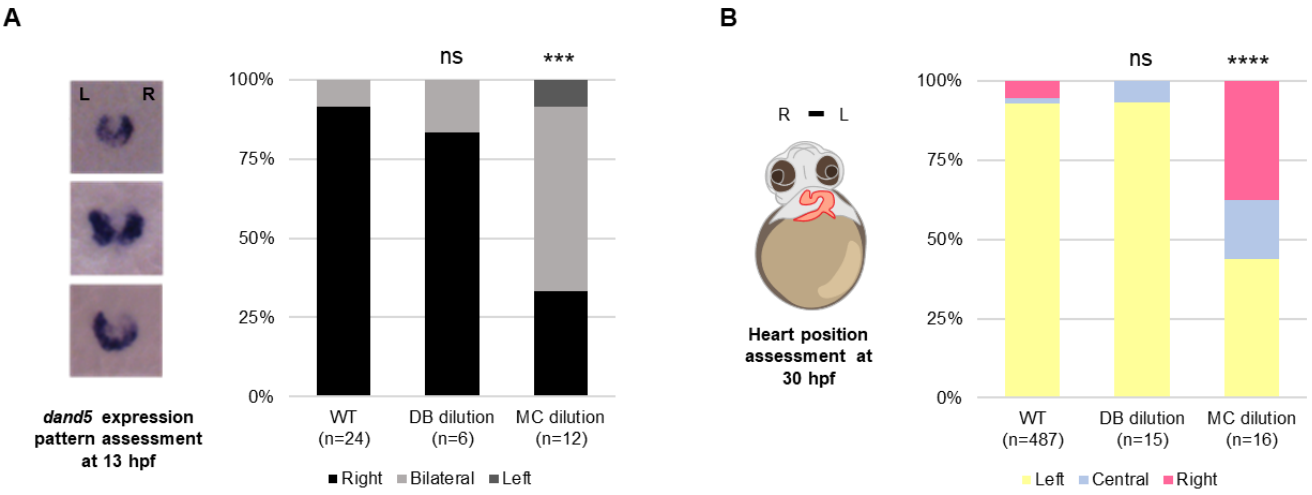

Figure 2.6: KV fluid dilution with Danieau's buffer does not affect left-right development.
(A) *dand5* expression pattern assessment at 13 hpf by *in situ* hybridization of control non manipulated embryos (n=24 embryos), danieau's buffer-diluted embryos (n=6 embryos) and methylcellulose-diluted embryos (n=12 embryos). ns, not significant; *** p<0,001; Fisher's Exact Test. (B) Heart position assessment at 30 hpf and scored for each control non injected embryos (n=487 embryos), Danieau's buffer-diluted embryos (n=15 embryos) and methylcellulose-diluted embryos (n=16 embryos). ns, not significant; **** p<0,0001; Fisher's Exact Test. L, left; R, right; DB, Danieau's buffer; MC, methylcellulose; hpf, hours post fertilization.

Thus, these results confirmed that changing KV fluid content transiently with a non-viscous buffer does not impact on flow physical properties and subsequently resulted in normal *dand5* expression pattern and later in correct heart position. Additionally, it revealed that our micromanipulation setup is a robust method to study KV fluid content in a stage specific time window.

Moreover, while MC dilution experiment does not discern between mechanosensory and chemosensory mechanisms, our results showed that by affecting both properties of the flow, through an increase of the fluid viscosity from 5 ss onwards, has a severe impact on LR development.

It is worth noticing that MC solutions are non-Newtonian fluids, meaning that its viscosity changes with shear rate, in contrast to Newtonian fluids, which viscosity remains constant no matter how fast they are forced to flow (Morozova et al., 2018). Furthermore, MC solutions follow a shear-thinning flow behavior as their viscosity decreases when the shear rate increases. Therefore, the specific fluid flow velocity patterns across the KV could affect differently the viscosity of the KV fluid diluted MC, which in theory could lead to inconsistent particle diffusion coefficients through the fluid and consequently EV accumulation at specific regions. Although, we did not observe any bias regarding the accumulation of particles during particle tracking for flow dynamic studies, to achieve a homogeneous viscous mixture, KV fluid

dilution experiments should be repeated using a Newtonian buffer, such as Ficoll (Qu & Breuer, 2020).

2.2.5. Fluid manipulations uncover mechanosensation for zebrafish left-right establishment

Concomitantly with this work, we found that KV has a unique capacity of recovery after fluid extraction. By using our micromanipulation method just to remove the KV fluid, we observed that manipulated KVs started to expand soon after fluid extraction (performed by Pedro Sampaio; BioRxiv Sampaio et al., 2022), indicating that the fluid secretion machinery mediated by CFTR (Navis et al., 2013; Roxo-Rosa et al., 2015) was not collaterally affected by the manipulation procedure and was able to recover the normal fluid volume. Furthermore, KV lumen recovery allowed us to monitor the flow dynamics as here described after fluid extraction.

Focusing on depleting KV fluid at 5 ss, as it was the developmental stage with highest sensitivity to this experiment, we found that embryos that showed a decreased angular velocity and persistent regional disoriented particle trajectories at 6 ss developed abnormal *dand5* expression pattern and laterality defects of the placement of internal organs, in the same proportion. In “Sham” control embryos and in 65% of the KV fluid extracted embryos, the strong counterclockwise movement was unchanged on all the stages followed fluid extraction leading the downregulation of *dand5* on the left sided cells and the corrected organ position (performed by Pedro Sampaio; BioRxiv Sampaio et al., 2022).

This further supports that directionality of the fluid flow is the most reliable asymmetric feature within the KV (Ferreira et al., 2017) and that embryos that did not recover flow dynamics fast enough until the 6 ss failed to break symmetry. Our results exposed unknown properties of the KV revealing an unprecedented recovery capacity of the embryo to continuously ensure the emergence of the symmetry break by re-inflate and re-circulate the fluid inside the KV, even in later stages when KV cells have become insensitive to flow dynamics.

Next, to expand our fluid dynamics perturbations within the developmental time window for flow-sensing mechanism, we challenged the KV recovery system by performing an additional fluid extraction one hour after the first intervention. Therefore, KV liquid was extracted at 5 ss and then at 7 ss in the same embryos, here referred to as double intervention. We predicted that in light of the chemosensory mechanism, even in the presence of a fast turnover of EV secretion, the double intervention would have a higher impact on EVs regular accumulation

within the KV cells than a single intervention at 5 ss and consequently would lead to more embryos with *dand5* symmetrically expressed. However, our results showed a similar proportion of bilateral *dand5* expression between the single intervention and the double intervention (data not shown), rejecting our hypothesis.

This data together with the results presented upon blocking different endocytic mechanisms showing no impact on laterality outcomes, rejects a flow-sensing mechanism dependent on constant accumulation and internalization of extracellular vesicles to trigger symmetry breaking. On the other hand, the directionality of the flow and the viscosity of the fluid have emerged as most robust elements for a consistent establishment of the LR asymmetry, advocating for the mechanosensory mechanism.

Section II – Another role of *syntenin-a*

2.2.6. Components involved in exosome biogenesis are expressed in the Kupffer's Vesicle

In order to have some insight about the vesicles that were being produced inside the KV cells, we took advantage of a KV specific microarray previously performed in our laboratory with WT embryos at 10 ss (unpublished data) that allowed us to identify the mRNA profile of these cells.

We observed that several exosome-related genes were highly expressed in the KV cells when comparing with the expression levels of genes known to have a role in the LR axis establishment, such as *foxj1a*, the master transcription factor involved in building KV cilia, *pkd2*, the monovalent cation-selective channel involved in flow sensing and transducing it into a calcium influx and *dand5,* the first asymmetrically expressed gene (summarized in Figure 2.7 A). Namely, Syndecans, Syntenin and Alix proteins, which form a complex involved in intraluminal vesicles biogenesis. Syndecans are heparan sulphate proteoglycans that bind to the endosomal membranes and recruit specific cargoes and Syntenin, the cytosolic adaptor protein that via its PDZ domain connects the Syndecans to Alix, which in turn is the auxiliary component of the ESCRT machinery that engages endosomal membrane inward budding and abscission (Grootjans et al., 2000; Baietti et al., 2012; Friand et al., 2015). Syndecans also function as co-receptors of growth factor receptors and integrins modulating cell migration, cell-cell interactions and cell-extracellular matrix interactions (Afratis et al., 2017). Likewise,

Syntenin is also involved in additional pathways depending on its binding partners, being implicated in cell division, neuronal development and tumor invasion (Shimada et al., 2019; Addi et al., 2020; Pradhan et al., 2020).

In zebrafish, three *syndecans* (2, 3 and 4) (Chen et al., 2004; Whiteford & Couchman, 2006; Lambaerts et al., 2012), two *syntenins* (a and b) (Lambaerts et al., 2012) and one ALIX, named *programmed cell death 6 interacting protein* (*pdcd6ip*) (Corbett et al., 2018) orthologues have been previously described. Moreover, Verweij and colleagues revealed recently that the Syndecan – Syntenin – Alix complex has conserved functions in zebrafish by showing that the number of CD63-pHluorin positive exosomes was reduced upon *syntenin-a* knockdown (Verweij et al., 2019). Within the KV cells, all *syndecans*, *syntenin-a* and *pdcd6ip* transcripts were detected within the range of the *dand5* and *pkd2* expression levels (Figure 2.7 A).

Next, we validated the microarray results by assessing the expression patterns of these genes through *in situ* hybridization both in zebrafish embryos of 4 ss and 10 ss, comprising the main time window where extracellular vesicles would potentially be secreted to the KV lumen, between the fluid flow sensing mechanism and its outcome, *dand5* downregulation. The *in situ* hybridization probe against *syntenin-a* showed a clear expression in the KV cells and notochord at 4 ss and 10 ss (Figure 2.7 B). *Syndecan 3* was firstly expressed only at the tailbud, in close proximity with the KV cells from the posterior side at 4 ss, and then it propagated through the pre-somitic mesoderm by the 10 ss (Figure 2.7 C). Interestingly, *syndecan 4* was expressed in the KV cells and the notochord (Figure 2.7 D), in a complementary fashion to the *syndecan 3* expression pattern suggesting complementary tissue-specific functions. Lastly, *in situ* hybridization against *pdcd6ip* showed a widely spread expression with an enrichment within the KV region at 4 ss that became more restricted to the KV cells at 10 ss (Figure 2.7 E). Unfortunately, we were not able to produce a reliable *syndecan 2 in situ* probe.

A

Ensembl ID	Gene Name	Description	Expression level *
ENSDARG00000036471	*dand5*	DAN domain family, member 5	8,35
ENSDARG00000059906	*sdc4*	syndecan 4	8,22
Gene ID: 337077	*sdc3*	syndecan 3	8,12
ENSDARG00000012513	*sdcbp*	syndecan binding protein (syntenin-a)	7,48
ENSDARG00000002731	*sdc2*	syndecan 2	6,62
ENSDARG00000101919	*foxj1a*	forkhead box J1a	6,11
ENSDARG00000025269	*pdcd6ip*	programmed cell death 6 interacting protein (ALIX)	4,09
ENSDARG00000014098	*pkd2*	polycystic kidney disease 2	3,56

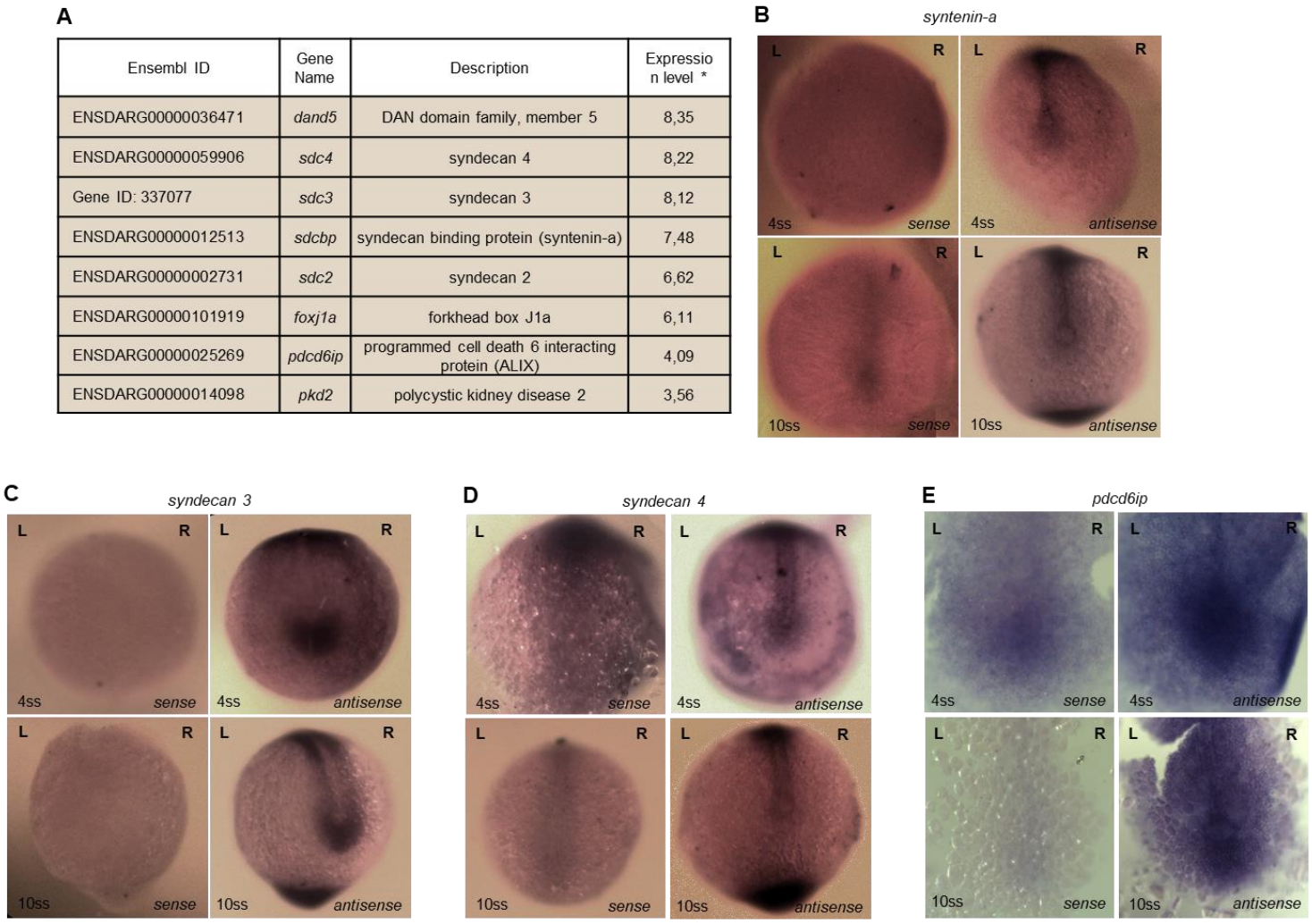

Figure 2.7: Syndecan – syntenin-a – pdcd6ip complex is expressed in Kupffer's Vesicle cells.
(A) Microarray analysis of KV-specific cells of 10 ss wildtype embryos. (B) Dorsal view of whole-mount *in situ* hybridization of sense and antisense probes for *syntenin-a* expression in embryos with 4 and 10 ss. (C) Dorsal view of whole-mount *in situ* hybridization of sense and antisense probes for *syndecan 3* expression in embryos with 4 and 10 ss. (D) Dorsal view whole-mount *in situ* hybridization of sense and antisense probes for *syndecan 4* expression in embryos with 4 and 10 ss. (E) Flat-mount *in situ* hybridization of sense and antisense probes for *pdcd6ip* expression in embryos with 4 and 10 ss. KV, Kupffer's Vesicle; L, left; R, right.

Being expressed at the right place and time, we speculated that these proteins could be involved in the formation of at least some of the CD63-pHluorin positive EVs that we observed within the KV lumen (section I). In fact, zebrafish *UDP-glucose dehydrogenase, ugdh,* mutants that are unable to produce proper heparan sulphate chains for the different proteoglycans, such as *syndecans*, developed abnormal symmetric *dand5* expression pattern. *Ugdh* mutants showed normal KV structure, ciliary length and fluid flow directionality, suggesting a role of heparan sulphate chains in restricting the flow sensing mechanism to the left sided KV cells (Superina et al., 2014).

2.2.7. Knockdown of *syntenin-a* affects dand5 expression pattern and heart situs

In a last attempt to test if EVs could be at the heart of the flow sensing mechanism, we decided to inhibit the formation of intraluminal vesicles and, consequently diminishing the number of exosomes secreted. For this purpose, we performed loss-of-function experiments using a morpholino targeting the translation start site of *syntenin-a* (*synta* MO) transcripts and its corresponding control morpholino (mismatch MO), previously validated in other studies to block Syntenin protein translation (Lambaerts et al., 2012) and to inhibit exosome formation (Verweij et al., 2019) in zebrafish embryos. However, injection of *synta* MO at one cell stage leads to the arrest of epiboly and impairment of convergent and extension movements during gastrulation (Figure 2.8 A, top panel), as formerly described (Lambaerts et al., 2012; Zhang et al., 2018).

Taking this result into consideration, we decided to inject the *synta* MO in a later developmental stage and specifically target the precursors of the KV, the dorsal forerunner cells (DFCs) to assess the cell-autonomous role of *syntenin-a* in the KV cells (Essner et al., 2005). By co-injecting the *synta* MO with the lineage tracer rhodamine dextran (10 kDa), we could later select the embryos that only showed fluorescence in the yolk cell and the KV cells (Figure 2.8 B) (Amack & Yost, 2004). Below we shall refer to these embryos as *synta* MO^{DFCs}.

Analysis of 8 ss embryos injected with *synta* MO^{DFCs} showed comparable embryonic development with control non injected embryos and mismatch MO^{DFCs} injected siblings (Figure 2.8 A bottom panel), confirming that we managed to bypass of the defects caused by the absence of *syntenin-a* during gastrulation.

Following MO^{DFCs} injections, embryos were analyzed regarding the *dand5* expression pattern, *spaw* expression pattern and heart lateralization outcome. Results revealed that control embryos showed the expected stronger expression of *dand5* on the right side of the KV at 13 hours post fertilization (hpf, corresponding to 8 ss) and an asymmetric expression of *spaw* on

the left side of LPM at 15 hpf (corresponding to 12 ss) (Figure 2.8 C and D). On the other hand, KV-specific *synta* knockdown resulted in a significant increase in embryos with defective symmetric or left sided expression pattern of *dand5* (24/65 embryos, 37% of the cases), when compared with WT non injected embryos (6/73 embryos; Fisher test with Bonferroni correction, p-value < 0.0001) and with control mismatch MO^{DFCs} injected embryos (4/35 embryos; Fisher test with Bonferroni correction, p-value < 0.01). Moreover, some DFCs *synta* morphants showed an overall decreased signal of *dand5* expression (data not shown). Consequently, *spaw* expression pattern became absent or bilateral in most of the cases, in contrast to WT embryos (12/19 embryos, 63% of cases; Fisher test with Bonferroni correction, p-value < 0.01).

To verify that defects in LR related gene expression patterns were specifically due to interference with *syntenin-a* expression and function, we co-injected *syntenin-a* RNA (50 pg *synta* RNA), which encodes an WT Syntenin-a protein insensitive to the *synta* MO, as previously described (Lambaerts et al., 2012). Co-injection of *synta* RNA with *synta* MO specifically into the DFCs led to a partial rescue in *dand5* expression pattern (4/15 embryos, 27% of the cases) to proportions comparable to the control non injected embryos (Fisher test with Bonferroni correction, p-value > 0.05).

Regarding heart development, control non injected and mismatch MO^{DFCs} injected embryos exhibited a normal leftward jogging of the heart at 30 hpf (193/210 embryos, 92%; and 26/27 embryos, 96%, respectively), while *synta* MO^{DFCs} morphants showed a strong and significant reduction of heart *situs* when compared to both controls (17/40 embryos, 43%; Fisher test with Bonferroni correction, p-value < 0.0001). Moreover, co-injection of *synta* MO^{DFCs} with 50 pg *synta* RNA^{DFCs} partially and significant rescued the heart *situs* (14/20 embryos, 70%; Fisher test with Bonferroni correction, p-value < 0.01 when compared to controls, p-value < 0.05 when compared to *synta* MO^{DFCs}). Similar results were obtained using a second morpholino (*synta*bis MO^{DFCs}) and analyzing *dand5* expression pattern and heart location in the zebrafish embryo body.

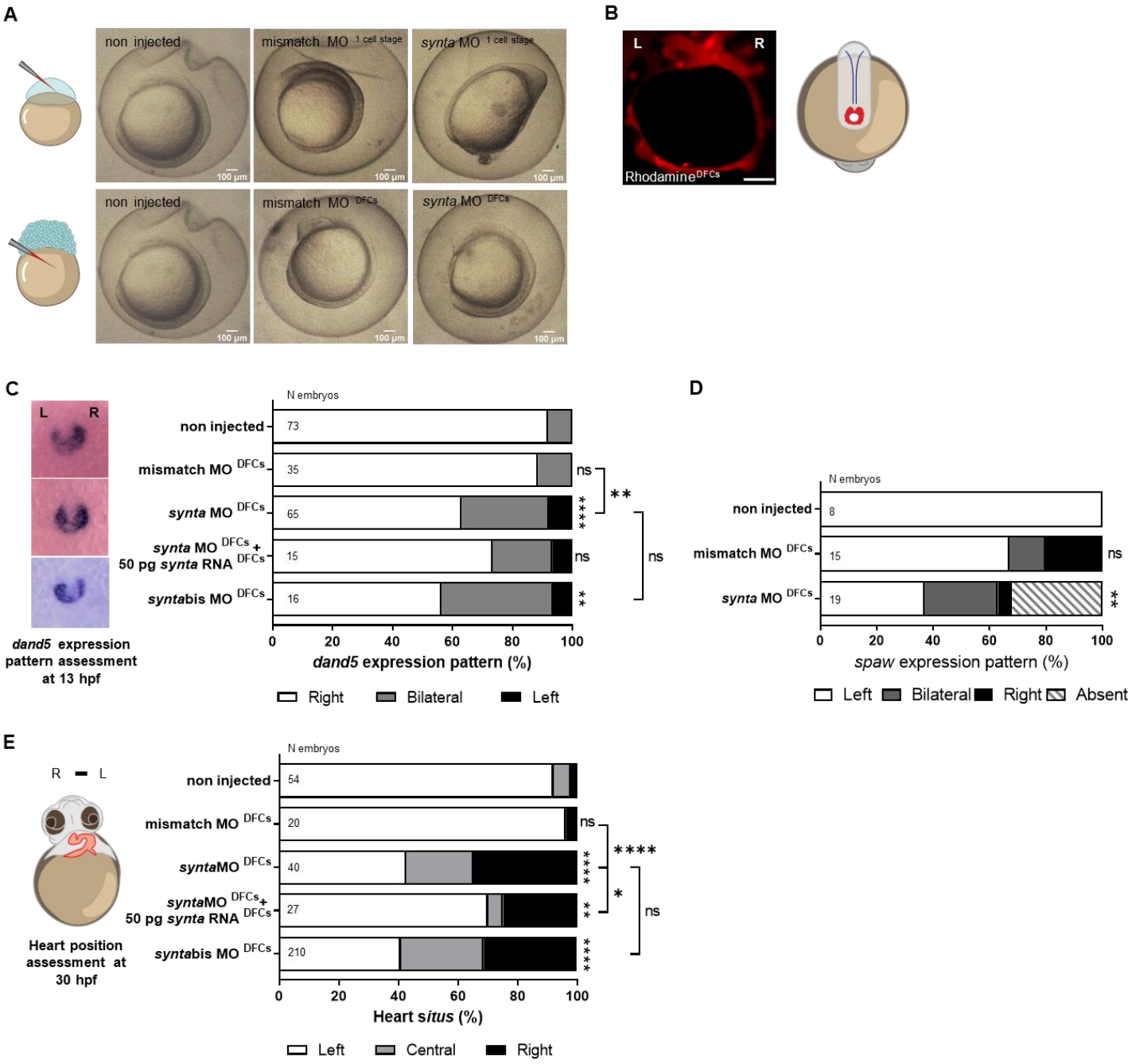

Figure 2.8: Kupffer's Vesicle – specific knockdown of *syntenin-a* overcomes gastrulation arrest and leads to LR defects.

(A) Schematic representation of morpholinos injections at 1 cell stage and at 512 cell stage, specifically for DFCs, and respective phenotypes observed upon injection of control mismatch MO and *synta* MO at 8 ss. (B) Rhodamine labelling at the KV showing the result of a successful injection of *synta* MO at 512 cell stage into DFCs and respective schematic representation. (C) *dand5* expression pattern assessment at 13 hpf by *in situ* hybridization of control non injected embryos (n= 73 embryos) and control mismatch MO ^{DFCs} (n= 35 embryos), *synta* MO ^{DFCs} (n= 65 embryos) *synta* MO ^{DFCs} combined with 50 pg of *syntenin-a* RNA ^{DFCs} (n= 15 embryos) and *synta*bis MO ^{DFCs} (n= 16 embryos) injected embryos. ns, not significant; * p<0.05; ** p<0.01; **** p<0,0001; Fisher's Exact Test. (D) *spaw* expression pattern assessment at 15 hpf by *in situ* hybridization of control non injected embryos (n= 8 embryos) and control mismatch MO ^{DFCs} (n= 15 embryos) and *synta* MO ^{DFCs} (n= 19 embryos) injected embryos. ** p<0.01; Fisher's Exact Test. (E) Heart position assessment at 30 hpf and scored for each control non injected embryos (n= 210 embryos) and injected embryos with control mismatch MO ^{DFCs} (n= 27 embryos), *synta* MO ^{DFCs} (n= 40 embryos), *synta* MO ^{DFCs} combined with 50 pg of *syntenin-a* RNA ^{DFCs} (n=

20 embryos) and *synta*bis MO ^{DFCs} (n= 54 embryos). DFCs, dorsal forerunner cells; KV, Kupffer's Vesicle; ss, somite stage; hpf, hours post fertilization; L, left; R, right. Scale bar, otherwise stated, represents 20 µm.

Thus, these data demonstrated that *syntenin-a* is functionally required for the LR axis establishment during the early stages of symmetry breaking.

2.2.8. Knockdown of *syntenin-a* alters fluid flow dynamics

Before analysing *syntenin-a* loss-of function experiments in the context of LR axis establishment, we needed to ensure that fluid flow dynamics were not affected. Otherwise, both chemosensory and mechanosensory properties of the flow would be perturbed, without being possible to discern on which process *syntenin-a* knockdown impacts.

To evaluate flow dynamics upon MO^{DFCs} injections, we recorded and tracked the native particles inside the KV of multiple embryos at 8 ss using high-speed video microscopy, as we previously described (Sampaio et al., 2014). We then quantified the effective flow angular velocity, which measures the magnitude of the directed counterclockwise movement of the tracked particles through a uniformly rotating sphere, as the circulating fluid in the KV (Ferreira et al., 2017; Juan et al., 2018). Angular velocity data were analyzed first dividing the KV in 8 radial sections and plotting the median angular velocity per section, as described in section I (Figure 2.9 A).

We observed that both controls non injected embryos and mismatch MO^{DFCs} injected embryos showed similar angular velocity flow maps, with a significant stronger directional flow at the anterior region, which was lost in *synta* MO^{DFCs} injected embryos (7, 7 and 8 embryos analyzed, respectively; one-way ANOVA Krustal-Wallis's test followed by Dunn's multiple comparison test, adjusted p-value < 0.01) (Figure 2.9 B). Additionally, *synta* MO^{DFCs} injected embryos showed a disorganized flow directionality on the left side of the KV (one-way ANOVA Krustal-Wallis's test followed by Dunn's multiple comparison test, adjusted p-value < 0.05) (Figure 2.9 D). No significant differences were observed within the posterior and right quadrants (one-way ANOVA Krustal-Wallis's test followed by Dunn's multiple comparison test, adjusted p-value > 0.05) (Figure 2.9 C and E). Moreover, co-injection of *synta* MO^{DFCs} with 50 pg *synta* RNA^{DFCs} significantly rescued the overall angular flow velocity when compared to *synta* MO^{DFCs} (one-way ANOVA Krustal-Wallis's test followed by Dunn's multiple comparison test, adjusted p-value < 0.05), to similar values observed in control groups (one-way ANOVA Krustal-Wallis's test followed by Dunn's multiple comparison test, adjusted p-value > 0.05) (Figure 2.9 F).

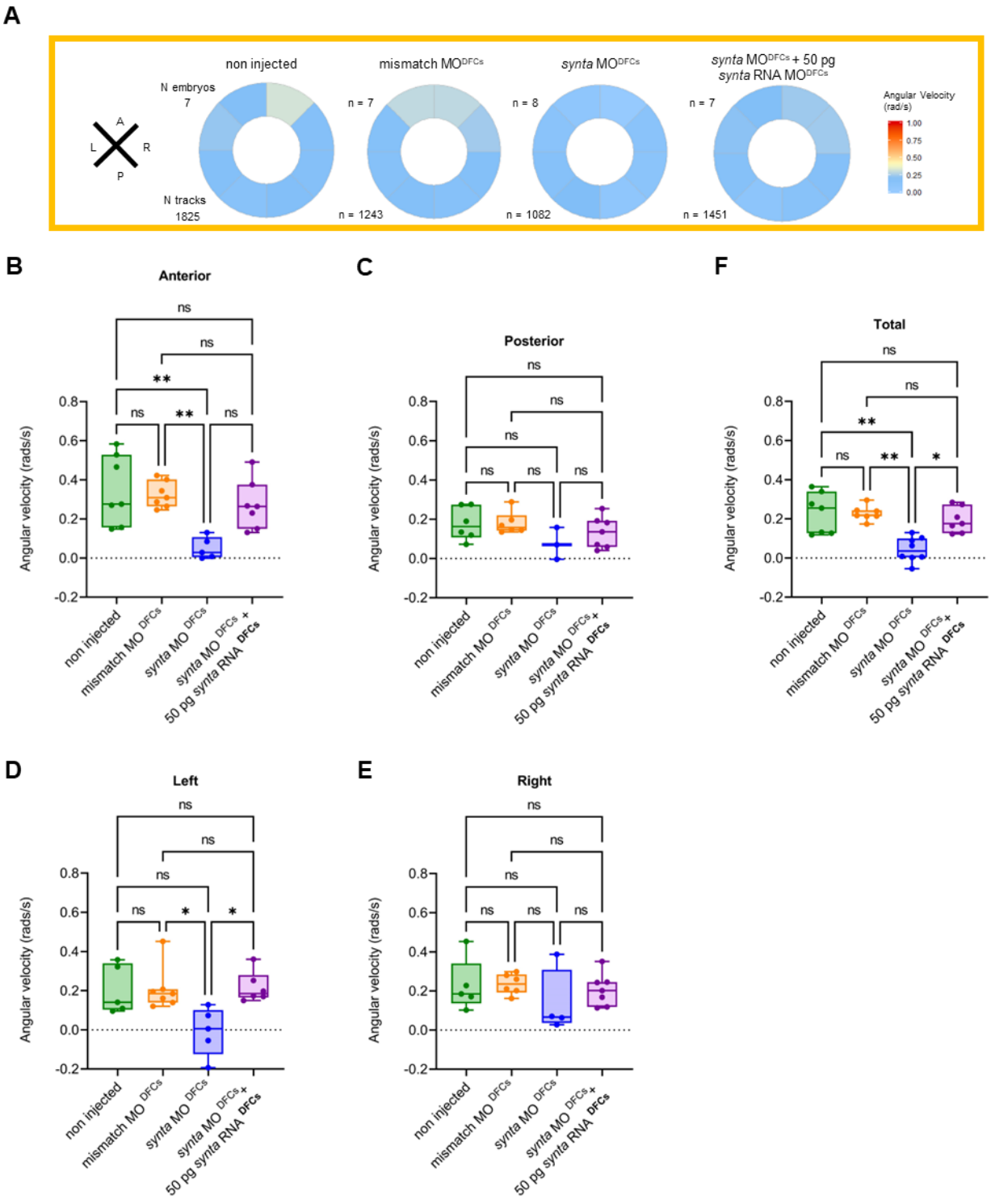

Figure 2.9: *Syntenin-a* knockdown impacts on fluid flow dynamics.
(A) Angular velocity polar plots at 8 ss for control non injected embryos (n= 7 embryos), mismatch MO ^{DFCs} (n= 7 embryos), *synta* MO ^{DFCs} (n= 8 embryos), and *synta* MO ^{DFCs} combined with 50 pg of *syntenin-a* RNA ^{DFCs} (n= 7 embryos) injected embryos. N tracks refers to the number of particle trajectories identified for quantification and respective angular velocity plots. Color code on polar plots states to the median angular velocity for all pooled embryos. (B-F) Quantification of angular velocities found for all tracks analyzed on the (B) anterior, (C) posterior, (D) left and (E) right quadrants and (F) total KV. ns, not significant; * p<0.05; ** p<0,01; non-parametric ANOVA test (Kruskal-Wallis) and *post hoc* analysis with Dunn's multiple comparisons tests. DFCs, dorsal forerunner cells; KV, Kupffer's Vesicle; ss, somite stage; A, anterior; P, posterior; L, left; R, right.

Our results demonstrated that *syntenin-a* downregulation leads to a general decrease in the angular velocity, most prominent in the anterior and the left sections of the KV. Given the impact on the fluid flow dynamics, we could no longer continue with the hypothesis that LR development defects upon the knockdown of *syntenin-a* might be solely due to a reduction in EV production within the KV cells.

2.2.9. Syntenin-a plays an additional role in regulating ciliary motility

The decreased angular velocity of flow was unexpected in the DFCs *synta* morphants, but since the fluid flow dynamics were recovered upon the rescue experiments, advocating for a specific function of *syntenin-a* rather than an off-target effect of the morpholino, we reasoned that *syntenin-a* could have an additional role in the KV cells. Therefore, we aimed to unravel the origin of the flow problems in the DFCs *synta* morphants.

The proper counterclockwise fluid flow is accomplished by the cumulative effect of correct ciliogenesis and KV remodeling (Kreiling et al., 2007; Oteiza et al., 2010; G. Wang et al., 2011; M. Zhang et al., 2012; Liu et al., 2019). As KV cilia length has a major impact in generating productive flow, by a power of 3 (Montenegro-Johnson et al., 2016; Pintado et al., 2017), we started by examining ciliary length through immunostaining for acetylated alpha tubulin, which labels the ciliary microtubules, at 8 ss (Figure 2.10 A). We quantified the ciliary length in 3D and found no significant differences between *synta* MO^{DFCs} injected embryos (6.27 ± 0.97 µm) and the control non injected (6.57 ± 0.76 µm) and mismatch MO^{DFCs} injected (6.58 ± 0.47 µm) embryos (Welch's ANOVA test with Dunnett's multiple comparisons test, adjusted p-value > 0.05) (Figure 2.10 B). The total number of cilia was not significantly different either (data not shown).

Subsequently, continuing the search for an explanation for the decreased angular flow velocity in *synta* MO^{DFCs} embryos we determined the ciliary beat frequency (CBF) through high-speed video microscopy analysis and did not find any difference between the treatments (non-injected embryos 37.59 Hz, mismatch MO^{DFCs} embryos 35.21 Hz and *synta* MO^{DFCs} embryos 35.71 Hz; ANOVA Krustal-Wallis's test with Dunn's multiple comparison test, adjusted p-value > 0.05) (Figure 2.10 C).

Next, we conducted an assay to assess the ciliary motility status by injecting a minimal amount of *arl13b-GFP* RNA (50 pg) into one cell staged embryos and performed live imaging at 8 ss (Figure 2.10 D). We have shown that by scanning the whole KV at a low speed in a slow scanning mode using a high pixel dwell time, it is possible to accurately distinguish the motile cilia from the immotile cilia and quantify them (Tavares et al., 2017).

We then track each motile and immotile cilium regarding its spatial distribution along the anterior – posterior axis (Figure 2.10 E). Clustering of motile cilia at the anterior region occurs during KV remodeling through cell rearrangements and has a direct impact on the fluid flow profile (Wang et al., 2012; Sampaio et al., 2014; Smith et al., 2014; Ferreira et al., 2017; Tavares et al., 2017). Our results showed that all conditions tested had a similar distribution with most cilia located at the anterior region (Figure 2.10 F). Although this means that KV re-shape is not compromised, it still does not provide an explanation for the decreased angular flow velocity in *synta* morphants.

By analyzing the number of motile and immotile cilia and plotting them according to its location within the KV, we observed that control non injected (n=23 embryos, 869 cilia) (Supplementary Movie 2.5) and mismatch MO^{DFCs} injected (n=17 embryos, 754 cilia) embryos had more motile cilia in general and specifically at the anterior region (ANOVA test with Tukey's multiple comparisons post-test, adjusted p-value < 0.01) and that the immotile cilia were evenly distributed between the two KV halves (ANOVA test with Tukey's multiple comparisons post-test, adjusted p-value > 0.05) (Figure 2.10 H and G), as previously described (Tavares et al., 2017). As for DFCs *synta* morphants (n=13 embryos, 482 cilia), motility was severely affected (Supplementary Movie 2.6). Motile cilia number was reduced at the expense of immotile cilia, as the total cilia number was maintained (mean motile cilia 19/36 cilia in *synta* MO^{DFCs} compared to 33/37 cilia in non-injected embryos and to 35/46 cilia in mismatch MO^{DFCs}). No further enrichment of motile cilia was observed at the anterior region (ANOVA test with Tukey's multiple comparisons post-test, adjusted p-value > 0.05) (Figure 2.10 I). Additionally, co-injection of *synta* MO^{DFCs} with 50 pg *synta* RNA^{DFCs} restored both the number of motile cilia (mean 32/40 cilia) and its distribution around the KV (ANOVA test with Tukey's multiple comparisons post-test, adjusted p-value < 0.01) (Figure 2.10 J).

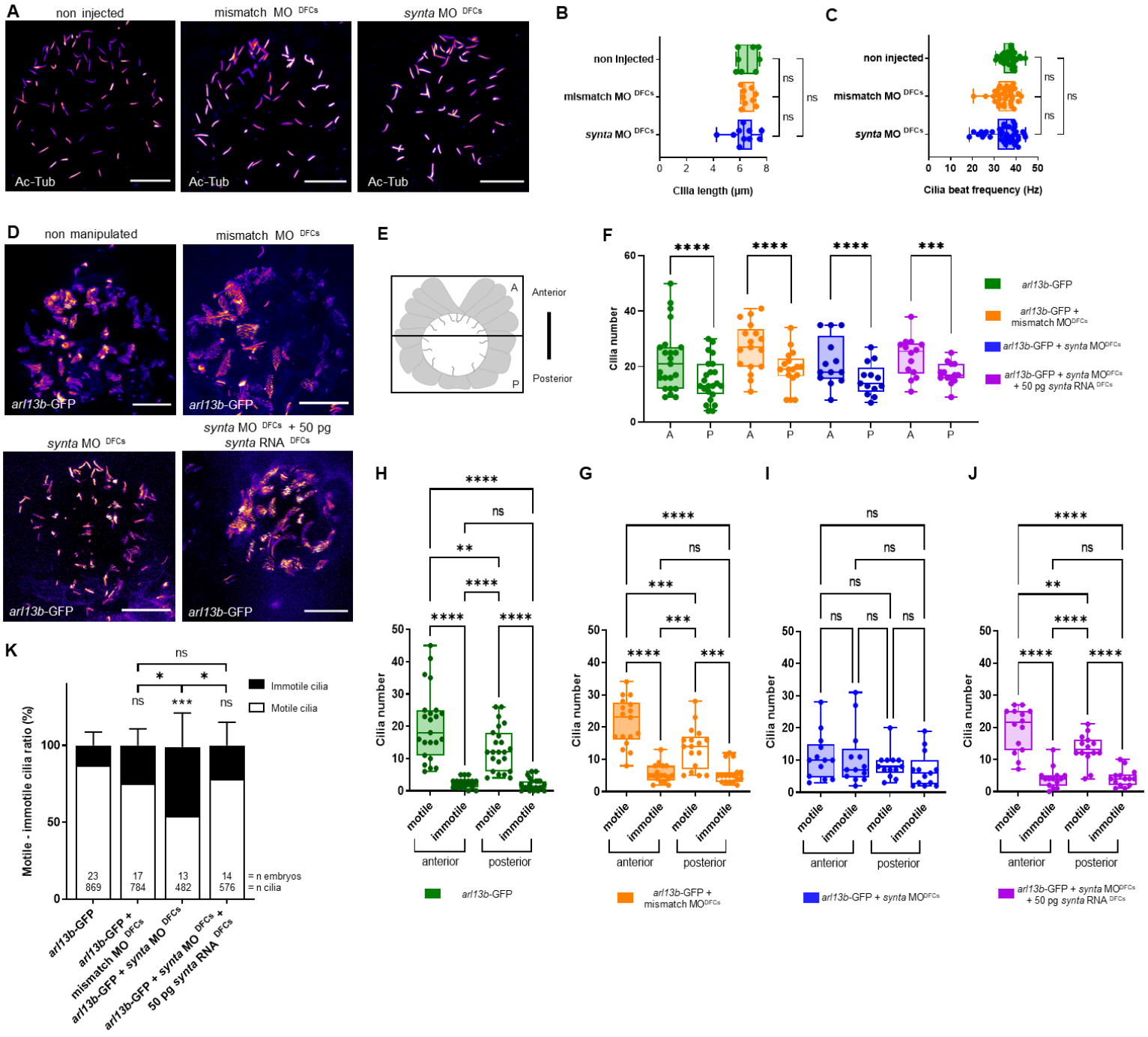

Figure 2.10: Kupffer's Vesicle – specific knockdown of *syntenin-a* affects cilia motility.

(A) Acetylated α-tubulin immunostaining for control non injected embryos and injected with control mismatch MO DFCs and *synta* MO DFCs at 8 ss showing KV labelled cilia. (B) 3D cilia length measurement in control non injected embryos (n=8 embryos, 461 cilia) and injected with control mismatch MO DFCs (n=9 embryos, 358 cilia) and *synta* MO DFCs (n=10 embryos, 447 cilia). ns, not significant; Welch's ANOVA test and *post hoc* analysis with Dunnett's multiple comparisons tests. (C) Cilia beat frequency quantification in control non injected embryos (n=4 embryos, 38 cilia) and injected with control mismatch MO DFCs (n=4 embryos, 35 cilia) and *synta* MO DFCs (n=4 embryos, 38 cilia). ns, not significant; non-parametric ANOVA test (Kruskal-Wallis) and *post hoc* analysis with Dunn's multiple comparisons tests. (D) KV cilia z-projection of live embryos injected with 50 pg *arl13b*-GFP RNA and later on injected with mismatch MO DFCs, *synta* MO DFCs, *synta* MO DFCs combined with 50 pg of *syntenin-a* RNA DFCs imaged at 8 ss. (E) Schematic representation of KV division used to compare the anterior-posterior cilia distribution. (F) Quantification of cilia number distributed along the anterior-posterior axis in 50 pg *arl13b*-GFP

RNA injected control embryos (n=23 embryos, 869 cilia) and injected with mismatch MO ^{DFCs} (n=17 embryos, 754 cilia), *synta* MO ^{DFCs} (n=13 embryos, 482 cilia), *synta* MO ^{DFCs} combined with 50 pg of *syntenin-a* RNA ^{DFCs} (n=14 embryos, 576 cilia). *** p<0.001; **** p<0,0001; one-way ANOVA test with Tukey's multiple comparisons post-test. (H-J) Distribution of motile and immotile cilia along the anterior-posterior axis quantified in (F) for 50 pg *arl13b*-GFP RNA injected control embryos (H) and injected with mismatch MO ^{DFCs} (G), *synta* MO ^{DFCs} (I), *synta* MO ^{DFCs} combined with 50 pg of *syntenin-a* RNA ^{DFCs} (J). ns; not significant; ** p<0.01; **** p<0,0001; one-way ANOVA test with Tukey's multiple comparisons post-test. (K) Percentages of ciliary motility assessed in previously quantified cilia in (F). ns; not significant; * p<0.05; *** p<0,001; Fisher's exact test. DFCs, dorsal forerunner cells; KV, Kupffer's Vesicle; ss, somite stage. Scale bar represents 20 μm.

Thus, loss of KV flow pattern and strength in *syntenin-a* morphants can be explained by the decrease of motile – immotile cilia ratio (Fisher test with Bonferroni correction, p-value < 0.001, when compared with controls; p-value < 0.05 when compared with mismatch MO^{DFCs} injected and rescued embryos) (Figure 2.10 K) and the disruption of the anterior cluster of motile cilia.

2.2.10. *Syntenin-a* regulates ciliary motility by modulating Notch signaling

Studies from our laboratory and others have pointed out that cilia within the LRO is regulated by Notch signaling. First, we showed that Notch ligand *deltaD* zebrafish mutants have shorter cilia and that overexpression of *deltaD* alone or of *notch intracellular domain, nicd*, were able to increase the ciliary length (Lopes et al., 2010). *DeltaD* is expressed in the KV cells and it was proposed to act autonomously through *foxj1a* (Lopes et al., 2010), as *foxj1a* morphants also have shorter or absent cilia in the KV (Stubbs et al., 2008; Yu et al., 2008). Later on, Tözser and colleagues showed by knocking down the Notch1 receptor, that *Xenopus* morphants phenocopied the zebrafish *deltaD* mutant shorter cilia at the frog LRO (Tözser et al., 2015). On the other hand, Notch signaling was implicated in motile – immotile cilia fate. Boskovski *et al.* reported that GALNT11, an N-acetylgalactosamine type O-glycosylation enzyme, activates Notch signaling through glycosylation of Notch receptor 1 regulating ciliary motility in the *Xenopus* LRO. Either by knocking down *galnt11* or *notch1*, the number of motile cilia was increased, whereas overexpression of *nicd* had the opposite effect (Boskovski et al., 2013). We then showed that regulation of ciliary motility by Notch signaling was conserved in the zebrafish LRO. We injected *arl13b-GFP* RNA, previously shown to increase ciliary length (Pintado et al., 2017) to normalize the length of cilia in all our manipulations and to be able to evaluate ciliary motility in live embryos. We then found that zebrafish *deltaD* mutants, similarly to *Xenopus notch1* morphants, have more motile cilia in expense of immotile cilia (Sampaio et al., 2014; Tavares et al., 2017).

Taking this into consideration, we questioned if the underlying reason for the differences in the motile – immotile cilia ratio observed in the *synta* morphants was related to an impairment of Notch signaling.

Syntenin is a cytoplasmic protein containing two adjacent PDZ domains (Grootjans et al., 1997), which confers to this protein a high capacity of protein-protein interaction and networking in order to build functional units within the cell (Nourry et al., 2003). Moreover, some Notch ligand intracellular domains cover PDZ binding motifs that enable an interaction with different PDZ adaptor proteins for further cellular localization and protein stability (Ascano et al., 2003; Wright et al., 2004; Adam et al., 2013; Tetzlaff et al., 2018). Interestingly, Syntenin was previously shown to physically interact with zebrafish DeltaD, by protein PDZ domain dimerization, which resulted in DeltaD protein stabilization at the cell membrane and, consequently, impairment of DeltaD internalization (Estrach et al., 2007). Ubiquitination and internalization of Notch ligands are essential to fully activate them in order to bind to Notch receptors and subsequently lead to Notch signaling activation (Itoh et al., 2003). Therefore, Syntenin – DeltaD binding limits Notch signaling induction in the neighboring cells (Estrach et al., 2007).

Thus, we assessed by immunostaining if DeltaD protein localization was being affected by loss-of-function of *syntenin-a*. We used a *sox17:GFP* transgenic line to identify the KV cells and performed the immunolabelling assay for DeltaD at 8 ss. DeltaD protein was found weakly localized within the KV cells of control non injected embryos (Figure 2.11 A), in line with the RNA expression previously described (Lopes et al., 2010). Further quantification of DeltaD fluorescence signal levels showed an increase of DeltaD within the KV cells of *synta* morphants when compared to WT embryos (student's t-test with Welch's correction, p-value < 0.05) (Figure 2.11 B), supporting a modulatory effect on DeltaD protein stability by Syntenin-a within the cells in zebrafish embryos.

To fully quantify the differences in protein levels, a more sensitive protein detection method such as western blot should be performed. However, *syntenin-a* knockdown injection only targeted the KV precursors and any difference would be diluted when performing a western blot with samples of whole embryos. So, we then analyzed DeltaD localization in another zebrafish tissue to confirm the phenotype observed within the KV cells. *DeltaD* is also expressed in the posterior tailbud of bud staged embryos (Figure 2.11 C) and, upon whole-embryo knockdown of *syntenin-a,* we observed an upregulation of DeltaD and a wider area of distribution supporting a relocalization of DeltaD between the plasma membrane and the endocytic compartments (student's t-test with Welch's correction, p-value < 0.05) (Figure 2.11 D and E).

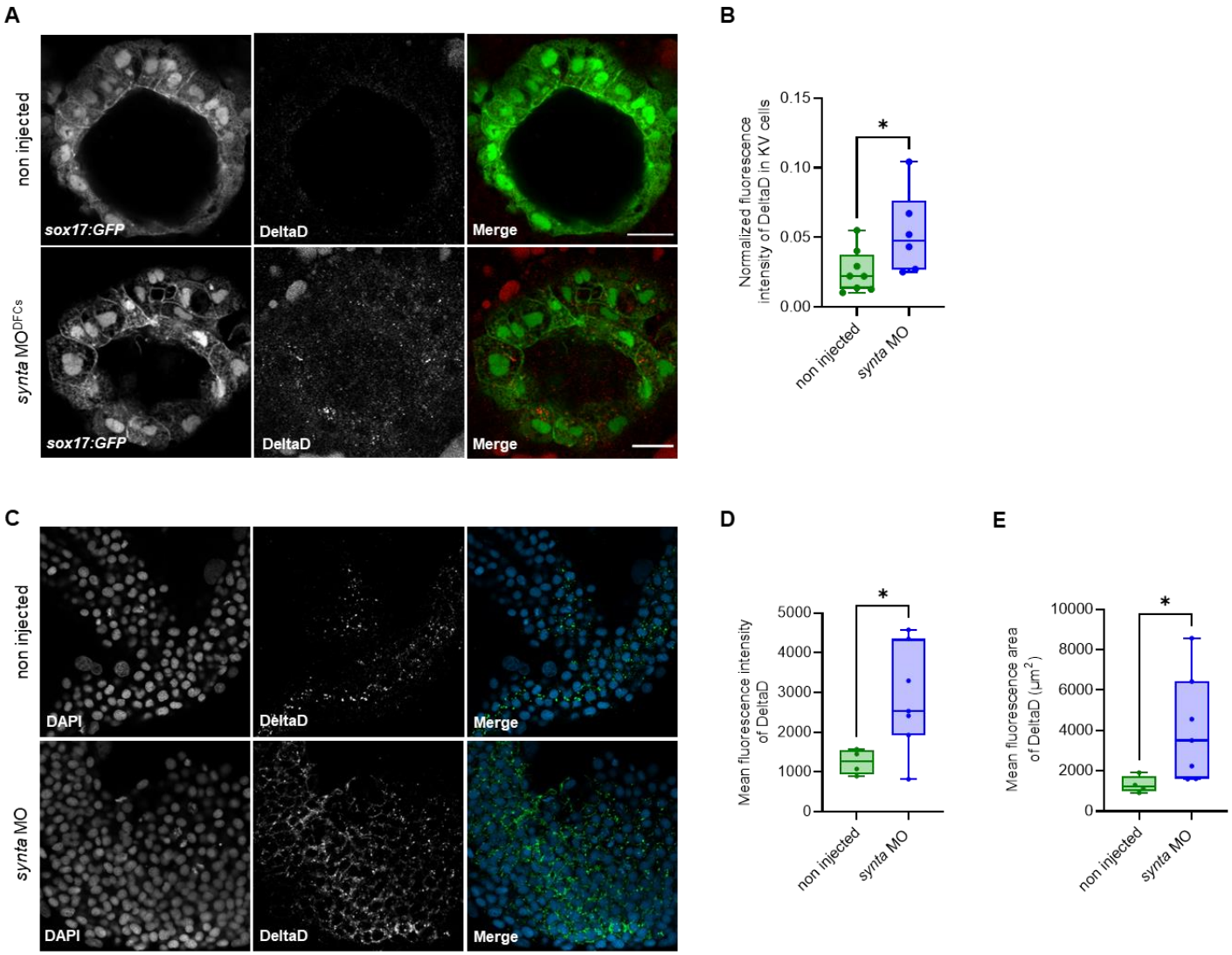

Figure 2.11: *Syntenin-a* enhances DeltaD protein stability.
(A) DeltaD immunostaining for *Tg(sox17:GFP)* non injected embryos and injected with *synta* MO^{DFCs} at 8 ss labelling DeltaD and Kupffer's Vesicle cells, respectively. (B) Measurement of DeltaD mean fluorescence intensity at the Kupffer's Vesicle cells of 8 ss control embryos (n=8 embryos) and *synta* MO^{DFCs} injected embryos (n=6 embryos), normalized to the background fluorescence signal. * $p<0.05$; Student's t-test with Welch's correction. (C) DeltaD and DAPI immunostaining for control non injected embryos and injected with *synta* MO at bud stage labelling DeltaD at the tailbud region. (D) Measurement of DeltaD mean fluorescence intensity at the tailbud cells of bud staged control embryos (n=4 embryos) and *synta* MO injected embryos (n=7 embryos). * $p<0.05$; Student's t test with Welch's correction. (E) Measurement of DeltaD mean fluorescence distribution area at the tailbud cells of bud staged control embryos (n=4 embryos) and *synta* MO injected embryos (n=7 embryos). * $p<0.05$; Student's t test with Welch's correction. DFCs, dorsal forerunner cells; ss, somite stage. Scale bar represents 20 µm.

Our results showed that downregulation of *syntenin-a* resulted in upregulated levels of DeltaD, in line with *in vitro* observations (Estrach et al., 2007) and, thus Notch signaling activation can further explain the increased number of immotile cilia within the KV and, consequently the loss of fluid flow dynamics

in *synta* morphants, by replicating *nicd* overexpression phenotype (Boskovski et al., 2013; Tavares et al., 2017).

Of note, some Notch ligands are known to have additional functions in a PDZ-dependent manner apart from initiating Notch signaling in the neighboring cells (Ascano et al., 2003; Wright et al., 2004). In case of DeltaD, it was found to mediate intercellular adhesion via Syntenin interaction (Estrach et al., 2007; Hava et al., 2009). Whereas Syntenin has been previously reported to localize at epithelial cell-cell contacts in different human cell lines (Zimmermann et al., 2001).

Cellular junctions play an essential role in KV maturation by promoting cohesion between the luminal epithelial cells during lumen expansion. Enrichment of *tight junction protein 1a (tjp1a)* and *claudin 5a (cldn5a)* expression at the apical side and *e-cadherin* at the basal membranes seal the intercellular space avoiding fluid leakage (Tay et al., 2013; Kim et al., 2017). Taking this into account, we asked if Syntenin – DeltaD could have an additional role in maintaining the cellular adhesion of the KV.

We assessed by immunostaining the Tjp1a protein levels and localization at 8 ss (Figure 2.12 A) and we observed that *synta* morphants had a reduction in the normalized fluorescence intensity of Tjp1a at the plasma membrane of KV cells (3.24 ± 0.58 ratio) when compared with control non-injected embryos (4.92 ± 1.34 ratio; Unpaired t-test with Welsh's correction, p-value < 0.05).

In order to determine if this difference had an influence on KV lumen expansion, we analyzed the impact of *syntenin-a* loss-of function on the KV volume. For that, we used whole-KV scans by filming live embryos with confocal live microscopy and measured the area of the KV delineated lumen for each focal plane, which the sum of all measurements resulted in the KV volume. Embryos injected with *synta* MO^{DFCs} presented significantly smaller KVs with 0.35 times the volume of control non-injected embryos and 0.26 times the volume of mismatch MO^{DFCs} injected embryos (*synta* morphant KV volume 19 × 10^3 µm^3 vs WT KV volume 54 × 10^3 µm^3; mismatch morphants KV volume 72 × 10^3 µm^3; Kruskal-Wallis ANOVA with Dunn's multiple comparisons test, p-value < 0.05 and p-value < 0.0001, respectively) (Figure 2.12 C). Co-injection of *synta* MO^{DFCs} with 50 pg *synta* RNA^{DFCs} restored the KV volume to 2.26 times the volume of *synta* morphants and to similar volumes of control embryos (43 × 10^3 µm^3; Kruskal-Wallis ANOVA with Dunn's multiple comparisons test, p-value < 0.05 and p-value > 0.05, respectively).

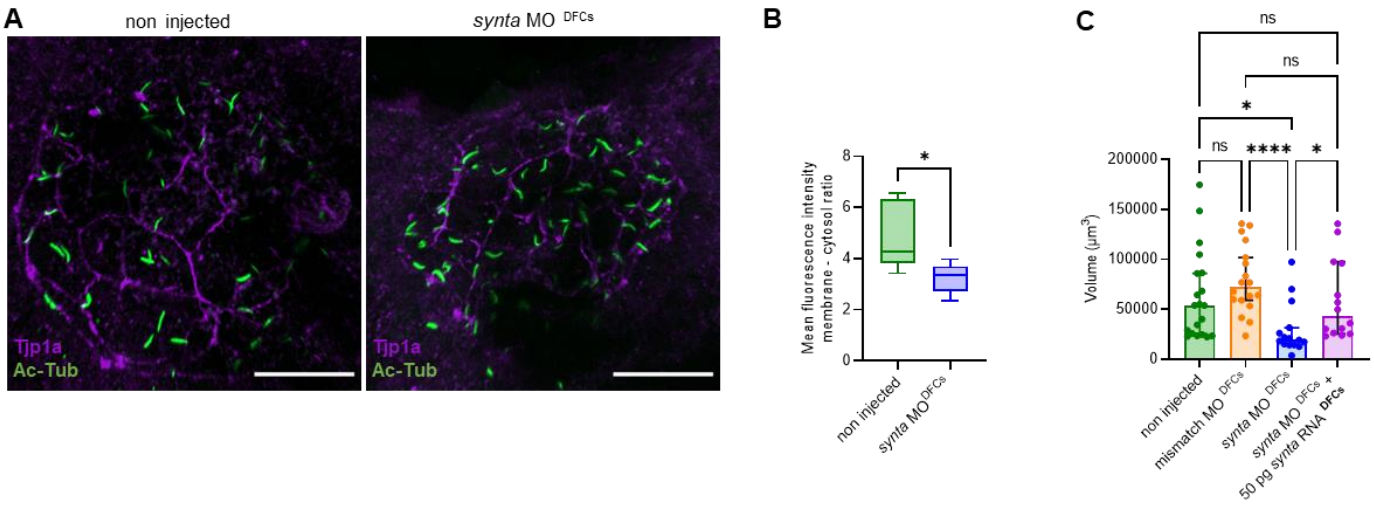

Figure 2.12: Syntenin-a downregulation impairs Kupffer's Vesicle volume.

(A) Acetylated alpha-tubulin and junction protein 1a (Tjp1a) immunostaining for control non injected embryos and injected with *synta* MO ^{DFCs} at 8 ss labelling KV cilia and apical membrane, respectively. (B) Measurement of Tjp1a mean fluorescence intensity at the KV cells plasma membrane of control embryos (n=5 embryos) and *synta* MO^{DFCs} injected embryos (n=6 embryos) normalized to the cytosolic signal. * p<0.05; Unpaired t-test with Welsh's correction. (C) Measurement of KV volume in control embryos (n= 20 embryos) and injected with mismatch MO ^{DFCs} (n=18 embryos), *synta* MO ^{DFCs} (n=15 embryos), *synta* MO ^{DFCs} combined with 50 pg of *syntenin-a* RNA ^{DFCs} (n=14 embryos). ns, not significant; * p<0.05; **** p<0,0001; Kruskal-Wallis one-way ANOVA analysis variance with Dunn's multiple comparisons test. DFCs, dorsal forerunner cells; KV, Kupffer's Vesicle; ss, somite stage. Scale represents 20 µm.

Considering the KV volume and the unchanged total number of cells in the KV, together our results suggest that reduction of *syntenin-a* levels impairs the full expansion of the KV lumen by disturbing the cohesiveness of KV cells, likely leading to fluid leakage through the intercellular space. At this point, more experiments would be needed to confirm that Syntenin-a-dependent maintenance of KV intercellular junctions is through DeltaD interaction. Nonetheless, decreased KV volumes in *synta* MO^{DFCs} most certainly contributed to the defective fluid flow dynamics observed in Figure 2.9 A.

Next, to further confirm the connection between Sintenin-a and DeltaD mediating ciliary motility regulation, we looked at the expression of the primary downstream targets of Notch signaling, the *hairy* and *enhancer of split*-related genes (referred to as *her* family in zebrafish) (Fischer & Gessler, 2007). Her factors are transcriptional repressors involved in the segmentation clock and binary cell fate decisions that are important for somitogenesis, stem cell maintenance and boundary formation (Kageyama et al., 2007).

During the KV half-life and the time-window for the LR asymmetry establishment, Notch signaling synchronizes the zebrafish segmentation clock between neighboring cells in the posterior pre-somitic mesoderm (Shankaran et al., 2007; Özbudak & Lewis, 2008). Moreover, we have previously showed

that Notch signaling specifically at the KV cells impacts directly on the transcription of *her12* and indirectly on the transcription of the motor dynein *dnah7* by affecting *foxj1a* transcription levels (Lopes et al., 2010; Tavares et al., 2017). *Her12* is at least one of the Notch signaling downstream targets responsible for modulating ciliary motility of KV cells. In 2017, we showed that *her12* was downregulated in *deltaD* zebrafish mutants and its overexpression recapitulated the *nicd* overexpression phenotype, showing more immotile cilia (Tavares et al., 2017).

To avoid any interference from the oscillatory expression levels of the *her12* at the KV neighboring cells part of the pre-somitic mesoderm (Gajewski et al., 2006; Shankaran et al., 2007) or any dilution of KV specific differences through analysis of whole-embryo expression levels, we decided to first isolate the KV cells by fluorescence-activated cell sorting (FACS). Although at 8 ss, the *Tg(sox17:GFP)* embryos show more GFP positive cells from the endodermal population besides the KV cells, different levels of GFP fluorescence intensity were sufficient to distinguish the KV population, which presents a higher level of GFP.

After sorting the KV cells of several pooled mismatch and *synta* injected morphants and control siblings, the total RNA was extracted and quantified by qPCR. Importantly, upon the knockdown of *syntenin-a*, we observed a significant 2.21-fold and 2.02-fold increase in the *her12* mRNA expression levels compared to control non-injected embryos and mismatch morphants, respectively (Welch ANOVA test with Dunnett's correction for multiple comparisons tests; p-value < 0.05) (Figure 2.13 A).

Analysis of *dnah7* expression levels revealed a significant 0.44-fold decrease in *synta* morphants compared to control non-injected embryos (Kruskal-Wallis ANOVA with Dunn's multiple comparisons test, p-value < 0.05), that was not sustained when compared to mismatch morphants (Kruskal-Wallis ANOVA with Dunn's multiple comparisons test, p-value > 0.05) (Figure 2.13 B). These observations may reflect the indirect influence of Notch signaling in the expression of *dnah7*. From previous studies we suspect that Notch signaling regulates *foxj1a* transcription (Lopes et al., 2010), which in turn is known to regulate *dnah7* transcription (Choksi et al., 2014; Tavares et al., 2017). Therefore, although *dnah7* is a reliable readout of *foxj1a* manipulations, it may not reflect Notch signaling responses.

Our observations point to a model where *syntenin-a* loss-of-function results in DeltaD upregulation and increased internalization, further activating Notch signaling in the neighboring cells that consequently increase the transcription of *her12,* triggering the molecular switch that will prevent cilia from beating. The increased numbers of immotile cilia, by altering the motile – immotile cilia ratio and their spatial distribution, negatively impact on productive fluid flow, that becomes no longer capable of breaking symmetry and leads to defective LR outcomes, such as in *dand5* and *spaw* expression

patterns and later on in heart placement. This data unraveled an upstream modulator of Notch signaling in ciliary motility cell fate.

Interestingly, we observed that the expression levels of *dand5* was significantly 0.39-fold and 0.41-fold decreased compared to control non-injected embryos and mismatch morphants, respectively (Welch ANOVA test with Dunnett's correction for multiple comparisons tests; p-value < 0.0001) (Figure 2.13 C). By *in situ* hybridization, we had previously indicated in this work that *dand5* expression pattern in *synta* MO^{DFCs} injected embryos appeared weak and mostly symmetric (Figure 2.8 C). These observations are in contrast to what we have reported for *pkd2* morphants, where we saw 62% of symmetric *dand5* expression pattern similar to *synta* morphants, but where the *dand5* relative expression levels were not altered when compared to WT embryos (Jacinto et al., 2021). As the total number of KV cells is unchanged, all together, these data suggested that *syntenin-a* loss-of-function, contrary to *pkd2* loss-of-function, affects *dand5* transcription. In fact, some *synta* morphants showed smaller *dand5* spatial mRNA domains, nearly absent (data not shown), recapitulating the vestigial *dand5* expression phenotype of *deltaD* mutants (Lopes et al., 2010). Therefore, this suggests that *syntenin-a* regulation of *dand5* transcription may also be through Notch signaling.

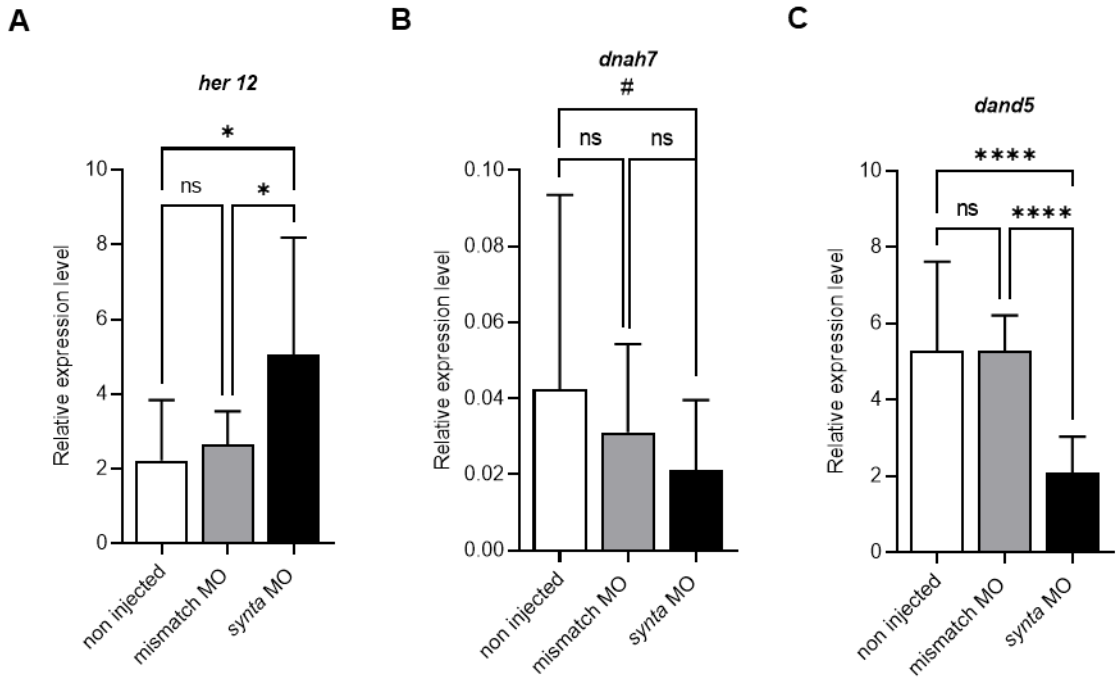

Figure 2.13: *Syntenin-a* regulates cilia motility through notch signaling and its downstream target *her12*.
(A-C) Quantification of relative expression levels of *her12* (A), *dnah7* (B) and *dand5* (C) by qPCR of sorted *sox17*:GFP positive KV cells at 8 somite stage of control non injected embryos and injected with mismatch MO and *synta* MO. ns, not significant; * p<0.05; **** p<0,0001; Welch ANOVA test with Dunnett's correction for multiple comparisons tests; # p<0.05; Kruskal-Wallis one-way ANOVA analysis variance with Dunn's multiple comparisons test. KV. Kupffer's Vesicle.

2.2.11. Notch signaling regulates motile – immotile cilia ratio through modulation of V-ATPase activity

We then interrogated about the underlying mechanism for the differences in the motile – immotile cilia ratio observed in the *synta* morphants and *deltaD* mutants when compared to each corresponding control embryos. For that, we examined a comparative transcriptomic analysis of KV precursors from WT and *deltaD* mutant embryos, already published by our laboratory (Tavares et al., 2017), to determine which genes could be implicated specifically in ciliary motility.

One gene, the *rabconnectin 3a* or *rbc3a*, caught our attention for showing a 16 ± 9-fold down regulation in *deltaD* mutants (Tavares et al., 2017). Rabconnectin 3a is a highly conserved protein in multicellular organisms containing 12 WD domains, responsible for protein-protein interactions (Nagano et al., 2002). In association with its partner, Rcb3b, Rbc3a was firstly described as a scaffold protein of Rab3 regulators on synaptic vesicles, most likely to modulate neurotransmitter loading and calcium-dependent exocytosis (Nagano et al., 2002; Kawabe et al., 2003). In zebrafish, Rabconnectin complex was found to temper V-ATPase activity by promoting the interaction of the cytosolic (V1) and the membrane (V0) subunits on the synaptic vesicles of hair cells (Einhorn et al., 2012) and to modulate vesicular endosome maturation in neural crest cells (Tuttle et al., 2014). Moreover, regulation of V-ATPase by Rbc3a has been associated with Notch signaling both in Drosophila and mammalian cells (Yan et al., 2009; Sethi et al., 2010).

On the other hand, V-ATPase has been well established to inhibit spermatozoa motility within the epididymis tract by regulating the luminal pH at the plasma membrane (Pastor-soler et al., 2003; Shum et al., 2009). Thus, we reasoned that Notch signaling could regulate ciliary motility in the KV cells by modulating the V-ATPase activity through the Rabconnectin complex.

Moreover, if *rbc3a* is one of the Notch signaling downstream targets, its expression should respond accordingly to Notch signaling manipulations. Analysis of *rbc3a* expression levels at 3 ss showed a significant 0.51-fold decrease in *deltaD* mutants (Student t-test with Welch's correction, p-value < 0.05) and a significant 3.4-fold increase in *her12* RNA injected embryos (Student t-test with Welch's correction, p-value < 0.01) when compared to WT embryos (Figure 2.14 A). Despite being maternally deposited in zebrafish embryos (data not shown), these results showed that *rbc3a* expression can be modulated by DeltaD – Notch signaling. As *her12* is thought to be a transcriptional repressor (Kageyama et al., 2007), regulation of *rbc3a* transcription is most likely to be indirect.

In WT zebrafish hair cells, the V1 cytosolic subunit of V-ATPase was found to co-localize with the V0 membrane subunit on synaptic vesicles, whereas in *rbc3a* mutant hair cells, V1 subunit disassembled

from its counterpart and became evenly distributed through the cytoplasm (Einhorn et al., 2012). Hence, we then tested if in our Notch manipulations we could detect any difference in V-ATPase localization profile, by performing an immunolabelling for V-ATPase V1A subunit. Importantly, we found that the V-ATPase was localized throughout the cytosol resembling a vesicular labelling pattern and was also concentrated at the plasma membrane on the apical side of some, but not all, KV cells (Figure 2.14 B). These observations supported a model in which V-ATPase is present at the plasma membrane, where it may be responsible for driving the proton flux into the extracellular space. We postulated that within the vicinity of a few cilia, an increase in protons could prevent ciliary beating. We further quantified the normalized fluorescence intensity signal from V-ATPase protein levels in the KV apical side. We observed that, in *deltaD* mutants, although not statistically different, there was a slightly decrease in the V-ATPase levels at the apical side of KV cells (ANOVA test with Tukey's correction for multiple comparisons tests, p-value > 0.05), while upon injection of 50 pg *her12* RNA there was a significant increase in the V-ATPase levels at the apical side of KV cells (ANOVA test with Tukey's correction for multiple comparisons tests, p-value < 0.05) when compared to WT embryos (Figure 2.14 C).

Our results showed that when Notch signaling is activated, through its downstream target *her12* overexpression, *rbc3a* is upregulated and V-ATPase signal increases at the plasma membrane.

Lastly, we independently evaluated whether V-ATPase activity was necessary for regulating the motile – immotile cilia ratio by incubating the zebrafish embryos with Concanamycin A, a specific V-ATPase inhibitor (Huss et al., 2002). We and others have shown that most KV cilia start as immotile at 3 ss and, then as KV matures and embryonic development progresses, cilia gradually acquire motility. By 8 ss, the majority of cilia had become motile (Yuan et al., 2015; Ferreira et al., 2017; Tavares et al., 2017). Importantly, V-ATPase activity has been reported to influence the KV cell number and cilia length, which are decreased when the pump is inhibited between one-cell and bud stage (Adams et al., 2006; Gokey et al., 2015). Therefore, we decided to inhibit the V-ATPase activity at the onset of ciliary motility between 3 ss and 4 ss, avoiding the secondary effects of V-ATPase function at early stages, and performed live imaging of KV cilia by confocal microscopy.

At this stage, we observed that in control WT embryos (n= 5 embryos) and in Concanamycin's solvent DMSO incubated embryos (n= 3 embryos) almost half of cilia are already motile (43 ± 22% and 50 ± 12%, respectively; Fisher test with Bonferroni correction, p-value > 0.05). On the other hand, embryos incubated with 200 nM of Concanamycin A (n= 11 embryos) showed a significant increase in the percentage of motile cilia (80 ± 12%; Fisher test with Bonferroni correction, p-value < 0.01 when

compared to WT embryos and p-value < 0.05 when compared to DMSO incubated embryos) (Figure 2.14 D).

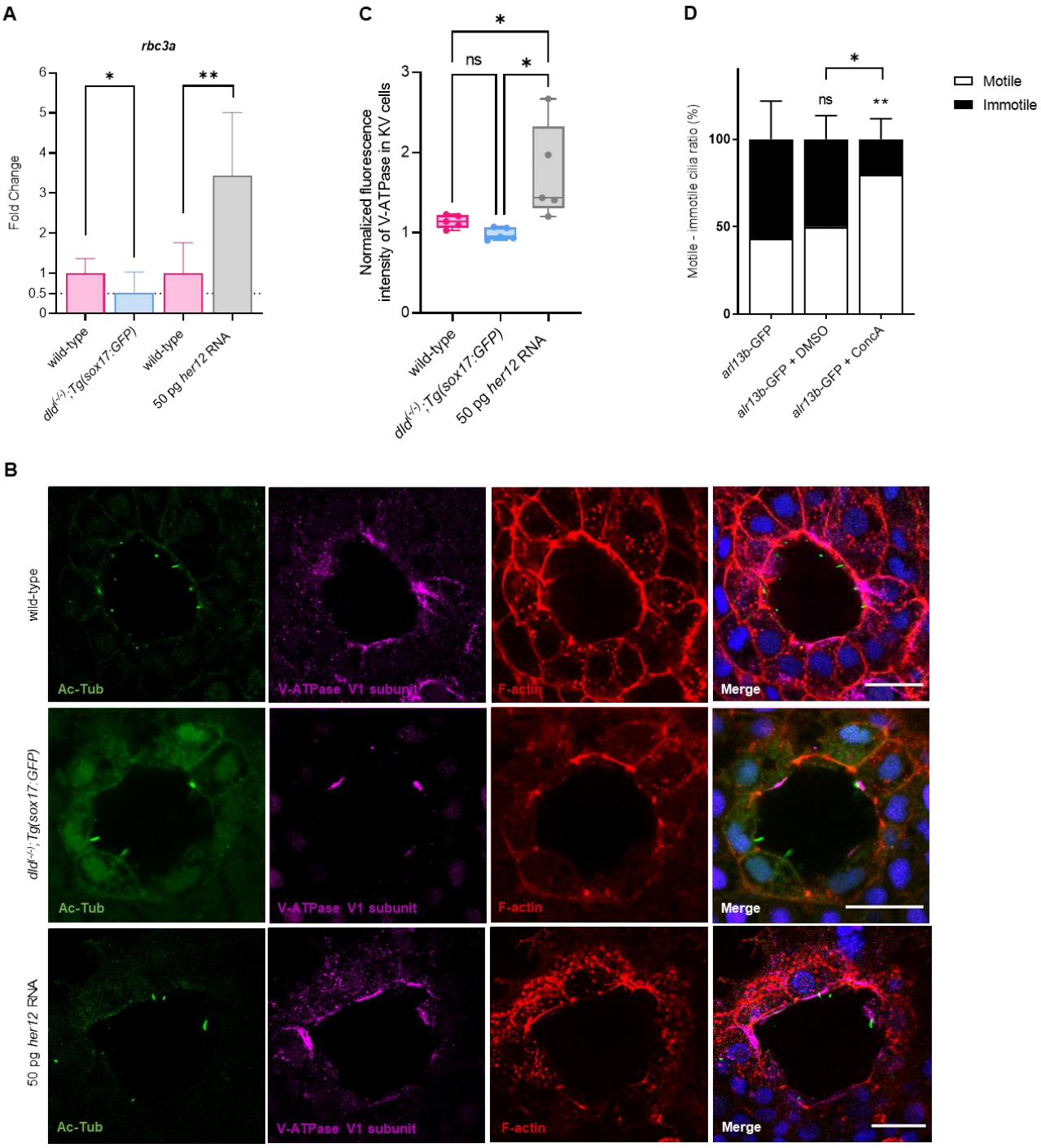

Figure 2. 14: Notch signaling may regulate ciliary motility through V-ATPase function.
(A) Transcription levels of *rbc3a*. Fold change in expression levels of *rbc3a* in whole embryos at 3 somite stage from wild-type control embryos, *dld(-/-);Tg(sox17:GFP)* embryos and 50 pg *her12* injected embryos. * p<0.05; ** p<0,01; Unpaired t-test with Welch's correction. (B) V-ATPase V1 subunit, acetylated tubulin and DAPI immunostaining for control non injected embryos, *dld(-/-);Tg(sox17:GFP)* embryos and 50 pg *her12* injected embryos at 3 somite stage on KV cells. (C) Measurement of V-ATPase V1 mean fluorescence intensity at the KV cells of 3 somite staged control embryos, normalized to the background fluorescence signal (n=5 embryos), *dld(-*

$^{/-}$);Tg(sox17:GFP) embryos (n= 5 embryos) and 50 pg *her12* injected embryos (n=5 embryos). ns; not significant; * p<0.05; ANOVA test with Tukey's correction for multiple comparisons tests. (D) Quantification of motile – immotile cilia ratio of 4 somite staged control embryos (n=5 embryos, 272 cilia) and embryos incubated for 30 minutes between 3 and 4 somite stages with DMSO (n=3 embryos, 76 cilia) or Concanamycin A, ConcA (n=11 embryos, 355 cilia). ns; not significant; * p<0.05; ** p<0,01; Fisher's exact test. KV, Kupffer's Vesicle. Scale bar represents 20 μm.

This experiment showed that an acute inhibition of V-ATPase activity for 30 minutes at 3 ss is enough to increase motile – immotile cilia ratio.

To undoubtedly show that *her12* and V-ATPase compose the molecular switch present at immotile ciliated cells that prevent the cilium from beating, live imaging recordings of fluorescently tagged *her12* or V-ATPase subunits transgenic lines coupled with *arl13b-GFP* to label the cilia would allow to correlate spatial distribution of Notch signaling effectors and motile and immotile cilia fate.

Altogether, we provided data that suggests Rabconnectin 3a and V-ATPase activity are modulated by Notch signaling and by its direct downstream effector *her12,* comprising a signaling cascade to fine-tune the number of motile and immotile cilia necessary for generating the optimal fluid flow capable of breaking symmetry.

2.3. DISCUSSION

How the fluid flow is sensed by the LRO cells is a more than 20-years old question, that has been tackled by several biologists and physicists and yet, a conclusive answer has not been provided. With this work, we combined confocal live microscopy with an in-house made micromanipulation setup to explore the biophysical properties of both the fluid flow and the LRO cells, during the LR symmetry breaking time-window, hoping to add new insights to the field, ultimately leading to resolve this mystery.

So far current observations are compatible with the mechanosensory and/or the chemosensory mechanism, without sufficient experimental data to fully support one of the models over the other.

The chemosensory-based mechanism proposes that a morphogen or vesicles-containing a signaling molecule are released unbiasedly into the lumen, where through the fluid flow current they are accumulated on the left side of the LRO triggering a calcium response (Nonaka et al., 1998; Tanaka et al., 2005). Visualization of these vesicles at the mouse LRO was accomplished by scanning and transmission electron microscopy and by live imaging of membranous parcels labelled with a lipophilic fluorescent dye (Tanaka et al., 2005). Interestingly, in our lab we also performed transmission electron microscopy of the zebrafish LRO (Tavares et al., 2017; Pinto et al., 2021). Despite our main objective was to analyze ciliary ultrastructure, we found that the KV lumen was also replenished of vesicles, ranging multiple sizes and shapes.

Taking advantage of the increasing knowledge from the extracellular vesicle (EV) field, we developed a transgenic line labelling CD63 positive EVs, to quantify and track them within the KV lumen. Concomitantly, we used our micromanipulation setup for extraction of KV fluid and further re-injection to change KV fluid content and study KV cells and EVs dynamics during the establishment of the biophysical mechanism of cilia-driven flow and the flow sensing mechanism. This methodology allowed us to test the reliability by which chemical cues can be detected by KV cells in the process of the LR axis determination. Our results argue against the chemosensory mechanism because no robust number of CD63 positive EVs was detected in the KV throughout all embryonic developmental stages tested and single KV quantification showed a highly variable number of CD63 positive EVs between embryos.

KV precursor cells, the dorsal forerunner cells, have unique endocytic properties when compared to the remaining deep cells during epibolic stages (Cooper & D'Amico, 1996). Here, we showed that differentiated KV cells retain internalization processes of 10 kDa membrane impermeant dextran dyes, but not of 70 kDa rhodamine-dextran dyes. However, general inhibition of endocytic pathways at 5 ss

had no consistent impacts on the LR axis patterning of the vertebrate body, assessed by the heart position of zebrafish embryos.

One could advocate that those manipulations at 5 ss may be too late to completely abolish the flow sensing mechanism. In fact, Yuan and colleagues have shown an increase in intraciliary calcium oscillations on the left side of KV between 1 ss and 4 ss that are transferred to the cells, inducing cytosolic waves between 5 ss and 10 ss (Yuan et al., 2015). Additionally, a directional flow of a yet low amplitude was shown between 3 ss and 5 ss, as KV cilia started to develop motility (Ferreira et al., 2017; Tavares et al., 2017). Therefore, by the 5 ss, the asymmetric signals could be already settled at KV cilia from the left side, triggering the signaling cascade necessary for *dand5* degradation at 8 ss (Lopes et al., 2010).

Nevertheless, our results showed that embryos manipulated at 5 ss, by diluting the KV fluid content with viscous methylcellulose, are still severely affected resulting in a high prevalence of symmetric *dand5* on the KV cells and defective heart position on the body. By impairing both mechanical and chemical cues for flow sensing mechanism, this experiment revealed that most embryos are still blind to the asymmetric cues for most of the initial steps of the fluid flow.

In the laboratory, we established the critical temporal map for the flow induced asymmetry, by extracting the fluid content at different time points. Results showed that the crucial time-window was between the 4 ss and 6 ss with a limited role during the 3 ss and the 7 ss (BioRxiv Sampaio et al., 2022). The 5 ss was the most susceptible stage upon the transient fluid extraction, but still the percentage of embryos with defects either on *dand5* expression pattern or organ *situs* did not exceed 35% of the cases. On the other hand, our KV fluid dilution with methylcellulose experiments led to 56% of the embryos showing defective LR axis patterns. Moreover, the fluid dilution with Danieau's buffer experiments showed that a rapid intervention in a time scale of a few minutes had no impact on LR development outcome, further supporting a cumulative role of flow dynamics throughout the entire time-window.

Our former hypothesis at the beginning of the Chapter proposed that EVs were secreted from the anterior side of the KV, rather than unbiasedly, due to an estimated higher shear stress produced at the plasma membrane by the cluster of motile cilia on the anterior-dorsal region (Solowiej-Wedderburn et al., 2019). Moreover, EVs released at the anterior region would be initially transported towards the left, leading to an asymmetric absorption pattern (Montenegro-Johnson et al., 2016; Ferreira et al., 2017). This model relied on evidence from endothelial cells showing that increased blood flow shear stress promoted recycling exocytosis of TRPV4 calcium channel to further induce cellular responses to the mechanical stimuli (Baratchi et al., 2014, 2016).

Clustering of motile cilia at the anterior region is achieved at 6 ss, through the process of cellular rearrangements during KV remodeling (Wang et al., 2012). At this developmental stage, we and others have shown that the number of motile cilia had overcome the number of immotile ones, without changing the total cilia number, contributing to the increase of the fluid flow amplitude specifically at the anterior pole and generally over time (Ferreira et al., 2017; Tavares et al., 2017).

Therefore, in light of the aforementioned model (Solowiej-Wedderburn et al., 2019), EVs would start to be secreted into the swirling motion fluid flow at 6 ss, which corresponds to the latest stages of the time-window that we found relevant for flow sensing mechanism. EVs would then have a limited time to accumulate on the left sided cells before KV cells become insensitive to external stimuli. This short time-window, however, would be sufficient if the secretion rate, transport and internalization or degradation rate were fast enough. Tanaka and colleagues had reported that nodal vesicular parcels were released every 5 to 15 seconds into the mouse node (Tanaka et al., 2005). Moreover, according to Ferreira's work using a simulated 9 – 14 ss flow pattern, they predicted that upon secretion of EVs, a LR concentration gradient can be established within 8 seconds, before particle diffusion counteracts mixing the fluid content into a uniform concentration (Ferreira et al., 2017). If we consider that this process starts at earlier stages, as 6 ss, it could take a longer time, due to slower fluid flow velocity magnitudes, perhaps in the order of minutes. Therefore, taking this line of thought, it is possible that secretion and transport can still lead to asymmetric EV distribution pattern within our timeline, but symmetry breaking would be yet dependent on the internalization rate.

The fluid flow has been also shown to induce actin-based cytoskeletal structures associated with endocytosis, like membrane ruffles, caused by the shear stress forces acting at the cell membranes (Samuel et al., 2012). Membrane ruffles positive endocytosis is characteristic of macropinocytosis, which would provide a rapid method to EV bulk internalization. However, our results showed that despite KV cells produce very dynamic actin-dependent membrane ruffles, that protrude stochastically from any side of the KV, macropinocytosis is not actively involved in engulfing KV fluid content nor in LR axis determination. On the other hand, changes in KV cell shapes are dependent on Rock2b – Myosin II activity, that modulate actin-myosin contractility, which in turn can regulate membrane protrusion initiation (Wang et al., 2012; Welf et al., 2020). Thus, we hypothesize that the observed actin-membrane protrusions are formed due to actin cortex fluctuations and they could contribute to the fast cell shape changes that occur during KV remodeling.

In conclusion, our results collectively do not support the chemosensory-sensing mechanism driven by EVs as the underlying reason for flow mediated symmetry breaking. On one hand, zebrafish embryos showed an unreliable number of CD63 positive EVs within the KV lumen. On the other hand,

comparing KV fluid replacement experiments showed that the laterality defects observed upon the methylcellulose replacement, which affects both mechano and chemosensory mechanisms, are in fact most likely due to the impairment of mechanical cues of the fluid flow, as impairment of chemical cues alone by pharmacologically inhibiting EV internalization did not further impact on LR axis development. Moreover, active induction of EV secretion at the anterior region caused by motile cilia movement dependent wall shear stress at 6 ss does not provide an explanation for the LR defects that arose from early stage KV fluid extractions.

We suggest that new mathematical models should be formulated considering the time-window for symmetry breaking that we found in the lab and the endocytic properties that we described for the LRO cells in this present work, to understand if the chemosensory mechanism is still a possibility and if so, in which conditions. For instance, as the wall shear stress driven EV secretion was not tested in this work, either unbiased or local secretion from the anterior side can still potentially occur. Moreover, different types of EVs, such as microvesicles and exosomes, can perform independent functions. Knowing the half-life of these EVs would be helpful in order to develop more accurate predictions and subsequently design more targeted experiments. Nevertheless, inhibiting endocytic processes, as performed in this work, would in theory impair the internalization of both EV populations.

Thus, the most promising theory is the mechanosensory-based mechanism in which immotile sensory cilia deflect in response to flow forces triggering a calcium influx through the polycystic complex Pkd1l1 – Pkd2 (McGrath et al., 2003; Field et al., 2011; Kamura et al., 2011), supported by similar evidence of a Pkd1 – Pkd2 complex working as mechanosensor in other systems, such as in kidney cells and endothelial cells (Nauli et al., 2003, 2006, 2008; Goetz et al., 2014; Praetorius, 2015).

Meanwhile, we have recently demonstrated that Pkd1l1 is located along KV cilia of zebrafish embryos (Roxo-Rosa & Lopes, 2019), equivalently to what was shown in the LRO of medaka embryos (Kamura et al., 2011). Moreover, Pkd1l1 and Pkd2 were shown to physically interact and morphants or mutants for each gene resulted in analogous LR phenotypes (Field et al., 2011; Kamura et al., 2011). Pkd2 was also demonstrated to mediate the intraciliary calcium oscillations and, subsequently, cytosolic calcium waves in the mouse LRO, similarly to previous reports in zebrafish KV (Yuan et al., 2015; Mizuno et al., 2020). Altogether, these observations support that Pkd1l1 and Pkd2 function in the same mechanotransduction pathway to integrate the mechanical signal of the cilia-driven fluid flow into cellular responses.

One major argument against the mechanosensory mechanism relies on the slow nature of fluid flow, that induces weak deflections on immotile cilia and, consequently the Pkd1l1 – Pkd2 mechanosensor complex would have to be extremely sensitive to elicit a fairly response (Cartwright et al., 2004, 2008).

Although fluid flow forces acting on immotile cilia revealed to be of the same order of magnitude as their variability along KV distribution and thermal fluctuations, Ferreira's simulations predicted that depending on the number of immotile cilia, temporal averaging of the mechanical signal can bypass the oscillatory noise (Ferreira et al., 2017). Therefore, the difference between immotile and motile cilia numbers must be tightly defined, to have an optimal ratio of cilia generating and sensing the fluid flow simultaneously.

While in some systems such as *Chlamydomonas reinhardtii*, initiation of ciliary motility was shown to be a final consequence of cilia assembly into a minimal length (Bottier et al., 2019), in vertebrates the beat onset seems to be a regulatory step by itself (Fakhro et al., 2011; Boskovski et al., 2013; Tavares et al., 2017; Bearce et al., 2022).

Studies from our laboratory and others have pointed out that cilia length and motility within the LRO are regulated independently by Notch signaling. First, we showed that by inhibiting Notch signaling, using *deltaD* mutants, the ciliary length was impaired and, inversely by supra-activating Notch signaling in WT embryos with *deltaD* and *nicd* overexpression, the ciliary length was increased compared to controls (Lopes et al., 2010). We then showed that *deltaD* mutants also have more motile cilia, while overexpression of *nicd* showed more immotile cilia, without affecting the total number of cilia (Sampaio et al., 2014; Tavares et al., 2017). By normalizing the ciliary size with *arl13b* overexpression (Pintado et al., 2017), we could overcome the cilia length differences that Notch signaling manipulations produce and successfully uncouple cilia length from cilia motility (Tavares et al., 2017).

Both ciliary length and motility phenotypes were reproduced by modulating Notch signaling in the *Xenopus* LRO, suggesting a conserved role of this pathway in the two species (Boskovski et al., 2013; Tözser et al., 2015). Nevertheless, these two functions of Notch signaling may not be independent and further studies are needed to understand the mechanistic relationship between ciliary length and motility.

This work showed that Notch signaling can be further regulated by Syntenin-a. This protein was previously shown to interact with multiple partners, mostly with membrane-bound proteins, regulating its subcellular trafficking (Latysheva et al., 2006; Beekman et al., 2012; Tudor et al., 2014; Tae et al., 2017). Although Syntenin has been extensively studied in the context of exosome

production and cancer invasion (Friand et al., 2015; Das et al., 2019; Kugeratski et al., 2021), it was also found highly enriched in human embryonic tissues (Zimmermann et al., 2001). Studies in *Xenopus* and zebrafish indicate that Syntenin plays an important role in early development regulating non-canonical Wnt-signaling and actin cytoskeleton, respectively, during convergent and extension movements (Luyten et al., 2008; Lambaerts et al., 2012; W. Zhang et al., 2018).

Moreover, Syntenin was found to directly bind and stabilize zebrafish DeltaD protein at the plasma membrane, reducing its internalization and consequently modulating Notch signaling and promoting intercellular adhesion *in vitro* (Estrach et al., 2007).

In our experiments, loss-of-function of *syntenin-a* led to a drastic increase in immotile cilia number within the KV, at the expense of the motile cilia number, resulting in a reduced fluid flow strength and directionality. Defective flow dynamics impaired the flow sensing mechanism evidenced by the lack of LR asymmetry in *dand5* and *spaw* expression patterns, which in turn caused an abnormal development of heart laterality.

Upregulation of Notch signaling showed by DeltaD protein and the downstream effector *her12* expression levels in *syntenin-a* morphants, positioned the role of Syntenin in the motile – immotile cilia ratio management upstream of Notch signaling.

Additionally, DeltaD was found to mediate intercellular adhesion by promoting human keratinocyte cohesiveness, via Syntenin interaction and independently of Notch signaling (Estrach et al., 2007). Our results showed that loss-of-function of *syntenin-a* decreased the fluorescence signal of tight junction protein 1a at the KV cells, suggesting a reduction in intercellular adhesion and further supporting the Syntenin – DeltaD regulatory mechanism described *in vitro* (Estrach et al., 2007) in live zebrafish embryos. Furthermore, *synta* morphants had significantly smaller KVs, which were restored to normal volumes upon rescue experiments with *synta* mRNA.

We hypothesize that in WT conditions, Syntenin-a directly interacts with DeltaD, stabilizing it at the plasma membrane, where DeltaD may contribute to sustaining the cellular adhesions between the KV cells. Concomitantly, Syntenin-a prevents DeltaD internalization, limiting Notch signaling activation, as the number of immotile cilia decreases throughout the KV development. Whereas, in *syntenin-a* morphants, DeltaD is no longer stabilized at the adhesion sites weakening the tightness between cells, which in turn may allow fluid leakage during KV inflation process and results in smaller KVs. DeltaD is then endocytosed, which activates this ligand via E3 ubiquitin ligases for subsequent binding to Notch receptors, enhancing the Notch signaling and *her12* transcription maintaining more cilia immotile for longer periods of time.

Syntenin-a, being expressed only in the KV cells within the tailbud, may also function to counteract the high levels of Notch signaling occurring at the tailbud to synchronize the segmentation clock and somitogenesis, from trans-activating abnormal Notch responses in the KV cells. It would be interesting to follow up this hypothesis, as our data is not enough to either support or reject it.

Next, in order to understand the molecular mechanism by which Notch signaling regulates ciliary motility, we looked into a tissue specific comparative transcriptomic analysis that showed *rabconnectin 3a*, a V-ATPase assembly regulator, was significantly downregulated in *deltaD* mutants (Tavares et al., 2017). This was particularly interesting because V-ATPase is responsible for maintaining spermatozoa flagella immotile by pumping protons to the extracellular space at the epididymis duct (Pastor-soler et al., 2003; Shum et al., 2009). Conversely, we found that *her12* overexpression led to an increase in *rabconnectin 3a* transcription and V-ATPase localization at the plasma membrane. This is consistent with more proton secretion into the KV lumen and more immotile cilia.

Going back to our transcriptomic microarray, we did not find any significantly difference in the expression levels of V-ATPase subunits in *deltaD* mutants when compared to control embryos (data not shown), suggesting that modulation of V-ATPase activity by Notch signaling is mostly post translational through Rabconnectin 3a-driven assembly.

By transiently inhibiting the V-ATPase activity, we also showed that the balance between motile and immotile cilia of KV cells was disrupted with more cilia beating at earlier stages, suggesting that low pH is necessary for preventing cilia from moving.

We hypothesize that a channel would be needed along the cilia to transduce the variations of extracellular pH into the ciliary axoneme. The acid-sensing ion channels (ASICs) may be potential candidates as they are proton-gated cation channels widely involved in sensory mediated responses (Cheng et al., 2018). Moreover, in zebrafish, ASICs were found to be expressed in the primary cilia of olfactory cells, most likely to respond to olfactory stimuli (Viña et al., 2015). Curiously, we found several ASICs expressed in the KV cells on our transcriptomic microarray at 8 – 10 ss.

Our observations point to a model where Notch signaling activation and, consequently *her12* transcription, up regulates *rabconnectin 3a* expression that in turn will trigger the molecular switch to stop cilia from beating. We hypothesize that Rabconnectin 3a promotes V-ATPase pump assembly at the endosomal vesicles that will be transported and recycled to the plasma membrane, as in epididymal cells (Shum et al., 2009). On the other hand, Rabconnectin 3a could drive V-ATPase assembly directly at its final location, as some membrane V0 subunits have been shown to be sufficient to target the proton pump specifically to the plasma membrane (Toei et al., 2010). At the plasma

membrane, V-ATPase promotes proton efflux to the vicinity of the cilium that may modulate second messengers' binding constants, such of calcium and calmodulin, to the ciliary axonemal proteins, inhibiting motility.

Taking this into account, it would be interesting to address the relationship between the transcription factor *her12* and Rabconnectin-3a. As *her12* belongs to a family of transcriptional repressors, the link may be indirect.

On the other hand, Rabconnectin complex was found to regulate Notch signaling. In Drosophila and human cell lines, *Rbc-3* mutant cells showed an impairment of V-ATPase activity which disrupted endocytic trafficking leading to an accumulation of Notch in the endocytic compartments (Yan et al., 2009; Sethi et al., 2010). Therefore, more studies would be needed to confirm the dynamics of Rabconnectin complex and Notch signaling interaction in the KV cells.

Curiously, during our studies we found that *syntenin-a* modulates *dand5* transcription at the KV cells. In fact, *dand5* production was found to be strongly reduced when Notch signaling was inhibited, either by pharmacological antagonists or in *deltaD* zebrafish mutants (Gourronc et al., 2007; Lopes et al., 2010). Similar effects were seen in *dand5* expression in the LRO of mouse embryos (Kitajima et al., 2013). Hence, these data suggest that *dand5* downregulation in *syntenin-a* morphants may be caused indirectly by Notch signaling defects.

Altogether, *syntenin-a* morphants revealed to be very similar to *nicd* overexpressed embryos, phenocopying the defects in the ratio between motile and immotile cilia numbers and the upregulation of *her12* transcription, both in opposition to *deltaD* mutants (Tavares et al., 2017). Supporting that Syntenin-a can be an upstream modulator of Notch signaling *in vitro* (Estrach et al., 2007) and *in vivo* (present work). We did not see, however, any difference in ciliary length upon loss-of-function of *syntenin-a*, in contrast to *deltaD* mutants, which may suggest that the ciliary motility is more sensitive to Notch signaling variations within the KV cells or that Syntenin-a separates the two ciliary functions of Notch signaling.

Moreover, we presented compiling data suggesting that Rabconnectin-3a and V-ATPase activity are at least some of the downstream effectors of Notch signaling that regulate the ciliary motility fate of KV cells. Such complex signaling pathway reinforces the importance of the correct balance between motile and immotile cilia numbers for the proper establishment of the LR axis, by producing a robust and heterogeneous patterned fluid flow, while having enough sensory cilia to transduce it into gene expression changes, ultimately breaking the LR symmetry.

Most likely due to the differences in the topography between zebrafish and mouse LROs, motile – immotile cilia ratio seems to be more relevant in zebrafish LR axis patterning, in opposition to the mouse, where two motile cilia were found to be sufficient to accomplish symmetry breaking (Shinohara et al., 2012).

2.4. SUPPLEMENTARY MATERIAL

Supplementary Movie 2. 1 – CD63-pHluorin positive vesicles inside of Kupffer's Vesicle lumen.
Time-lapse of Tg(CD63-pHluorin) embryo at 5 ss, oriented with anterior and left sides of the KV to the top and left sides of the page, recorded by airyscan confocal microscopy using a 40x lens. Non manipulated embryo shows CD63-pHluorin positive extracellular vesicles within the Kupffer's Vesicle lumen being transported by the fluid flow.

Supplementary Movie 2. 2 – Kupffer's Vesicle liquid dilution procedure.
Time-lapse of an example of a wild-type embryo at 5 ss, oriented with anterior and left sides of the KV to the top and left sides of the page, recorded at 50 fps and played at 100 fps. The KV liquid was extract and diluted in approximately one µl of fluorescent solution priorly loaded into the needle and then, after a few seconds, the resulting mixed liquid was re-injected into the KV until it reached the initial volume.

Supplementary Movie 2. 3 – Example of a manipulated embryo at 5 ss which Kupffer's Vesicle fluid was diluted in Danieau's buffer.
Sequence of processed brightfield images of a 7 ss KV showing particles tracking for angular flow velocity quantification, oriented with anterior and left sides of the KV to the top and left sides of the page, recorded at 60 fps and played at 20 fps.

Supplementary Movie 2. 4 – Example of a manipulated embryo at 5 ss which Kupffer's Vesicle fluid was diluted in 1.5% of Methylcellulose.
Sequence of processed brightfield images of a 7 ss KV showing particles tracking for angular flow velocity quantification, oriented with anterior and left sides of the KV to the top and left sides of the page, recorded at 60 fps and played at 20 fps.

Supplementary Movie 2. 5 – Scan of a wild-type Kupffer's Vesicle showing motile and immotile cilia.
Embryo was injected with 50 pg of *alr13b*-GFP mRNA at 1 cell stage and imaged at 8 ss, oriented with anterior and left sides of the KV to the top and left sides of the page, recorded by confocal microscopy using a 40x lens. Motile cilia appear as a blurry cone and immotile cilia appear as sharp and bright stiff signal.

Supplementary Movie 2. 6 – Scan of a *syntenin-a* morphant Kupffer's Vesicle showing motile and immotile cilia.
Embryo was injected with 50 pg of *alr13b*-GFP mRNA at 1 cell stage, then injected with synta MO^{DFCs} at 512 cell stage, and finally imaged at 8 ss. Oriented with anterior and left sides of the KV to the top and left sides of the page, the embryo was recorded by confocal microscopy using a 40x lens. Motile cilia appear as a blurry cone and immotile cilia appear as sharp and bright stiff signal.

Supplementary Table 2. 1 – Linear mixed-effects model fit: Results for dilution experiments.
Fixed effects coefficient estimates are given. Model information: Number of observations: 16622; Number of embryos: 30. Fixed effects coefficients: 12; Random effects coefficients 90; Covariance parameters: 7. Model formula: AAV ~ 1 + Group*LR + Group*PA + Group*Time + (1 + Group | EmbryoID). Results relate to Figures 5c-f. Model formula: AAV ~ 1 + Intervention*LR + Intervention*PA + Intervention*Time + (1 + Intervention | EmbryoID). *** indicates p<0.001; ** indicates p<0.01; * indicates p<0.05. DB: Danieaus' buffer; MC, methylcellulose; LR, left – right; AP, anterior – posterior.

Name	Estimate	Lower CI	Upper CI	p-value
(Regression line intercept)	0.25148	0.20891	0.29405	6.8705E-31 ***
DB injection	0.070724	-0.030824	0.17227	0.17223
MC injection	-0.12344	-0.19256	-0.05431	0.00046626 ***
Left-right axis	0.0042626	-0.008177	0.016702	0.50182
Posterior-anterior axis	0.16135	0.14901	0.17369	4.4137E-142 ***
Somite stage	0.021413	0.013687	0.029139	5.6349E-08 ***
Interaction: DB injection and left-right axis	-0.012356	-0.027636	0.002925	0.11301
Interaction: MC injection and left-right axis	0.026366	0.008478	0.044254	0.0038681 ***
Interaction: DB injection and posterior-anterior axis	-0.02139	-0.036997	-0.00578	0.0072282 ***
Interaction: MC injection and posterior-anterior axis	-0.073208	-0.092273	-0.05414	5.4857E-14 ***
Interaction: DB injection and time	-0.012635	-0.022248	-0.00302	0.0099937 ***
Interaction: MC injection and time	-0.0004407	-0.012174	0.011293	0.94131

2.5. REFERENCES

Adam, M. G., Berger, C., Feldner, A., Yang, W. J., Wüstehube-Lausch, J., Herberich, S. E., Pinder, M., Gesierich, S., Hammes, H. P., Augustin, H. G., & Fischer, A. (2013). Synaptojanin-2 binding protein stabilizes the notch ligands DLL1 and DLL4 and inhibits sprouting angiogenesis. *Circulation Research*, *113*(11), 1206–1218. https://doi.org/10.1161/CIRCRESAHA.113.301686

Adams, D. S., Robinson, K. R., Fukumoto, T., Yuan, S., Craig, R., Yelick, P., Kuo, L., Mcsweeney, M., & Levin, M. (2006). Early, H+ -V-ATPase-dependent proton flux is necessary for consistent left-right patterning of non-mammalian vertebrates. *Development (Cambridge, England)*, *133*(9), 1657–1671. https://doi.org/10.1242/dev.02341.Early

Addi, C., Presle, A., Frémont, S., Cuvelier, F., Rocancourt, M., Milin, F., Schmutz, S., Chamot-Rooke, J., Douché, T., Duchateau, M., Giai Gianetto, Q., Salles, A., Ménager, H., Matondo, M., Zimmermann, P., Gupta-Rossi, N., & Echard, A. (2020). The Flemmingsome reveals an ESCRT-to-membrane coupling via ALIX/syntenin/syndecan-4 required for completion of cytokinesis. *Nature Communications*, *11*(1), 1941. https://doi.org/10.1038/s41467-020-15205-z

Afratis, N. A., Nikitovic, D., Multhaupt, H. A. B., Theocharis, A. D., Couchman, J. R., & Karamanos, N. K. (2017). Syndecans – key regulators of cell signaling and biological functions. *FEBS Journal*, *284*(1), 27–41. https://doi.org/10.1111/febs.13940

Amack, J. D., & Yost, H. J. (2004). The T Box Transcription Factor No Tail in Ciliated Cells Controls Zebrafish Left-Right Asymmetry. *Current Biology*, *14*(8), 685–690. https://doi.org/10.1016/j

Ascano, J. M., Beverly, L. J., & Capobianco, A. J. (2003). The C-terminal PDZ-ligand of JAGGED1 is essential for cellular transformation. *Journal of Biological Chemistry*, *278*(10), 8771–8779. https://doi.org/10.1074/jbc.M211427200

Baietti, M. F., Zhang, Z., Mortier, E., Melchior, A., Degeest, G., Geeraerts, A., Ivarsson, Y., Depoortere, F., Coomans, C., Vermeiren, E., Zimmermann, P., & David, G. (2012). Syndecan-syntenin-ALIX regulates the biogenesis of exosomes. *Nature Cell Biology*, *14*(7), 677–685. https://doi.org/10.1038/ncb2502

Baratchi, S., Almazi, J. G., Darby, W., Arnan, F. J. T., & Peter, M. (2016). Shear stress mediates exocytosis of functional TRPV4 channels in endothelial cells. *Cellular and Molecular Life Sciences : CMLS*, *73*(3), 649–666. https://doi.org/10.1007/s00018-015-2018-8

Baratchi, S., Tovar-Lopez, F. J., Khoshmanesh, K., Grace, M. S., Darby, W., Almazi, J., Mitchell, A., & McIntyre, P. (2014). Examination of the role of transient receptor potential vanilloid type 4 in endothelial responses to shear forces. *Biomicrofluidics*, *8*(4), 044117. https://doi.org/10.1063/1.4893272

Bearce, E. A., Irons, Z. H., Craig, S. B., Kuhns, C. J., Sabazali, C., Farnsworth, D. R., Miller, A. C., & Grimes, D. T. (2022). Daw1 regulates the timely onset of cilia motility during development. *Development (Cambridge, England)*, *149*(12), dev200017. https://doi.org/10.1242/dev.200017

Beekman, J. M., Vervoort, S. J., Dekkers, F., van Vessem, M. E., Vendelbosch, S., Brugulat-Panès, A., van Loosdregt, J., Braat, A. K., & Coffer, P. J. (2012). Syntenin-mediated regulation of Sox4 proteasomal degradation modulates transcriptional output. *Oncogene*, *31*(21), 2668–2679.

https://doi.org/10.1038/onc.2011.445

Behrndt, M., Salbreux, G., Campinho, P., Hauschild, R., Oswald, F., Roensch, J., Grill, S. W., & Heisenberg, C.-P. (2012). Forces driving epithelial spreading in zebrafish gastrulation. *Science (New York, N.Y.)*, *338*(6104), 257–260. https://doi.org/10.1126/science.1224143

Blum, M., & Ott, T. (2018). Animal left–right asymmetry. *Current Biology*, *28*(7), R301–R304. https://doi.org/10.1016/j.cub.2018.02.073

Bordbar, A., Taassob, A., & Kamali, R. (2018). Diffusion and convection mixing of non-Newtonian liquids in an optimized micromixer. *Canadian Journal of Chemical Engineering*, *96*(8), 1829–1836. https://doi.org/10.1002/cjce.23113

Boskovski, M. T., Yuan, S., Pedersen, N. B., & Goth, C. K. (2013). The Heterotaxy gene, GALNT11, glycosylates Notch to orchestrate cilia type and laterality. *Nature*, *504*(7480), 456–459. https://doi.org/10.1038/nature12723.The

Bottier, M., Thomas, K. A., Dutcher, S. K., & Bayly, P. V. (2019). How Does Cilium Length Affect Beating? *Biophysical Journal*, *116*(7), 1292–1304. https://doi.org/10.1016/j.bpj.2019.02.012

Cartwright, J. H. E., Piro, N., Piro, O., & Tuval, I. (2008). Fluid Dynamics of Nodal Flow and Left – Right Patterning in Development. *Developmental Dynamics : An Official Publication of the American Association of Anatomists*, *237*(12), 3477–3490. https://doi.org/10.1002/dvdy.21672

Cartwright, J. H. E., Piro, O., & Tuval, I. (2004). Fluid-dynamical basis of the embryonic development of left – right asymmetry in vertebrates. *Proceedings of the National Academy of Sciences of the United States of America*, *101*(19), 7234–7239. https://doi.org/10.1073/pnas.0402001101

Chen, E., Hermanson, S., & Ekker, S. C. (2004). Syndecan-2 is essential for angiogenic sprouting during zebrafish development. *Blood*, *103*(5), 1710–1719. https://doi.org/10.1182/blood-2003-06-1783

Cheng, Y. R., Jiang, B. Y., & Chen, C. C. (2018). Acid-sensing ion channels: Dual function proteins for chemo-sensing and mechano-sensing. *Journal of Biomedical Science*, *25*(1), 46. https://doi.org/10.1186/s12929-018-0448-y

Choksi, S. P., Babu, D., Lau, D., Yu, X., & Roy, S. (2014). Systematic discovery of novel ciliary genes through functional genomics in the zebrafish. *Development (Cambridge, England)*, *141*(17), 3410–3419. https://doi.org/10.1242/dev.108209

Chung, W. S., & Stainier, D. Y. R. (2008). Intra-Endodermal Interactions Are Required for Pancreatic β Cell Induction. *Developmental Cell*, *14*(4), 582–593. https://doi.org/10.1016/j.devcel.2008.02.012

Compagnon, J., Barone, V., Rajshekar, S., Kottmeier, R., Pranjic-Ferscha, K., Behrndt, M., & Heisenberg, C.-P. (2014). The Notochord Breaks Bilateral Symmetry by Controlling Cell Shapes in the Zebrafish Laterality Organ. *Developmental Cell*, *31*(6), 774–783. https://doi.org/10.1016/j.devcel.2014.11.003

Cooper, M. S., & D'Amico, L. A. (1996). A cluster of noninvoluting endocytic cells at the margin of the zebrafish blastoderm marks the site of embryonic shield formation. *Developmental Biology*, *180*(1), 184–198. https://doi.org/10.1006/dbio.1996.0294

Corbett, M. A., van Eyk, C. L., Webber, D. L., Bent, S. J., Newman, M., Harper, K., Berry, J. G., Azmanov, D. N., Woodward, K. J., Gardner, A. E., Slee, J., Pérez-Jurado, L. A., MacLennan, A. H., & Gecz, J. (2018).

Pathogenic copy number variants that affect gene expression contribute to genomic burden in cerebral palsy. *NPJ Genomic Medicine*, *3*, 33. https://doi.org/10.1038/s41525-018-0073-4

Das, S. K., Sarkar, D., Emdad, L., & Fisher, P. B. (2019). MDA-9/Syntenin: An emerging global molecular target regulating cancer invasion and metastasis. *Advances in Cancer Research*, *144*, 137–191. https://doi.org/10.1016/bs.acr.2019.03.011

Delling, M., Indzhykulian, A. A., Liu, X., Li, Y., Xie, T., Corey, D. P., & Clapham, D. E. (2016). Primary cilia are not calcium-responsive mechanosensors. *Nature*, *531*(7596), 656–660. https://doi.org/10.1038/nature17426

Doherty, G. J., & McMahon, H. T. (2009). Mechanisms of endocytosis. *Annual Review of Biochemistry*, *78*(March), 857–902. https://doi.org/10.1146/annurev.biochem.78.081307.110540

Ducharme, J., & Farinotti, R. (1996). Clinical pharmacokinetics and metabolism of chloroquine. Focus on recent advancements. *Clinical Pharmacokinetics*, *31*(4), 257–274. https://doi.org/10.2165/00003088-199631040-00003

Eeden, F. J. M. Van, Granato, M., Schach, U., Brand, M., Furutani-seiki, M., Haffter, P., Hammerschmidt, M., Heisenberg, C., Jiang, Y., Kane, D. A., Kelsh, N., Mullins, M. C., Odenthal, J., Warga, R. M., Allende, M. L., Weinberg, E. S., & Nüsslein-volhard, C. (1996). Mutations affecting somite formation and patterning in the zebrafish, Danio rerio. *Development*, *123*, 153–164.

Einhorn, Z., Trapani, J. G., Liu, Q., & Nicolson, T. (2012). Rabconnectin3 Promotes Stable Activity of the H+ Pump on Synaptic Vesicles in Hair Cells. *The Journal of Neuroscience : The Official Journal of the Society for Neuroscience*, *32*(32), 11144–11156. https://doi.org/10.1523/JNEUROSCI.1705-12.2012

England, S. J., Campbell, P. C., Banerjee, S., & Swanson, A. J. (2017). Identification and Expression Analysis of the Complete Family of Zebrafish pkd Genes. *Frontiers in Cell and Developmental Biology*, *5*, 5. https://doi.org/10.3389/fcell.2017.00005

Essner, J. J., Amack, J. D., Nyholm, M. K., Harris, E. B., & Yost, H. J. (2005). Kupffer's vesicle is a ciliated organ of asymmetry in the zebrafish embryo that initiates left-right development of the brain, heart and gut. *Development (Cambridge, England*, *132*(6), 1247–1260. https://doi.org/10.1242/dev.01663

Estrach, S., Legg, J., & Watt, F. M. (2007). Syntenin mediates Delta1-induced cohesiveness of epidermal stem cells in culture. *Journal of Cell Science*, *120*(Pt 16), 2944–2952. https://doi.org/10.1242/jcs.016253

Fakhro, K. a, Choi, M., Ware, S. M., Belmont, J. W., Towbin, J. a, Lifton, R. P., Khokha, M. K., & Brueckner, M. (2011). Rare copy number variations in congenital heart disease patients identify unique genes in left-right patterning. *Proceedings of the National Academy of Sciences of the United States of America*, *108*(7), 2915–2920. https://doi.org/10.1073/pnas.1019645108

Ferreira, J. V., Da Rosa Soares, A., Ramalho, J., Carvalho, C. M., Cardoso, M. H., Pintado, P., Carvalho, A. S., Beck, H. C., Matthiesen, R., Zuzarte, M., Girao, H., Van Niel, G., & Pereira, P. (2022). LAMP2A regulates the loading of proteins into exosomes. *Science Advances*, *8*(12), eabm1140. https://doi.org/10.1126/sciadv.abm1140

Ferreira, , Fukui, H., Chow, R., Vilfan, A., & Vermot, J. (2019). The cilium as a force sensor-myth versus reality. *Journal of Cell Science*, *132*(14). https://doi.org/10.1242/jcs.213496

Ferreira, , Pakula, G., Klaeyle, L., Fukui, H., Vilfan, A., Supatto, W., & Vermot, J. (2018). Chiral Cilia Orientation in the Left-Right Organizer. *Cell Reports*, *25*(8), 2008-2016.e4. https://doi.org/10.1016/j.celrep.2018.10.069

Ferreira, , Vilfan, A., Jülicher, F., Supatto, W., & Vermot, J. (2017). Physical limits of flow sensing in the left-right organizer. *ELife*, *6*, e25078. https://doi.org/10.7554/eLife.25078

Field, S., Riley, K.-L., Grimes, D. T., Hilton, H., Simon, M., Powles-Glover, N., Siggers, P., Bogani, D., Greenfield, A., & Norris, D. P. (2011). Pkd1l1 establishes left-right asymmetry and physically interacts with Pkd2. *Development (Cambridge, England)*, *138*(6), 1131–1142. https://doi.org/10.1242/dev.058149

Fischer, A., & Gessler, M. (2007). Delta-Notch-and then? Protein interactions and proposed modes of repression by Hes and Hey bHLH factors. *Nucleic Acids Research*, *35*(14), 4583–4596. https://doi.org/10.1093/nar/gkm477

Friand, V., David, G., & Zimmermann, P. (2015). Syntenin and syndecan in the biogenesis of exosomes. *Biology of the Cell*, *107*(10), 331–341. https://doi.org/10.1111/boc.201500010

Gajewski, M., Elmasri, H., Girschick, M., Sieger, D., & Winkler, C. (2006). Comparative analysis of her genes during fish somitogenesis suggests a mouse/chick-like mode of oscillation in medaka. *Development Genes and Evolution*, *216*(6), 315–332. https://doi.org/10.1007/s00427-006-0059-6

Goetz, J., Steed, E., Ferreira, R., Ramspacher, C., Boselli, F., Charvin, G., Liebling, M., Wyart, C., & Schwab, Y. (2014). Endothelial Cilia Mediate Low Flow Sensing during Zebrafish Vascular Development. *Cell Reports*, *6*(5), 799–808. https://doi.org/10.1016/j.celrep.2014.01.032

Gokey, J. J., Dasgupta, A., Amack, J. D., & Medical, U. (2015). The V-ATPase accessory protein Atp6ap1b mediates dorsal forerunner cell proliferation and left-right asymmetry in zebrafish. *Developmental Biology*, *407*(1), 115–130. https://doi.org/10.1016/j.ydbio.2015.08.002.The

Gokey, J. J., Ji, Y., Tay, H. G., Litts, B., & Amack, J. D. (2016). Kupffer's vesicle size threshold for robust left-right patterning of the zebrafish embryo. *Developmental Dynamics : An Official Publication of the American Association of Anatomists*, *245*(1), 22–33. https://doi.org/10.1002/dvdy.24355

Gourronc, F., Ahmad, N., Nedza, N., Eggleston, T., & Rebagliati, M. (2007). Nodal Activity Around Kupffer's Vesicle Depends on the T-Box Transcription Factors Notail and Spadetail and on Notch Signaling. *Developmental Dynamics : An Official Publication of the American Association of Anatomists*, *236*(8), 2131–2146. https://doi.org/10.1002/dvdy.21249

Grimes, D. T., & Burdine, R. D. (2017). Left – Right Patterning : Breaking Symmetry to Asymmetric Morphogenesis. *Trends in Genetics*, *33*(9), 616–628. https://doi.org/10.1016/j.tig.2017.06.004

Grootjans, J. J., Reekmans, G., Ceulemans, H., & David, G. (2000). Syntenin-syndecan binding requires syndecan-synteny and the co-operation of both PDZ domains of syntenin. *The Journal of Biological Chemistry*, *275*(26), 19933–19941. https://doi.org/10.1074/jbc.M002459200

Grootjans, J. J., Zimmermann, P., Reekmans, G., Smets, A., Degeest, G., Dürr, J., & David, G. (1997). Syntenin, a PDZ protein that binds syndecan cytoplasmic domains. *Proceedings of the National Academy of Sciences of the United States of America*, *94*(25), 13683–13688. https://doi.org/10.1073/pnas.94.25.13683

Hamada, H., & Tam, P. P. L. (2014). Mechanisms of left-right asymmetry and patterning: driver, mediator and responder. *F1000prime Reports*, *6*(110). https://doi.org/10.12703/P6-110

Hashimoto, H., Rebagliati, M., Ahmad, N., Muraoka, O., Kurokawa, T., Hibi, M., & Suzuki, T. (2004). The Cerberus/Dan-family protein Charon is a negative regulator of Nodal signaling during left-right patterning in zebrafish. *Development (Cambridge, England)*, *131*(8), 1741–1753. https://doi.org/10.1242/dev.01070

Hava, D., Forster, U., Matsuda, M., Cui, S., Link, B. A., Eichhorst, J., Wiesner, B., Chitnis, A., & Abdelilhah-Seyfried, S. (2009). Apical membrane maturation and cellular rosette formation during morphogenesis of the zebrafish lateral line. *Journal of Cell Science*, *122*(5), 687–695. https://doi.org/10.1242/jcs.032102

Huss, M., Ingenhorst, G., König, S., Gaßel, M., Dröse, S., Zeeck, A., Altendorf, K., & Wieczorek, H. (2002). Concanamycin A, the specific inhibitor of V-ATPases, binds to the VO subunit c. *The Journal of Biological Chemistry*, *277*(43), 40544–40548. https://doi.org/10.1074/jbc.M207345200

Itoh, M., Kim, C. H., Palardy, G., Oda, T., Jiang, Y. J., Maust, D., Yeo, S. Y., Lorick, K., Wright, G. J., Ariza-McNaughton, L., Weismann, A. M., Lewis, J., Chandrasekharappa, S. C., & Chitnis, A. B. (2003). Mind bomb is a ubiquitin ligase that is essential for efficient activation of notch signaling by delta. *Developmental Cell*, *4*(1), 67–82. https://doi.org/10.1016/S1534-5807(02)00409-4

Jacinto, R., Sampaio, P., Roxo-Rosa, M., Pestana, S., & Lopes, S. S. (2021). Pkd2 Affects Cilia Length and Impacts LR Flow Dynamics and Dand5. *Frontiers in Cell and Developmental Biology*, *9*, 624531. https://doi.org/10.3389/fcell.2021.624531

Ji, Y., Buel, S. M., & Amack, J. D. (2016). Mutations in zebrafish pitx2 model congenital malformations in Axenfeld-Rieger syndrome but do not disrupt left-right placement of visceral organs. *Developmental Biology*, *416*(1), 69–81. https://doi.org/10.1016/j.ydbio.2016.06.010

Juan, T., Géminard, C., Coutelis, J. B., Cerezo, D., Polès, S., Noselli, S., & Fürthauer, M. (2018). Myosin1D is an evolutionarily conserved regulator of animal left-right asymmetry. *Nature Communications*, *9*(1). https://doi.org/10.1038/s41467-018-04284-8

Kageyama, R., Ohtsuka, T., & Kobayashi, T. (2007). The Hes gene family: Repressors and oscillators that orchestrate embryogenesis. *Development (Cambridge, England)*, *134*(7), 1243–1251. https://doi.org/10.1242/dev.000786

Kamura, K., Kobayashi, D., Uehara, Y., Koshida, S., Iijima, N., Kudo, A., Yokoyama, T., & Takeda, H. (2011). Pkd1l1 complexes with Pkd2 on motile cilia and functions to establish the left-right axis. *Development (Cambridge, England)*, *138*(6), 1121–1129. https://doi.org/10.1242/dev.058271

Kawabe, H., Sakisaka, T., Yasumi, M., Shingai, T., Izumi, G., Nagano, F., Deguchi-Tawarada, M., Takeuchi, M., Nakanishi, H., & Takai, Y. (2003). A novel rabconnectin-3-binding protein that directly binds a GDP/GTP exchange protein for Rab3A small G protein implicated in Ca2+-dependent exocytosis of neurotransmitter. *Genes to Cells : Devoted to Molecular & Cellular Mechanisms*, *8*(6), 537–546. https://doi.org/10.1046/j.1365-2443.2003.00655.x

Kim, J., Bae, S., Lee, H. S., Park, J., & Kim, K. (2017). Claudin5a is required for proper inflation of Kupffer ’ s vesicle lumen and organ laterality. *PloS One*, *12*(8), e0182047.

https://doi.org/10.1371/journal.pone.0182047

Kimmel, C. B., Ballard, W. W., Kimmel, S. R., Ullmann, B., & Schilling, T. F. (1995). Stages of embryonic development of the zebrafish. *Developmental Dynamics*, *203*(3), 253–310. https://doi.org/10.1002/aja.1002030302

Kitajima, K., Oki, S., Ohkawa, Y., Sumi, T., & Meno, C. (2013). Wnt signaling regulates left – right axis formation in the node of mouse embryos. *Developmental Biology*, *380*(2), 222–232. https://doi.org/10.1016/j.ydbio.2013.05.011

Koivusalo, M., Welch, C., Hayashi, H., Scott, C. C., Kim, M., Alexander, T., Touret, N., Hahn, K. M., & Grinstein, S. (2010). Amiloride inhibits macropinocytosis by lowering submembranous pH and preventing Rac1 and Cdc42 signaling. *Journal of Cell Biology*, *188*(4), 547–563. https://doi.org/10.1083/jcb.200908086

Kramer-Zucker, A. G., Olale, F., Haycraft, C. J., Yoder, B. K., Schier, A. F., & Drummond, I. A. (2005). Cilia-driven fluid flow in the zebrafish pronephros, brain and Kupffer's vesicle is required for normal organogenesis. *Development (Cambridge, England)*, *132*(8), 1907–1921. https://doi.org/10.1242/dev.01772

Kreiling, J. A., Prabhat, Williams, G., & Creton, R. (2007). Analysis of Kupffer's vesicle in zebrafish embryos using a cave automated virtual environment. *Developmental Dynamics : An Official Publication of the American Association of Anatomists*, *236*(7), 1963–1969. https://doi.org/10.1002/dvdy.21191

Kugeratski, F. G., Hodge, K., Lilla, S., McAndrews, K. M., Zhou, X., Hwang, R. F., Zanivan, S., & Kalluri, R. (2021). Quantitative proteomics identifies the core proteome of exosomes with syntenin-1 as the highest abundant protein and a putative universal biomarker. In *Nature Cell Biology* (Vol. 23, Issue 6). Springer US. https://doi.org/10.1038/s41556-021-00693-y

Kwan, K. M., Fujimoto, E., Grabher, C., Mangum, B. D., Hardy, M. E., Campbell, D. S., Parant, J. M., Yost, H. J., Kanki, J. P., & Chien, C. Bin. (2007). The Tol2kit: A multisite gateway-based construction Kit for Tol2 transposon transgenesis constructs. *Developmental Dynamics : An Official Publication of the American Association of Anatomists*, *236*(11), 3088–3099. https://doi.org/10.1002/dvdy.21343

Lambaerts, K., Van Dyck, S., Mortier, E., Ivarsson, Y., Degeest, G., Luyten, A., Vermeiren, E., Peers, B., David, G., & Zimmermann, P. (2012). Syntenin, a syndecan adaptor and an Arf6 phosphatidylinositol 4,5-bisphosphate effector, is essential for epiboly and gastrulation cell movements in zebrafish. *Journal of Cell Science*, *125*(Pt 5), 1129–1140. https://doi.org/10.1242/jcs.089987

Latysheva, N., Muratov, G., Rajesh, S., Padgett, M., Hotchin, N. A., Overduin, M., & Berditchevski, F. (2006). Syntenin-1 is a new component of tetraspanin-enriched microdomains: mechanisms and consequences of the interaction of syntenin-1 with CD63. *Molecular and Cellular Biology*, *26*(20), 7707–7718. https://doi.org/10.1128/MCB.00849-06

Li, L., Wan, T., Wan, M., Liu, B., Cheng, R., & Zhang, R. (2015). The effect of the size of fluorescent dextran on its endocytic pathway. *Cell Biology International*, *39*(5), 531–539. https://doi.org/10.1002/cbin.10424

Liu, J., Zhu, C., Ning, G., Yang, L., Cao, Y., & Id, S. H. (2019). Chemokine signaling links cell-cycle

progression and cilia formation for left – right symmetry breaking. *PLoS Biology*, *17*(8), e3000203. https://doi.org/10.1371/journal.pbio.3000203

Long, S., Ahmad, N., & Rebagliati, M. (2003). The zebrafish nodal-related gene southpaw is required for visceral and diencephalic left-right asymmetry. *Development (Cambridge, England)*, *130*(11), 2303–2316. https://doi.org/10.1242/dev.00436

Longair, M. H., Baker, D. A., & Armstrong, J. D. (2011). Simple neurite tracer: Open source software for reconstruction, visualization and analysis of neuronal processes. *Bioinformatics*, *27*(17), 2453–2454. https://doi.org/10.1093/bioinformatics/btr390

Lopes, S. S., Lourenço, R., Pacheco, L., Moreno, N., Kreiling, J., & Saúde, L. (2010). Notch signalling regulates left-right asymmetry through ciliary length control. *Development (Cambridge, England)*, *137*(21), 3625–3632. https://doi.org/10.1242/dev.054452

Luyten, A., Mortier, E., Van Campenhout, C., Taelman, V., Degeest, G., Wuytens, G., Lambaerts, K., David, G., Bellefroid, E. J., & Zimmermann, P. (2008). The postsynaptic density 95/disc-large/zona occludens protein syntenin directly interacts with frizzled 7 and supports noncanonical Wnt signaling. *Molecular Biology of the Cell*, *19*(4), 1594–1604. https://doi.org/10.1091/mbc.e07-08-0832

Marques, S., Borges, A. C., Silva, A. C., Freitas, S., Cordenonsi, M., & Belo, J. A. (2004). The activity of the Nodal antagonist Cerl-2 in the mouse node is required for correct L/R body axis. *Genes & Development*, *18*(19), 2342–2347. https://doi.org/10.1101/gad.306504.2342

McGrath, J., Somlo, S., Makova, S., Tian, X., & Brueckner, M. (2003). Two populations of node monocilia initiate left-right asymmetry in the mouse. *Cell*, *114*(1), 61–73. https://doi.org/10.1016/S0092-8674(03)00511-7

Mizuno, K., Shiozawa, K., Katoh, T. A., Minegishi, K., Ide, T., Ikawa, Y., Nishimura, H., Takaoka, K., Itabashi, T., Iwane, A. H., Nakai, J., Shiratori, H., & Hamada, H. (2020). Role of Ca2+ transients at the node of the mouse embryo in breaking of left-right symmetry. *Science Advances*, *6*(30). https://doi.org/10.1126/sciadv.aba1195

Montague, T. G., Gagnon, J. A., & Schier, A. F. (2018). Conserved regulation of nodal-mediated left-right patterning in zebrafish and mouse. *Development (Cambridge, England)*, *145*(24), dev171090. https://doi.org/10.1242/dev.171090

Montenegro-Johnson, T. D., Baker, D. I., Smith, D. J., & Lopes, S. S. (2016). Three-dimensional flow in Kupffer's Vesicle. *Journal of Mathematical Biology*, *73*(3), 705–725. https://doi.org/10.1007/s00285-016-0967-7

Moreno-Ayala, R., Olivares-Chauvet, P., Schäfer, R., & Junker, J. P. (2021). Variability of an Early Developmental Cell Population Underlies Stochastic Laterality Defects. *Cell Reports*, *34*(2), 108606. https://doi.org/10.1016/j.celrep.2020.108606

Morozova, S., Schmidt, P. W., Metaxas, A., Bates, F. S., Lodge, T. P., & Dutcher, C. S. (2018). Extensional Flow Behavior of Methylcellulose Solutions Containing Fibrils. *ACS Macro Letters*, *7*(3), 347–352. https://doi.org/10.1021/acsmacrolett.8b00042

Nagano, F., Kawabe, H., Deguchi-tawarada, M., & Takeuchi, M. (2002). Rabconnectin-3 , a Novel Protein That Binds Both GDP / GTP Exchange Protein and GTPase- activating Protein for Rab3 Small G

Protein Family *. *The Journal of Biological Chemistry*, *277*(12), 9629–9632. https://doi.org/10.1074/jbc.C100730200

Nauli, S. M., Alenghat, F. J., Luo, Y., Williams, E., Vassilev, P., Li, X., Elia, A. E. H., Lu, W., Brown, E. M., Quinn, S. J., Ingber, D. E., & Zhou, J. (2003). Polycystins 1 and 2 mediate mechanosensation in the primary cilium of kidney cells. *Nature Genetics*, *33*(2), 129–137. https://doi.org/10.1038/ng1076

Nauli, S. M., Kawanabe, Y., Kaminski, J. J., Pearce, W. J., Ingber, D. E., & Zhou, J. (2008). Endothelial Cilia Are Fluid Shear Sensors That Regulate Calcium Signaling and Nitric Oxide Production Through Polycystin-1. *Circulation*, *117*(9), 1161–1171. https://doi.org/10.1161/CIRCULATIONAHA.107.710111

Nauli, S. M., Rossetti, S., Kolb, R. J., Alenghat, F. J., Consugar, M. B., Harris, P. C., Ingber, D. E., Loghman-adham, M., & Zhou, J. (2006). Loss of Polycystin-1 in Human Cyst-Lining Epithelia Leads to Ciliary Dysfunction. *Journal of the American Society of Nephrology : JASN*, *17*(4), 1015–1025. https://doi.org/10.1681/ASN.2005080830

Navis, A., Marjoram, L., & Bagnat, M. (2013). Cftr controls lumen expansion and function of Kupffer's vesicle in zebrafish. *Development (Cambridge, England)*, *140*(8), 1703–1712. https://doi.org/10.1242/dev.091819

Niel, G. Van, Angelo, G. D., & Raposo, G. (2018). Shedding light on the cell biology of extracellular vesicles. *Nature Reviews. Molecular Cell Biology*, *19*(4), 213–228. https://doi.org/10.1038/nrm.2017.125

Nonaka, S., Tanaka, Y., Okada, Y., Takeda, S., Harada, A., Kanai, Y., Kido, M., & Hirokawa, N. (1998). Randomization of left-right asymmetry due to loss of nodal cilia generating leftward flow of extraembryonic fluid in mice lacking KIF3B motor protein. *Cell*, *95*(6), 829–837. https://doi.org/10.1016/S0092-8674(00)81705-5

Nourry, C., Grant, S. G. N., & Borg, J. P. (2003). PDZ domain proteins: plug and play! *Science Signaling*, *179*, 1–13. https://doi.org/10.1126/stke.2003.179.re7

Okada, Y., Takeda, S., Tanaka, Y., Belmonte, J. C. I., & Hirokawa, N. (2005). Mechanism of nodal flow: A conserved symmetry breaking event in left-right axis determination. *Cell*, *121*(4), 633–644. https://doi.org/10.1016/j.cell.2005.04.008

Ortega, F. G., Roefs, M. T., Perez, D. D. M., Kooijmans, S. A., Jong, O. G. De, Sluijter, J. P., Schiffelers, R. M., & Vader, P. (2019). Interfering with endolysosomal trafficking enhances release of bioactive exosomes. *Nanomedicine: Nanotechnology, Biology, and Medicine*, *20*, 102014. https://doi.org/10.1016/j.nano.2019.102014

Oteiza, P., Köppen, M., Concha, M. L., & Heisenberg, C. P. (2008). Origin and shaping of the laterality organ in zebrafish. *Development (Cambridge, England)*, *135*(16), 2807–2813. https://doi.org/10.1242/dev.022228

Oteiza, P., Köppen, M., Krieg, M., Pulgar, E., Farias, C., Melo, C., Preibisch, S., Müller, D., Tada, M., Hartel, S., Heisenberg, C. P., & Concha, M. L. (2010). Planar cell polarity signalling regulates cell adhesion properties in progenitors of the zebrafish laterality organ. *Development (Cambridge, England)*, *137*(20), 3459–3468. https://doi.org/10.1242/dev.049981

Özbudak, E. M., & Lewis, J. (2008). Notch signalling synchronizes the zebrafish segmentation clock but

is not needed to create somite boundaries. *PLoS Genetics*, *4*(2), e15. https://doi.org/10.1371/journal.pgen.0040015

Pastor-soler, N., Litvin, T. N., Silva, N. Da, Chen, Y., Brown, D., Buck, J., Levin, L. R., & Breton, S. (2003). Bicarbonate-regulated Adenylyl Cyclase (sAC) Is a Sensor That Regulates pH-dependent V-ATPase Recycling. *The Journal of Biological Chemistry*, *278*(49), 49523–49529. https://doi.org/10.1074/jbc.M309543200

Pintado, P., Sampaio, P., Tavares, B., Smith, D. J., & Lopes, S. S. (2017). Dynamics of cilia length in left – right development. *Royal Society Open Science*, *4*(3), 161102. http://dx.doi.org/10.1098/rsos.161102

Pinto, A. L., Rasteiro, M., Bota, C., Pestana, S., Sampaio, P., Hogg, C., Burgoyne, T., & Lopes, S. S. (2021). Zebrafish motile cilia as a model for primary ciliary dyskinesia. *International Journal of Molecular Sciences*, *22*(16), 8361. https://doi.org/10.3390/ijms22168361

Pols, M. S., & Klumperman, J. (2009). Trafficking and function of the tetraspanin CD63. *Experimental Cell Research*, *315*(9), 1584–1592. https://doi.org/10.1016/j.yexcr.2008.09.020

Pradhan, A. K., Maji, S., Das, S. K., Emdad, L., Sarkar, D., & Fisher, P. B. (2020). MDA-9/Syntenin/SDCBP: New insights into a unique multifunctional scaffold protein. *Cancer Metastasis Reviews*, *39*(3), 769–781. https://doi.org/10.1007/s10555-020-09886-7.MDA-9/Syntenin/SDCBP

Praetorius, H. A. (2015). The primary cilium as sensor of fluid flow: new building blocks to the model. A review in the theme: cell signaling: proteins, pathways and mechanisms. *American Journal of Physiology. Cell Physiology*, *308*(3), 198–208. https://doi.org/10.1152/ajpcell.00336.2014

Qu, Z., & Breuer, K. S. (2020). Effects of shear-thinning viscosity and viscoelastic stresses on flagellated bacteria motility. *Physical Review Fluids*, *5*, 073103. https://doi.org/10.1103/PhysRevFluids.5.073103

Rathbun, L. I., Colicino, E. G., Manikas, J., Connell, J. O., Krishnan, N., Reilly, N. S., Coyne, S., Garrastegui, A., Freshour, J., Santra, P., Manning, M. L., Amack, J. D., & Hehnly, H. (2020). Cytokinetic bridge triggers de novo lumen formation in vivo. *Nature Communications*, *11*(1), 1269. https://doi.org/10.1038/s41467-020-15002-8

Roxo-Rosa, M., Jacinto, R., Sampaio, P., & Lopes, S. S. (2015). The zebrafish Kupffer's vesicle as a model system for the molecular mechanisms by which the lack of Polycystin-2 leads to stimulation of CFTR. *Biology Open*, *4*(11), 1356–1366. https://doi.org/10.1242/bio.014076

Roxo-Rosa, M., & Lopes, S. S. (2019). The Zebrafish Kupffer's Vesicle: A Special Organ in a Model Organism to Study Human Diseases. *In Zebrafish in Biomedical Research. IntechOpen*. https://doi.org/10.5772/intechopen.88266%0D

Sampaio, P., Ferreira, , Guerrero, A., Pintado, P., Tavares, B., Amaro, J., Smith, A. A., Montenegro-Johnson, T., Smith, D. J., & Lopes, S. S. (2014). Left-Right Organizer Flow Dynamics: How Much Cilia Activity Reliably Yields Laterality? *Developmental Cell*, *29*(6), 716–728. https://doi.org/10.1016/j.devcel.2014.04.030

Sampaio, P., Pestana, S., Guerrero, A., Telley, I. A., Smith, D. J., & Lopes, S. S. (2022). Fluid manipulations uncover mechanosensation for zebrafish left-right establishment during one-hour time interval. *BioRxiv*, 2022.04.21.489023. https://doi.org/10.1101/2022.04.21.489023

Samuel, S. P., Jain, N., Dowd, F. O., Paul, T., Gerard, V. A., Gun, Y. K., & Prina-mello, A. (2012). Multifactorial determinants that govern nanoparticle uptake by human endothelial cells under flow. *International Journal of Nanomedicine*, *7*, 2943–2956. https://doi.org/10.2147/IJN.S30624

Saydmohammed, M., Yagi, H., Calderon, M., Clark, M. J., Feinstein, T., Sun, M., Stolz, D. B., Watkins, S. C., Amack, J. D., Lo, C. W., & Tsang, M. (2018). Vertebrate myosin 1d regulates left–right organizer morphogenesis and laterality. *Nature Communications*, *9*(1), 1–11. https://doi.org/10.1038/s41467-018-05866-2

Schweickert, A., Vick, P., Getwan, M., Weber, T., Schneider, I., Eberhardt, M., Beyer, T., Pachur, A., & Blum, M. (2010). The Nodal Inhibitor Coco Is a Critical Target of Leftward Flow in Xenopus. *Current Biology*, *20*(8), 738–743. https://doi.org/10.1016/j.cub.2010.02.061

Schweickert, A., Weber, T., Beyer, T., Vick, P., Bogusch, S., Feistel, K., & Blum, M. (2007). Cilia-Driven Leftward Flow Determines Laterality in Xenopus. *Current Biology*, *17*(1), 60–66. https://doi.org/10.1016/j.cub.2006.10.067

Sethi, N., Yan, Y., Debra, Q., Schupbach, T., & Kang, Y. (2010). Rabconnectin-3 Is a Functional Regulator of Mammalian Notch Signaling. *The Journal of Biological Chemistry*, *5*(45), 34757–34764. https://doi.org/10.1074/jbc.M110.158634

Shankaran, S. S., Sieger, D., Schröter, C., Czepe, C., Pauly, M. C., Laplante, M. A., Becker, T. S., Oates, A. C., & Gajewski, M. (2007). Completing the set of h/E(spl) cyclic genes in zebrafish: her12 and her15 reveal novel modes of expression and contribute to the segmentation clock. *Developmental Biology*, *304*(2), 615–632. https://doi.org/10.1016/j.ydbio.2007.01.004

Shimada, T., Yasuda, S., Sugiura, H., & Yamagata, K. (2019). Syntenin: PDZ Protein Regulating Signaling Pathways and Cellular Functions. *International Journal of Molecular Sciences*, *20*(17). https://doi.org/10.3390/ijms20174171

Shinohara, K., Kawasumi, A., Takamatsu, A., Yoshiba, S., Botilde, Y., Motoyama, N., Reith, W., Durand, B., Shiratori, H., & Hamada, H. (2012). Two rotating cilia in the node cavity are sufficient to break left-right symmetry in the mouse embryo. *Nature Communications*, *3*, 622. https://doi.org/10.1038/ncomms1624

Shum, W. W. C., Da Silva, N., Brown, D., & Breton, S. (2009). Regulation of luminal acidification in the male reproductive tract via cell-cell crosstalk. *Journal of Experimental Biology*, *212*(Pt 11), 1753–1761. https://doi.org/10.1242/jeb.027284

Smith, D., Gaffney, E., & Blake, J. (2007). Discrete cilia modelling with singularity distributions: Application to the embryonic node and the airway surface liquid. In *Bulletin of Mathematical Biology* (Vol. 69, Issue 5). https://doi.org/10.1007/s11538-006-9172-y

Smith, D., Montenegro-Johnson, T., & Lopes, S. (2014). Organized chaos in Kupffer's vesicle: How a heterogeneous structure achieves consistent left-right patterning. *Bioarchitecture*, *4*(3), 119–125. https://doi.org/10.4161/19490992.2014.956593

Solowiej-Wedderburn, J., Smith, D. J., Lopes, S. S., & Montenegro-johnson, T. D. (2019). Wall stress enhanced exocytosis of extracellular vesicles as a possible mechanism of left-right symmetry-breaking in vertebrate development. *Journal of Theoretical Biology*, *460*, 220–226.

https://doi.org/10.1016/j.jtbi.2018.10.015

Stubbs, J. L., Oishi, I., Izpisúa Belmonte, J. C., & Kintner, C. (2008). The forkhead protein Foxj1 specifies node-like cilia in Xenopus and zebrafish embryos. *Nature Genetics*, *40*(12), 1454–1460. https://doi.org/10.1038/ng.267

Supatto, W., Fraser, S. E., & Vermot, J. (2008). An All-Optical Approach for Probing Microscopic Flows in Living Embryos. *Biophysical Journal*, *95*(4), L29–L31. https://doi.org/10.1529/biophysj.108.137786

Supatto, W., & Vermot, J. (2011). From Cilia Hydrodynamics to Zebrafish Embryonic Development. In *Current topics in developmental biology* (1st ed., Vol. 95). Elsevier Inc. https://doi.org/10.1016/B978-0-12-385065-2.00002-5

Superina, S., Borovina, A., & Ciruna, B. (2014). Analysis of maternal-zygotic ugdh mutants reveals divergent roles for HSPGs in vertebrate embryogenesis and provides new insight into the initiation of left–right asymmetry. *Developmental Biology*, *387*(2), 154–166. https://doi.org/10.1016/j.ydbio.2014.01.013

Tae, N., Lee, S., Kim, O., Park, J., Na, S., & Lee, J.-H. (2017). Syntenin promotes VEGF-induced VEGFR2 endocytosis and angiogenesis by increasing ephrin-B2 function in endothelial cells. *Oncotarget*, *8*(24), 38886–38901. https://doi.org/10.18632/oncotarget.16452

Tanaka, Y., Okada, Y., & Hirokawa, N. (2005). FGF-induced vesicular release of Sonic hedgehog and retinoic acid in leftward nodal flow is critical for left-right determination. *Nature*, *435*(7039), 172–177. https://doi.org/10.1038/nature03494

Tavares, B., Jacinto, R., Sampaio, P., Pestana, S., Pinto, A., Vaz, A., Roxo-Rosa, M., Gardner, R., Lopes, T., Schilling, B., Henry, I., Saúde, L., & Lopes, S. S. (2017). Notch/Her12 signalling modulates, motile/immotile cilia ratio downstream of Foxj1a in zebrafish left-right organizer. *ELife*, *6*, e25165. https://doi.org/10.7554/eLife.25165

Tay, H. G., Schulze, S. K., Compagnon, J., Foley, F. C., Heisenberg, C., Yost, H. J., Abdelilah-seyfried, S., & Amack, J. D. (2013). Lethal giant larvae 2 regulates development of the ciliated organ Kupffer's vesicle. *Development (Cambridge, England)*, *140*(7), 1550–1559. https://doi.org/10.1242/dev.087130

Tetzlaff, F., Adam, M. G., Feldner, A., Moll, I., Menuchin, A., Rodriguez-Vita, J., Sprinzak, D., & Fischer, A. (2018). MPDZ promotes DLL4-induced notch signaling during angiogenesis. *ELife*, *7*, 1–21. https://doi.org/10.7554/eLife.32860

Thisse, C., & Thisse, B. (2008). High-resolution in situ hybridization to whole-mount zebrafish embryos. *Nature Protocols*, *3*(1), 59–69. https://doi.org/10.1038/nprot.2007.514

Toei, M., Saum, R., & Forgac, M. (2010). Regulation and isoform function of the V-ATPases. *Biochemistry*, *49*(23), 4715–4723. https://doi.org/10.1021/bi100397s.Regulation

Tözser, J., Earwood, R., Kato, A., Brown, J., Tanaka, K., Didier, R., Megraw, T. L., Blum, M., & Kato, Y. (2015). TGF-β Signaling Regulates the Differentiation of Motile Cilia. *Cell Reports*, *11*(7), 1000–1007. https://doi.org/10.1016/j.celrep.2015.04.025

Tudor, C., te Riet, J., Eich, C., Harkes, R., Smisdom, N., Bouhuijzen Wenger, J., Ameloot, M., Holt, M., Kanger, J. S., Figdor, C. G., Cambi, A., & Subramaniam, V. (2014). Syntenin-1 and ezrin proteins link

activated leukocyte cell adhesion molecule to the actin cytoskeleton. *The Journal of Biological Chemistry*, *289*(19), 13445–13460. https://doi.org/10.1074/jbc.M113.546754

Tuttle, A. M., Hoffman, T. L., & Schilling, T. F. (2014). Rabconnectin-3a Regulates Vesicle Endocytosis and Canonical Wnt Signaling in Zebrafish Neural Crest Migration. *PLoS Biology*, *12*(5), e1001852. https://doi.org/10.1371/journal.pbio.1001852

Verweij, F., Bebelman, M., Jimenez, C., Vallejo, J., Janssen, H., Neefjes, J., Knol, J. C., Haas, R., Piersma, S., Baglio, S. R., Verhage, M., Middeldorp, J. M., Zomer, A., Rheenen, J. Van, Coppolino, M., Hurbain, I., Raposo, G., Smit, M., Toonen, R., … Pegtel, D. M. (2016). Quantifying exosome secretion from single cells reveals a modulatory role for GPCR signaling. *The Journal of Cell Biology*, *217*(3), 1129–1142. https://doi.org/10.1083/jcb.201703206

Verweij, F., Revenu, C., Arras, G., Dingli, F., Loew, D., Pegtel, D. M., Follain, G., Allio, G., Goetz, J. G., Zimmermann, P., Herbomel, P., Del Bene, F., Raposo, G., & van Niel, G. (2019). Live Tracking of Inter-organ Communication by Endogenous Exosomes In Vivo. *Developmental Cell*, *48*(4), 573-589.e4. https://doi.org/10.1016/j.devcel.2019.01.004

Viña, E., Parisi, V., Abbate, F., Cabo, R., Guerrera, M. C., Laurà, R., Quirós, L. M., Pérez-Varela, J. C., Cobo, T., Germanà, A., Vega, J. A., & García-Suárez, O. (2015). Acid-sensing ion channel 2 (ASIC2) is selectively localized in the cilia of the non-sensory olfactory epithelium of adult zebrafish. *Histochemistry and Cell Biology*, *143*(1), 59–68. https://doi.org/10.1007/s00418-014-1264-4

Wang, G., Cadwallader, A. B., Jang, D. S., Tsang, M., Yost, H. J., & Amack, J. D. (2011). The Rho kinase rock2b establishes anteroposterior asymmetry of the ciliated Kupffer's vesicle in zebrafish. *Development (Cambridge, England)*, *138*(1), 45–54. https://doi.org/10.1242/dev.052985

Wang, G., Manning, M. L., & Amack, J. D. (2012). Regional cell shape changes control form and function of Kupffer's vesicle in the zebrafish embryo. *Developmental Biology*, *370*(1), 52–62. https://doi.org/10.1016/j.cmet.2012.08.002.

Wang, L. H., Rothberg, K. G., & Anderson, R. G. W. (1993). Mis-assembly of clathrin lattices on endosomes reveals a regulatory switch for coated pit formation. *The Journal of Cell Biology*, *123*(5), 1107–1117. https://doi.org/10.1083/jcb.123.5.1107

Welf, E. S., Miles, C. E., Huh, J., Fiolka, R., Welf, E. S., Miles, C. E., Huh, J., Sapoznik, E., Chi, J., Driscoll, M. K., Isogai, T., Noh, J., Weems, A., Pohlkamp, T., Dean, K., Fiolka, R., Molgoner, A., & Danuser, G. (2020). Actin-Membrane Release Initiates Cell Protrusions. *Developmental Cell*, *55*(6), 723-736.e8. https://doi.org/10.1016/j.devcel.2020.11.024

Whiteford, J. R., & Couchman, J. R. (2006). A conserved NXIP motif is required for cell adhesion properties of the syndecan-4 ectodomain. *Journal of Biological Chemistry*, *281*(43), 32156–32163. https://doi.org/10.1074/jbc.M605553200

Wright, G. J., Leslie, J. D., Ariza-McNaughton, L., & Lewis, J. (2004). Delta proteins and MAGI proteins: An interaction of Notch ligands with intracellular scaffolding molecules and its significance for zebrafish development. *Development*, *131*(22), 5659–5669. https://doi.org/10.1242/dev.01417

Yan, Y., Denef, N., & Schüpbach, T. (2009). The vacuolar proton pump (V-ATPase) is required for Notch signaling and endosomal trafficking in Drosophila. *Developmental Cell*, *17*(3), 387–402.

https://doi.org/10.1016/j.devcel.2009.07.001.The

Yoshiba, S., Shiratori, H., Kuo, I. Y., Kawasumi, A., Shinohara, K., Nonaka, S., Asai, Y., Sasaki, G., Belo, J. A., Sasaki, H., Nakai, J., Dworniczak, B., Ehrlich, B., Pennekamp, P., & Hamada, H. (2012). Cilia at the node of mouse embryos sense fluid flow for left-right determination via Pkd2. *Science (New York, N.Y.)*, *338*(6104), 226–231. https://doi.org/10.1038/nature13314.A

Yu, X., Ng, C. P., Habacher, H., & Roy, S. (2008). Foxj1 transcription factors are master regulators of the motile ciliogenic program. *Nature Genetics*, *40*(12), 1445–1453. https://doi.org/10.1038/ng.263

Yuan, S., Zhao, L., Brueckner, M., & Sun, Z. (2015). Intraciliary Calcium Oscillations Initiate Vertebrate Left-Right Asymmetry. *Current Biology : CB*, *25*(5), 556–567. https://doi.org/10.1016/j.cub.2014.12.051

Zhang, M., Zhang, J., Lin, S.-C., & Meng, A. (2012). β-Catenin 1 and β-catenin 2 play similar and distinct roles in left-right asymmetric development of zebrafish embryos. *Development (Cambridge, England)*, *139*(11), 2009–2019. https://doi.org/10.1242/dev.074435

Zhang, W., Zhang, Y., Li, S., Wu, Z., Yan, Y., & Li, Y. (2018). Prmt7 regulates epiboly and gastrulation cell movements by facilitating syntenin. *Acta Biochimica et Biophysica Sinica*, *50*(12), 1280–1287. https://doi.org/10.1093/abbs/gmy136

Zimmermann, P., Tomatis, D., Rosas, M., Grootjans, J., Leenaerts, I., Degeest, G., Reekmans, G., Coomans, C., & David, G. (2001). Characterization of syntenin, a syndecan-binding PDZ protein, as a component of cell adhesion sites and microfilaments. *Molecular Biology of the Cell*, *12*(2), 339–350. https://doi.org/10.1091/mbc.12.2.339

CHAPTER 3.

PRIMARY CILIARY DYSKINESIA – CHARACTERIZATION OF A NEW *ZMYND10* VARIANT

3. INTRODUCTION

Primary ciliary dyskinesia (PCD; OMIM 244400) is a rare and heterogeneous syndromic condition that arises from motile cilia dysfunction, including lack or reduced number of cilia, uncoordinated ciliary beat pattern and abnormal ciliary beat frequency, in different organs but mostly affecting the respiratory system (Stannard et al., 2004; Schwabe et al., 2008; Boon, Smits, et al., 2014; Raidt et al., 2014; Bustamante-marin et al., 2019).

Ineffective or complete absent beating of motile cilia impairs the mucus upward transport from the middle ear, the paranasal sinuses and the bronchial tree, resulting in poor clearance of the upper and lower airways. Consequently, bacterial pathogens accumulated in the mucus layer proliferate causing a vicious cycle of recurrent infections, starting at an early age (Mullowney et al., 2014). Upper airway infections are characterized by chronic rhinitis, rhinorrhea or nasal congestion, sinusitis, nasal polyps and persistent otitis media, that often result in conductive hearing loss and speech/language delay (Goutaki et al., 2016). PCD children also develop wet and productive cough, most likely as a reflex to compensate for the lack of mucociliary clearance (Leigh et al., 2016). Lower airway infections, such as recurrent bronchitis and pneumonia, irreversibly affect lung structure and function leading to the development of bronchiectasis in 50% of PCD children by 8 years of age and in all PCD adults (Kennedy, Noone, et al., 2007). Pulmonary function decline can evolve to severe lung obstructive disease and end-stage respiratory failure, in some cases requiring long-term oxygen supplementation and lung transplantation (Frija-Masson et al., 2017).

Moreover, ciliary motility impairment affects thoracic and abdominal organ laterality position within the body. In the absence of a cilia-driven fluid flow within the embryonic structure left-right organizer (LRO), the left-right asymmetric axis is no longer established and the embryo laterality remains unbiased, leading to a randomization of the final internal organ position (Nonaka et al., 1998; McGrath & Brueckner, 2003). Accordingly, 50% of PCD patients have laterality defects, most of them present *situs inversus*, a complete reversal of organ arrangement, referred to as Kartagener's syndrome (Kartagener, 1933). Additionally, roughly one-tenth of the PCD cases fall into a category of *situs ambiguous*, representing any combination of partial reversal of visceral organ position and often linked to congenital heart disease (CHD) (Kennedy, Omran, et al., 2007; Shapiro et al., 2014). In fact, while in the general population, *situs inversus* and *situs ambiguous* are associated with 2 – 5% and 3% of CHD cases, respectively (Zhu et al., 2006; Harrison et al., 2016), within the PCD population, the CHD related to *situs ambiguous* prevalence is 200-fold increased (Kennedy, Noone, et al., 2007; Kennedy, Omran, et al., 2007; Best et al., 2019).

PCD is also characterized by fertility problems. Depending on the mutated PCD gene, 75% of male PCD patients have shown infertility, caused by dysfunction of either spermatozoa flagella or efferent duct motile cilia (Höben et al., 2018; Aprea, Nöthe-Menchen, et al., 2021). In contrast, 61% of female PCD individuals were considered to have sub-fertility, associated with an impairment of fallopian tube cilia motility in transporting the oocyte to the uterus (Raidt et al., 2015; Vanaken et al., 2017).

In a lower extent, PCD patients can also present hydrocephalus due to ciliary dysfunction of ependymal cells that result in defective cerebrospinal fluid flow during brain development and adult life (Boon, Wallmeier, et al., 2014; Amirav et al., 2016; Wallmeier et al., 2019).

Thus, clinical presentation of PCD is heterogenous, and patients show different combinations of symptoms, some of which vary over time. This phenotypical variance among PCD patients accounts for the complex genetic origin of this disorder, with more than 50 different genes being already associated with PCD (Wallmeier et al., 2020).

Within the cilia, motility is supported by highly conserved appendages composed of axonemal outer and inner dynein arms (ODA and IDA), microtubule inner proteins, radial spokes, nexin-links, central pair complex and CCDC39/CCDC40 molecular ruler (Ishikawa, 2017). Mutations on proteins coded by this group of genes can lead to structural defects, with absence of one or more components, and microtubule disorganization.

Moreover, within the cytoplasm, several proteins are responsible for folding, stabilization and assembly of the axonemal outer and inner dyneins arms. These dynein axonemal assembly factors (DNAAFs) interact not only with each other but also with heat shock chaperones, functioning as co-chaperones for a step-wise assembly process of dynein arm subunits into multi-protein complexes, before being delivered to the cilia or flagella (Desai et al., 2017; Aprea, Raidt, et al., 2021).

Some studies suggested that dynein subunits are firstly sequestered into specialized membrane-less organelles, where DNAAFs and chaperones rapidly flux through to coordinate dynein arm preassembly (Horani et al., 2018; Huizar et al., 2018). Then, DNAAFs were proposed to divide into early and late pre-assembly complexes, composed by at least DNAAF5/HEATR2 (Horani et al., 2012) – DNAAF13/SPAG1 (Knowles et al., 2013) – DNAAF2/KTU (Omran et al., 2008) and DNAAF2 – DNAAF4/DYX1C1 (Tarkar et al., 2013) – DNAAF6/PIH1D3 (Paff et al., 2017), respectively. Moreover, DNAAF2 would function as a link between the two complexes, establishing a temporal sequence for DNAAFs action (Tarkar et al., 2013; Paff et al., 2017; Horani et al., 2018). In opposition to this mechanism, another study suggested that specific dynein subunits were assembled independently by different DNAAFs, where DNAAF7/ZMYND10 was shown to promote protein stabilization and assembly of

dynein heavy chains (Mali et al., 2018). These authors further proposed that dynein intermediate and light chains were assembled in parallel via the PIH (heat shock binding) domain of other chaperones, such as DNAAF2, DNAAF6 and DNAAF15/PIH1D2 (Yamaguchi et al., 2018), while DNAAF13 and DNAAF4 would provide a stable platform for final dynein arm assembly (Mali et al., 2018). Thus, more in-depth studies are needed in order to establish the exact mechanism by which DNAAFs bring together the subunits of dynein arms.

Independently of the dynein assembly process, mature complexes are then deployed to cilia by the intraflagellar transport (IFT) system. Therefore, mutations in DNAAFs lead to a complete or partial absence of both outer and inner dynein arms from the ciliary axoneme, severely affecting cilia and flagella motility (Aprea, Raidt, et al., 2021).

Lastly, PCD can be caused by mutations in genes involved in different steps of multiciliogenesis, such as *MCIDAS*, the transcriptional regulator that mediates multiple cilia formation program (Boon, Wallmeier, et al., 2014); *CCNO*, the protein responsible for centriole amplification and migration at later stages of differentiation for multiple ciliary docking (Wallmeier et al., 2014; Amirav et al., 2016) and FOXJ1, the transcription factor for the cilia motility program (Wallmeier et al., 2019). In all cases, resulting in reduced generation of multiple motile cilia (RGMC).

However, 20 – 30% of individuals with clinical manifestations compatible with PCD cannot be explained by mutations on any known PCD gene, meaning that further studies are still needed to fully characterize the whole spectrum of disease-causing genes (Marshall et al., 2015; Wallmeier et al., 2020).

Mutations in most of PCD genes follow an autosomal recessive trait with a few exceptions showing an X-chromosomal recessive inheritance, such as mutations in *RPGR*, *retinitis pigmentosa GTPase regulator* gene, *OFD1, oral-facial-digital syndrome type 1* gene and *DNAAF6* (Krawczyński & Witt, 2004; A. Moore et al., 2006; Paff et al., 2017; Bukowy-Bieryllo et al., 2019) and an autosomal dominant inheritance, such as mutations in *FOXJ1* (Wallmeier et al., 2019).

Due to its recessive trait, PCD is a fairly rare disease with a prevalence ranging from 1 in 10.000 to 1 in 20.000 children (Rubbo & Lucas, 2017). However, significant differences in PCD frequencies were found across Europe with a higher PCD prevalence observed in a British Asian population (approximately 1 in 2000), mostly due to high incidence of consanguinity (O'Callaghan et al., 2010) and a much lower prevalence found in many other countries, for instances in Estonia and Romania, probably due to lower general government expenditure on health (Kuehni et al., 2010).

Moreover, PCD prevalence was also profoundly underestimated in Portugal, approximately 1 in 200.000 children (Kuehni et al., 2010), which correlated with the absence of essential techniques, such as ciliary function analysis and genetic testing, within the country, with most of PCD diagnosis relying only on transmission electron microscopy (TEM) assessment (Strippoli et al., 2012).

Lack of highly specialized diagnostic centers and lack of awareness about the disease by general practitioners also contributed to the underestimation of PCD incidence. In fact, an international survey reported that 37% of positive patients had more than 40 medical consultations regarding their PCD-related symptoms before getting a referral for PCD testing (Behan, Galvin, et al., 2016). Additionally, apart from *situs inversus*, PCD clinical manifestations are not so suspicious and sometimes patients can present milder symptoms resulting in missed or later age diagnosis (Dehlink et al., 2016).

Different clinical diagnostic predictive tools are now available to guide general practitioners through the relevant medical history of patients and determine which ones need a referral for PCD testing (Djakow et al., 2012; Behan, Dimitrov, et al., 2016; Leigh et al., 2016).

Regarding PCD diagnosis, it should be performed only in specialized centers by experienced multidisciplinary teams using recommended diagnostic pipelines. The European respiratory society guidelines endorse the practice of nasal nitric oxide (nNO) measurements, high-speed video microscopy analysis (HVMA), transmission electron microscopy (TEM) assessment and genetic screening (Barbato et al., 2009; Lucas et al., 2017). While the American thoracic society (ATS) recommends the use of nNO measurements, TEM assessment and genetic testing (Shapiro et al., 2018).

Measurement of nNO is a quick and almost noninvasive technique and involves sampling expired gas from one nostril via a stationary chemiluminescence analyzer using either velum closure breathing maneuvers in patients with more than six years old or tidal breathing maneuvers in patients with less than six years old (Marthin & Nielsen, 2013; Lucas et al., 2017). Although the underlying mechanism is largely unknown, levels of nNO are mainly low in PCD patients (less than 77 nl/min) when compared to healthy control individuals (250 – 300 nl/min) (Collins et al., 2014). However, some PCD mutations, mainly in cases resulting in normal ciliary ultrastructure by conventional TEM, nNO levels were found in the lower range of normal (78 – 125 nl/min) or even comparable to normal values (Marthin & Nielsen, 2011; Shapiro et al., 2020; Raidt et al., 2022). Lower nNO values can also occur due to acute viral respiratory infections or sinusitis. Therefore, analysis of nNO alone is not sufficient to rule in or out PCD, but combined with a strong clinical history, it has a highly predictive value (Dalrymple & Kenia, 2019).

Assessment of ciliary function by high-speed video microscopy analysis (HVMA) involves sampling epithelial respiratory cells from nasal or bronchial brush biopsies and recording the ciliary movement with a high-speed camera, between 120 and 500 frames per second (Lucas et al., 2017). Both ciliary beat pattern (CBP) and frequency (CBF) are analyzed in slow-motion replays and characterized either by a normal recovery and power strokes comparable to healthy control cilia, a complete absence or partial reduced ciliary movement, a stiff beating, a reduced amplitude or a circular rotation movement (Kempeneers et al., 2019). Some ultrastructural defects have been associated with specific patterns of ciliary beating, for instances, mutations affecting both ODA and IDA result in immotile cilia, mutations affecting only ODA severely impact on ciliary movement but a minimal residual beating is sometimes observed, mutations in genes coding for proteins of radial spokes and central pair apparatus lead to rotatory movement when cilia are observed from a top view and mutations in *CCDC39, CCDC40* and some *DNAH11* variants result in hyperkinetic cilia (Chilvers et al., 2003; Raidt et al., 2014; Blanchon et al., 2020). Nevertheless, other mutations can cause very subtle ciliary beating abnormalities that are difficult to detect and can be easily missed (reviewed by Wallmeier et al., 2020).

Conducting HVMA involves an expensive set up and depends on extensive expertise and training of the microscopists, who can still be subjective and introduce some observer bias. Moreover, HVMA still lacks standardization methods for cell processing and ciliary assessment (Shapiro et al., 2018) although efforts are being made every year at the European Respiratory Society conferences. External factors such as secondary infections, environmental pollutants, inflammatory mediators and pharmacological agents can also affect indirectly the ciliary movement (Merkus et al., 2001; Hofmann et al., 2004; Joskova et al., 2020). Therefore, new recommendations have been proposed, including repetition of HVMA from different biopsies or following cell culture (Dalrymple & Kenia, 2019; Kempeneers et al., 2019). New softwares for CBF measurement (Smith et al., 2012) and more quantitative analysis of CBP, as for example the weighted distance traveled by the cilium per second being

the most reliable parameter found (Papon et al., 2012; Blanchon et al., 2020), have also been developed.

In fact, our laboratory was deeply involved in the creation of a PCD diagnostic team in Portugal, according to the European respiratory society guidelines (Lucas et al., 2017). After 8 years, we now have a consortium of several clinical and research units that work together to collectively improve the research and diagnostic status of PCD in our country (Constant et al., 2018). Moreover, we have specialized ourselves in HVMA, after intensive training, and we recently published for the first time the normal range of CBF and CBP observed in a healthy volunteer Portuguese control group, as well as, in a Portuguese PCD patient group (Sampaio et al., 2021). Concomitantly, we developed a new software for a semi-automatic detection of ciliary beat frequencies in the recorded movies, allowing a fast and unbiased data analysis and consequently, making HVMA a better PCD diagnostic test and easier to implement in future diagnostic centers (Sampaio et al., 2021).

On the other hand, samples from nasal or bronchial epithelial cells can also be used to assess the ciliary ultrastructure by TEM (Papon et al., 2010). Typical hallmarks of abnormal cilia include lack or truncated ODAs (50% of PCD cases); lack of simultaneously ODAs and IDAs (15% of PCD cases) and lack of IDAs with microtubular disorganization (26% of PCD cases) (Leigh et al., 2016). However, concurrently with the discover of new PCD genes along the years, more cases of normal ciliary ultrastructure or easily missed subtle abnormalities have been described, ranging from 17 to 30% of the PCD patients (Boon, Smits, et al., 2014; Kouis et al., 2017). This includes some *DNAH11* variants (Schwabe et al., 2008; Blanchon et al., 2020) and mutations in nexin-dynein link proteins (Wirschell et al., 2013), microtubule inner proteins (Ta-Shma et al., 2018), radial spokes (Knowles et al., 2014) and central pair apparatus (Dougherty et al., 2020). Additionally, IDA structure and consequently IDA defects are sometimes difficult to identify, as they are less electron dense resulting in low contrast of these structures compared with other ciliary components, and they are less frequent along the ciliary axoneme (Barbato et al., 2009). Thus, presence of typical hallmarks in more than 50%

of cilia cross sections is sufficient to indicate a PCD diagnosis (Shapiro et al., 2016; Lucas et al., 2017), whereas samples showing ciliary abnormalities in less than 50% of cilia cross sections require additional testing (Shoemark et al., 2020).

Although TEM was considered the gold standard PCD test once, it is still a laborious and expensive technique, performed and analyzed only by highly trained technicians (Dalrymple & Kenia, 2019). Electron microscopic tomography (Shoemark & Hogg, 2013) and cryo-electron tomography (Lin et al., 2014) may resolved some subtle abnormalities observed by conventional TEM but are extremely specialized techniques and not widely available.

Molecular genetic screening is highly recommended by the American thoracic society for PCD diagnosis in patients with strong clinical phenotypes (Shapiro et al., 2018). Either by using whole-exome techniques or extended genetic panels specific for PCD genes, previously reported PCD causing variants can be easily identified in genomic DNA samples extracted from patient's blood. One disease causing mutation in each allele must occur in the same PCD gene for a positive diagnosis. In case of lack of known mutations, observed sequence variants should be ranked following the international recommendations into benign, likely benign, unknown significance, likely pathogenic and pathogenic (Richards et al., 2015). Furthermore, potential PCD causing mutations should be confirmed by Sanger sequencing, correlated with the phenotype assessed by any other PCD diagnostic test, and checked by segregation analysis (Lucas et al., 2017). On the other hand, large heterozygous genomic deletions, large intragenic duplications and deep intronic mutations, reported in some PCD patients, are missed by some sequencing technologies (Duquesnoy et al., 2007; Knowles et al., 2013). Moreover, in particular for *HYDIN,* PCD genes can also be difficult to sequence, due to equivalent segments within the paralogous gene, complicating the analysis of local variants (Olbrich et al., 2012). Hence, molecular genetic testing is sufficient to confirm a diagnosis in the presence of PCD causing mutations, but it cannot rule out a positive diagnosis in the absence of known mutations (Lucas et al., 2017).

Patients with high clinical suspicion for PCD without a definitive diagnosis by any of these tests should remain under clinical monitoring by a specialist and be further tested as more diagnostic tools become available and new genes are discovered.

In fact, one of the more recent and powerful diagnostic techniques is the immunofluorescence (IF) labelling assay, that by now has been used mostly as a research tool due to lack of sufficient clinical evidence for the diagnostic accuracy assessment (Fliegauf et al., 2005; Dalrymple & Kenia, 2019). Nevertheless, the European respiratory society agrees that, in case of validated antibodies, the IF assay can be valuable in clinical settings, providing new insights for resource-limited PCD diagnostic centers (Lucas et al., 2017; Rumman et al., 2017). In a PCD diagnostic perspective, no extra collection method are needed for this method, as samples from the nasal or bronchial respiratory epithelial cells for HVMA and TEM can be also used to visualize the distribution of ciliary components, within the cell and along the length of the ciliary axoneme by using fluorescently tagged antibodies against ciliary proteins (Omran & Loges, 2009). At this point, the advantages of IF labelling protocol are that single ciliated cells, in contrast to the undisrupted epithelial clusters necessary for HVMA, and fewer cells, in opposition to the large number of cells required for TEM analysis, are enough to achieve a definitive result and thus reduce the need for repeated nasal brushing in the same patient (Shoemark et al., 2017). Additionally, air-dried samples in glass slides can be easily transported to faraway performing laboratories, in opposition to HVMA that must be executed right after the nasal brushing or at least as soon as possible after collection (Omran & Loges, 2009; Reula et al., 2021).

At the laboratory, IF protocols are simpler to implement and optimize, easier to perform on a daily basis and do not require specialized expensive equipment when compared to TEM analysis. Moreover, Shoemark and colleagues evaluated the expenditure of these two techniques and confirmed that IF labelling can cost up to 8 times less per sample than TEM analysis (Shoemark et al., 2017). The median time for processing and analyzing a sample was also significantly less, with IF protocols requiring 14 days and TEM protocols requiring 27 days (Shoemark et al., 2017).

When analyzing the distribution of ciliary components under confocal or fluorescent microscopes, absence or misplacement of protein labelling can be indicative of PCD. A similar sensitivity to TEM analysis was achieved by using a combined panel of antibodies against the ciliary proteins DNAH5 (an outer arm dynein), DNALI1 (an inner arm dynein), GAS8 (a protein from the dynein regulatory complex, the nexin link) and RSPH9 (a radial spoke component) to detect ciliary defects in a cohort of prospective PCD patients (Shoemark et al., 2017). Surprisingly, the same diagnostic rate by IF labelling was observed by an independent laboratory (Baz-Redón et al., 2020).

Additionally, IF labelling can be particularly effective, over conventional TEM, regarding PCD cases with normal ciliary ultrastructure. For instance, radial spoke mutations, such as in *RSPH1, RSPH4* and *RSPH9*, can be easily resolved by single labelling of RSPH9, as it is absent in all cases (Frommer et al., 2015). Mutations in *HYDIN* and *SPEF2*, two genes that code for proteins from the central pair apparatus, can also be detected by the absence of SPEF2 labelling from the ciliary axonemes (Dougherty et al., 2020). Lastly, IDA components that are sometimes difficult to observe by TEM can be clearly visible by antibody against DNALI1 staining and consequently IDA defects result in absence of DNALI1 immunofluorescent signal (Shoemark et al., 2017).

Interestingly, mutations in the outer dynein *DNAH11*, that is usually present at the proximal region of the ciliary axoneme, can result in different phenotypes. Depending on the PCD causing variant, faulty DNAH11 protein can be absent from the ciliary axoneme without affecting most of ODA components and subsequently leading to neglectable changes by TEM analysis. In these cases, a diagnosis can be given by IF labelling of DNAH11, that becomes absent, and of DNAH9, that shifts from the distal part of the ciliary axoneme to become pan-axonemal (Dougherty et al., 2016). On the other hand, some *DNAH11* variants cannot be resolved by IF as they do not affect the proper protein localization within the axoneme, thus resulting in a normal distribution of the antibody (Dougherty et al., 2016).

Another limitation of IF technique is that by labelling specific proteins of interest, defects in unrelated proteins could be missed. This issue could be overpassed in the future as the full spectrum of PCD genes is being discovered and the antibodies for the respective proteins are being produced and validated (Liu et al., 2020).

In summary, IF labelling assays seem to be a reliable diagnostic technique for PCD, having a comparable diagnostic accuracy to TEM analysis, with the benefits of being faster, cost-effective and easy to implement. Nonetheless and similarly to the other PCD diagnostic tests, IF should not be used as a stand-alone test to exclude PCD.

The purpose of this work was to evaluate the procedure of IF method for confirming a positive PCD diagnosis in two siblings (subjects #1291156 and #1880724) that shared the same *ZMYND10* mutation. We had previously described this new variant for the first time by HVMA, TEM and genetic screening for one of the patients (Sampaio et al., 2021). Using a research panel of ten antibodies against ciliary proteins, we now analyzed the distribution of ciliary components in both siblings to infer about the performance of IF analysis by comparing the obtained results with previously published data.

We confirmed that the IF method was easy to implement in our laboratory and optimization of antibody dilutions was performed successfully using respiratory ciliated cells from healthy control volunteers. Moreover, we found that IF labelling is accurate and sensitive to intrinsic patient variability, reinforcing the use of this technique not only in clinical research but also in PCD diagnosis.

Our laboratory now performs HVMA and IF and our Lisbon consortium is the only one in Portugal performing all the essential PCD diagnostic tests recommended by the European respiratory society guidelines: nNO, TEM and HVMA. Thus, we want to further implement IF labelling assay as a daily basis technique in our laboratory to improve the PCD diagnosis in our country, either by enabling distant primary and secondary care centers to easily send us air-dried samples from their prospective patients in glass slides for posterior testing in our premises or by providing training to other institutes to correctly use this technique. Our long-term aim is to investigate the accuracy and limitations of IF as a diagnostic tool for PCD in diagnostic cohort studies, composed by Portuguese PCD patients. Ultimately, providing additional evidence to change the current guidelines to accept IF in PCD diagnostic pipelines and consequently enhancing PCD diagnosis in resource-limited countries.

3.1. EXPERIMENTAL PROCEDURES

Sample collection and preparation

Sample collection was performed at the patient's baseline health state. Certified technicians collected nasal cells from the inferior turbinate nasal epithelia (Lucas et al., 2017) using a cytological brush (0134, Fisaude, Spain). Cells were immersed in culture medium 199 (Gibco - Life technologies) buffer supplemented with 1% of Penicillin-Streptomycin (15140122, ThermoFisher Scientific).

For high-speed video microscopy analysis, cell samples were spread onto a glass slide delimited using silicone grease (Z273554, Dow Corning Corporation), to make a sealed compartment avoiding overflowing, and covered with a coverslip. Samples were processed within 3 hours after sampling.

For immunofluorescence analysis, cell samples were spread onto glass slides, air-dried in a laminar flow hood and stored at -80ºC until use. At least ten slide preparations should be stored in order to allow different antibody testing or repetition in case of inconclusive result.

High-speed video microscopy analysis

Samples were examined in an inverted transmission light microscope (Nikon Eclipse Ti-U) with a 100× oil immersion objective lens (1.30 NA) at 25ºC. Only multiciliated cell clusters presenting undisrupted epithelial edges free of mucus and debris were recorded (Thomas et al., 2008) using a high-speed FASTCAM MC2 camera (Photron Europe, Limited) controlled with PFV (Photron FASTCAM Viewer) software. Following the European Respiratory society guidelines, small videos were recorded at 200 frames per second (fps), in order to visualize at least four frames throughout the beat cycle, for ciliary beta pattern evaluation (Lucas et al., 2017). Moreover, ten different clusters were imaged, eight from the sideway edge and two from the anterior edge (top view).

The ciliary movement was analyzed in 30-60 fps replays and ciliary beat frequency was measured using the CiliarMove software (Sampaio et al., 2021). Video recordings were archived for audit purposes.

Immunofluorescence analysis

The immunofluorescence analyses of human respiratory cells followed the protocol previously described by Omran's lab (Omran & Loges, 2009).

After thawing the samples, cells were incubated with 4% paraformaldehyde for 15 minutes for fixation of the axoneme and axonemal structures. Then washed 3 times with 1x PBS (Phosphate-buffered saline solution) and incubated in 0.2% Triton X-100 for 10 minutes for cell permeabilization. The slides were blocked overnight at 4ºC with 1% skim milk, to avoid nonspecific binding. Incubation with the primary antibodies in 1% skim milk was performed for 3 hours at room temperature on the next day.

The following primary antibodies were used: mouse monoclonal or rabbit monoclonal antibodies anti-acetylated tubulin (1:1000 dilution; T7451, Sigma-Aldrich or 5335, Cell Signaling); mouse monoclonal antibody anti-DNAH11 (Dougherty et al., 2016) and rabbit polyclonal antibodies anti-DNAH5 (1:500 dilution; HPA037470) (Fliegauf et al., 2005), anti-DNAH9 (HPA052641) (Loges et al., 2018); anti-DNAI1 (1:300 dilution; HPA021649) (Whitfield et al., 2019); anti-DNAI2 (1:500 dilution; HPA050565) (Höben et al., 2018); anti-DNALI1 (1:300 dilution, HPA028305) (Liu et al., 2020); anti-GAS8 (1:500 dilution, HPA041311) (Olbrich et al., 2015); anti-RSPH9 (1:400 dilution, HPA031703) (Frommer et al., 2015); anti-CCDC39 (1:300 dilution; HPA035364) (Merveille et al., 2011) and anti-SPEF2 (1:200 dilution; HPA039606) (Dougherty et al., 2020). The monoclonal antibody against DNAH11 was kindly offered by Niki Loges from Omran's lab, whereas the other antibodies were purchased from Atlas Antibodies, unless otherwise stated.

The slides were washed 5 times with 1x PBS at room temperature and then incubated with the secondary antibodies for 30 min at room temperature. Cross adsorbed secondary antibodies, including Alexa Fluor 488-conjugated goat antibodies to mouse (1:1,000, A1108) and Alexa Fluor 546-conjugated goat antibodies to rabbit (1:1,000, A11010) were purchased from Molecular Probes (Invitrogen). Nuclei DNA was stained with Hoechst 33342 (1:1000; 14533, Sigma-Aldrich).

Immunofluorescence images were taken using a Zeiss Widefield Axioimager Z2 fluorescence microscope with a Zeiss Plan-Apochromat 63x oil immersion objective (1.4 NA). The obtained pattern for the antibody labelling in subjects #1291156 and #1880724 was compared to the ones observed in health control samples, being classified as normal, decreased, absent or proximal/distal regarding the location within the ciliary axoneme.

3.2. RESULTS

Heymut Omran's lab, in the University Children's Hospital Muenster, Germany, was the pioneer in using IF labelling for PCD research and has been establishing IF analysis as a complement to PCD diagnostic measures over the last years (Omran & Loges, 2009). In order to implement the IF protocol from nasal epithelial ciliated cells in our lab as a PCD research tool and posteriorly assess the viability of using it as a PCD diagnostic test, I went to Heymut Omran's lab, for training under the supervision of Petra Pennekamp and Niki Loges.

Regarding our Portuguese PCD patient cohort, we decided to perform the IF studies to fully characterize the ciliary protein distribution in samples with a new variant of *ZMYND10*. We had previously identified this mutation in one child (subject #1880724) and described it accordingly with nasal nitric oxide (nNO) measurements, high-speed video microscopy analysis (HVMA), transmission electron microscopy (TEM) assessment and genetic testing (Sampaio et al., 2021). However, this family has an older daughter also with PCD (subject #1291156). Interestingly, subject #1291156 has *situs inversus,* whereas subject #1880724 has a normal organ arrangement (Figure 3.1 A). Thus, we decided to study both siblings as it would allow us to test IF sensitivity between different patients with the same mutation and concomitantly test if the patient with left – right abnormalities could have evolved to more severe respiratory outcomes.

Mutations in *ZMYND10* were first described to cause PCD in 2013 (D. Moore et al., 2013; Zariwala et al., 2013). At the time, ZMYND10 was known to be a zinc finger protein with four conserved classical LxxLL protein-binding motifs and a C-terminal MYND zinc-finger domain, which suggested that it could require interacting partners for its function (Albee et al., 2013), and it was previously associated with several types of cancer (Agathanggelou et al., 2003). Being up-regulated during ciliogenesis (Ross et al., 2007), ZMYND10 was found mainly localized within the cytoplasm (Albee et al., 2013; Zariwala et al., 2013).

At the molecular level, ZMYND10 was found to interact with the dynein axonemal assembly factor (DNAAF) 11/LRRC6 (D. Moore et al., 2013; Zariwala et al., 2013), and to co-localize with most DNAAFs in the liquid phase separation organelles (Huizar et al., 2018), suggesting that ZMYND10 could also be part of the preassembly dynein complex and thus be a DNAAF by itself. Studies in *Drosophila, Xenopus* and zebrafish support a conservative role of ZMYND10 as a DNAAF (D. Moore et al., 2013; Zariwala et al., 2013; Kobayashi et al., 2017). While in studies with *Chlamydomonas* and *Paramecium tetraurelia*, ZMYND10 was found to affect cilia length and basal body/centriole number, suggesting additional roles in maintenance of ciliary structure and function (Albee et al., 2013; Shi et al., 2021).

More recently, two *Zmynd10* mutant mice were developed in order to further understand the molecular contribution of ZMYND10 in dynein preassembly (Cho et al., 2018; Mali et al., 2018). Mali and colleagues showed that ZMYND10 interacts with HSP90 co-chaperone FKBP8 and chaperone HSP90 to mediate specifically dynein heavy chain stability and preassembly. In *Zmynd10* mutant, dynein heavy chains, such as DNAH5, are unable to bind to the dynein intermediate and light chains, causing overall protein instability and consequently axonemal dynein degradation (Mali et al., 2018). On the other hand, Cho and colleagues showed that ZMYND10 also modulates the preassembly of dynein intermediate chains by directly promoting DNAI1 stability (Cho et al., 2018).

Either way, *ZMYND10* mutations in PCD patients were shown to result in lack of ODA and IDA at the ciliary ultrastructure when evaluated by TEM and an absence of DNAH5 (ODA component) and DNALI1 (IDA component) signal by IF labelling (D. Moore et al., 2013; Zariwala et al., 2013). Consequently, PCD patients presented a complete absence of ciliary motility confirmed by HVMA (D. Moore et al., 2013; Zariwala et al., 2013; Sampaio et al., 2021). Clinical features included low levels of nNO, respiratory symptoms, *situs inversus* and infertility (Zariwala et al., 2013; Kurkowiak et al., 2016). Different *ZMYND10* missense mutations and frameshift deletions contribute to 3% of the overall PCD cases worldwide (Kurkowiak et al., 2016).

In Portugal, we have reported two different cases, one PCD patient showing a homozygous c.[510+1delG] splice donor mutation that followed the classical DNAAF phenotype (subject #1880724), hereby further studied, and another PCD patient with a previously described homozygous c.[1136A>G] missense mutation that presented a much milder phenotype with normal TEM and CBF within normal ranges (Zariwala et al., 2013; Sampaio et al., 2021).

As the subject #1291156 (sister of #1880724) data was not described in Sampio et al. (2021), we will analyze it here and compare it with the sibling data. Examples of previous TEM analysis performed by Andreia Pinto, a PCD Portuguese consortium partner, are shown in Figure 3.1 B depicting ciliary cross-sections of respiratory epithelial samples for both siblings.

Thorough quantification of ciliary ultrastructure defects revealed distinct profiles between the two subjects. While subject #1291156 presented a consistent absence of both ODA and IDA, without any additional microtubule defect, subject #1880724 showed absence of either both ODA and IDA or only ODA and an increased number of abnormalities regarding the central pair apparatus and microtubule organization (Figure 3.1 C). Thus, TEM analysis showed that these two patients have the same phenotype concerning other *ZMYND10* variants affecting ODA and IDA, and therefore it would be sufficient to provide a positive diagnosis with PCD.

To execute the IF analysis, nasal brushings were performed by certified technicians from our institute in order to obtain live epithelial ciliated cells. Firstly, we analyzed the ciliary function, as subject #1291156 had no prior record, and compared to the CBF of our Portuguese healthy control group, ranging from 6.10 to 9.13 Hz (Supplementary Movie 3.1).

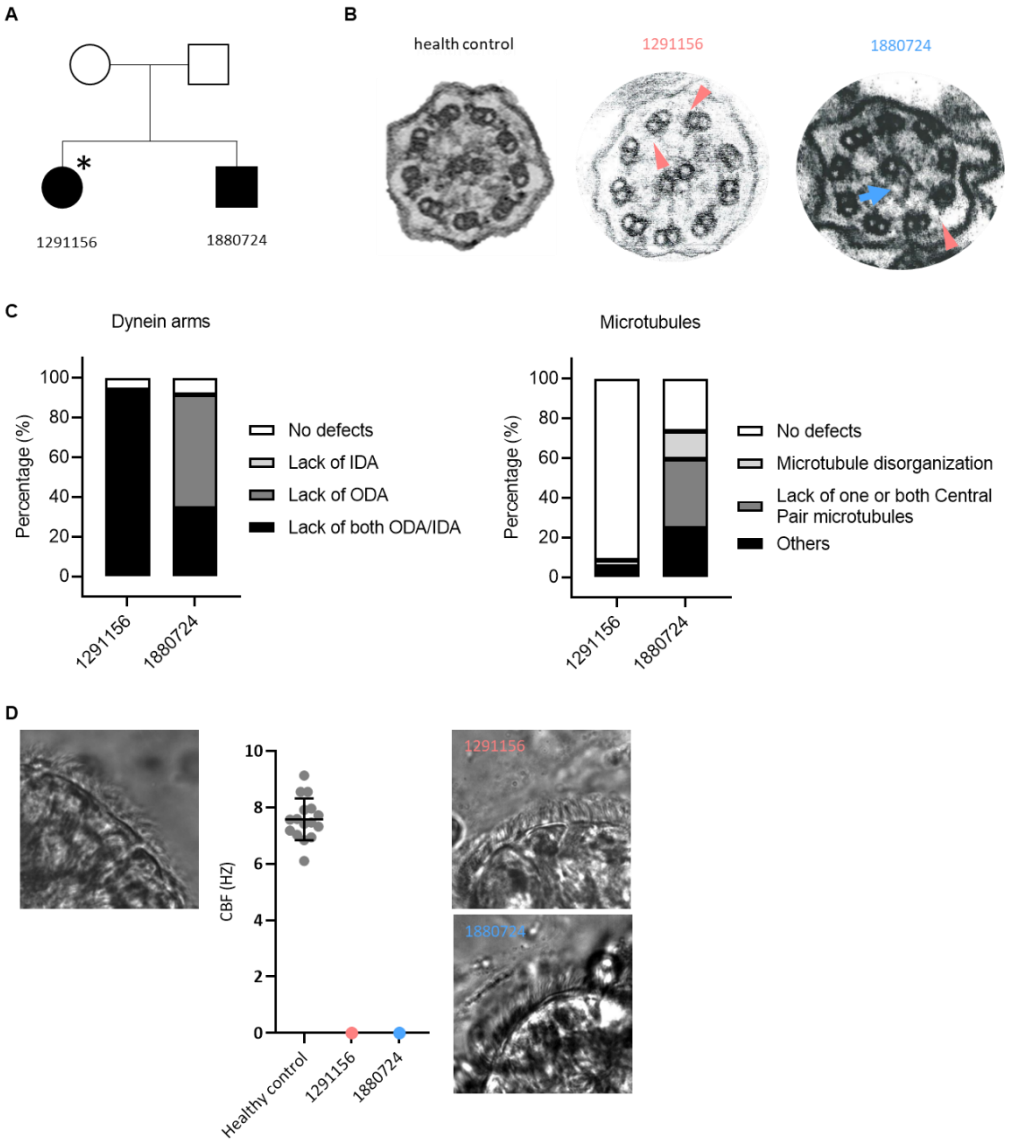

Figure 3.1: New ZMYND10 variant causes primary ciliary dyskinesia.
(A) Pedigree of a family harboring the c.[510+1delG] splice donor mutation in *ZMYND10* gene. Unaffected parents are shown in white and PCD siblings (subjects #1291156 and #1880724) are in black. Asterisk indicates *situs inversus* defect. (B) Examples of cross-sectioned respiratory cilia from the respiratory epithelium of an healthy control individual, subject #1291156 and subject #1880724 by transmission electron microscopy. (C) Quantification of dynein arms and microtubules-related defects in subject #1291156 (n=221 cilia) and subject #1880724 (n=57 cilia) observed in B. (D) Ciliary beat frequency (Hz) of the healthy control group (n=16 individuals) and of the subjects #1291156 and #1880724. Means from 10 samples per individual are displayed. Examples of multiciliated clusters used for analysis are shown.

Both siblings presented several epithelial ciliated edges with more than 10 cells, indicating that the cell collection was successful and the epithelium structure was preserved. Recording of ciliary movement showed that both siblings had static cilia, with complete absence of motility (CBF = 0 Hz) (Figure 3.1 D; Supplementary Movie 3.2 and Supplementary Movie 3.3), in agreement with the lack of axonemal dynein motors.

Secondly, the remaining cells were prepared for IF labelling assays. We double-stained every slide with anti-acetylated alpha tubulin in order to identify the ciliary axonemal microtubules and to co-localize these with the second antibody for the ciliary protein of interest. Most studies using IF as a complement for PCD diagnosis rely on the staining of DNAH5, one outer dynein heavy chain, and of DNALI1, a light intermediate chain of the inner dynein arm, both usually expressed across the entire ciliary axoneme (Fliegauf et al., 2005; Shoemark et al., 2017). In *ZMYND10* mutations, DNAH5 has been reported to be mostly absent from cilia, but sometimes it can be seen at the proximal region of the axoneme, while DNALI1 was only reported at the apical membrane region of the cell in one study and completely absent in the others (D. Moore et al., 2013; Zariwala et al., 2013; Kurkowiak et al., 2016).

Staining of DNAH5 in both subjects #1291156 and #1880724 revealed a constant abnormal signal in every analyzed cell when compared to the signal of healthy control cells (Figure 3.2 A). In #1291156 samples, DNAH5 was mostly absent from cilia, whereas in #1880724, it was either completely or distally absent, and in both cases an accumulation of DNAH5 at cytoplasmic foci or at the proximal ciliary regions was observed (Figure 3.2 B).

Regarding the DNALI1 staining, both siblings presented a decreased to completely absent signal for IDA. In subject #1880724 samples, a few cells were seen to have normal DNALI1 signal (Figure 3.3 A and B), in agreement with the differences detected by TEM analysis. Thus, in a low extent, IDA seem to enter the cilium more easily in #1880724 samples.

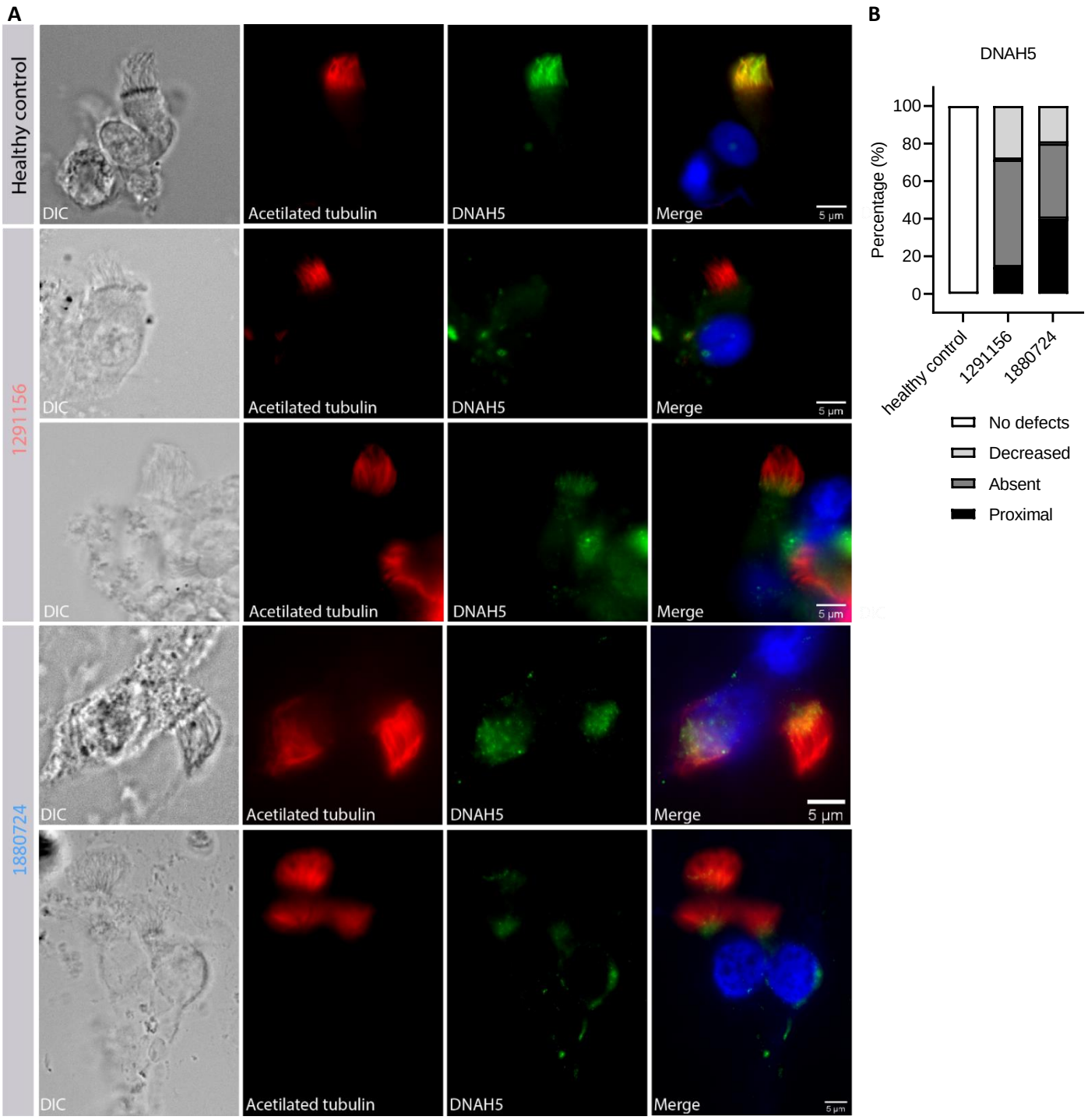

Figure 3.2: DNAH5 localization is affected by the new ZMYND10 variant.
(A) Immunolabelling of ciliary microtubules with acetylated alpha tubulin and the axonemal outer dynein DNAH5 in respiratory ciliated cells of a healthy control volunteer (n=16 cells), subject 1291156 (n=7 cells) and subject 1880724 (n=15 cells). DIC, differential interference contrast microscopy (brightfield). (B) Quantification of fluorescence signal patterns in cilia observed in A.

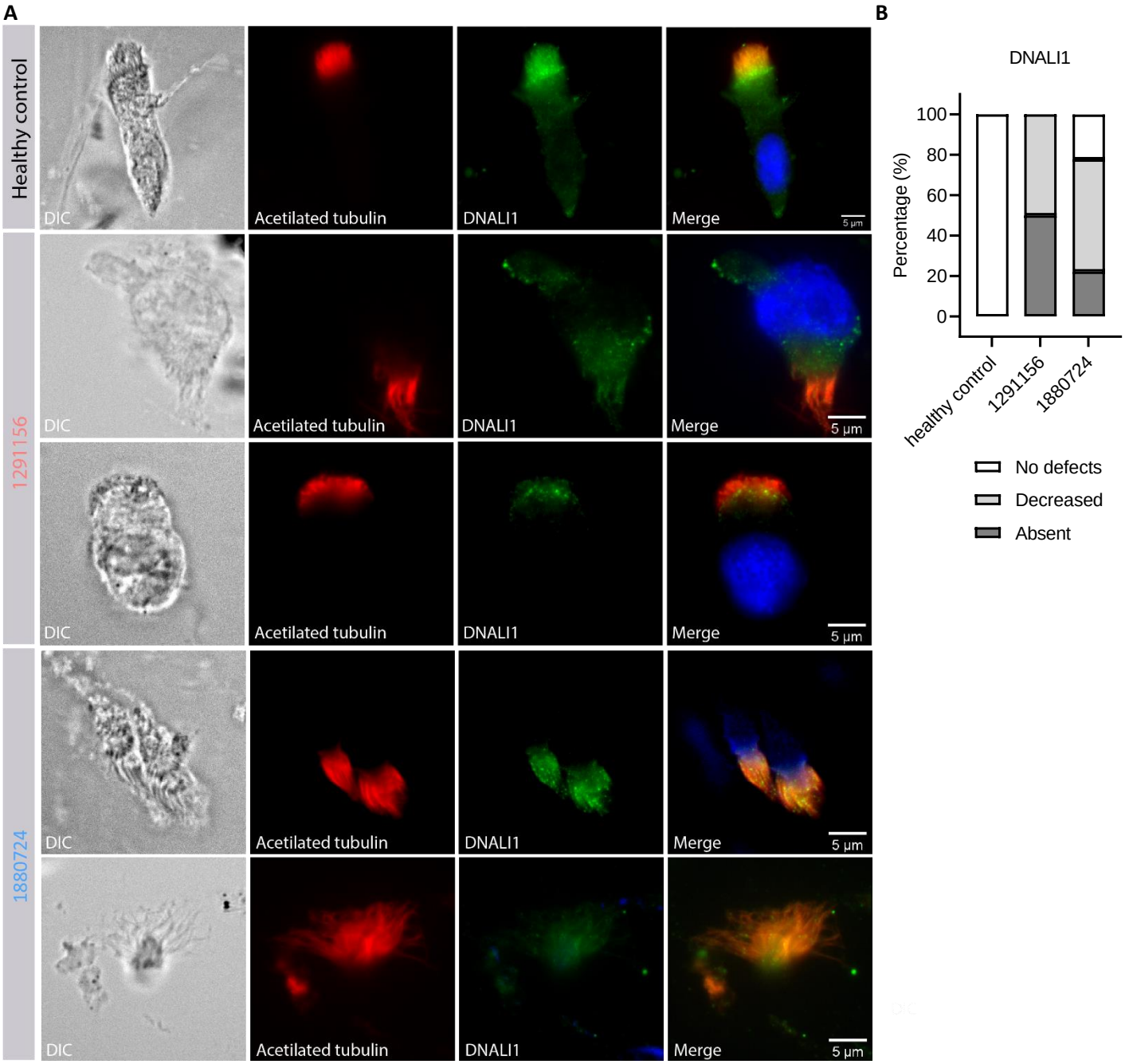

Figure 3.3: DNALI1 localization is affected by the new ZMYND10 variant.
(A) Immunolabelling of ciliary microtubules with acetylated alpha tubulin and the axonemal inner dynein DNALI1 in respiratory ciliated cells of a healthy control volunteer (n=8 cells), subject 1291156 (n=6 cells) and subject 1880724 (n=9 cells). DIC, differential interference contrast microscopy (brightfield). (B) Quantification of the fluorescence signal patterns in cilia observed in A.

We then analyzed the localization of another dynein heavy chain, DNAH9. In contrast to the subtype III DNAH5, DNAH9 belongs to the outer dynein subtype II being present only at the distal end of the ciliary axoneme in control respiratory epithelial cells (Figure 3.4 A) (Fliegauf et al., 2005). There are no

reports of DNAH9 distribution in *ZMYND10* mutant respiratory cells. However, DNAH9 was found to interact with DNAH5 by co-immunoprecipitation and it becomes absent from the ciliary axonemes when DNAH5 is no longer present (Loges et al., 2018). We found that both subjects #1291156 and #1880724 lacked any staining for DNAH9 within the cilia and a diffuse signal appeared at the cytoplasm, but indistinguishable from background signal (Figure 3.4 A and B). Thus, DNAH9 assembly into the cilia is compromised in *ZMYND10* mutations, supporting a mechanism where DNAH9 depends on other ODA components to become localized at the distal region of the axoneme.

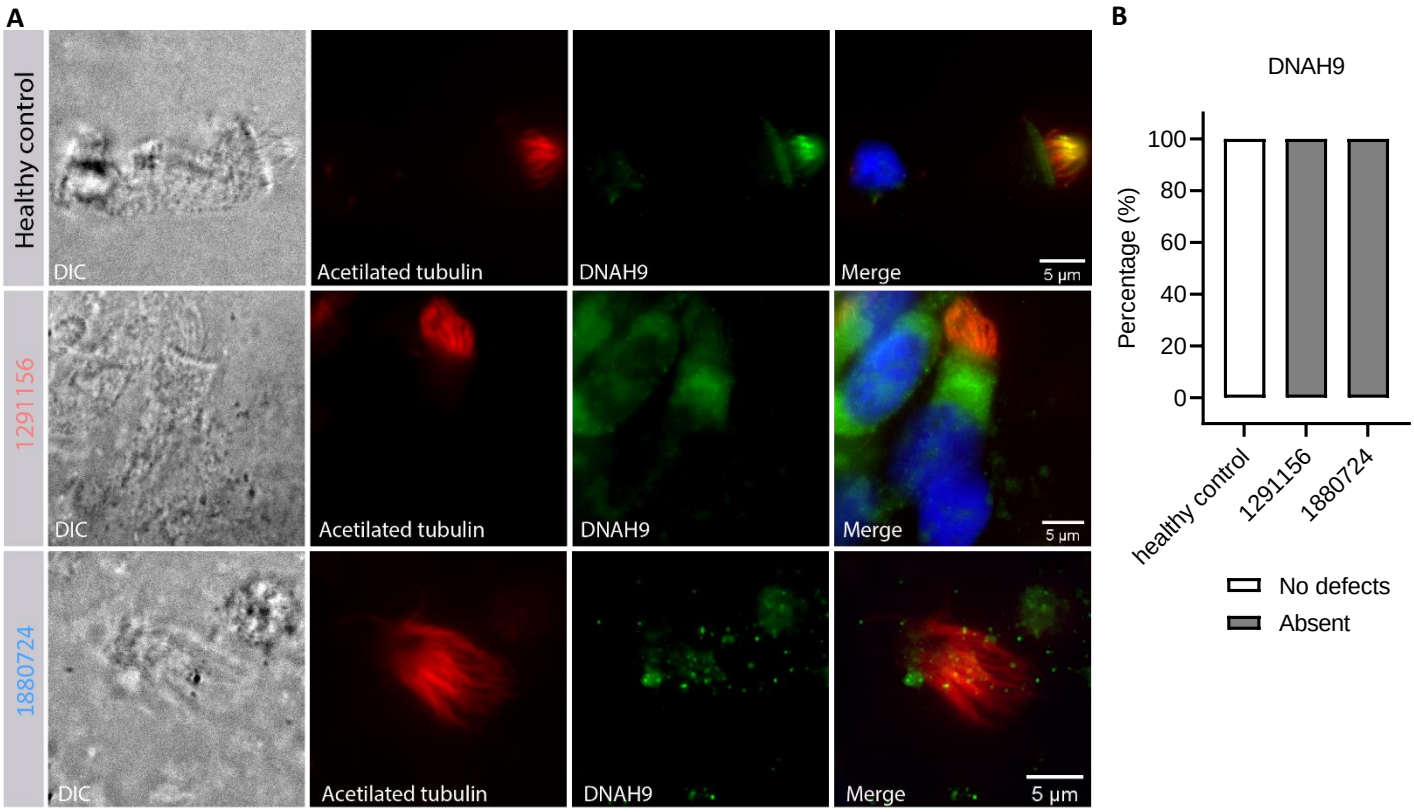

Figure 3.4: DNAH9 localization is affected by the new ZMYND10 variant.
(A) Immunolabelling of ciliary microtubules with acetylated alpha tubulin and the axonemal outer dynein subtype II DNAH9 in respiratory ciliated cells of a healthy control volunteer (n=16 cells), subject 1291156 (n=5 cells) and subject 1880724 (n=9 cells). DIC, differential interference contrast microscopy (brightfield). (B) Quantification of the fluorescence signal patterns in cilia observed in A.

On the other hand, the outer dynein heavy chain subtype I, DNAH11, is known to be located only at the proximal end of the ciliary axoneme when compared with the pan-axonemal localization of acetylated tubulin (Figure 3.5 A) (Dougherty et al., 2016). Although there is no record of DNAH11 distribution regarding specifically *ZMYND10* mutations, a normal proximal localization of DNAH11 was observed in most patients with DNAAFs mutations, such as for

DNAAF1, DNAAF2, DNAAF3 and *DNAAF4*, as well as in *DNAH5, DNAH9* and *DNAI2* mutant respiratory cells (Dougherty et al., 2016; Loges et al., 2018). Conversely, it was described before that *DNAH11* mutations do not affect ODA nor IDA assembly (Schwabe et al., 2008). Therefore, DNHA11 appeared to evolve distinctively from the other outer dyneins, where the integrity of ODA and IDA seems to be independent of its trafficking and assembly into the axoneme.

We thus analyzed the DNAH11 distribution in both siblings and within the respiratory epithelial cells from subjects #1291156 and #1880724, DNAH11 was consistently observed at the proximal region of the ciliary axonemes (Figure 3.5 A). Supporting that, similarly to other DNAAFs, ZMYND10 is not involved in DNAH11 stability nor in its preassembly in the cytoplasm.

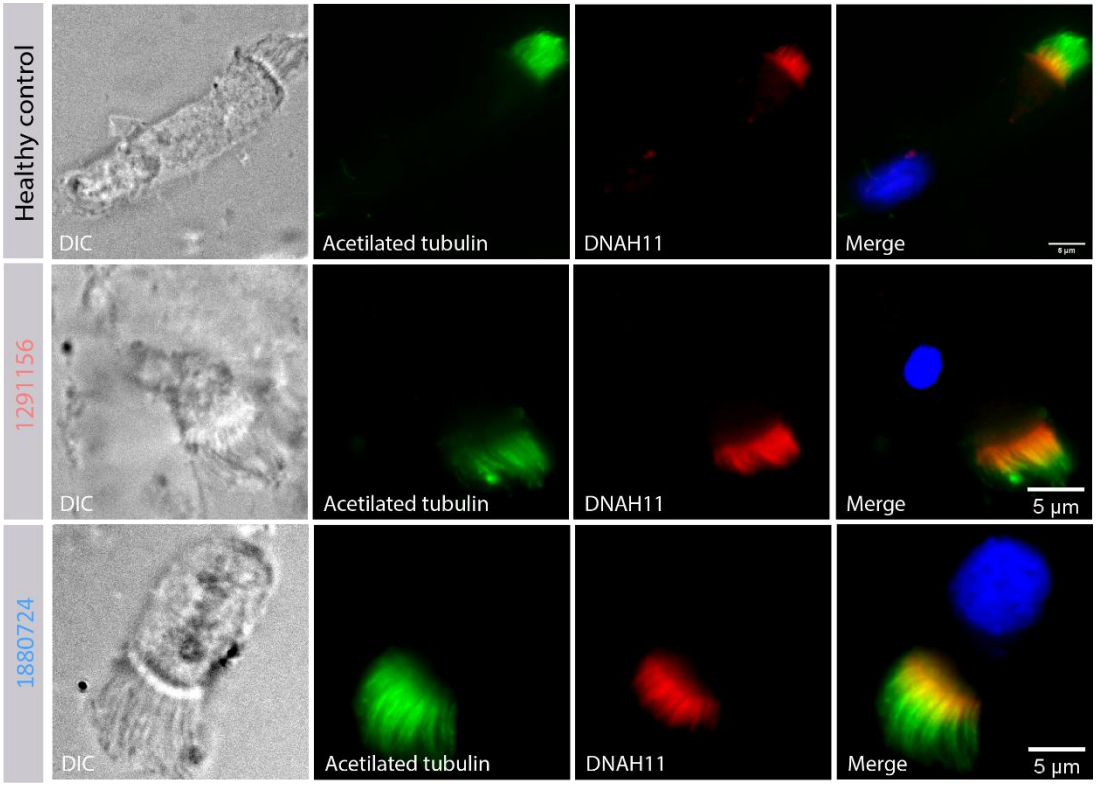

Figure 3.5: DNAH11 localization is not affected by the new ZMYND10 variant.
Immunolabelling of ciliary microtubules with acetylated alpha tubulin and the axonemal outer dynein DNAH11 in respiratory ciliated cells of a healthy control volunteer (n=10 cells), subject 1291156 (n=10 cells) and subject 1880724 (n=12 cells). DIC, differential interference contrast microscopy (brightfield).

Regarding the outer dynein intermediate chains, DNAI1 and DNAI2, IF labelling assays have demonstrated that both proteins are localized across the entire ciliary axoneme (Figure 3.6 A and Figure 3.7 A) (Höben et al., 2018; Loges et al., 2018). DNAI1 and DNAI2 depend on the

other ODA components and DNAAFs-driven pre-assembly in the cytoplasm in order to be successfully deployed into the cilia (Höben et al., 2018). In *ZMYND10* mutant respiratory cells, only DNAI2 has been reported and immunolabelling revealed it was completely absent from the ciliary axonemes without further accumulation in the cytoplasm (Kurkowiak et al., 2016), which has been attributed to rapid protein degradation to avoid cellular stress caused by non-functional ODA complexes (Cho et al., 2018). In contrast, DNAI2 stability in *Zmynd10* mutant mice was not severely affected and protein accumulation was spotted within the cytoplasm (Mali et al., 2018).

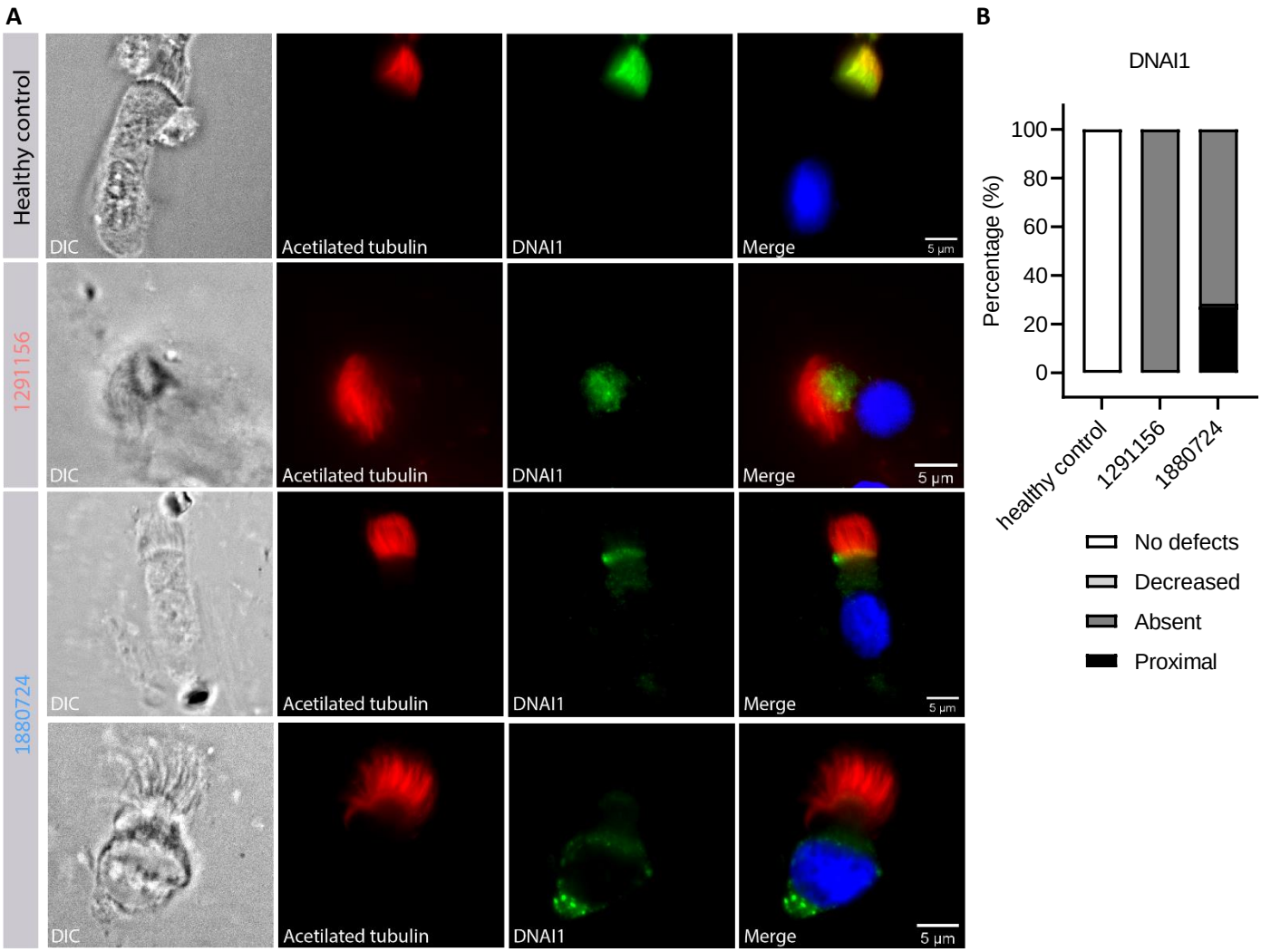

Figure 3.6: DNAI1 localization is affected by the new ZMYND10 variant.
(A) Immunolabelling of ciliary microtubules with acetylated alpha tubulin and the axonemal outer dynein intermediate chain DNAI1 in respiratory ciliated cells of a healthy control volunteer (n=10 cells), subject 1291156 (n=10 cells) and subject 1880724 (n=11 cells). DIC, differential interference contrast microscopy (brightfield). (B) Quantification of the fluorescence signal patterns in cilia observed in A.

We then analyzed the distribution of both DNAI1 and DNAI2 in the respiratory epithelial cells from subjects #1291156 and #1880724. In general, DNAI1 and DNAI2 were absent from the ciliary axoneme of *ZMYND10* mutant cells (Figure 3.6 B and Figure 3.7 B) and a constant accumulation of either diffused or local signal was observed within the cytoplasm for both proteins (Figure 3.6 A and Figure 3.7 A). Moreover, accumulation of DNAI1 at the proximal region of the axoneme was also observed in a minority of cells from subject #1880724 (Figure 3.6 A). Therefore, to some extent dynein intermediate chains are still present in subjects #1291156 and #1880724 cells.

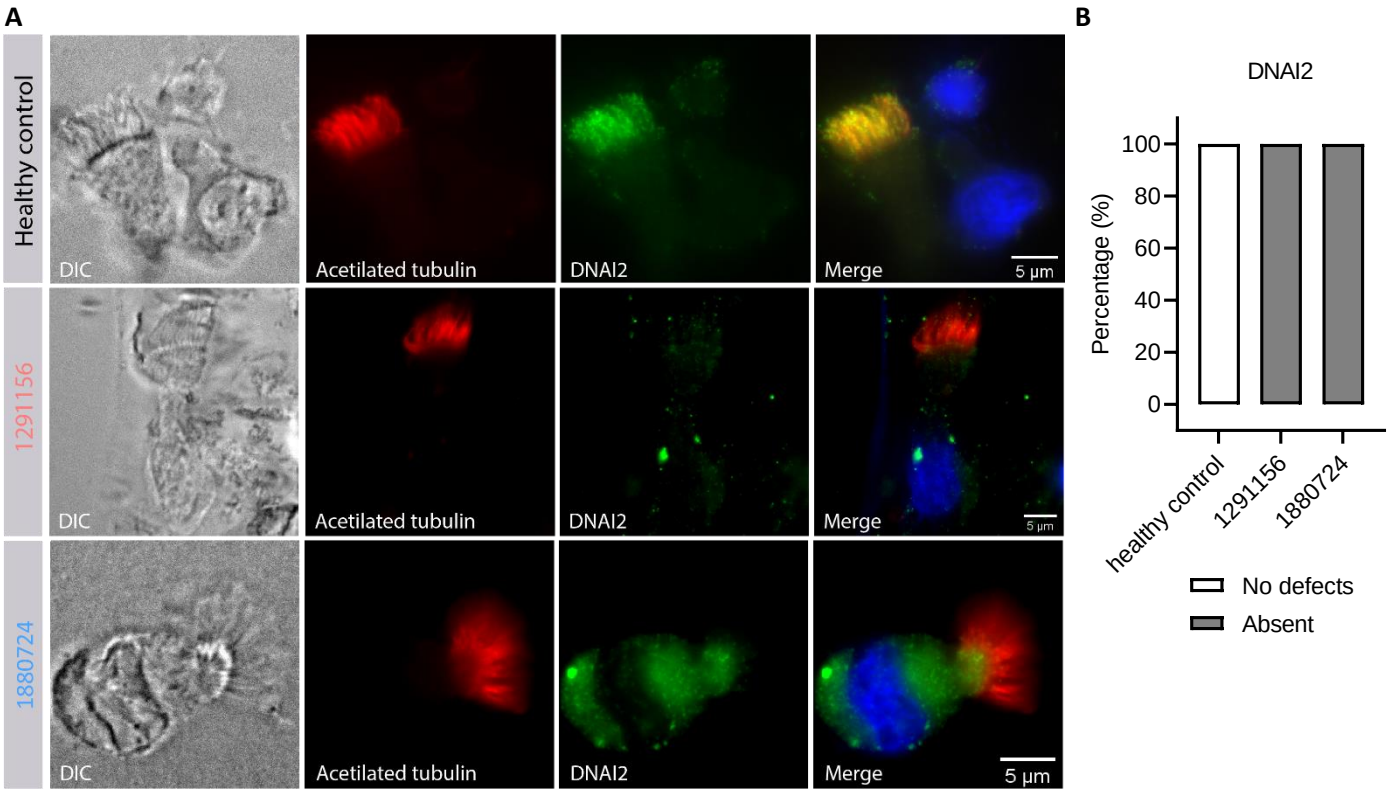

Figure 3.7: DNAI2 localization is affected by the new ZMYND10 variant.
(A) Immunolabelling of ciliary microtubules with acetylated alpha tubulin and the axonemal outer dynein intermediate chain DNAI2 in respiratory ciliated cells of a healthy control volunteer (n=10 cells), subject 1291156 (n=5 cells) and subject 1880724 (n=5 cells). DIC, differential interference contrast microscopy (brightfield). (B) Quantification of the fluorescence signal patterns in cilia observed in A.

As TEM analysis showed a few additional defects regarding microtubule disorganization and central pair microtubule number in respiratory epithelial samples from the subject #1880724, we further evaluated the distribution of CCDC39. This protein is part of the molecular ruler complex together with CCDC40 (Becker-Heck et al., 2011; Merveille et al., 2011). The ruler complex is responsible for providing the necessary anchoring sites for the 96 nm repeat length

and arrangements of ciliary axonemal components for motility (Oda et al., 2014). Mutations in both *CCDC39* and *CCDC40* result in absence of IDA components and nexin-dynein regulatory complex (N-DRC) proteins and consequently present structural disorganization, with mislocalization of peripheral microtubules and abnormal number of central pair microtubules (Becker-Heck et al., 2011; Merveille et al., 2011).

In subjects #1291156 and #1880724 respiratory cells, CCDC39 was present along the ciliary axoneme and thus did not differ from the healthy control cells (Supplementary Figure 3.1), as previously shown for other *ZMYND10* mutations (Kurkowiak et al., 2016). Therefore, we assumed that the tubular abnormalities observed by TEM were probably due to some degree of cellular degeneration.

We then analyzed some components of the N-DRC, radial spokes and central pair apparatus. Although defects in these proteins have not been reported in *ZMYND10* mutant cells, we took the opportunity to optimize the antibodies against the respective proteins and to fully characterize the phenotype of the new variant that our PCD patients' harbor.

We used primary antibodies for Gas8, a N-DRC constituent (Olbrich et al., 2015), RSPH9, one of the radial spoke proteins (Frommer et al., 2015) and SPEF2, a central pair- associated protein (Dougherty et al., 2020). The staining showed a strong ciliary localization for the three proteins in healthy control volunteer cells as well as in #1291156 and #1880724 respiratory cells (Supplementary Figure 3.2 for Gas8; Supplementary Figure 3.3 for RSPH9 and Supplementary Figure 3.4 for SPEF2). Thus confirming that absence of motility in subjects #1291156 and #1880724 caused by *ZMYND10* mutation is entirely due to lack of functional ODA and IDA motor complexes and does not affect additional motility appendages.

In conclusion, the IF method was implemented and optimized successfully in our laboratory. Overall results from subjects #1291156 and #1880724 were compatible with data from HVMA and TEM analysis previously performed as well as published data for other *ZMYND10* variants.

3.3. DISCUSSION

Formerly in Portugal, only patients with strong PCD clinical phenotype would undergo PCD testing by TEM (Fermeiro et al., 2010; Strippoli et al., 2012). However, this pipeline has been proved to miss almost 30% of PCD cases, as many of the increasing number of PCD mutated genes result in normal ciliary ultrastructure or subtle abnormalities that are easily neglected by conventional TEM (Jackson et al., 2016).

Importantly, we have been benefiting from the foundation of the Better Experimental Screening and Treatment for Primary Ciliary Dyskinesia (BESTcilia) consortium (Germany, 2016). This initiative allowed for important advances in the characterization of clinical course and for developing programs to enhance the diagnostic accuracy by establishing PCD diagnostic centers in different countries that were unable to meet the European respiratory society diagnostic guidelines (Sousa et al., 2018).

Now, we have a PCD consortium devoted to improving the PCD diagnosis in Portugal (Constant et al., 2018). Particularly in our laboratory, we are responsible for performing high-speed video microscopy analysis of samples coming from different regions of the country. In fact, we were able to determine for the first time the normal range of ciliary beat frequency for the Portuguese healthy community and for a Portuguese PCD patient group. Moreover, within the consortium, we developed a semi-automated software to measure the frequency of ciliary movement in a reliable fashion and easy to apply in other PCD diagnostic centers (Sampaio et al., 2021).

With this work, we wanted to further establish another PCD diagnostic test in the laboratory, the IF for the characterization of the proteins present in the ciliary axoneme. We took the advantage of a new *ZMYND10* variant found in the Portuguese PCD patient group to fully characterize and optimize the main available antibodies that cover the major ultrastructural defects in PCD.

IF labelling assays proved to be an easy to implement reliable method, as most patterns regarding presence, absence or abnormal localization for every antibody reproduced previously published data. Moreover, we could resolve the additional defects present in #1880724 cells by TEM. Tubular disorganization was not reported in *ZMYND10* mutations and we confirmed by IF that the new *ZMYND10* variant described here does not cause it either.

Furthermore, IF results showed some variability in the faulty pattern of ODA and IDA proteins between the sibling samples, in agreement with the TEM results, which may be due to patient variability.

We hypothesized that inconsistent results regarding the protein accumulation of, for instance, DNAH5, DNAI1 and DNAI2 in the cytoplasm may occur due to different life-stages of respiratory epithelial cells. Immature ciliated cells would have more protein signal as they have had less time to induce protein degradation, while mature ciliated cells have already degraded most of the non-functional complexes, resulting in complete absence of fluorescent signal.

This could be particularly challenging in cases where a small standard panel is used first and then a second panel must be determined, as specific mutations can lead to absence of ODAs from the entire ciliary axoneme and others to a partial absence from the distal end. Nevertheless, a PCD positive diagnosis can be achieved, without establishing the disease-causing gene, when other methods corroborate the results, such as nNO measurements, HVMA and/or TEM analysis.

Moreover, we did not observe significant changes in the IF results that correlated with the different internal organ *situs* between the samples from subject #1291156, which has *situs inversus* and the samples from subject #1880724, which has *situs solitus*. A retrospective comparison in the UK also found that respiratory symptoms and disease progression were similar between patients with and without *situs inversus* of the same age (McManus et al., 2003).

Although studies from the left – right field have already placed the establishment of organ position during the early stages of embryonic development, these studies show that *situs inversus* has no further effect *per se* on later stages of the chronic airway disease part of PCD and subsequently that laterality evolve independently of the respiratory symptoms.

Interestingly, organ final position is widely considered as randomized in PCD patients due to the presence of roughly 50 – 50% of *situs solitus* and *situs inversus.* In the absence of ciliary motility to drive the process of symmetry breaking, left and right sides are set unbiasedly within the body and consequently thoracic and abdominal organs are displayed towards one side or the other. In *situs inversus*, as the arrangement between the organs is conserved, patients can be asymptomatic and have a normal life expectancy (Channabasappa et al., 2013). However, 6 to 10% of the total PCD cases show a laterality defect within the broad spectrum of partial variations between *situs solitus* and *situs inversus,* referred to as *situs ambiguous* (Kennedy, Omran, et al., 2007; Shapiro et al., 2014; Best et al., 2019). The underlying reason for the low prevalence of these cases in PCD is unknown. It would be tempting to speculate that in case of a partial randomization between all laterality possibilities, most of them would result in fetal death or fetal abnormalities, as they would compromise the arrangement of the organs between them. Indeed, a recent study showed that in a large cohort of PCD patients carrying a *DNAH5* mutation, only 7.6% of the cases had *situs ambiguous*, while *Dnah5* mutant

mice showed *situs ambiguous* in 40% of the cases when observed prenatally, which did not survive postnatally (Nöthe-Menchen et al., 2019). Overall, there is a low survival rate of *situs ambiguous* both in humans and mice.

Nonetheless, presence of laterality abnormalities, specifically *situs inversus*, has been shown to contribute to an earlier diagnosis and thus allowing PCD patients to be treated accordingly sooner (Coren et al., 2002; Kuehni et al., 2010). On the other way, it shows how difficult it can be to recognize PCD in patients with normal *situs* and how important it is to develop new diagnostic tools to detect patients and identify new disease-causing genes that are not involved in the establishment of organ laterality.

In fact, mutations in genes coding components of the N-DRC, radial spokes and central pair apparatus have not been associated with *situs inversus* (reviewed by Wallmeier et al., 2020). Moreover, these mutations usually do not greatly affect the ultrastructure of the ciliary axoneme, which can make difficult the PCD diagnosis by conventional TEM. Thus, IF labelling assays and specifically application of the analysis in a daily routine of antibodies against proteins of N-DRC, radial spokes and central pair apparatus can be extremely advantageous for PCD diagnosis.

Having all of this into account, we are in favor of the implementation of IF analysis not only when another PCD test is not available, but also for both improvement of PCD diagnostics and as a PCD clinical research tool. However, a consensus from the European respiratory society is still needed, mostly regarding the IF considerations during data analysis. Total number of cells, standard panel of antibodies, as well as secondary panels and number of nasal brushing repetitions are some parameters that must be determined in the next pipelines in order to achieve standardization between centers.

In a country with about 10 million people, more than 100 samples were analyzed by our laboratory in the last years, with 34 being fully characterized following the European respiratory society guidelines and reaching a final diagnosis positive for PCD (18 patients) or PCD-excluded (16 patients) (Sampaio et al., 2021). Twenty more samples had the ciliary function analyzed by me and one of which was considered as “likely to have PCD” due to a hyperkinetic phenotype of ciliary movement coupled with an absence of DNAH11 from the ciliary axonemes by IF. Hence, showing the great potential for the growth of IF application, as a useful PCD diagnostic test in Portugal.

3.4. SUPPLEMENTARY MATERIAL

Supplementary Movie 3. 1 – Example of a sideway view of beating respiratory cilia from a healthy control volunteer.
Cilia exhibit a normal ciliary beat pattern characterized by two active motions, the recovery stroke and the power stroke. Mucociliary clearance capacity does not seem compromised. Ciliary movement was recorder at 500 fps and played at 60 fps.

Supplementary Movie 3. 2 – Example of a sideway view of respiratory cilia from # 1291156 sibling.
Cilia exhibit lack any type of movement with a rigid profile. Mucus accumulation, due to absence of mucociliary clearance. Ciliary movement was recorder at 500 fps and played at 60 fps.

Supplementary Movie 3. 3 – Example of a sideway view of respiratory cilia from # 1880724 sibling.
Cilia exhibit lack any type of movement with a rigid profile. Mucus accumulation, due to absence of mucociliary clearance. Ciliary movement was recorder at 500 fps and played at 60 fps.

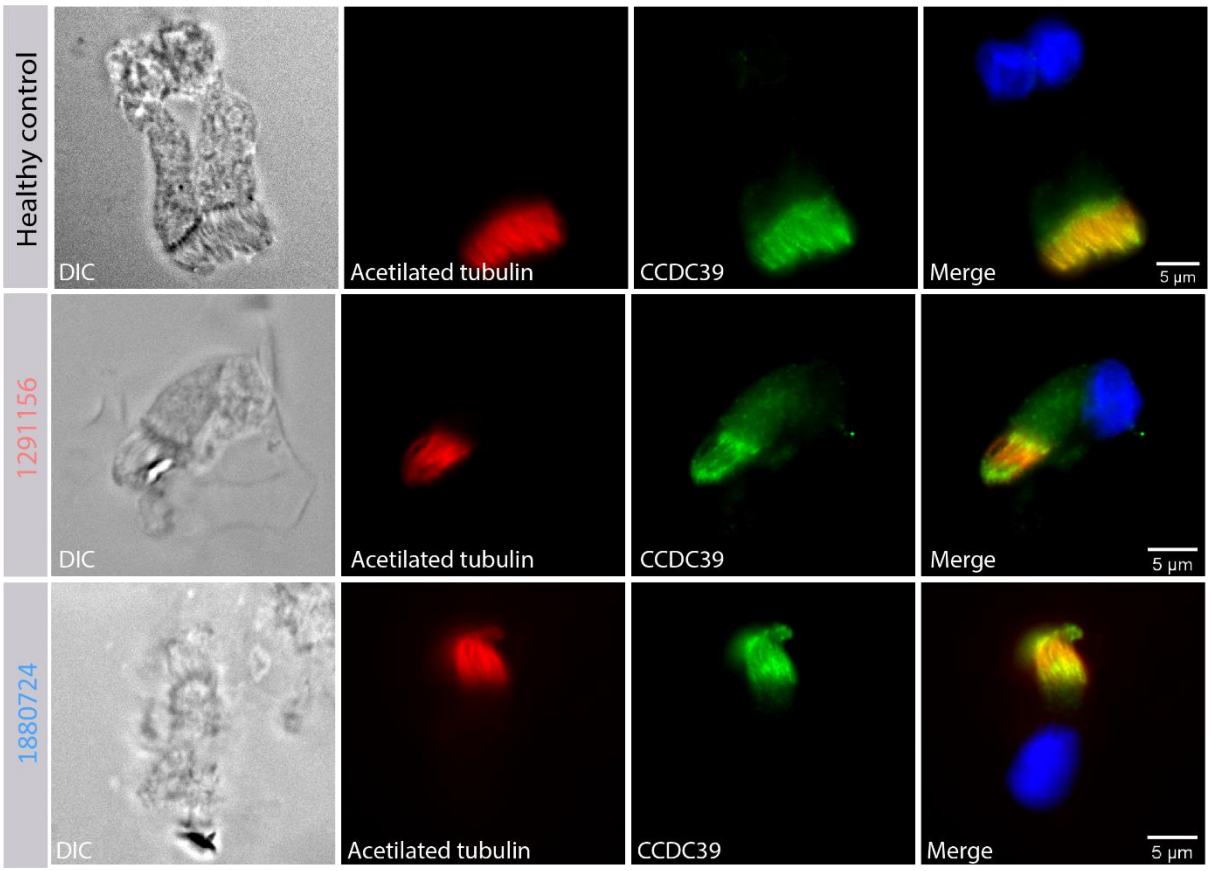

Supplementary Figure 3.1: CCDC39 localization is not affected by the new ZMYND10 variant.
Immunolabelling of ciliary microtubules with acetylated alpha tubulin and one component of the ruler complex, CCDC39, in respiratory ciliated cells of a healthy control volunteer (n=10 cells), subject 1291156 (n=4 cells) and subject 1880724 (n=7 cells). DIC, differential interference contrast microscopy (brightfield).

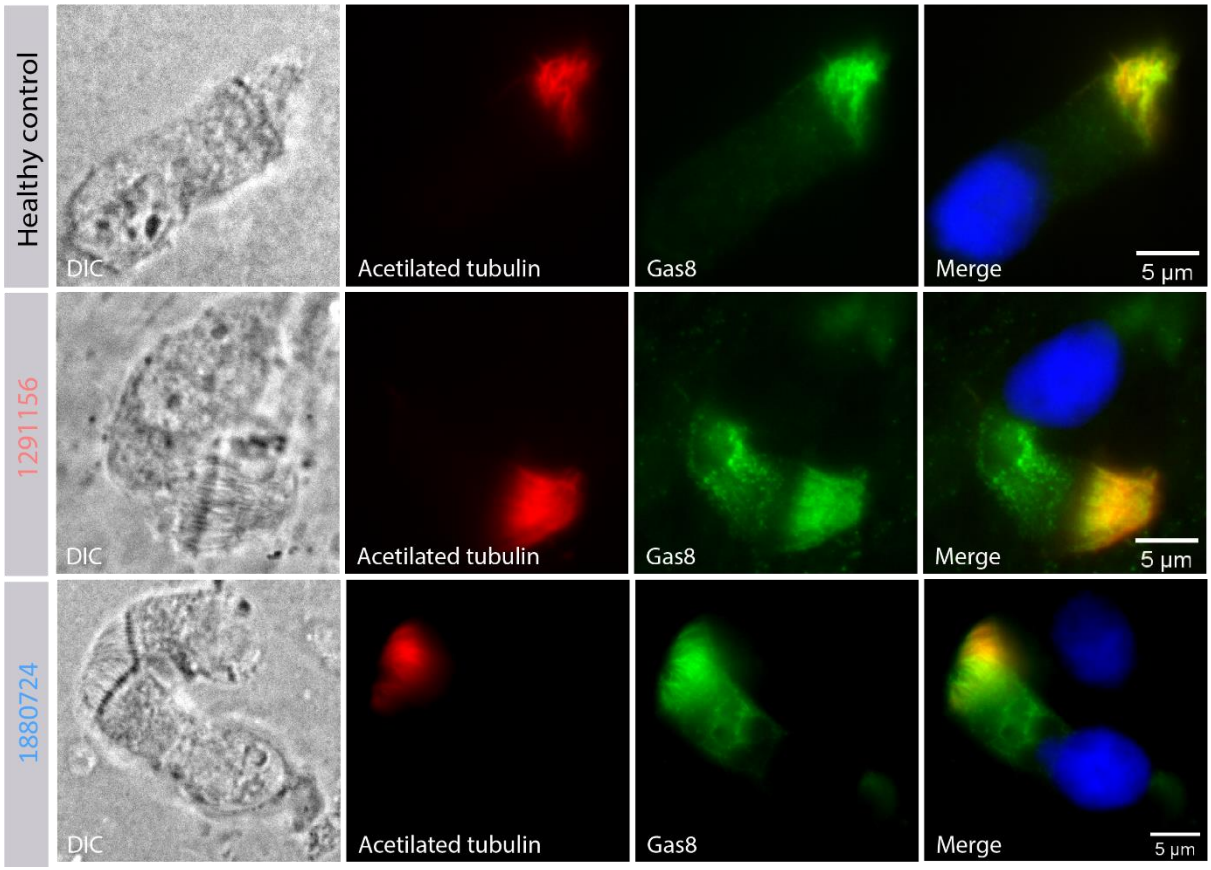

Supplementary Figure 3.2: Gas8 localization is not affected by the new ZMYND10 variant.
Immunolabelling of ciliary microtubules with acetylated alpha tubulin and one component of the nexin-dynein regulatory complex, Gas8, in respiratory ciliated cells of a healthy control volunteer (n=10 cells), subject 1291156 (n=26 cells) and subject 1880724 (n=7 cells). DIC, differential interference contrast microscopy (brightfield).

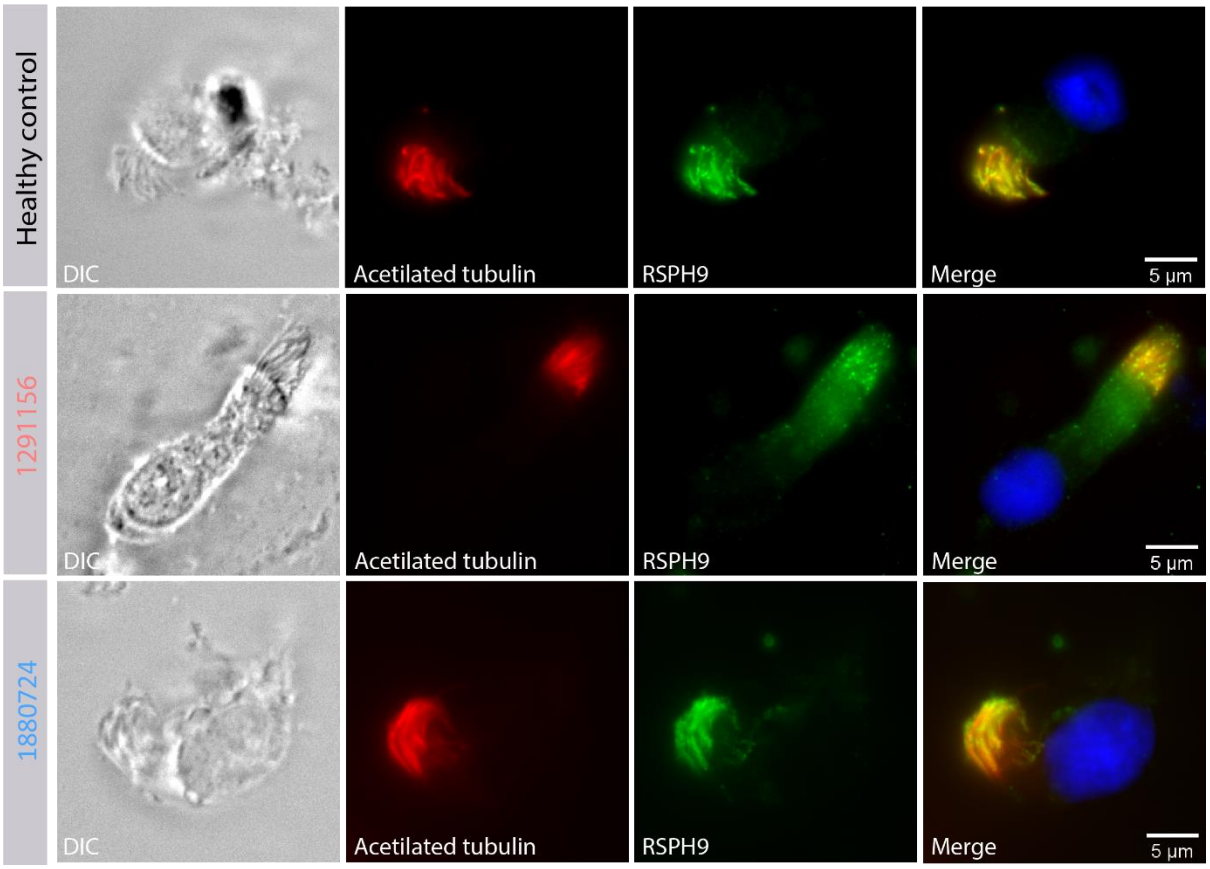

Supplementary Figure 3.3: RSPH9 localization is not affected by the new ZMYND10 variant.
Immunolabelling of ciliary microtubules with acetylated alpha tubulin and one component of the radial spokes, RSPH9, in respiratory ciliated cells of a healthy control volunteer (n=10 cells), subject 1291156 (n=8 cells) and subject 1880724 (n=7 cells). DIC, differential interference contrast microscopy (brightfield).

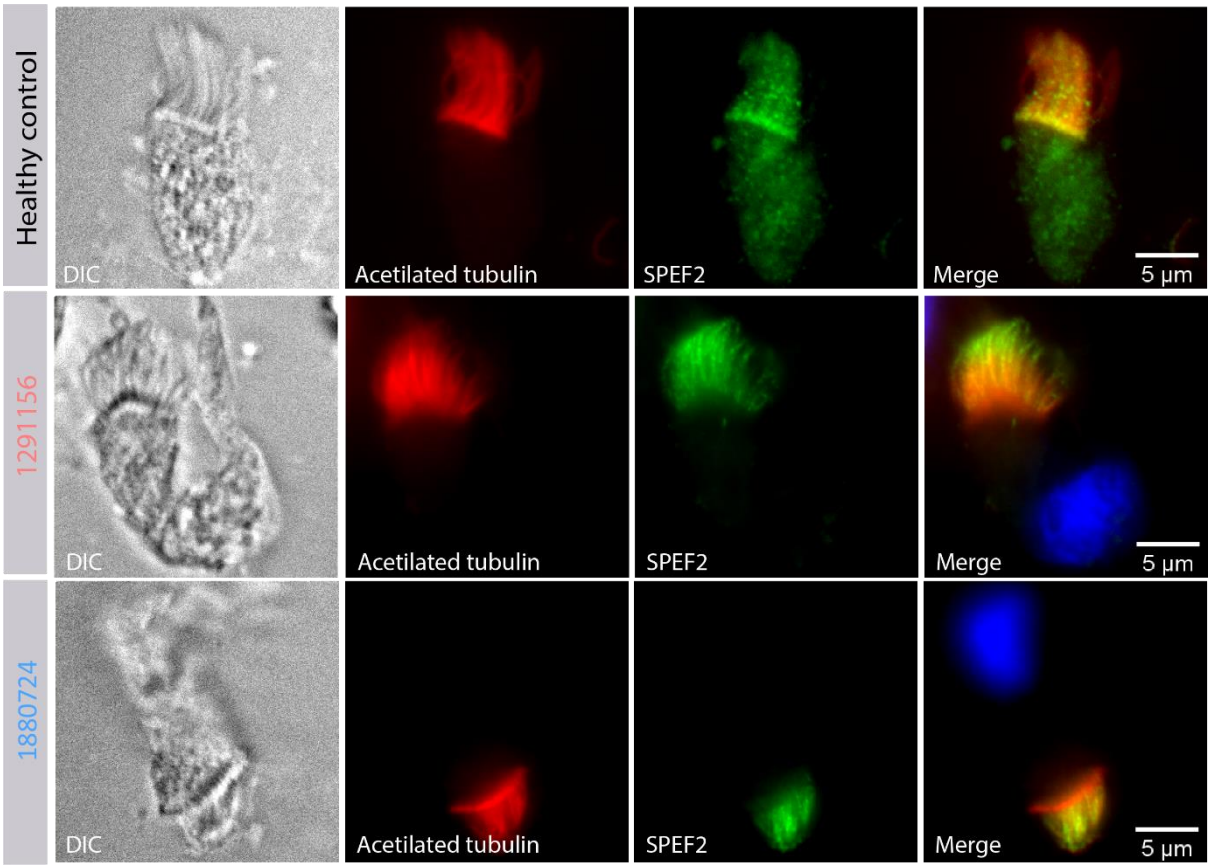

Supplementary Figure 3.4: SPEF2 localization is not affected by the new ZMYND10 variant.
Immunolabelling of ciliary microtubules with acetylated alpha tubulin and one component of the central pair appendages, SPEF2, in respiratory ciliated cells of a healthy control volunteer (n=11 cells), subject 1291156 (n=11 cells) and subject 1880724 (n=11 cells). DIC, differential interference contrast microscopy (brightfield).

3.5. REFERENCES

Agathanggelou, A., Dallol, A., Zöchbauer-Müller, S., Morrissey, C., Honorio, S., Hesson, L., Martinsson, T., Fong, K. M., Kuo, M. J., Yuen, P. W., Maher, E. R., Minna, J. D., & Latif, F. (2003). Epigenetic inactivation of the candidate 3p21.3 suppressor gene BLU in human cancers. *Oncogene*, *22*(10), 1580–1588. https://doi.org/10.1038/sj.onc.1206243

Albee, A. J., Kwan, A. L., Lin, H., Granas, D., Stormo, G. D., & Dutcher, S. K. (2013). Identification of cilia genes that affect cell-cycle progression using whole-genome transcriptome analysis in chlamydomonas reinhardtti. *G3: Genes, Genomes, Genetics*, *3*(6), 979–991. https://doi.org/10.1534/g3.113.006338

Amirav, I., Wallmeier, J., Loges, N. T., Menchen, T., Pennekamp, P., Mussaffi, H., Abitbul, R., Avital, A., Bentur, L., Dougherty, G. W., Nael, E., Lavie, M., Olbrich, H., Werner, C., Kintner, C., Omran, H., & Israeli PCD Consortium Investigators. (2016). Systematic Analysis of CCNO Variants in a Defined Population : Implications for Clinical Phenotype and. *Human Mutation*, *37*(4), 396–405. https://doi.org/10.1002/humu.22957

Aprea, I., Nöthe-Menchen, T., Dougherty, G. W., Raidt, J., Loges, N. T., Kaiser, T., Wallmeier, J., Olbrich, H., Strünker, T., Kliesch, S., Pennekamp, P., & Omran, H. (2021). Motility of efferent duct cilia aids passage of sperm cells through the male reproductive system. *Molecular Human Reproduction*, *27*(3), gaab009. https://doi.org/10.1093/molehr/gaab009

Aprea, I., Raidt, J., Höben, I. M., Loges, N. T., Nöthe-Menchen, T., Pennekamp, P., Olbrich, H., Kaiser, T., Biebach, L., Tüttelmann, F., Horvath, J., Schubert, M., Krallmann, C., Kliesch, S., & Omran, H. (2021). Defects in the cytoplasmic assembly of axonemal dynein arms cause morphological abnormalities and dysmotility in sperm cells leading to male infertility. In *PLoS Genetics* (Vol. 17, Issue 2). https://doi.org/10.1371/journal.pgen.1009306

Barbato, A., Frischer, T., Kuehni, C. E., Snijders, D., Azevedo, I., Baktai, G., Bartoloni, L., Eber, E., Escribano, A., Haarman, E., Hesselmar, B., Hogg, C., Jorissen, M., Lucas, J., Nielsen, K. G., O'Callaghan, C., Omran, H., Pohunek, P., Strippoli, M. P. F., & Bush, A. (2009). Primary ciliary dyskinesia: A consensus statement on diagnostic and treatment approaches in children. *The European Respiratory Journal*, *34*(6), 1264–1276. https://doi.org/10.1183/09031936.00176608

Baz-Redón, N., Rovira-Amigo, S., Fernández-Cancio, M., Castillo-Corullón, S., Cols, M., Caballero-Rabasco, M. A., Asensio, Ó., Martín de Vicente, C., Martínez-Colls, M., Torrent-Vernetta, A., de Mir-Messa, I., Gartner, S., Iglesias-Serrano, I., Díez-Izquierdo, A., Polverino, E., Amengual-Pieras, E., Amaro-Rodríguez, R., Vendrell, M., Mumany, M., … Moreno-Galdó, A. (2020). Immunofluorescence Analysis as a Diagnostic Tool in a Spanish Cohort of Patients with Suspected Primary Ciliary Dyskinesia. *Journal of Clinical Medicine*, *9*(11), 3603. https://doi.org/10.3390/jcm9113603

Becker-Heck, A., Zohn, I. E., Okabe, N., Pollock, A., Lenhart, K. B., Sullivan-Brown, J., McSheene, J., Loges, N. T., Olbrich, H., Haeffner, K., Fliegauf, M., Horvath, J., Reinhardt, R., Nielsen, K. G., Marthin, J. K., Baktai, G., Anderson, K. V., Geisler, R., Niswander, L., … Burdine, R. D. (2011). The coiled-coil domain containing protein CCDC40 is essential for motile cilia function and left-right axis formation. *Nature Genetics*, *43*(1), 79–84. https://doi.org/10.1038/ng.727

Behan, L., Dimitrov, B., Kuehni, C., Hogg, C., CArrol, M., Evans, H., Goutaki, M., Harris, A., Packham, S., Walker, W., & Lucas, J. (2016). PICADAR: A diagnostic predictive tool for primary ciliary dyskinesia. *The European Respiratory Journal*, *47*(4), 1103–1112. https://doi.org/10.1183/13993003.01551-2015

Behan, L., Galvin, A. D., Rubbo, B., Masefield, S., Copeland, F., Manion, M., Rindlisbacher, B., Redfern, B., & Lucas, J. S. (2016). Diagnosing primary ciliary dyskinesia: An international patient perspective. *The European Respiratory Journal*, *48*(4), 1096–1107. https://doi.org/10.1183/13993003.02018-2015

Best, S., Shoemark, A., Rubbo, B., Patel, M. P., Fassad, M. R., Dixon, M., Rogers, A. V, Hirst, R. A., Rutman, A., Ollosson, S., Jackson, C. L., Goggin, P., Thomas, S., Pengelly, R., Cullup, T., Pissaridou, E., Hayward, J., Onoufriadis, A., Callaghan, C. O., … Hogg, C. (2019). Risk factors for situs defects and congenital heart disease in primary ciliary dyskinesia. *Thorax*, *74*(2), 203–205. https://doi.org/10.1136/thoraxjnl-2018-212104

Blanchon, S., Legendre, M., Bottier, M., Tamalet, A., Montantin, G., Collot, N., Faucon, C., Dastot, F., Copin, B., Clement, A., Filoche, M., Coste, A., Amselem, S., Escudier, E., Papon, J.-F., & Louis, B. (2020). Deep phenotyping , including quantitative ciliary beating parameters , and extensive genotyping in primary ciliary dyskinesia. *Journal of Medical Genetics*, *57*(4), 237–244. https://doi.org/10.1136/jmedgenet-2019-106424

Boon, M., Smits, A., Cuppens, H., Jaspers, M., Proesmans, M., Dupont, L. J., Vermeulen, F. L., Daele, S. Van, Malfroot, A., Godding, V., Jorissen, M., & Boeck, K. De. (2014). Primary ciliary dyskinesia : critical evaluation of clinical symptoms and diagnosis in patients with normal and abnormal ultrastructure. *Orphanet Journal of Rare Diseases*, *9*, 11. https://doi.org/10.1186/1750-1172-9-11

Boon, M., Wallmeier, J., Ma, L., Loges, N. T., Jaspers, M., Olbrich, H., Dougherty, G. W., Raidt, J., Werner, C., Amirav, I., Hevroni, A., Abitbul, R., Avital, A., Soferman, R., Wessels, M., Callaghan, C. O., Chung, E. M. K., Rutman, A., Hirst, R. A., … Omran, H. (2014). MCIDAS mutations result in a mucociliary clearance disorder with reduced generation of multiple motile cilia. *Nature Communications*, *5*, 4418. https://doi.org/10.1038/ncomms5418

Bukowy-Bieryllo, Z., Rabiasz, A., Dabrowski, M., Pogorzelski, A., Wojda, A., Dmenska, H., Grzela, K., Sroczynski, J., Witt, M., & Zietkiewicz, E. (2019). Truncating mutations in exons 20 and 21 of OFD1 can cause primary ciliary dyskinesia without associated syndromic symptoms. *Journal of Medical Genetics*, *56*(11), 769–777. https://doi.org/10.1136/jmedgenet-2018-105918

Bustamante-marin, X. M., Yin, W., Sears, P. R., Werner, M. E., Brotslaw, E. J., Mitchell, B. J., Jania, C. M., Zeman, K. L., Rogers, T. D., Herring, L. E., Refabe, L., Thomas, L., Amselem, S., Escudier, E., Legendre, M., Grubb, B. R., Knowles, M. R., Zariwala, M. A., & Ostrowski, L. E. (2019). Lack of GAS2L2 Causes PCD by Impairing Cilia Orientation and Mucociliary Clearance. *American Journal of Human Genetics*, *104*(2), 229–245. https://doi.org/10.1016/j.ajhg.2018.12.009

Channabasappa, S. M., Mohan, H. S., & Sarma, J. (2013). A patient with situs inversus totalis presenting for emergency laparoscopic appendectomy: Consideration for safe anesthetic management. In *Anesthesia, essays and researches* (Vol. 7, Issue 1, pp. 127–129). https://doi.org/10.4103/0259-1162.114019

Chilvers, M. A., Rutman, A., & O'Callaghan, C. (2003). Ciliary beat pattern is associated with specific ultrastructural defects in primary ciliary dyskinesia. *The Journal of Allergy and Clinical*

Immunology, *112*(3), 518–524. https://doi.org/10.1016/S0091-6749(03)01799-8

Cho, K. J., Noh, S. H., Han, S. M., Choi, W. Il, Kim, H. Y., Yu, S., Lee, J. S., Rim, J. H., Lee, M. G., Hildebrandt, F., & Gee, H. Y. (2018). ZMYND10 stabilizes intermediate chain proteins in the cytoplasmic pre-assembly of dynein arms. *PLoS Genetics*, *14*(3), 1–21. https://doi.org/10.1371/journal.pgen.1007316

Collins, S. A., Gove, K., Walker, W., & Lucas, J. S. A. (2014). Nasal nitric oxide screening for primary ciliary dyskinesia: Systematic review and meta-analysis. *The European Respiratory Journal*, *44*(6), 1589–1599. https://doi.org/10.1183/09031936.00088614

Constant, C., Sousa, R., Pinto, A., Sampaio, P., & Lopes, S. S. (2018). Nova Era no Diagnóstico da Discinesia Ciliar Primária. *Acta Pediátrica Portuguesa*, *49*(3), 235–242. https://doi.org/10.21069/APP.2018.14652

Coren, M., Meeks, M., Morrison, I., Buchdahl, R., & Bush, A. (2002). Primary ciliary dyskinesia: Age at diagnosis and symptom history. *Acta Paediatrica (Oslo, Norway : 1992)*, *91*(6), 667–669. https://doi.org/10.1080/080352502760069089

Dalrymple, R. A., & Kenia, P. (2019). European Respiratory Society guidelines for the diagnosis of primary ciliary dyskinesia: A guideline review. *Archives of Disease in Childhood: Education and Practice Edition*, *104*(5), 265–269. https://doi.org/10.1136/archdischild-2017-312902

Dehlink, E., Hogg, C., Carr, S. B., Bush, A., Dehlink, E., Hogg, C., Carr, S. B., & Bush, A. (2016). Clinical phenotype and current diagnostic criteria for primary ciliary dyskinesia. *Expert Review of Respiratory Medicine*, *10*(11), 1163–1175. https://doi.org/10.1080/17476348.2016.1242414

Desai, P. B., Dean, A. B., & Mitchell, D. R. (2017). Cytoplasmic preassembly and trafficking of axonemal dyneins. In *Dyneins: The Biology of Dynein Motors: Second Edition* (Second Edi). Elsevier Inc. https://doi.org/10.1016/B978-0-12-809471-6.00004-8

Djakow, J., Rozehnalova, E., Havlisova, M., Svobodova, T., & Pohunek, P. (2012). Clinical index to evaluate the risk of primary ciliary dyskinesia in children. *European Respiratory Journal*, *40*(Suppl. 56), 2844.

Dougherty, G. W., Loges, N. T., Klinkenbusch, J. A., Olbrich, H., Pennekamp, P., Menchen, T., Raidt, J., Wallmeier, J., Werner, C., Westermann, C., Ruckert, C., Mirra, V., Hjeij, R., Memari, Y., Durbin, R., Kolb-kokocinski, A., Praveen, K., Kashef, M. A., Kashef, S., … Omran, H. (2016). DNAH11 Localization in the Proximal Region of Respiratory Cilia Defines Distinct Outer Dynein Arm Complexes. *American Journal of Respiratory Cell and Molecular Biology*, *55*(2), 213–224. https://doi.org/10.1165/rcmb.2015-0353OC

Dougherty, G. W., Olbrich, H., Hjeij, R., Loges, N. T., Amirav, I., Philipsen, M. C., Marthin, J. K., Nielsen, K. G., Sutharsan, S., Raidt, J., Werner, C., Pennekamp, P., Dworniczak, B., & Omran, H. (2020). SPEF2- and HYDIN -Mutant Cilia Lack the Central Pair – associated Protein SPEF2 , Aiding Primary Ciliary Dyskinesia Diagnostics. *American Journal of Respiratory Cell and Molecular Biology*, *62*(3), 382–396. https://doi.org/10.1165/rcmb.2019-0086OC

Duquesnoy, P., Escudier, E., Bridoux, A., Escalier, D., Rayet, I., Amselem, S., Marcos, E., & Vojtek, A. (2007). A common variant in combination with a nonsense mutation in a member of the thioredoxin

family causes primary ciliary dyskinesia. *Proceedings of the National Academy of Sciences of the United States of America*, *104*(9), 3336–3341. https://doi.org/10.1073/pnas.0611405104

Fermeiro, J., Bandeira, T., Lobo, L., & Pereira, L. (2010). Primary ciliary dyskinesia revisited: Based on three clinical reports. *Revista Portuguesa de Pneumologia*, *16*(5), 837–847. https://doi.org/10.1016/s0873-2159(15)30076-3

Fliegauf, M., Olbrich, H., Horvath, J., Wildhaber, J. H., Zariwala, M. A., Kennedy, M., Knowles, M. R., & Omran, H. (2005). Mislocalization of DNAH5 and DNAH9 in Respiratory Cells from Patients with Primary Ciliary Dyskinesia. *American Journal of Respiratory and Critical Care Medicine*, *171*(12), 1343–1349. https://doi.org/10.1164/rccm.200411-1583OC

Frija-Masson, J., Bassinet, L., Honoré, I., Dufeu, N., Housset, B., Coste, A., Papon, J. F., Escudier, E., Burgel, P. R., & Maître, B. (2017). Clinical characteristics, functional respiratory decline and follow-up in adult patients with primary ciliary dyskinesia. *Thorax*, *72*(2), 154–160. https://doi.org/10.1136/thoraxjnl-2015-207891

Frommer, A., Hjeij, R., Loges, N. T., Edelbusch, C., Jahnke, C., Raidt, J., Werner, C., Wallmeier, J., Große-Onnebrink, J., Olbrich, H., Cindrić, S., Jaspers, M., Boon, M., Memari, Y., Durbin, R., Kolb-Kokocinski, A., Sauer, S., Marthin, J. K., Nielsen, K. G., … Omran, H. (2015). Immunofluorescence analysis and diagnosis of primary ciliary dyskinesia with radial spoke defects. *American Journal of Respiratory Cell and Molecular Biology*, *53*(4), 563–573. https://doi.org/10.1165/rcmb.2014-0483OC

Germany, W. W.-U. M. (2016). *Better experimental screening and treatment for primary ciliary dyskinesia*. Accessed at 23th August 2022. https://doi.org/10.1080/01913123.2016.1270815

Goutaki, M., Meier, A. B., Halbeisen, F. S., Lucas, J. S., Dell, S. D., Maurer, E., Casaulta, C., Jurca, M., Spycher, B. D., & Kuehni, C. E. (2016). Clinical manifestations in primary ciliary dyskinesia: Systematic review and meta-analysis. *The European Respiratory Journal*, *48*(4), 1081–1095. https://doi.org/10.1183/13993003.00736-2016

Harrison, M. J., Shapiro, A. J., & Kennedy, M. P. (2016). Congenital Heart Disease and Primary Ciliary Dyskinesia. *Paediatric Respiratory Reviews*, *18*, 25–32. https://doi.org/10.1016/j.prrv.2015.09.003

Höben, I. M., Hjeij, R., Olbrich, H., Dougherty, G. W., Nöthe-Menchen, T., Aprea, I., Frank, D., Pennekamp, P., Dworniczak, B., Wallmeier, J., Raidt, J., Nielsen, K. G., Philipsen, M. C., Santamaria, F., Venditto, L., Amirav, I., Mussaffi, H., Prenzel, F., Wu, K., … Omran, H. (2018). Mutations in C11orf70 Cause Primary Ciliary Dyskinesia with Randomization of Left/Right Body Asymmetry Due to Defects of Outer and Inner Dynein Arms. *American Journal of Human Genetics*, *102*(5), 973–984. https://doi.org/10.1016/j.ajhg.2018.03.025

Hofmann, T., Gugatschga, M., Koidl, B., & Wolf, G. (2004). Influence of preservatives and topical steroids on ciliary beat frequency in vitro. *Archives of Otolaryngology--Head & Neck Surgery*, *130*(4), 440–445. https://doi.org/10.1001/archotol.130.4.440

Horani, A., Druley, T. E., Zariwala, M. A., Patel, A. C., Levinson, B. T., Arendonk, L. G. Van, Thornton, K. C., Giacalone, J. C., Albee, A. J., Wilson, K. S., Turner, E. H., Nickerson, D. A., Shendure, J., Bayly, P. V, Leigh, M. W., Knowles, M. R., Brody, S. L., Dutcher, S. K., & Ferkol, T. W. (2012). Whole-Exome Capture and Sequencing Identifies HEATR2 Mutation as a Cause of Primary Ciliary Dyskinesia. *The American Journal of Human Genetics*, *91*(4), 685–693. https://doi.org/10.1016/j.ajhg.2012.08.022

Horani, A., Ustione, A., Huang, T., Firth, A. L., Pan, J., Gunsten, S. P., Haspel, J. A., Piston, D. W., & Brody, S. L. (2018). Establishment of the early cilia preassembly protein complex during motile ciliogenesis. *Proceedings of the National Academy of Sciences of the United States of America*, *115*(6), E1221–E1228. https://doi.org/10.1073/pnas.1715915115

Huizar, R. L., Lee, C., Boulgakov, A. A., Horani, A., Tu, F., Marcotte, E. M., Brody, S. L., & Wallingford, J. B. (2018). A liquid-like organelle at the root of motile ciliopathy. *ELife*, *7*, e38497. https://doi.org/10.7554/eLife.38497

Ishikawa, T. (2017). Axoneme structure from motile cilia. *Cold Spring Harbor Perspectives in Biology*, *9*(1), a028076. https://doi.org/10.1101/cshperspect.a028076

Jackson, C. L., Behan, L., Collins, S. A., Goggin, P. M., Adam, E. C., Coles, J. L., Evans, H. J., Harris, A., Lackie, P., Packham, S., Page, A., Thompson, J., Walker, W. T., Kuehni, C., & Lucas, J. S. (2016). Accuracy of diagnostic testing in primary ciliary dyskinesia. *The European Respiratory Journal*, *47*(3), 837–848. https://doi.org/10.1183/13993003.00749-2015

Joskova, M., Mokry, J., & Franova, S. (2020). Respiratory Cilia as a Therapeutic Target of Phosphodiesterase Inhibitors. *Frontiers in Pharmacology*, *11*, 1–11. https://doi.org/10.3389/fphar.2020.00609

Kartagener, M. (1933). Zur Pathogenese der Bronchiektasien. Bronchiektasien bei situs inversus viscerum. *Beitr Klin Tuberk*, *83*, 489–501.

Kempeneers, C., Seaton, C., Garcia Espinosa, B., & Chilvers, M. A. (2019). Ciliary functional analysis : Beating a path towards standardization. *Pediatric Pulmonology*, *54*(10), 1627–1638. https://doi.org/10.1002/ppul.24439

Kennedy, M. P., Noone, P. G., Leigh, M. W., Zariwala, M. A., Minnix, S. L., Knowles, M. R., & Molina, P. L. (2007). High-resolution CT of patients with primary ciliary dyskinesia. *American Journal of Roentgenology*, *188*(5), 1232–1238. https://doi.org/10.2214/AJR.06.0965

Kennedy, M. P., Omran, H., Leigh, M. W., Dell, S., Morgan, L., Molina, P. L., Robinson, B. V, Minnix, S. L., Olbrich, H., Severin, T., Ahrens, P., Lange, L., Morillas, H. N., Noone, P. G., Zariwala, M. A., & Knowles, M. R. (2007). Congenital Heart Disease and Other Heterotaxic Defects in a Large Cohort of Patients With Primary Ciliary Dyskinesia. *Circulation*, *115*, 2814–2821. https://doi.org/10.1161/CIRCULATIONAHA.106.649038

Knowles, M. R., Ostrowski, L. E., Leigh, M. W., Sears, P. R., Davis, S. D., Wolf, W. E., Hazucha, M. J., Carson, J. L., Olivier, K. N., Sagel, S. D., Rosenfeld, M., Ferkol, T. W., Dell, S. D., Milla, C. E., Randell, S. H., Yin, W., Sannuti, A., Metjian, H. M., Noone, P. G., … Zariwala, M. A. (2014). Mutations in RSPH1 Cause Primary Ciliary Dyskinesia with a Unique Clinical and Ciliary Phenotype. *American Journal of Respiratory and Critical Care Medicine*, *189*(6), 707–717. https://doi.org/10.1164/rccm.201311-2047OC

Knowles, M. R., Ostrowski, L. E., Loges, N. T., Hurd, T., Leigh, M. W., Huang, L., Wolf, W. E., Carson, J. L., Hazucha, M. J., Yin, W., Davis, S. D., Dell, S. D., Ferkol, T. W., Sagel, S. D., Olivier, K. N., Jahnke, C., Olbrich, H., Werner, C., Raidt, J., … Zariwala, M. A. (2013). Mutations in SPAG1 cause primary ciliary dyskinesia associated with defective outer and inner dynein arms. *American Journal of Human Genetics*, *93*(4), 711–720. https://doi.org/10.1016/j.ajhg.2013.07.025

Kobayashi, D., Asano-hoshino, A., Nakakura, T., Nishimaki, T., Ansai, S., Kinoshita, M., Ogawa, M., Hagiwara, H., & Yokoyama, T. (2017). Loss of zinc finger MYND-type containing 10 (zmynd10) affects cilia integrity and axonemal localization of dynein arms, resulting in ciliary dysmotility, polycystic kidney and scoliosis in medaka (Oryzias latipes). *Developmental Biology*, *10*. https://doi.org/10.1016/j.ydbio.2017.08.016

Kouis, P., Yiallouros, P. K., Middleton, N., Evans, J. S., Kyriacou, K., & Papatheodorou, S. (2017). Prevalence of primary ciliary dyskinesia in consecutive referrals of suspect cases and the transmission electron microscopy detection rate: a systematic review and meta-analysis. *Pediatric Research*, *81*(3), 398–405. https://doi.org/10.1038/pr.2016.263

Krawczyński, M. R., & Witt, M. (2004). PCD and RP: X-linked inheritance of both disorders? *Pediatric Pulmonology*, *38*(1), 88–89. https://doi.org/10.1002/ppul.30001

Kuehni, C. E., Frischer, T., Strippoli, M. P., Maurer, E., Bush, A., Nielsen, K. G., Escribano, A., Lucas, J. S., Yiallouros, P., Omran, H., Eber, E., O'Callaghan, C., Snijders, D., & Barbato, A. (2010). Factors influencing age at diagnosis of primary ciliary dyskinesia in European children. *The European Respiratory Journal*, *36*(6), 1248–1258. https://doi.org/10.1183/09031936.00001010

Kurkowiak, M., Ziętkiewicz, E., Greber, A., Voelkel, K., Wojda, A., Pogorzelski, A., & Witt, M. (2016). ZMYND10 - Mutation analysis in Slavic patients with primary ciliary dyskinesia. *PLoS ONE*, *11*(1), 1–14. https://doi.org/10.1371/journal.pone.0148067

Leigh, M. W., Ferkol, T. W., Davis, S. D., Lee, H., Rosenfeld, M., Dell, S. D., Sagel, S. D., Milla, C., Olivier, K. N., Sullivan, K. M., Zariwala, M. A., Pittman, J. E., Shapiro, A., Carson, J. L., Krischer, J., Hazucha, M. J., & Knowles, M. R. (2016). Clinical Features and Associated Likelihood of Primary Ciliary Dyskinesia in Children and Adolescents. *Annals of the American Thoracic Society*, *13*(8), 1305–1313. https://doi.org/10.1513/AnnalsATS.201511-748OC

Lin, J., Yin, W., Smith, M. C., Song, K., Leigh, M. W., Zariwala, M. A., Knowles, M. R., Ostrowski, L. E., & Nicastro, D. (2014). Cryo-electron tomography reveals ciliary defects underlying human RSPH1 primary ciliary dyskinesia. *Nature Communications*, *5*, 5727. https://doi.org/10.1038/ncomms6727

Liu, Z., Nguyen, Q. P. H., Guan, Q., Albulescu, A., Erdman, L., Mahdaviyeh, Y., Kang, J., Ouyang, H., Hegele, R. G., Moraes, T., Goldenberg, A., Dell, S. D., & Mennella, V. (2020). A quantitative super-resolution imaging toolbox for diagnosis of motile ciliopathies. *Science Translational Medicine*, *12*(535), eaay0071. https://doi.org/10.1126/scitranslmed.aay0071

Loges, N. T., Antony, D., Maver, A., Deardorff, M. A., Güleç, E. Y., Gezdirici, A., Nöthe-Menchen, T., Höben, I. M., Jelten, L., Frank, D., Werner, C., Tebbe, J., Wu, K., Goldmuntz, E., Čuturilo, G., Krock, B., Ritter, A., Hjeij, R., Bakey, Z., … Schmidts, M. (2018). Recessive DNAH9 Loss-of-Function Mutations Cause Laterality Defects and Subtle Respiratory Ciliary-Beating Defects. *American Journal of Human Genetics*, *103*(6), 995–1008. https://doi.org/10.1016/j.ajhg.2018.10.020

Lucas, J. S., Barbato, A., Collins, S. A., Goutaki, M., Behan, L., Caudri, D., Dell, S., Eber, E., Escudier, E., Hirst, R. A., Hogg, C., Jorissen, M., Latzin, P., Legendre, M., Leigh, M. W., Midulla, F., Nielsen, K. G., Omran, H., Papon, J. F., … Kuehni, C. E. (2017). European Respiratory Society guidelines for the diagnosis of primary ciliary dyskinesia. *The European Respiratory Journal*, *49*(1), 1601090. https://doi.org/10.1183/13993003.01090-2016

Mali, G. R., Yeyati, P. L., Mizuno, S., Dodd, D. O., Tennant, P. A., Keighren, M. A., Lage, P. Zur, Shoemark, A., Garcia-Munoz, A., Shimada, A., Takeda, H., Edlich, F., Takahashi, S., Kreigsheim, A. von, Jarman, A. P., & Mill, P. (2018). ZMYND10 functions in a chaperone relay during axonemal dynein assembly. *ELife*, *7*(Ic), 1–27. https://doi.org/10.7554/eLife.34389

Marshall, C. R., Scherer, S. W., Zariwala, M. A., Lau, L., Paton, T. A., Stockley, T., Jobling, R. K., Ray, P. N., Knowles, M. R., Consortium, F. C., Hall, D. A., Dell, S. D., & Kim, R. H. (2015). Whole-Exome Sequencing and Targeted Copy Number Analysis in Primary Ciliary Dyskinesia. *G3: Genes, Genomes, Genetics*, *5*(8), 1775–1781. https://doi.org/10.1534/g3.115.019851

Marthin, J., & Nielsen, K. (2011). Choice of nasal nitric oxide technique as first-line test for primary ciliary dyskinesia. *The European Respiratory Journal*, *37*(3), 559–565. https://doi.org/10.1183/09031936.00032610

Marthin, J., & Nielsen, K. (2013). Hand-Held Tidal Breathing Nasal Nitric Oxide Measurement - A Promising Targeted Case-Finding Tool for the Diagnosis of Primary Ciliary Dyskinesia. *PLoS ONE*, *8*(2), e57262. https://doi.org/10.1371/journal.pone.0057262

McGrath, J., & Brueckner, M. (2003). Cilia are at the heart of vertebrate left-right asymmetry. *Current Opinion in Genetics and Development*, *13*(4), 385–392. https://doi.org/10.1016/S0959-437X(03)00091-1

McManus, I. C., Mitchison, H. M., Chung, E. M. K., Stubbings, G. F., & Martin, N. (2003). Primary ciliary dyskinesia (Siewert's/Kartagener's syndrome): respiratory symptoms and psycho-social impact. *BMC Pulmonary Medicine*, *3*, 4. https://doi.org/10.1186/1471-2466-3-4

Merkus, P., Romeijn, S. G., Verhoef, J. C., Merkus, F. W., & Schouwenburg, P. F. (2001). Classification of cilio-inhibiting effects of nasal drugs. *The Laryngoscope*, *111*(4 Pt 1), 595–602. https://doi.org/10.1097/00005537-200104000-00008

Merveille, A. C., Davis, E. E., Becker-Heck, A., Legendre, M., Amirav, I., Bataille, G., Belmont, J., Beydon, N., Billen, F., Clément, A., Clercx, C., Coste, A., Crosbie, R., De Blic, J., Deleuze, S., Duquesnoy, P., Escalier, D., Escudier, E., Fliegauf, M., … Amselem, S. (2011). CCDC39 is required for assembly of inner dynein arms and the dynein regulatory complex and for normal ciliary motility in humans and dogs. *Nature Genetics*, *43*(1), 72–78. https://doi.org/10.1038/ng.726

Moore, A., Escudier, E., Roger, G., Tamalet, A., Pelosse, B., Marlin, S., Clément, A., Geremek, M., Delaisi, B., Bridoux, A. M., Coste, A., Witt, M., Duriez, B., & Amselem, S. (2006). RPGR is mutated in patients with a complex X linked phenotype combining primary ciliary dyskinesia and retinitis pigmentosa. *Journal of Medical Genetics*, *43*(4), 326–333. https://doi.org/10.1136/jmg.2005.034868

Moore, D., Onoufriadis, A., Shoemark, A., Simpson, M., Zur Lage, P., De Castro, S. C., Bartoloni, L., Gallone, G., Petridi, S., Woollard, W., Antony, D., Schmidts, M., Didonna, T., Makrythanasis, P., Bevillard, J., Mongan, N., Djakow, J., Pals, G., Lucas, J., … Mitchison, H. (2013). Mutations in ZMYND10, a gene essential for proper axonemal assembly of inner and outer dynein arms in humans and flies, cause primary ciliary dyskinesia. *American Journal of Human Genetics*, *93*(2), 346–356. https://doi.org/10.1016/j.ajhg.2013.07.009

Mullowney, T., Manson, D., Kim, R., Stephens, D., Shah, V., & Dell, S. (2014). Primary Ciliary Dyskinesia and Neonatal Respiratory Distress. *Pediatrics*, *134*(6), 1160–1166.

https://doi.org/10.1542/peds.2014-0808

Nonaka, S., Tanaka, Y., Okada, Y., Takeda, S., Harada, A., Kanai, Y., Kido, M., & Hirokawa, N. (1998). Randomization of left-right asymmetry due to loss of nodal cilia generating leftward flow of extraembryonic fluid in mice lacking KIF3B motor protein. *Cell*, *95*(6), 829–837. https://doi.org/10.1016/S0092-8674(00)81705-5

Nöthe-Menchen, T., Wallmeier, J., Pennekamp, P., Höben, I., Olbrich, H., Loges, N., Raidt, J., Dougherty, G., Hjeij, R., Dworniczak, B., & Omran, H. (2019). Randomization of Left-right Asymmetry and Congenital Heart Defects: The Role of DNAH5 in Humans and Mice. *Circulation. Genomic and Precision Medicine*, *10.1161/CI*, Advance online publication. https://doi.org/10.1161/CIRCGEN.119.002686

O'Callaghan, C., Chetcuti, P., & Moya, E. (2010). High prevalence of primary ciliary dyskinesia in a British Asian population. *Archives of Disease in Childhood*, *95*(1), 51–52. https://doi.org/10.1136/adc.2009.158493

Oda, T., Yanagisawa, H., Kamiya, R., & Kikkawa, M. (2014). A molecular ruler determines the repeat length in eukaryotic cilia and flagella. *Science (New York, N.Y.)*, *346*(6211), 857–860. https://doi.org/10.1126/science.1260214

Olbrich, H., Cremers, C., Loges, N. T., Werner, C., Nielsen, K. G., Marthin, J. K., Philipsen, M., Wallmeier, J., Pennekamp, P., Menchen, T., Edelbusch, C., Dougherty, G. W., Schwartz, O., Thiele, H., Altmüller, J., Rommelmann, F., & Omran, H. (2015). Loss-of-Function GAS8 Mutations Cause Primary Ciliary Dyskinesia and Disrupt the Nexin-Dynein Regulatory Complex. *American Journal of Human Genetics*, *97*(4), 546–554. https://doi.org/10.1016/j.ajhg.2015.08.012

Olbrich, H., Schmidts, M., Werner, C., Onoufriadis, A., Loges, N. T., Raidt, J., Banki, N. F., Shoemark, A., Burgoyne, T., Al Turki, S., Hurles, M. E., Köhler, G., Schroeder, J., Nürnberg, G., Nürnberg, P., Chung, E. M. K., Reinhardt, R., Marthin, J. K., Nielsen, K. G., … Omran, H. (2012). Recessive HYDIN mutations cause primary ciliary dyskinesia without randomization of left-right body asymmetry. *American Journal of Human Genetics*, *91*(4), 672–684. https://doi.org/10.1016/j.ajhg.2012.08.016

Omran, H., Kobayashi, D., Olbrich, H., Tsukahara, T., Loges, N. T., Hagiwara, H., Zhang, Q., Leblond, G., O'Toole, E., Hara, C., Mizuno, H., Kawano, H., Fliegauf, M., Yagi, T., Koshida, S., Miyawaki, A., Zentgraf, H., Seithe, H., Reinhardt, R., … Takeda, H. (2008). Ktu/PF13 is required for cytoplasmic pre-assembly of axonemal dyneins. *Nature*, *456*(7222), 611–616. https://doi.org/10.1038/nature07471

Omran, H., & Loges, N. T. (2009). Immunofluorescence staining of ciliated respiratory epithelial cells. In *Methods in cell biology* (Vol. 91, Issue 08). Elsevier Masson SAS. https://doi.org/10.1016/S0091-679X(08)91007-4

Paff, T., Loges, N. T., Aprea, I., Wu, K., Bakey, Z., Haarman, E. G., Daniels, J. M. A., Sistermans, E. A., Bogunovic, N., Dougherty, G. W., Matter, A., Olbrich, H., Werner, C., Pals, G., Ho, I. M., Schmidts, M., Omran, H., & Micha, D. (2017). Mutations in PIH1D3 Cause X-Linked Primary Ciliary Dyskinesia with Outer and Inner Dynein Arm Defects. *American Journal of Human Genetics*, *100*(1), 160–168. https://doi.org/10.1016/j.ajhg.2016.11.019

Papon, J. F., Bassinet, L., Cariou-Patron, G., Zerah-Lancner, F., Vojtek, A. M., Blanchon, S., Crestani, B., Amselem, S., Coste, A., Housset, B., Escudier, E., & Louis, B. (2012). Quantitative analysis of ciliary

beating in primary ciliary dyskinesia: a pilot study. *Orphanet Journal of Rare Diseases*, *7*, 1–11. https://doi.org/10.1186/1750-1172-7-78

Papon, J. F., Coste, A., Roudot-Thoraval, F., Boucherat, M., Roger, G., Tamalet, A., Vojtek, A. M., Amselem, S., & Escudier, E. (2010). A 20-year experience of electron microscopy in the diagnosis of primary ciliary dyskinesia. *The European Respiratory Journal*, *35*(5), 1057–1063. https://doi.org/10.1183/09031936.00046209

Raidt, J., Krenz, H., Tebbe, J., Große-Onnebrink, J., Olbrich, H., Loges, N. T., Biebach, L., Schmalstieg, C., Keßler, C., Wallmeier, J., Dworniczak, B., Pennekamp, P., Dugas, M., Werner, C., & Omran, H. (2022). Limitations of Nasal Nitric Oxide Measurement for Diagnosis of Primary Ciliary Dyskinesia with Normal Ultrastructure. *Annals of the American Thoracic Society*, *19*(8), 1275–1284. https://doi.org/10.1513/AnnalsATS.202106-728OC

Raidt, J., Wallmeier, J., Hjeij, R., Onnebrink, G., Pennekamp, P., Loges, N. T., Olbrich, H., Ha, K., Dougherty, G. W., Omran, H., & Werner, C. (2014). Ciliary beat pattern and frequency in genetic variants of primary ciliary dyskinesia. *The European Respiratory Journal*, *44*(6), 1579–1588. https://doi.org/10.1183/09031936.00052014

Raidt, J., Werner, C., Menchen, T., Dougherty, G. W., Olbrich, H., Loges, N. T., Schmitz, R., Pennekamp, P., & Omran, H. (2015). Ciliary function and motor protein composition of human fallopian tubes. *Human Reproduction (Oxford, England)*, *30*(12), 2871–2880. https://doi.org/10.1093/humrep/dev227

Reula, A., Pitarch-fabregat, J., Milara, J., Cortijo, J., Mata-roig, M., Milian, L., & Armengot, M. (2021). High-Speed Video Microscopy for Primary Ciliary Dyskinesia Diagnosis: A Study of Ciliary Motility Variations with Time and Temperature. *Diagnostics (Basel, Switzerland)*, *11*(7), 1301. https://doi.org/10.3390/diagnostics11071301

Richards, S., Aziz, N., Bale, S., Bick, D., Das, S., Gastier-Foster, J., Grody, W. W., Hegde, M., Lyon, E., Spector, E., Voelkerding, K., Rehm, H. L., & Committee, A. L. Q. A. (2015). Standards and guidelines for the interpretation of sequence variants: a joint consensus recommendation of the American College of Medical Genetics and Genomics and the Association for Molecular Pathology. *Genetics in Medicine : Official Journal of the American College of Medical Genetics*, *17*(5), 405–424. https://doi.org/10.1038/gim.2015.30.Standards

Ross, A. J., Dailey, L. A., Brighton, L. E., & Devlin, R. B. (2007). Transcriptional profiling of mucociliary differentiation in human airway epithelial cells. *American Journal of Respiratory Cell and Molecular Biology*, *37*(2), 169–185. https://doi.org/10.1165/rcmb.2006-0466OC

Rubbo, B., & Lucas, J. S. (2017). Clinical care for primary ciliary dyskinesia : current challenges and future directions. *European Respiratory Review : An Official Journal of the European Respiratory Society*, *26*(145), 170023. https://doi.org/10.1183/16000617.0023-2017

Rumman, N., Jackson, C., Collins, S., Goggin, P., Coles, J., & Lucas, J. S. (2017). Diagnosis of primary ciliary dyskinesia: Potential options for resource-limited countries. *European Respiratory Review : An Official Journal of the European Respiratory Society*, *26*(143), 160058. https://doi.org/10.1183/16000617.0058-2016

Sampaio, P., da Silva, M. F., Vale, I., Roxo-Rosa, M., Pinto, A., Constant, C., Pereira, L., Quintão, C. M., & Lopes, S. S. (2021). CiliarMove: new software for evaluating ciliary beat frequency helps find novel

mutations by a Portuguese multidisciplinary team on primary ciliary dyskinesia. *ERJ Open Research*, *7*(1), 00792–02020. https://doi.org/10.1183/23120541.00792-2020

Schwabe, G. C., Hoffmann, Ã. K., Loges, N. T., Birker, D., Rossier, C., Santi, M. M. De, Olbrich, H., Fliegauf, M., Failly, M., Liebers, U., Collura, M., Gaedicke, G., Mundlos, S., Wahn, U., Blouin, J., Niggemann, B., Omran, H., Antonarakis, S. E., & Bartoloni, L. (2008). Primary Ciliary Dyskinesia Associated With Normal Axoneme Ultrastructure Is Caused by DNAH11 Mutations. *Human Mutation*, *29*(2), 289–298. https://doi.org/10.1002/humu

Shapiro, A., Davis, S. D., Polineni, D., Manion, M., Rosenfeld, M., Dell, S. D., Chilvers, M. A., Ferkol, T. W., Zariwala, M. A., Sagel, S. D., Josephson, M., Morgan, L., Yilmaz, O., Olivier, K. N., Milla, C., Pittman, J. E., Leigh Anne Daniels, M., Jones, M. H., Janahi, I. A., … Lavergne, V. (2018). Diagnosis of primary ciliary dyskinesia: An official American thoracic society clinical practice guideline. *American Journal of Respiratory and Critical Care Medicine*, *197*(12), e24–e39. https://doi.org/10.1164/rccm.201805-0819ST

Shapiro, A., Davis, S., Ferkol, T., Dell, S., Rosenfeld, M., Olivier, K. N., Sagel, S. D., Milla, C., Zariwala, M. A., Wolf, W., Carson, J. L., Hazucha, M. J., Burns, K., Robinson, B., Knowles, M. R., Leigh, M. W., & Consortium, G. D. of M. C. (2014). Laterality Defects Other Than Situs Inversus Totalis in Primary Ciliary Dyskinesia Insights Into Situs Ambiguus and Heterotaxy. *Chest*, *146*(5), 1176–1186. https://doi.org/10.1378/chest.13-1704

Shapiro, A., Dell, S., Gaston, B., O'Connor, M., Marozkina, N., Manion, M., Hazucha, M. J., & Leigh, M. W. (2020). Nasal nitric oxide measurement in primary ciliary dyskinesia a technical paper on standardized testing protocols. *Annals of the American Thoracic Society*, *17*(2), E1–E12. https://doi.org/10.1513/AnnalsATS.201904-347OT

Shapiro, A., Zariwala, M. A., Ferkol, T., Davis, S. D., Sagel, S. D., Dell, S. D., Rosenfeld, M., Olivier, K. N., Milla, C., Daniel, S. J., Kimple, A. J., Manion, M., Knowles, M. R., & Leigh, M. W. (2016). Diagnosis, monitoring, and treatment of primary ciliary dyskinesia: PCD foundation consensus recommendations based on state of the art review. *Pediatric Pulmonology*, *51*(2), 115–132. https://doi.org/10.1002/ppul.23304

Shi, L., Shen, X., Chi, Y., & Shen, Y. (2021). Primary ciliary dyskinesia relative protein ZMYND10 is involved in regulating ciliary function and intraflagellar transport in Paramecium tetraurelia. *European Journal of Protistology*, *77*, 125756. https://doi.org/10.1016/j.ejop.2020.125756

Shoemark, A., Boon, M., Brochhausen, C., Bukowy-Bieryllo, Z., de Santi, M. M., Goggin, P., Griffin, P., Hegele, R. G., Hirst, R. A., Leigh, M. W., Lupton, A., MacKenney, K., Omran, H., Pache, J. C., Pinto, A., Reinholt, F. P., Schroeder, J., Yiallouros, P., & Escudier, E. (2020). International consensus guideline for reporting transmission electron microscopy results in the diagnosis of Primary Ciliary Dyskinesia (BEAT PCD TEM Criteria). *The European Respiratory Journal*, *55*(4), 1900725. https://doi.org/10.1183/13993003.00725-2019

Shoemark, A., Frost, E., Dixon, M., Ollosson, S., Kilpin, K., Patel, M., Scully, J., Rogers, A. V, Mitchison, H. M., Bush, A., & Hogg, C. (2017). Accuracy of Immuno fluorescence in the Diagnosis of Primary Ciliary Dyskinesia. *American Journal of Respiratory and Critical Care Medicine*, *196*(1), 94–101. https://doi.org/10.1164/rccm.201607-1351OC

Shoemark, A., & Hogg, C. (2013). Electron tomography of respiratory cilia. *Thorax*, *68*(2), 190–191. https://doi.org/10.1136/thoraxjnl-2012-202938

Smith, C. M., Djakow, J., Free, R. C., Djakow, P., Lonnen, R., Williams, G., Pohunek, P., Hirst, R. A., Easton, A. J., Andrew, P. W., & O'Callaghan, C. (2012). CiliaFA: A research tool for automated, high-throughput measurement of ciliary beat frequency using freely available software. *Cilia*, *1*, 1–7. https://doi.org/10.1186/2046-2530-1-14

Sousa, R., Constant, C., Bandeira, T., & Pereira, L. (2018). Primary Ciliary Dyskinesia : Updates on Diagnosis , Follow-Up and Treatment. *Portuguese Journal of Pediatrics*, *49*(3), 342–349. https://doi.org/10.25754/pjp.2018.13575

Stannard, W., Rutman, A., Wallis, C., & O'Callaghan, C. (2004). Central microtubular agenesis causing primary ciliary dyskinesia. *American Journal of Respiratory and Critical Care Medicine*, *169*(5), 634–637. https://doi.org/10.1164/rccm.200306-782OC

Strippoli, M. P. F., Frischer, T., Barbato, A., Snijders, D., Maurer, E., Lucas, J. S. A., Eber, E., Karadag, B., Pohunek, P., Zivkovic, Z., Escribano, A., O'callaghan, C., Bush, A., & Kuehni, C. E. (2012). Management of primary ciliary dyskinesia in European children: Recommendations and clinical practice. *European Respiratory Journal*, *39*(6), 1482–1491. https://doi.org/10.1183/09031936.00073911

Ta-Shma, A., Hjeij, R., Perles, Z., Dougherty, G. W., Abu Zahira, I., Letteboer, S. J. F., Antony, D., Darwish, A., Mans, D. A., Spittler, S., Edelbusch, C., Cindrić, S., Nöthe-Menchen, T., Olbrich, H., Stuhlmann, F., Aprea, I., Pennekamp, P., Loges, N. T., Breuer, O., … Omran, H. (2018). Homozygous loss-of-function mutations in MNS1 cause laterality defects and likely male infertility. *PLoS Genetics*, *14*(8), e1007602. https://doi.org/10.1371/journal.pgen.1007602

Tarkar, A., Loges, N. T., Slagle, C. E., Francis, R., Dougherty, G. W., Tamayo, J. V., Shook, B., Cantino, M., Schwartz, D., Jahnke, C., Olbrich, H., Werner, C., Raidt, J., Pennekamp, P., Abouhamed, M., Hjeij, R., Köhler, G., Griese, M., Li, Y., … Omran, H. (2013). DYX1C1 is required for axonemal dynein assembly and ciliary motility. *Nature Genetics*, *45*(9), 995–1003. https://doi.org/10.1038/ng.2707

Thomas, B., Rutman, A., & O'Callaghan, C. (2008). Disrupted ciliated epithelium shows slower ciliary beat frequency and increased dyskinesia. *The European Respiratory Journal*, *34*(2), 401–404. https://doi.org/10.1183/09031936.00153308

Vanaken, G. J., Bassinet, L., Boon, M., Mani, R., Honoré, I., Papon, J.-F. P., Cuppens, H., Jaspers, M., Lorent, N., Coste, A., Escudier, E., Amselem, S., Maitre, B., Legendre, M., & Christin-Maitre, S. (2017). Infertility in an adult cohort with primary ciliary dyskinesia: phenotype–gene association. *The European Respiratory Journal*, *50*(6), 1750314. https://doi.org/10.1183/13993003.00314-2017

Wallmeier, J., Al-mutairi, D. A., Chen, C., Loges, N. T., Pennekamp, P., Menchen, T., Ma, L., Shamseldin, H. E., Olbrich, H., Dougherty, G. W., Werner, C., Alsabah, B. H., Köhler, G., Jaspers, M., Boon, M., Griese, M., Schmitt-grohé, S., Zimmermann, T., Koerner-rettberg, C., … Omran, H. (2014). Mutations in CCNO result in congenital mucociliary clearance disorder with reduced generation of multiple motile cilia. *Nature Genetics*, *46*(6), 646–651. https://doi.org/10.1038/ng.2961

Wallmeier, J., Frank, D., Shoemark, A., Nöthe-Menchen, T., Cindric, S., Olbrich, H., Loges, N. T., Aprea, I., Dougherty, G. W., Pennekamp, P., Kaiser, T., Mitchison, H. M., Hogg, C., Carr, S. B., Zariwala, M. A., Ferkol, T., Leigh, M. W., Davis, S. D., Atkinson, J., … Omran, H. (2019). De Novo Mutations in FOXJ1

Result in a Motile Ciliopathy with Hydrocephalus and Randomization of Left / Right Body Asymmetry. *American Journal of Human Genetics*, *105*(5), 1030–1039. https://doi.org/10.1016/j.ajhg.2019.09.022

Wallmeier, J., Nielsen, K. G., Kuehni, C. E., Lucas, J. S., Leigh, M. W., Zariwala, M. A., & Omran, H. (2020). Motile ciliopathies. *Nature Reviews Disease Primers*, *6*(1), 77. https://doi.org/10.1038/s41572-020-0209-6

Whitfield, M., Thomas, L., Bequignon, E., Schmitt, A., Stouvenel, L., Montantin, G., Tissier, S., Duquesnoy, P., Copin, B., Chantot, S., Whitfield, M., Thomas, L., Bequignon, E., Schmitt, A., & Stouvenel, L. (2019). Mutations in DNAH17 , Encoding a Sperm-Specific Axonemal Outer Dynein Arm Heavy Chain , Cause Isolated Male Infertility Due to Asthenozoospermia. *American Journal of Human Genetics*, *105*(1), 198–212. https://doi.org/10.1016/j.ajhg.2019.04.015

Wirschell, M., Olbrich, H., Werner, C., Tritschler, D., Bower, R., Sale, W. S., Loges, N. T., Pennekamp, P., Lindberg, S., Stenram, U., Carlén, B., Horak, E., Köhler, G., Nürnberg, P., Nürnberg, G., Porter, M. E., & Omran, H. (2013). The nexin-dynein regulatory complex subunit DRC1 is essential for motile cilia function in algae and humans. *Nature Genetics*, *45*(3), 262–268. https://doi.org/10.1038/ng.2533

Yamaguchi, H., Oda, T., Kikkawa, M., & Takeda, H. (2018). Systematic studies of all PIH proteins in zebrafish reveal their distinct roles in axonemal dynein assembly. *ELife*, *7*, e36979. https://doi.org/10.7554/eLife.36979.001

Zariwala, M. A., Gee, H. Y., Kurkowiak, M., Al-Mutairi, D. A., Leigh, M. W., Hurd, T. W., Hjeij, R., Dell, S. D., Chaki, M., Dougherty, G. W., Adan, M., Spear, P. C., Esteve-Rudd, J., Loges, N. T., Rosenfeld, M., Diaz, K. A., Olbrich, H., Wolf, W. E., Sheridan, E., … Hildebrandt, F. (2013). ZMYND10 is mutated in primary ciliary dyskinesia and interacts with LRRC6. *American Journal of Human Genetics*, *93*(2), 336–345. https://doi.org/10.1016/j.ajhg.2013.06.007

Zhu, L., Belmont, J. W., & Ware, S. M. (2006). Genetics of human heterotaxias. *European Journal of Human Genetics*, *14*(1), 17–25. https://doi.org/10.1038/sj.ejhg.5201506

CHAPTER 4.

DISCUSSION

4. INTRODUCTION

The correct asymmetric displacement of visceral organs within the LR body plan is of utmost importance for the proper alignment and connection of the organs with each other, ultimately leading to a functional multisystem. When the LR axis development is perturbed, pathological conditions arise compromising the wellbeing of 1 in 10000 people (Lin et al., 2014). While *situs inversus* and *situs ambiguous* have been mostly studied under the primary ciliary dyskinesia (PCD) field, this disorder only accounts for 20 – 25% of the individuals with laterality defects (Deng et al., 2014). Moreover, the LR axis establishment remains an attractive field with many unresolved questions involving cellular communication, ciliary motility, hydrodynamics at microscales and genetic signaling cascades.

Throughout the development of my PhD project, we intended to provide new insights into different steps of the LR axis patterning. Firstly, we had previously found that Notch signaling was regulating the motile – immotile cilia fate and we pursued this pathway searching for new players, as a disequilibrium in ciliary motility ratio has catastrophic effects on fluid flow production within the zebrafish LR organizer (LRO). Then, we tackled how fluid flow is perceived by the surrounding cells, a 20 years old question, and we presented compiling data towards the mechanosensory hypothesis. Lastly, we implemented another molecular test in order to improve our laboratory response towards the PCD diagnostic challenges that we found in Portugal.

4.1. Building an optimal fluid flow with proper motile – immotile cilia ratio

It was Afzelius, who firstly proposed that ciliary motility was triggering the LR axis establishment in a yet to discover embryonic structure (Afzelius, 1976). Twenty years later, ciliary motility was experimentally demonstrated at the mouse node (Supp et al., 1997, 1999; Nonaka et al., 1998; Okada et al., 1999), then at the rabbit notochordal plate and the medaka Kupffer's Vesicle (Okada et al., 2005), at the zebrafish Kupffer's Vesicle (Essner et al., 2005) and lastly, at the *Xenopus* gastrocoel roof plate (Schweickert et al., 2007). Although different species present LROs with distinct topographies, ciliary motility is conserved among most vertebrates, playing an essential role in symmetry breaking (Essner et al., 2002). On the other hand, immotile cilia are also present. Mouse and *Xenopus* display motile cilia at the center of the LRO and immotile cilia at the periphery, whereas in zebrafish immotile cilia are evenly

distributed in the LRO (McGrath et al., 2003; Yoshiba et al., 2012; Boskovski et al., 2013; Tavares et al., 2017).

Interestingly, at least within mouse and zebrafish LROs, most cilia start as immotile and progressively become motile during the time-window for LR axis establishment while other cilia remain completely immotile (McGrath et al., 2003; Yoshiba et al., 2012; Yuan et al., 2015; Ferreira et al., 2017; Tavares et al., 2017). According to our and others cilia quantifications from the zebrafish KV, the number of motile cilia ranges between 27 – 33% at 4 ss, 63 – 76% at 5 – 6 ss and 84 – 90% at 8 ss (Yuan et al., 2015; Tavares et al., 2017). A small discrepancy was reported by Ferreira and colleagues that saw consistently less immotile cilia at 3 ss and around 98% of motile cilia at 8 ss (Ferreira et al., 2017), which may be a reflection of different imaging scan protocols used to distinguish motile from immotile cilia or perhaps different zebrafish strains.

Together this data suggests that immotile cilia also play an important role in symmetry breaking and motile – immotile cilia ratio must be regulated throughout the KV development. Our laboratory and others have previously shown that Notch signaling modulates the number of motile and immotile cilia, without affecting the total number of cilia within the zebrafish and *Xenopus* LROs (Boskovski et al., 2013; Tözser et al., 2015; Tavares et al., 2017). Moreover, we found that Notch signaling effect on cilia motility was in part caused by an upregulation of the *her12* transcription factor (Tavares et al., 2017). With this work (Chapter 2), we further discovered that Syntenin, a cytoplasmatic adaptor protein, was also involved in the establishment of motile – immotile cilia ratio, as an upstream regulator of Notch signaling.

In vitro studies showed that Syntenin directly interacts with zebrafish DeltaD, stabilizing DeltaD protein at the plasma membrane and consequently preventing its internalization and ubiquitination, necessary for Notch signaling activation (Estrach et al., 2007). In zebrafish live embryos, we showed that loss-of function of *syntenin-a* increased DeltaD protein levels and altered DeltaD localization, that became distributed between the plasma membrane and the endocytic compartments. *Her12* expression levels were also increased in *syntenin-a* morphants, confirming the Notch signaling activation. In agreement with our previous study, ultimately, these embryos had decreased numbers of motile cilia, which severely affected the fluid flow dynamics, triggering early and late LR defects, as shown by *dand5* symmetric expression pattern and heart *situs* randomization, respectively.

Moreover, we found subsequent downstream targets of Notch signaling involved in ciliary motility. The Notch signaling effector Her12 was shown to increase *rabconnectin 3a* transcription, which in turn increased V-ATPase localization at the plasma membrane, while in *deltaD* mutants, *rabconnectin 3a* expression levels and V-ATPase fluorescent signals were

decreased. We also inhibited V-ATPase activity with Concanamycin A and showed an increased motile cilia number at early stages of the LR axis development. To our best knowledge, this treatment is unique in increasing motile cilia number at 4 ss to comparable proportions to those found at 8 somite staged wildtype embryos (around 80% of motile cilia) (Tavares et al., 2017).

The role of proton flux in the LR axis development is controversial. First, inhibition of H^+/K^+-ATPase proton pump, from 1 to 1000 cell stage, randomized the expression patterns of *nodal* and *pitx2* at the LPM, without affecting cilia (Kawakami et al., 2005). Second, knockdown studies for different V-ATPase subunits resulted in a reduced number of KV cells and shorter cilia (Chen et al., 2012; Gokey et al., 2015). The time-window for V-ATPase contribution was narrowed down to between 1 cell stage and 90% epiboly stage, which indicates a role in DFCs, prior to the KV formation (Adams et al., 2006; Gokey et al., 2015). We now showed a new function of V-ATPase in KV ciliary motility, suggesting that proton flux affects both early and late steps of the LR establishment. At this point, apart from the ciliary number and length phenotypes, we do not know the implications of having more motile cilia at earlier stages, on the *dand5* mRNA degradation nor on the position of visceral organs. Nevertheless, embryos incubated with Concanamycin A from bud stage to 6 ss demonstrated a lack of significant laterality defects in heart looping (Gokey et al., 2015).

Aside from ciliary motility, we found that DFCs *syntenin-a* morphants showed a reduction of Tjp1a levels at the KV luminal surface and decreased KV lumen volumes. Suggesting that *syntenin-a* loss-of-function weakens the KV cell cohesiveness, allowing fluid leakage between the intercellular spaces during KV lumen expansion. To confirm this hypothesis, injection of rhodamine dextran into the KV lumen would provide a direct visualization on fluorescent fluid leakage. Curiously, Estrach and colleagues showed that Syntenin and zebrafish DeltaD interaction, besides regulating Notch signaling, promoted intercellular adhesion (Estrach et al., 2007), in line with our results. Nevertheless, evaluation of tight junction proteins such as Tjp1a and Claudin5a, within the KV cells and quantification of KV volume should be performed in *deltaD* mutants in order to further assess the contribution of DeltaD in adherent junctions *in vivo*.

Taking all results into consideration, we suggest a simplified model where:

(i) In wildtype conditions during late epiboly stages, embryos start to express *foxj1a*, the master transcriptional factor that drives the motile ciliary program in all DFCs (Stubbs et al., 2008; Yu et al., 2008; Zhang et al., 2012). At bud stage, Notch signaling is activated at the posterior side of the KV cells, leading to the upregulation of *her12* (Tavares et al., 2017), which in turn increases the levels of *rabconnectin 3a.* From this point onwards, the complex

Rabconnectin drives the assembly of membrane (V0) and cytosolic (V1) V-ATPase subunits, that by the 3 ss is mostly enriched at the plasma membrane. Facing the extracellular KV lumen, the V-ATPase pumps protons at the vicinity of cilia in order to keep them immotile. At 4 ss, *syntenin-a* is expressed in the KV cells and stabilizes DeltaD protein at the plasma membrane, limiting Notch signaling and consequently the downstream molecular switch, as cilia start to acquire motility. At the plasma membrane, DeltaD may accumulate at the adherent junctions and contribute to cellular tightness during KV lumen expansion.

(ii) In *syntenin-a* morphants, DeltaD is not stabilized at the plasma membrane causing endocytosis-driven DeltaD activation and subsequently a Notch signaling overactivation. Increased levels of *her12* sustain the assembly of V-ATPase at the plasma membrane, maintaining cilia immotile for longer periods of time. On the other hand, intercellular adhesions are defective, which compromises the capacity of KV cells to properly seal the lumen during Cftr-driven fluid influx, resulting in smaller KVs. Both abnormal motile – immotile cilia ratio and KV volume negatively affect the fluid flow effectiveness in breaking symmetry.

Whether Notch signaling dictates which cilia will persist forever immotile or regulates gradually the transition from immotile to motile, remains debatable. Previous work from Ferreira and Yuan may point towards the latter hypothesis, as embryos between 9 and 16 ss, showed the lowest number of immotile cilia, around 5 ± 4%, and in some cases reaching a complete absence of immotile cilia (Yuan et al., 2015; Ferreira et al., 2017). This data agrees with our published work showing that all KV cilia had an ultrastructure characteristic of motile cilia with clearly visible dynein arms, when observed either by transmitted electron microscopy or live imaging with a fluorescent tagged *dnal1* (Tavares et al., 2017). Suggesting that, in contrast to mouse and *Xenopus*, cilia immotility is temporary in zebrafish and eventually all cilia will become motile.

Ciliary motility also plays an important function within the respiratory epithelial cells, fallopian duct cells, spermatozoa and brain ependymal cells driving mucociliary clearance, egg transport, cell locomotion and cerebrospinal fluid flow, respectively. Interestingly, a recent paper proposed that Daw1, a homolog of *Chlamydomonas* ODA16, regulates the timely onset of ciliary motility in different zebrafish structures by enhancing the transport efficiency of ODAs into the cilium (Bearce et al., 2022). On one hand, *daw1* morphants and mutants showed significant defects in several LR outcomes and otolith generation, a process dependent on motile cilia present in the zebrafish ear (Gao et al., 2010; Stooke-Vaughan et al., 2012; Bearce et al., 2022). On the other hand, all *daw1* mutants showed a curly down tail phenotype at embryonic stages, due to lack of ciliary motility at the central canal, that was gradually recovered throughout development and later on only 20% of the fish exhibited spinal curve

defects at adulthood (Bearce et al., 2022). Therefore, ODA16/*daw1* seems to be required for establishing cilia motility quickly, which has strong implications on early stages and short-lived structures, such as the LRO, and milder to no effects on later stages (Ahmed et al., 2008; Bearce et al., 2022). In agreement, *Daw1* mice mutants showed prominent laterality defects and minor effects on respiratory cilia movement (Solomon et al., 2017).

It would be noteworthy to see if Daw1 and the mechanism described here are "talking to each other" to coordinate motile – immotile cilia ratio, for instance by evaluating if V-ATPase activity inhibition can rescue the immotile cilia phenotype observed in the KV of *daw1* mutants.

In summary, KV cilia motility is tightly regulated in a time-dependent manner to generate a proper fluid flow capable of breaking symmetry. In return, this leads us to the question of how strong the flow needs to be for a reliable LR axis development.

4.2. Biophysical role of the flow: mechanosensation over chemosensation

Several studies have been demonstrating that a slow cilia-driven fluid flow is enough to trigger a molecular response in the surrounding cells. In mice, Hamada's group showed that the leftward fluid flow velocity starts as low as 1 µm/s, which is sufficient to induce *dand5* mRNA downregulation on the left side, several hours before the flow attain its full speed of around 15 – 20 µm/s (Okada et al., 1999; Nakamura et al., 2012; Shinohara et al., 2012). Moreover, slowing the fluid flow during the entire time-window with a low concentration of methylcellulose (0.5%) revealed that all embryos achieved a dominant left-sided Nodal signaling even if it had been induced at both sides of the LPM (Shinohara et al., 2012). In agreement, we showed that the fluid flow within the zebrafish LRO progressively increases, as more immotile cilia turn into motile (Tavares et al., 2017). We also found that, although *dand5* asymmetric expression pattern becomes visible at the same time that the fluid flow becomes stronger at 8 ss (Sampaio et al., 2014), the crucial time-window for LR successful outcome is much earlier, between 4 and 6 ss, characterized by a lower magnitude of flow (BioRxiv, Sampaio et al., 2022). With this work, we also found that a low fluid viscosity plays an important role in setting an optimal flow.

Additionally, it was shown that mouse mutants with only two motile cilia developed a normal LR gene expression irrespectively of their position within the LRO cavity (Shinohara et al., 2012). In the zebrafish LRO, the symmetry breaking event seems to be more dependent on motile cilia number, with previous calculations estimating a minimum of 30 cilia for a robust

LR axis establishment (Sampaio et al., 2014; Smith et al., 2014). Interestingly though, titration of *dnah7* morpholino into zebrafish to generate embryos with only few motile cilia clustered either on the left or right side of the LRO showed a concordant internal heart arrangement on the same side as the motile cilia (Sampaio et al., 2014). The latter experiment suggested that in zebrafish a few motile cilia are also sufficient to generate a fluid flow capable of symmetry breaking, while laterality is strongly dependent on motile cilia localization.

The remaining question is how such mild fluid flow is perceived by the cells. The chemosensation model proposes that morphogens or vesicles containing signaling molecules are secreted into the LRO lumen and carried by the directional fluid flow towards the left side, where they accumulate, triggering a response either by being internalized by the cells or activating a membrane receptor (Nonaka et al., 1998; Okada et al., 1999; Takeda et al., 1999; Tanaka et al., 2005; Cartwright et al., 2007, 2020; Montenegro-Johnson et al., 2016; Ferreira et al., 2017; Solowiej-Wedderburn et al., 2019).

Recent studies in mice simulated different models for extracellular vesicle (EVs) secretion: (i) unbiasedly extended release; (ii) motile cilia stress-induced release and (iii) directly from motile cilia release (Gallagher & Smith, 2020). When compared with experimental results from mice mutants with few motile cilia, this theoretical data suggested that symmetrical secretion of vesicles throughout the LRO is the only model capable of generating some leftward bias in particle accumulation (Shinohara et al., 2012; Gallagher & Smith, 2020). On the other hand, studies in zebrafish suggested a preferential localized secretion of vesicles from the anterior region of the KV, as they would be firstly transported towards the left side facilitating a left biased concentration gradient before particle diffusion and chaotic advection efficiently homogenize the KV fluid (Montenegro-Johnson et al., 2016; Ferreira et al., 2017; Solowiej-Wedderburn et al., 2019). Additionally, Solowiej-Wedderburn et al. (2019) took into consideration the effect of blood flow shear stress on promoting exocytosis in other systems (Baratchi et al., 2014, 2016) and hypothesized that the strong fluid flow at the KV anterior region could enhance the release of extracellular vesicles (Solowiej-Wedderburn et al., 2019). However, no experimental evidence has definitely shown the presence or relevance of EVs nor how the Pkd1l1 – Pkd2 ciliary complex would be integrated in the model in light of the chemosensory mechanism.

In order to test this hypothesis, we used a new in-house method developed to manipulate the KV fluid content in a highly spatio-temporally controlled manner and combined it with genetics and live imaging microscopy. Our results showed that the number of CD63 positive EVs transported by the fluid flow was too low and too variable between embryos precluding the evaluation of EV accumulation in a sided manner. Moreover, uptake of small particles, such

as 10 kDa rhodamine dextrans, seem to occur across the entire KV, without a persistent bias between the left and right sides. Additionally, pharmacological inhibition of different endocytic pathways did not affect heart laterality. Thus, altogether no endocytic evidence was found for supporting a chemosensing mechanism in the establishment of the zebrafish LR axis.

In opposition, the mechanosensory hypothesis proposes that the fluid flow is perceived by bending of the immotile cilia where a ciliary mechanosensor would transduce flow force into a calcium signal (McGrath et al., 2003; Tabin & Vogan, 2003). This model is supported by the observations that a Pkd1l1 – Pkd2 ciliary complex is present in several LROs, such as in mice (Field et al., 2011), medaka (Kamura et al., 2011) and more recently shown by our group in zebrafish (Roxo-Rosa & Lopes, 2019).

On one hand, Pkd2 is a monovalent cation-selective channel (transient receptor potential polycystic channel, TRPP2) and widely accepted to drive a calcium response upon fluid flow stimuli within kidney and endothelial cells (Nauli et al., 2003, 2008; Goetz et al., 2014) and within the LRO (McGrath et al., 2003; Schottenfeld et al., 2007; Yuan et al., 2015; Mizuno et al., 2020). In mice and zebrafish, *Pkd2* mutations impair the symmetry breaking, with most animals showing high proportions of symmetric *dand5* expression patterns, either bilateral or absence of Nodal signaling and *situs* defects (Pennekamp et al., 2002; Schottenfeld et al., 2007; Yoshiba et al., 2012; Jacinto et al., 2021).

On the other hand, *Pkd1l1* is a paralogue of the *polycystic kidney disease 1* gene (PKD1), and it is expected to be the mechanosensory partner that interacts with *Pkd2* within the LRO (Field et al., 2011; Kamura et al., 2011). However the underlying mechanism by which Pkd1l1 senses the fluid flow and modulates Pkd2 activity is still largely unknown (Ferreira et al., 2019; Little & Norris, 2021). Interestingly, two distinct *Pkd1l1* mutations affected differently the LR axis establishment in mice (Grimes et al., 2016). One *Pkd1l1*$^{rks/rks}$ point mutation, considered to be a non-null allele, phenocopied *Pkd2* mutant by showing most embryos with loss of Nodal signaling in the LPM and, later on, a complete penetrance of right pulmonary isomerism (Pennekamp et al., 2002; Field et al., 2011). In contrast, a putative *pkd1l1*$^{tm1/tm1}$ null allele showed opposing phenotypes with most embryos having bilateral Nodal signaling activation in the LPM and subsequently an increased incidence of left pulmonary isomerism (Grimes et al., 2016). *Dand5* expression pattern was symmetric in both mutants, however *Dand5* expression levels were found to be downregulated in *pkd1l1*$^{tm1/tm1}$ mutants, hence explaining the differences observed in LPM Nodal signaling (Field et al., 2011; Grimes et al., 2016). Based on this data, Grimes and colleagues suggested a model where, in the absence of flow, Pkd1l1 acts as upstream repressor of Pkd2, and upon fluid flow induction, Pkd1l1 is repressed, allowing Pkd2 to activate and initiate the calcium influx (Grimes et al., 2016; Little & Norris,

2021). However, evaluation of the direct impact of these mutations on calcium signaling is still lacking. Zebrafish mutants or morphants for *pkd1l1* are also missing and it could be a useful tool to further understand the relationship between flow, *pdk1l1* and *pkd2*.

Moreover, re-introduction of Pkd2 specifically on mice immotile cilia rescued *Pkd2* mouse mutant phenotype (Yoshiba et al., 2012), thus supporting the mechanosensory model and leading us to the next question regarding how many immotile cilia are needed for proper flow-sensing. Although this seems a relevant matter, the information available is limited.

Studies from *Dpcd* mouse mutants, mentioned above as having only two or three motile cilia, showed that they also have less 30% of cilia overall and yet they are still capable of perceiving the generated slow flow given the correct LR gene expression patterns (Shinohara et al., 2012). Nevertheless, a total of 157 – 141 cilia were found within these mutant LROs, which is significantly more than the average of a wildtype zebrafish LRO, that is 44 ± 12 cilia (Tavares et al., 2017).

Ferreira and colleagues performed mathematical simulations, assuming the ciliary motility status and the subsequent calculated angular flow velocity of embryos with 3 ss, 8 ss and 9 – 14 ss, to infer about the feasibility of immotile cilia-based mechanosensation. Predictions from embryos at 3 ss, when roughly half of the cilia are still immotile (44%), indicated that the fluid flow was too slow and irregular to be sensed. While in embryos between 8 and 14 ss embryos, when the fluid flow is more robust, the number of immotile cilia (2 – 5%) was predicted to be insufficient to distinguish the productive flow forces from the oscillatory noise (Ferreira et al., 2017). Suggesting that, in some way, fluid flow forces and immotile cilia number could reach a balance along these two time points. Additionally, for a robust flow sensing mechanism, a temporal averaging of forces acting on 3 immotile cilia on the same side was found to be the minimum necessary (Ferreira et al., 2017).

In agreement with this, we found that during the crucial time-window for symmetry breaking, the number of immotile cilia ranges between 24 – 37% (Tavares et al., 2017), providing enough sensory cilia to perceive the fluid flow. New simulations taking into consideration the observed sensitive stages could be performed seeking further clarification.

Hence, from 4 to 6 ss, the zebrafish LRO seems to attain an equilibrium between motile and immotile cilia number to efficiently generate a productive fluid flow while simultaneously sensing it. However, as immotile cilia are evenly distributed around the LRO, (Tavares et al., 2017), and the fluid flow speed and viscosity do not show any bias towards the left or right side (Ferreira et al., 2017), how asymmetry of *dand5* expression is established on the left side of the LRO remains unanswered.

Some models, in pursuit of a common origin for symmetry breaking across the animal kingdom, have suggested that an intrinsic chiral component of the cytoskeleton, referred to as F-molecule, oriented accordingly with the AP and DV axes could drive the establishment of the third axis and thus be at the heart of LR asymmetry (Blum & Ott, 2018). A few recent studies have tried to shed some light into the chirality of some LR-related features.

Intriguingly, both in mouse and zebrafish LROs, continuous fluid flow was found to affect ciliary bending angle that became significantly different at later stages, after the symmetry breaking (Ferreira et al., 2018; BioRxiv, Katoh et al., 2022). Although fluid flow had already been involved in positive feedback loops to adjust the basal body orientation and refine cilia polarity in *Xenopus* multiciliated cells (Mitchell et al., 2007; Guirao et al., 2010), the biological meaning of this ciliary angle chirality has not been fully addressed in the context of LR axis establishment. While in mouse, the fluid flow affects mostly the left sided cilia (BioRxiv, Katoh et al., 2022), in zebrafish, the right sided cilia went from the mirror image of the left sided cilia at 3 ss to exhibit an asymmetric dextral chirality, following the fluid flow direction, at 8 ss (Ferreira et al., 2018). Ferreira and colleagues argued that this phenomenon could optimize the flow directionality or signaling molecule recognition, but our own results reject this hypothesis as asymmetric cilia chirality arises too late, past the sensitive stages for flow sensing.

On the other hand, Katoh and colleagues claimed that Pkd2 seemed to be mainly localized on the dorsal side of each immotile cilia from the mouse LRO (BioRxiv, Katoh et al., 2022). Asymmetric and unilateral distribution of ion channels along the ciliary membrane was also reported in human sperm flagella (Miller et al., 2018). Katoh et al. further proposed that, due to its polarized arrangement, Pkd2 channel would open in response to an increase in membrane tension on the ciliary dorsal side, possibly by stretching the mechanosensor Pkd1l1, which is achieved by a ventral bending of the cilium. While the leftward fluid flow causes a ventral bending only on left sided cilia, the artificial rightward fluid flow would ventrally bend the cilia from the right side, reconciling previous experimental data (Nonaka et al., 2002).

Additionally, Katoh showed by using optical tweezers that an artificial mechanical stimulus of 1,5 hours could elicit a Pkd2-dependent calcium increase in immotile cilia and *Dand5* mRNA downregulation in the same cells (BioRxiv, Katoh et al., 2022). Thus, suggesting that flow and Pkd2 asymmetric localization within cilia, integrates the molecular mechanism of the mechanosensory model. Yet, this study is still in preprint at the time of the thesis publication and needs to complete the peer reviewing process, therefore conclusions should be taken prudently.

4.3. Pkd2-mediated calcium signaling

Both in mouse and zebrafish LROs, a Pkd2-dependent response was detected at early stages, concordant with the time-window of lower magnitude flow that we detected for symmetry breaking (McGrath et al., 2003; Takao et al., 2013; Yuan et al., 2015; Mizuno et al., 2020). Moreover, a ciliary localization of Pkd2 is crucial for optimal intraciliary calcium oscillations on the left sided LRO cells (Yoshiba et al., 2012). The calcium signals are transferred from the cilia to the cytosol, triggering a further release of calcium ions from internal storage organelles, such as the endoplasmic reticulum, through the inositol phosphate (IP) pathway (Sarmah et al., 2005; Jurynec et al., 2008; Francescatto et al., 2010; Yuan et al., 2015; Mizuno et al., 2020). Thus, amplifying and propagating the calcium waves through the LRO cells.

Furthermore, Pkd2-dependent calcium signaling targets Ca^{2+}/calmodulin-dependent kinase (CaMK-II) phosphorylation, leading to a transient activation of CaMK-II enzyme on the left side of zebrafish LRO, anytime between 6 and 10 ss until 16 ss (Francescatto et al., 2010; Rothschild et al., 2011). However, the underlying mechanism by which calcium signaling, and perhaps CaMK-II, result in *dand5* mRNA downregulation is poorly understood.

In mice, a previous study showed that *Dand5* expression level and, subsequently, its expression pattern are determined post-transcriptionally in a 3'-UTR dependent manner (Nakamura et al., 2012). Twenty years later, the same laboratory found that the RNA binding protein Bicaudal-C (Bicc1) interacts with 3'-UTR of *Dand5* and recruits the Ccr4-Not deadenylase complex, known to mediate mRNA decay by shortening of mRNA poly(A) tails (reviewed by Temme et al., 2014), which most likely induces *Dand5* mRNA downregulation (Minegishi et al., 2021).

An accompanying paper in *Xenopus*, showed that Bicc1-dependent post transcriptional regulation of *Dand5* is conserved in frog LRO (Maerker et al., 2021). Moreover, Maerker and colleagues found another player in this process, the Dicer1, an enzyme involved primarily in the production of small non-coding microRNAs, which in turn mediate the fine-tuning of gene expression (reviewed by Vergani-Junior et al., 2021). Alternatively, Dicer1 could act independently from microRNAs through other non-canonical mechanisms (Pong & Gullerova, 2018).

Lastly in zebrafish, *bicc1* is expressed in the LRO (Bouvrette et al., 2010) and maternal zygotic *dicer1* mutants showed a bilateral expression of *dand5*, that was retained for longer periods of time when compared with wildtype embryos (Maerker et al., 2021), suggesting that this pathway is also safeguarded in fish LRO.

4.4. After the fluid flow-sensing mechanism, the desensitization phase

Since cilia-driven fluid flow determines the LR asymmetry at early stages, when the flow speed is low, we then questioned about the relevance of the strong flow. It is plausible that an increase in flow magnitude could sustain or amplify the asymmetries previously established, enhancing the robustness of this process.

In mice, strong directional flow was suggested to modulate DAND5 distribution around the LRO, in order to completely abolish Nodal activity on that region (Inácio et al., 2013). During the symmetry breaking time-window, DAND5 protein followed a concordant pattern to the *Dand5* mRNA, resulting in an asymmetric Nodal signaling activation, detected by increased Smad2 phosphorylation on the left side (Kawasumi et al., 2011; Inácio et al., 2013). Then, in a strong flow-dependent manner, DAND5 became bilaterally present in the LRO and later on, the signal was no longer detected on the LRO right side. At this point, DAND5 was only observed at the left side, concomitantly with the decrease in Smad2 phosphorylation. The authors proposed that changes in DAND5 localization occurred by protein secretion into the lumen, translocation and uptake by the left sided cells, and claimed that it was crucial for ceasing Nodal signaling in a precise timely fashion (Inácio et al., 2013). Indeed, previous results from Shinohara and colleagues showed that incubating embryos with a mild concentration of 0.5% methylcellulose during the initial slow flow time-window and, then transferred them to 1% methylcellulose, abolishing the flow for the rest of the development, did not affect the overall LR asymmetry but in some cases Nodal signaling was activated on both sides (left sided dominant) (Shinohara et al., 2012). Thus, supporting a later role of flow and DAND5 in maintaining the asymmetries.

In zebrafish, although never tested owing to the absence of functional Dand5 antibodies, protein translocation seems unlikely. In contrast to mice, that induce the expression of *Dand5* and *Nodal* within the same crown cells around the LRO, zebrafish display two distinct regions, being *dand5* expressed at the KV cells and *spaw* at an non-overlapping dorsal domain straight above the KV (Hashimoto et al., 2004). Thus, Dand5 protein from the right side of the KV would have to travel a long way, not only through the KV lumen but also through the left sided KV cells, to reach Spaw from the left side. Moreover, peri-nodal *Nodal* becomes asymmetrically expressed in mice, but never in zebrafish (Long et al., 2003; Kawasumi et al., 2011). Suggesting that a sustained action of Dand5 may be needed on both sides of the KV. Nevertheless, experimental data is necessary to confirm or reject this hypothesis in zebrafish, as for example evaluation of Smad2 phosphorylation expression timing and pattern or mass spectrometry analysis of KV liquid for Dand5 presence.

On the other hand, the strong flow could be just a trivial consequence of the continuous transition of immotile to motile cilia. As mentioned above, cilia acquire motility progressively covering a time-window where motile and immotile cilia proportions are balanced for optimal symmetry breaking to a period where immotile cilia number are insufficient to reliably sense the flow (Ferreira et al., 2017; Tavares et al., 2017). Therefore, one could suggest that turning all cilia motile would completely abolish the flow sensing mechanism carried by the immotile cilia, thus desensitizing the KV cells to further signals. In fact, *dand5* is still expressed around the KV, strongly on the right side, by the 14 ss (data not shown), supporting that the strong fluid flow has no impact thereafter on *dand5* mRNA degradation.

4.5. Characterization of a new Portuguese *ZMYND10* variant while contributing for PCD diagnosis in Portugal

In the last years, a great effort has been made to improve the PCD diagnosis in Portugal. First, it was performed solely based on few conventional TEM results and, currently, we have a multidisciplinary group responsible for performing the analysis of nasal nitric oxide, evaluation of the ciliary function by high-speed video microscopy, evaluation of the ciliary ultrastructure by TEM and identification of PCD-causing mutations by genetic testing (Fermeiro et al., 2010; Strippoli et al., 2012; Constant et al., 2018; Sampaio et al., 2021). Thus, meeting the European respiratory society diagnostic guidelines (Lucas et al., 2017; Sousa et al., 2018).

We now established IF labelling assays for respiratory ciliated cells in the laboratory as a daily basis technique for PCD testing. Furthermore, we extensively characterized, based on the commercially available and previously validated antibodies, a *ZMYND10* variant that we had identified in one Portuguese family (Sampaio et al., 2021). Here, it was also reported the localization of the ciliary proteins DNAH9, DNAH11, DNAI1, Gas8, RSPH9 and SPEF2 in *ZMYND10* mutant respiratory cells.

PCD diagnosis can be challenging, mostly in countries with limited resources, as in Portugal. But, on a long-term perspective, a good PCD diagnostic algorithm is likely to decrease laborious, expensive and unnecessary diagnostic and therapeutic interventions. Additionally, identification of the genetic cause of PCD is necessary for the participation in international network registries, which will be certainly useful to stratify PCD patients into research projects and randomized clinical trials, as new treatments are being developed (Goutaki & Shoemark, 2022).

To date, only one randomized placebo-controlled trial on continuous usage of azithromycin therapy in PCD patients was published. Excitingly, the experimental group had fewer exacerbations and bacterial infections during the 6-month study (Kobbernagel et al., 2020), but long-term studies are needed to evaluate the subsequent impact on lung function. More recently, a PCD clinical trial network was created to boost the implementation of new clinical trials, by bringing a sufficient number of patients, patient organizations and pharmaceutical companies together (Raidt et al., 2022). Therefore, it is expected that new treatment approaches will emerge in the next few years.

Ultimately, we want to create disease awareness and provide cost-effective alternatives to our primary and secondary care centers in order to enhance and expand the access of the Portuguese community to a better PCD diagnosis and to prospective care.

4.6. FINAL REMARKS

LR axis development and PCD fields have been continuously benefiting from each other's discoveries, involving studies such as, biochemical and genetic manipulations to live imaging, fluid mechanics and computational modelling. Thus, exponentially growing hand in hand in the last century.

I hope that with this work we also shed new light into some aspects of the zebrafish LR and PCD fields. We revealed an endocytic capacity of KV cells that does not seem to impact on the LR axis establishment, further compiling data supporting the mechanosensory model over the chemosensory. Additionally, we discovered an upstream modulator and downstream targets of Notch signaling involved in cilia motility fate, exposing a common feature between LRO cells and respiratory cells as acidic pH seems to modulate the cilia movement in both. Lastly, we characterized new PCD causing mutations by means of IF labelling assays.

As almost 30% of PCD cases remain without an identifiable genetic cause, we are looking forward to see how PCD clinical studies or development of new diagnostic tools and discovery of other LR related genes will contribute to a greater good.

4.7. REFERENCES

Adams, D. S., Robinson, K. R., Fukumoto, T., Yuan, S., Craig, R., Yelick, P., Kuo, L., Mcsweeney, M., & Levin, M. (2006). Early, H+ -V-ATPase-dependent proton flux is necessary for consistent left-right patterning of non-mammalian vertebrates. *Development (Cambridge, England)*, *133*(9), 1657–1671. https://doi.org/10.1242/dev.02341.Early

Afzelius, B. a. (1976). A human syndrome caused by immotile cilia. *Science*, *193*(4250), 317–319. https://doi.org/10.1126/science.1084576

Ahmed, N. T., Gao, C., Lucker, B. F., Cole, D. G., & Mitchell, D. R. (2008). ODA16 aids axonemal outer row dynein assembly through an interaction with the intraflagellar transport machinery. *The Journal of Cell Biology*, *183*(2), 313–322. https://doi.org/10.1083/jcb.200802025

Baratchi, S., Almazi, J. G., Darby, W., Arnan, F. J. T., & Peter, M. (2016). Shear stress mediates exocytosis of functional TRPV4 channels in endothelial cells. *Cellular and Molecular Life Sciences : CMLS*, *73*(3), 649–666. https://doi.org/10.1007/s00018-015-2018-8

Baratchi, S., Tovar-Lopez, F. J., Khoshmanesh, K., Grace, M. S., Darby, W., Almazi, J., Mitchell, A., & McIntyre, P. (2014). Examination of the role of transient receptor potential vanilloid type 4 in endothelial responses to shear forces. *Biomicrofluidics*, *8*(4), 044117. https://doi.org/10.1063/1.4893272

Bearce, E. A., Irons, Z. H., Craig, S. B., Kuhns, C. J., Sabazali, C., Farnsworth, D. R., Miller, A. C., & Grimes, D. T. (2022). Daw1 regulates the timely onset of cilia motility during development. *Development (Cambridge, England)*, *149*(12), dev200017. https://doi.org/10.1242/dev.200017

Blum, M., & Ott, T. (2018). Animal left–right asymmetry. *Current Biology*, *28*(7), R301–R304. https://doi.org/10.1016/j.cub.2018.02.073

Boskovski, M. T., Yuan, S., Pedersen, N. B., & Goth, C. K. (2013). The Heterotaxy gene, GALNT11, glycosylates Notch to orchestrate cilia type and laterality. *Nature*, *504*(7480), 456–459. https://doi.org/10.1038/nature12723.The

Bouvrette, D. J., Sittaramane, V., Heidel, J. R., Chandrasekhar, A., & Bryda, E. C. (2010). Knockdown of bicaudal C in zebrafish (Danio rerio) causes cystic kidneys: A nonmammalian model of polycystic kidney disease. *Comparative Medicine*, *60*(2), 96–106.

Cartwright, J. H. E., Piro, N., Piro, O., & Tuval, I. (2007). Embryonic nodal flow and the dynamics of nodal vesicular parcels. *Journal of the Royal Society, Interface*, *4*(12), 49–55. https://doi.org/10.1098/rsif.2006.0155

Cartwright, J. H. E., Piro, O., & Tuval, I. (2020). Chemosensing versus mechanosensing in nodal and Kupffer's vesicle cilia and in other left-right organizer organs. *Philosophical Transactions of the Royal Society B: Biological Sciences*, *375*(1792). https://doi.org/10.1098/rstb.2019.0566

Chen, Y., Wu, B., Xu, L., Li, H., Xia, J., Yin, W., Li, Z., Shi, D., Li, S., Lin, S., Shu, X., & Pei, D. (2012). A SNX10/V-ATPase pathway regulates ciliogenesis in vitro and in vivo. *Cell Research*, *22*(2), 333–345. https://doi.org/10.1038/cr.2011.134

Constant, C., Sousa, R., Pinto, A., Sampaio, P., & Lopes, S. S. (2018). Nova Era no Diagnóstico da Discinesia Ciliar Primária. *Acta Pediátrica Portuguesa*, *49*(3), 235–242. https://doi.org/10.21069/APP.2018.14652

Deng, H., Xia, H., & Deng, S. (2014). Genetic basis of human left-right asymmetry disorders. *Expert*

Reviews in Molecular Medicine, *16*, e19. https://doi.org/10.1017/erm.2014.22

Essner, J. J., Amack, J. D., Nyholm, M. K., Harris, E. B., & Yost, H. J. (2005). Kupffer's vesicle is a ciliated organ of asymmetry in the zebrafish embryo that initiates left-right development of the brain, heart and gut. *Development (Cambridge, England*, *132*(6), 1247–1260. https://doi.org/10.1242/dev.01663

Essner, J. J., Vogan, K. J., Wagner, M. K., Tabin, C. J., Yost, H. J., & Brueckner, M. (2002). Conserved function for embryonic nodal cilia. *Nature*, *418*(6893), 37–38. https://doi.org/10.1038/418037a

Estrach, S., Legg, J., & Watt, F. M. (2007). Syntenin mediates Delta1-induced cohesiveness of epidermal stem cells in culture. *Journal of Cell Science*, *120*(Pt 16), 2944–2952. https://doi.org/10.1242/jcs.016253

Fermeiro, J., Bandeira, T., Lobo, L., & Pereira, L. (2010). Primary ciliary dyskinesia revisited: Based on three clinical reports. *Revista Portuguesa de Pneumologia*, *16*(5), 837–847. https://doi.org/10.1016/s0873-2159(15)30076-3

Ferreira, R. R., Fukui, H., Chow, R., Vilfan, A., & Vermot, J. (2019). The cilium as a force sensor-myth versus reality. *Journal of Cell Science*, *132*(14). https://doi.org/10.1242/jcs.213496

Ferreira, R. R., Pakula, G., Klaeyle, L., Fukui, H., Vilfan, A., Supatto, W., & Vermot, J. (2018). Chiral Cilia Orientation in the Left-Right Organizer. *Cell Reports*, *25*(8), 2008-2016.e4. https://doi.org/10.1016/j.celrep.2018.10.069

Ferreira, R. R., Vilfan, A., Jülicher, F., Supatto, W., & Vermot, J. (2017). Physical limits of flow sensing in the left-right organizer. *ELife*, *6*, e25078. https://doi.org/10.7554/eLife.25078

Field, S., Riley, K.-L., Grimes, D. T., Hilton, H., Simon, M., Powles-Glover, N., Siggers, P., Bogani, D., Greenfield, A., & Norris, D. P. (2011). Pkd1l1 establishes left-right asymmetry and physically interacts with Pkd2. *Development (Cambridge, England)*, *138*(6), 1131–1142. https://doi.org/10.1242/dev.058149

Francescatto, L., Rothschild, S. C., Myers, A. L., & Tombes, R. M. (2010). The activation of membrane targeted CaMK-II in the zebrafish Kupffer's vesicle is required for left-right asymmetry. *Development (Cambridge, England)*, *137*(16), 2753–2762. https://doi.org/10.1242/dev.049627

Gallagher, M. T., & Smith, D. J. (2020). Simulations of particle tracking in the oligociliated mouse node and implications for left-right symmetry breaking mechanics. *Philosophical Transactions of the Royal Society of London. Series B, Biological Sciences*, *375*(1792), 20190161. https://doi.org/10.1098/rstb.2019.0161

Gao, C., Wang, G., Amack, J. D., & Mitchell, D. R. (2010). Oda16/Wdr69 is essential for axonemal dynein assembly and ciliary motility during zebrafish embryogenesis. *Developmental Dynamics : An Official Publication of the American Association of Anatomists*, *239*(8), 2190–2197. https://doi.org/10.1002/dvdy.22355.Oda16/Wdr69

Goetz, J., Steed, E., Ferreira, R., Ramspacher, C., Boselli, F., Charvin, G., Liebling, M., Wyart, C., & Schwab, Y. (2014). Endothelial Cilia Mediate Low Flow Sensing during Zebrafish Vascular Development. *Cell Reports*, *6*(5), 799–808. https://doi.org/10.1016/j.celrep.2014.01.032

Gokey, J. J., Dasgupta, A., Amack, J. D., & Medical, U. (2015). The V-ATPase accessory protein Atp6ap1b mediates dorsal forerunner cell proliferation and left-right asymmetry in zebrafish. *Developmental Biology*, *407*(1), 115–130. https://doi.org/10.1016/j.ydbio.2015.08.002.The

Goutaki, M., & Shoemark, A. (2022). Diagnosis of Primary Ciliary Dyskinesia. *Clinics in Chest Medicine*, *43*(1), 127–140. https://doi.org/10.1016/j.ccm.2021.11.008

Grimes, D. T., Keynton, J. L., Buenavista, M. T., Jin, X., Patel, S. H., Kyosuke, S., Vibert, J., Williams, D.

J., Hamada, H., Hussain, R., Nauli, S. M., & Norris, D. P. (2016). Genetic Analysis Reveals a Hierarchy of Interactions between Polycystin- Encoding Genes and Genes Controlling Cilia Function during Left-Right Determination. *PLoS Genetics*, *12*(6), e1006070. https://doi.org/10.1371/journal.pgen.1006070

Guirao, B., Meunier, A., Mortaud, S., Aguilar, A., Corsi, J. M., Strehl, L., Hirota, Y., Desoeuvre, A., Boutin, C., Han, Y. G., Mirzadeh, Z., Cremer, H., Montcouquiol, M., Sawamoto, K., & Spassky, N. (2010). Coupling between hydrodynamic forces and planar cell polarity orients mammalian motile cilia. *Nature Cell Biology*, *12*(4), 341–350. https://doi.org/10.1038/ncb2040

Hashimoto, H., Rebagliati, M., Ahmad, N., Muraoka, O., Kurokawa, T., Hibi, M., & Suzuki, T. (2004). The Cerberus/Dan-family protein Charon is a negative regulator of Nodal signaling during left-right patterning in zebrafish. *Development (Cambridge, England)*, *131*(8), 1741–1753. https://doi.org/10.1242/dev.01070

Inácio, J. M., Marques, S., Nakamura, T., Shinohara, K., Meno, C., Hamada, H., & Belo, J. A. (2013). The dynamic right-to-left translocation of Cerl2 is involved in the regulation and termination of Nodal activity in the mouse node. *PloS One*, *8*(3), e60406. https://doi.org/10.1371/journal.pone.0060406

Jacinto, R., Sampaio, P., Roxo-Rosa, M., Pestana, S., & Lopes, S. S. (2021). Pkd2 Affects Cilia Length and Impacts LR Flow Dynamics and Dand5. *Frontiers in Cell and Developmental Biology*, *9*, 624531. https://doi.org/10.3389/fcell.2021.624531

Jurynec, M. J., Xia, R., Mackrill, J. J., Gunther, D., Crawford, T., Flanigan, K. M., Abramson, J. J., Howard, M. T., & Grunwald, D. J. (2008). Selenoprotein N is required for ryanodine receptor calcium release channel activity in human and zebrafish muscle. *Proceedings of the National Academy of Sciences of the United States of America*, *105*(34), 12485–12490. https://doi.org/10.1073/pnas.0806015105

Kamura, K., Kobayashi, D., Uehara, Y., Koshida, S., Iijima, N., Kudo, A., Yokoyama, T., & Takeda, H. (2011). Pkd1l1 complexes with Pkd2 on motile cilia and functions to establish the left-right axis. *Development (Cambridge, England)*, *138*(6), 1121–1129. https://doi.org/10.1242/dev.058271

Katoh, T. A., Omori, T., Mizuno, K., & Sai, X. (2022). Immotile cilia of the mouse node sense a fluid flow – induced mechanical force for left-right symmetry breaking. *BioRxiv*, *04.11.487968*. https://doi.org/2022.04.11.487968

Kawakami, Y., Raya, A., Raya, R. M., Rodríguez-Esteban, C., & Izpisúa Belmonte, J. C. (2005). Retinoic acid signalling links left – right asymmetric patterning and bilaterally symmetric somitogenesis in the zebrafish embryo. *Nature*, *435*(7039), 165–171. https://doi.org/10.1038/nature03512

Kawasumi, A., Nakamura, T., Iwai, N., Yashiro, K., Saijoh, Y., Belo, J. A., Shiratori, H., & Hamada, H. (2011). Left-right asymmetry in the level of active Nodal protein produced in the node is translated into left-right asymmetry in the lateral plate of mouse embryos. *Developmental Biology*, *353*(2), 321–330. https://doi.org/10.1016/j.ydbio.2011.03.009

Kobbernagel, H. E., Buchvald, F. F., Haarman, E. G., Casaulta, C., Collins, S. A., Hogg, C., Kuehni, C. E., Lucas, J. S., Moser, C. E., Quittner, A. L., Raidt, J., Rosthøj, S., Sørensen, A. L., Thomsen, K., Werner, C., Omran, H., & Nielsen, K. G. (2020). Efficacy and safety of azithromycin maintenance therapy in primary ciliary dyskinesia (BESTCILIA): a multicentre , double-blind , randomised , placebo-controlled phase 3 trial. *The Lancet. Respiratory Medicine*, *8*(5), 493–505. https://doi.org/10.1016/S2213-2600(20)30058-8

Lin, Krikov, S., Riehle-Colarusso, T., Frías, J., Belmont, J., Anderka, M., Geva, T., Getz, K., & Botto, L. (2014). Laterality defects in the national birth defects prevention study (1998-2007): Birth prevalence and descriptive epidemiology. *American Journal of Medical Genetics. Part A*, *164*(10), 2581–2591. https://doi.org/10.1002/ajmg.a.36695

Little, R. B., & Norris, D. P. (2021). Right, left and cilia: How asymmetry is established. *Seminars in Cell and Developmental Biology*, *110*, 11–18. https://doi.org/10.1016/j.semcdb.2020.06.003

Long, S., Ahmad, N., & Rebagliati, M. (2003). The zebrafish nodal-related gene southpaw is required for visceral and diencephalic left-right asymmetry. *Development (Cambridge, England)*, *130*(11), 2303–2316. https://doi.org/10.1242/dev.00436

Lucas, J. S., Barbato, A., Collins, S. A., Goutaki, M., Behan, L., Caudri, D., Dell, S., Eber, E., Escudier, E., Hirst, R. A., Hogg, C., Jorissen, M., Latzin, P., Legendre, M., Leigh, M. W., Midulla, F., Nielsen, K. G., Omran, H., Papon, J. F., … Kuehni, C. E. (2017). European Respiratory Society guidelines for the diagnosis of primary ciliary dyskinesia. *The European Respiratory Journal*, *49*(1), 1601090. https://doi.org/10.1183/13993003.01090-2016

Maerker, M., Getwan, M., Dowdle, M. E., McSheene, J. C., Gonzalez, V., Pelliccia, J. L., Hamilton, D. S., Yartseva, V., Vejnar, C., Tingler, M., Minegishi, K., Vick, P., Giraldez, A. J., Hamada, H., Burdine, R. D., Sheets, M. D., Blum, M., & Schweickert, A. (2021). Bicc1 and Dicer regulate left-right patterning through post-transcriptional control of the Nodal inhibitor Dand5. *Nature Communications*, *12*(1), 1–15. https://doi.org/10.1038/s41467-021-25464-z

McGrath, J., Somlo, S., Makova, S., Tian, X., & Brueckner, M. (2003). Two populations of node monocilia initiate left-right asymmetry in the mouse. *Cell*, *114*(1), 61–73. https://doi.org/10.1016/S0092-8674(03)00511-7

Miller, M. R., Kenny, S. J., Mannowetz, N., Mansell, S. A., Wojcik, M., Mendoza, S., Zucker, R. S., Xu, K., & Lishko, P. V. (2018). Asymmetrically Positioned Flagellar Control Units Regulate Human Sperm Rotation. *Cell Reports*, *24*(10), 2606–2613. https://doi.org/10.1016/j.celrep.2018.08.016

Minegishi, K., Rothé, B., Komatsu, K. R., Ono, H., Ikawa, Y., Nishimura, H., Katoh, T. A., Kajikawa, E., Sai, X., Miyashita, E., Takaoka, K., Bando, K., Kiyonari, H., Yamamoto, T., Saito, H., Constam, D. B., & Hamada, H. (2021). Fluid flow-induced left-right asymmetric decay of Dand5 mRNA in the mouse embryo requires a Bicc1-Ccr4 RNA degradation complex. *Nature Communications*, *12*(1), 4071. https://doi.org/10.1038/s41467-021-24295-2

Mitchell, B., Jacobs, R., Li, J., Chien, S., & Kintner, C. (2007). A positive feedback mechanism governs the polarity and motion of motile cilia. *Nature*, *447*(7140), 97–101. https://doi.org/10.1038/nature05771

Mizuno, K., Shiozawa, K., Katoh, T. A., Minegishi, K., Ide, T., Ikawa, Y., Nishimura, H., Takaoka, K., Itabashi, T., Iwane, A. H., Nakai, J., Shiratori, H., & Hamada, H. (2020). Role of Ca2+ transients at the node of the mouse embryo in breaking of left-right symmetry. *Science Advances*, *6*(30). https://doi.org/10.1126/sciadv.aba1195

Montenegro-Johnson, T. D., Baker, D. I., Smith, D. J., & Lopes, S. S. (2016). Three-dimensional flow in Kupffer's Vesicle. *Journal of Mathematical Biology*, *73*(3), 705–725. https://doi.org/10.1007/s00285-016-0967-7

Nakamura, T., Saito, D., Kawasumi, A., Shinohara, K., Asai, Y., Takaoka, K., Dong, F., Takamatsu, A., Belo, J. A., Mochizuki, A., & Hamada, H. (2012). Fluid flow and interlinked feedback loops establish left-right asymmetric decay of Cerl2 mRNA. *Nature Communications*, *3*, 1322. https://doi.org/10.1038/ncomms2319

Nauli, S. M., Alenghat, F. J., Luo, Y., Williams, E., Vassilev, P., Li, X., Elia, A. E. H., Lu, W., Brown, E. M., Quinn, S. J., Ingber, D. E., & Zhou, J. (2003). Polycystins 1 and 2 mediate mechanosensation in the primary cilium of kidney cells. *Nature Genetics*, *33*(2), 129–137. https://doi.org/10.1038/ng1076

Nauli, S. M., Kawanabe, Y., Kaminski, J. J., Pearce, W. J., Ingber, D. E., & Zhou, J. (2008). Endothelial

Cilia Are Fluid Shear Sensors That Regulate Calcium Signaling and Nitric Oxide Production Through Polycystin-1. *Circulation*, *117*(9), 1161–1171. https://doi.org/10.1161/CIRCULATIONAHA.107.710111

Nonaka, S., Shiratori, H., Saijoh, Y., & Hamada, H. (2002). Determination of left-right patterning of the mouse embryo by artificial nodal flow. *Nature*, *418*(6893), 96–99. https://doi.org/10.1038/nature00849

Nonaka, S., Tanaka, Y., Okada, Y., Takeda, S., Harada, A., Kanai, Y., Kido, M., & Hirokawa, N. (1998). Randomization of left-right asymmetry due to loss of nodal cilia generating leftward flow of extraembryonic fluid in mice lacking KIF3B motor protein. *Cell*, *95*(6), 829–837. https://doi.org/10.1016/S0092-8674(00)81705-5

Okada, Y., Nonaka, S., Tanaka, Y., Saijoh, Y., Hamada, H., & Hirokawa, N. (1999). Abnormal nodal flow precedes situs inversus in iv and inv mice. *Molecular Cell*, *4*(4), 459–468. https://doi.org/10.1016/S1097-2765(00)80197-5

Okada, Y., Takeda, S., Tanaka, Y., Belmonte, J. C. I., & Hirokawa, N. (2005). Mechanism of nodal flow: A conserved symmetry breaking event in left-right axis determination. *Cell*, *121*(4), 633–644. https://doi.org/10.1016/j.cell.2005.04.008

Pennekamp, P., Karcher, C., Fischer, A., Schweickert, A., Skryabin, B., Horst, J., Blum, M., & Dworniczak, B. (2002). The ion channel polycystin-2 is required for left-right axis determination in mice. *Current Biology*, *12*(11), 938–943. https://doi.org/10.1016/S0960-9822(02)00869-2

Pong, S. K., & Gullerova, M. (2018). Noncanonical functions of microRNA pathway enzymes - Drosha, DGCR8, Dicer and Ago proteins. *FEBS Letters*, *592*(17), 2973–2986. https://doi.org/10.1002/1873-3468.13196

Raidt, J., Maitre, B., Pennekamp, P., Altenburg, J., Anagnostopoulou, P., Bloemsma, L. D., Boon, M., Borrelli, M., Brinkmann, F., Carr, S. B., Carroll, M. P., Castillo-corullón, S., Coste, A., Cutrera, R., Dehlink, E., Damien, M., Destouches, S., Cicco, M. E. Di, Dixon, L., … Nielsen, K. G. (2022). The disease-specific clinical trial network for Primary Ciliary Dyskinesia (PCD-CTN). *ERJ Open Research*, *8*(3), 00139–02022. https://doi.org/10.1183/23120541.00139-2022

Rothschild, S. C., Francescatto, L., Drummond, I. A., & Tombes, R. M. (2011). CaMK-II is a PKD2 target that promotes pronephric kidney development and stabilizes cilia. *Development (Cambridge, England)*, *138*(16), 3387–3397. https://doi.org/10.1242/dev.066340

Roxo-Rosa, M., & Lopes, S. S. (2019). The Zebrafish Kupffer's Vesicle: A Special Organ in a Model Organism to Study Human Diseases. *In Zebrafish in Biomedical Research. IntechOpen*. https://doi.org/10.5772/intechopen.88266%0D

Sampaio, P., da Silva, M. F., Vale, I., Roxo-Rosa, M., Pinto, A., Constant, C., Pereira, L., Quintão, C. M., & Lopes, S. S. (2021). CiliarMove: new software for evaluating ciliary beat frequency helps find novel mutations by a Portuguese multidisciplinary team on primary ciliary dyskinesia. *ERJ Open Research*, *7*(1), 00792–02020. https://doi.org/10.1183/23120541.00792-2020

Sampaio, P., Ferreira, R. R., Guerrero, A., Pintado, P., Tavares, B., Amaro, J., Smith, A. A., Montenegro-Johnson, T., Smith, D. J., & Lopes, S. S. (2014). Left-Right Organizer Flow Dynamics: How Much Cilia Activity Reliably Yields Laterality? *Developmental Cell*, *29*(6), 716–728. https://doi.org/10.1016/j.devcel.2014.04.030

Sampaio, P., Pestana, S., Guerrero, A., Telley, I. A., Smith, D. J., & Lopes, S. S. (2022). Fluid manipulations uncover mechanosensation for zebrafish left-right establishment during one-hour time interval. *BioRxiv*, 2022.04.21.489023. https://doi.org/10.1101/2022.04.21.489023

Sarmah, B., Latimer, A. J., Appel, B., & Wente, S. R. (2005). Inositol polyphosphates regulate zebrafish

left-right asymmetry. *Developmental Cell*, *9*(1), 133–145. https://doi.org/10.1016/j.devcel.2005.05.002

Schottenfeld, J., Sullivan-Brown, J., & Burdine, R. D. (2007). Zebrafish curly up encodes a Pkd2 ortholog that restricts left-side-specific expression of southpaw. *Development (Cambridge, England)*, *134*(8), 1605–1615. https://doi.org/10.1242/dev.02827

Schweickert, A., Weber, T., Beyer, T., Vick, P., Bogusch, S., Feistel, K., & Blum, M. (2007). Cilia-Driven Leftward Flow Determines Laterality in Xenopus. *Current Biology*, *17*(1), 60–66. https://doi.org/10.1016/j.cub.2006.10.067

Shinohara, K., Kawasumi, A., Takamatsu, A., Yoshiba, S., Botilde, Y., Motoyama, N., Reith, W., Durand, B., Shiratori, H., & Hamada, H. (2012). Two rotating cilia in the node cavity are sufficient to break left-right symmetry in the mouse embryo. *Nature Communications*, *3*, 622. https://doi.org/10.1038/ncomms1624

Smith, D., Montenegro-Johnson, T., & Lopes, S. (2014). Organized chaos in Kupffer's vesicle: How a heterogeneous structure achieves consistent left-right patterning. *Bioarchitecture*, *4*(3), 119–125. https://doi.org/10.4161/19490992.2014.956593

Solomon, G. M., Francis, R., Chu, K. K., Birket, S. E., Gabriel, G., Trombley, J. E., Lemke, K. L., Klena, N., Turner, B., Tearney, G. J., Lo, C. W., & Rowe, S. M. (2017). Assessment of ciliary phenotype in primary ciliary dyskinesia by micro-optical coherence tomography. *JCI Insight*, *2*(5), e91702. https://doi.org/10.1172/jci.insight.91702

Solowiej-Wedderburn, J., Smith, D. J., Lopes, S. S., & Montenegro-johnson, T. D. (2019). Wall stress enhanced exocytosis of extracellular vesicles as a possible mechanism of left-right symmetry-breaking in vertebrate development. *Journal of Theoretical Biology*, *460*, 220–226. https://doi.org/10.1016/j.jtbi.2018.10.015

Sousa, R., Constant, C., Bandeira, T., & Pereira, L. (2018). Primary Ciliary Dyskinesia : Updates on Diagnosis , Follow-Up and Treatment. *Portuguese Journal of Pediatrics*, *49*(3), 342–349. https://doi.org/10.25754/pjp.2018.13575

Stooke-Vaughan, G. A., Huang, P., Hammond, K. L., Schier, A. F., & Whitfield, T. T. (2012). The role of hair cells, cilia and ciliary motility in otolith formation in the zebrafish otic vesicle. *Development (Cambridge, England)*, *139*(10), 1777–1787. https://doi.org/10.1242/dev.079947

Strippoli, M. P. F., Frischer, T., Barbato, A., Snijders, D., Maurer, E., Lucas, J. S. A., Eber, E., Karadag, B., Pohunek, P., Zivkovic, Z., Escribano, A., O'callaghan, C., Bush, A., & Kuehni, C. E. (2012). Management of primary ciliary dyskinesia in European children: Recommendations and clinical practice. *European Respiratory Journal*, *39*(6), 1482–1491. https://doi.org/10.1183/09031936.00073911

Stubbs, J. L., Oishi, I., Izpisúa Belmonte, J. C., & Kintner, C. (2008). The forkhead protein Foxj1 specifies node-like cilia in Xenopus and zebrafish embryos. *Nature Genetics*, *40*(12), 1454–1460. https://doi.org/10.1038/ng.267

Supp, D. M., Brueckner, M., Kuehn, M. R., Witte, D. P., Lowe, L. A., Mcgrath, J., Corrales, J., & Potter, S. S. (1999). Targeted deletion of the ATP binding domain of left-right dynein confirms its role in specifying development of left-right asymmetries. *Development (Cambridge, England)*, *126*(23), 5495–5504. https://doi.org/10.1242/dev.126.23.5495

Supp, D. M., Witte, D. P., Potter, S. S., & Brueckner, M. (1997). Mutation of an axonemal dynein affects left–right asymmetry in inversus viscerum mice. *Nature*, *389*(6654), 963–966. https://doi.org/10.1097/MPG.0b013e3181a15ae8.Screening

Tabin, C. J., & Vogan, K. J. (2003). A two-cilia model for vertebrate left-right axis specification. *Genes*

& Development, *17*(1), 1–6. https://doi.org/10.1101/gad.1053803

Takao, D., Nemoto, T., Abe, T., Kiyonari, H., Kajiura-kobayashi, H., Shiratori, H., & Nonaka, S. (2013). Asymmetric distribution of dynamic calcium signals in the node of mouse embryo during left – right axis formation. *Developmental Biology*, *376*(1), 23–30. https://doi.org/10.1016/j.ydbio.2013.01.018

Takeda, S., Yonekawa, Y., Tanaka, Y., Okada, Y., Nonaka, S., & Hirokawa, N. (1999). Left-right asymmetry and kinesin superfamily protein KIF3a: New insights in determination of laterality and mesoderm induction by KIF3A(-/-) mice analysis. *The Journal of Cell Biology*, *145*(4), 825–836. https://doi.org/10.1083/jcb.145.4.825

Tanaka, Y., Okada, Y., & Hirokawa, N. (2005). FGF-induced vesicular release of Sonic hedgehog and retinoic acid in leftward nodal flow is critical for left-right determination. *Nature*, *435*(7039), 172–177. https://doi.org/10.1038/nature03494

Tavares, B., Jacinto, R., Sampaio, P., Pestana, S., Pinto, A., Vaz, A., Roxo-Rosa, M., Gardner, R., Lopes, T., Schilling, B., Henry, I., Saúde, L., & Lopes, S. S. (2017). Notch/Her12 signalling modulates, motile/immotile cilia ratio downstream of Foxj1a in zebrafish left-right organizer. *ELife*, *6*, e25165. https://doi.org/10.7554/eLife.25165

Temme, C., Simonelig, M., & Wahle, E. (2014). Deadenylation of mRNA by the CCR4-NOT complex in Drosophila: molecular and developmental aspects. *Frontiers in Genetics*, *5*, 143. https://doi.org/10.3389/fgene.2014.00143

Tözser, J., Earwood, R., Kato, A., Brown, J., Tanaka, K., Didier, R., Megraw, T. L., Blum, M., & Kato, Y. (2015). TGF-β Signaling Regulates the Differentiation of Motile Cilia. *Cell Reports*, *11*(7), 1000–1007. https://doi.org/10.1016/j.celrep.2015.04.025

Vergani-Junior, C. A., Tonon-da-Silva, G., Inan, M. D., & Mori, M. A. (2021). DICER: structure, function, and regulation. *Biophysical Reviews*, *13*(6), 1081–1090. https://doi.org/10.1007/s12551-021-00902-w

Yoshiba, S., Shiratori, H., Kuo, I. Y., Kawasumi, A., Shinohara, K., Nonaka, S., Asai, Y., Sasaki, G., Belo, J. A., Sasaki, H., Nakai, J., Dworniczak, B., Ehrlich, B., Pennekamp, P., & Hamada, H. (2012). Cilia at the node of mouse embryos sense fluid flow for left-right determination via Pkd2. *Science (New York, N.Y.)*, *338*(6104), 226–231. https://doi.org/10.1038/nature13314.A

Yu, X., Ng, C. P., Habacher, H., & Roy, S. (2008). Foxj1 transcription factors are master regulators of the motile ciliogenic program. *Nature Genetics*, *40*(12), 1445–1453. https://doi.org/10.1038/ng.263

Yuan, S., Zhao, L., Brueckner, M., & Sun, Z. (2015). Intraciliary Calcium Oscillations Initiate Vertebrate Left-Right Asymmetry. *Current Biology : CB*, *25*(5), 556–567. https://doi.org/10.1016/j.cub.2014.12.051

Zhang, M., Zhang, J., Lin, S.-C., & Meng, A. (2012). β-Catenin 1 and β-catenin 2 play similar and distinct roles in left-right asymmetric development of zebrafish embryos. *Development (Cambridge, England)*, *139*(11), 2009–2019. https://doi.org/10.1242/dev.074435